Constitutive Modeling of Bio-Cemented Sands for Earthquake Engineering Applications

By

MAYA EL KORTBAWI
DISSERTATION

Submitted in partial satisfaction of the requirements for the degree of

DOCTOR OF PHILOSOPHY

in

Civil and Environmental Engineering

in the

OFFICE OF GRADUATE STUDIES

of the

UNIVERSITY OF CALIFORNIA

DAVIS

Approved:

Katerina Ziotopoulou, Chair

Ross W. Boulanger

Jason T. DeJong

Committee in Charge

2022

To my support system, my parents Rock and Marie,

my sisters Nadine and Céline,

and my biggest fan Elie

Table of Contents

List of Figures ..... **viii**

List of Tables ..... **xv**

ABSTRACT ..... **xvi**

ACKNOWLEDGMENTS ..... **xix**

CHAPTER 1 Introduction **1**

1.1 Background 1

1.2 Overview of Dissertation 4

1.3 Dissertation organization 5

CHAPTER 2 Mechanical behavior of bio-cemented sands: state-of-the-art review of experimental and numerical developments **9**

2.1 Introduction 10

2.2 Considered experimental studies 18

2.3 Experimental observations from past studies on bio-cemented sands 21

2.3.1 Microstructure changes 21

2.3.2 Stiffness-related engineering properties 24

2.3.3 Strength-related engineering properties 27

2.4 Synthesis and discussion of behaviors of bio-cemented sands 30

2.4.1 Metrics of cementation 30

2.4.2 Monotonic behavior: Pre- and post-yielding 33

2.4.3 Cyclic behavior 40

2.5 Continuum models for bio-cemented sands 48

2.5.1 Available constitutive models and approaches 48

2.5.2 Discussion and recommendations 51

2.6 Summary and concluding remarks 53

CHAPTER 3 Axisymmetric simulations of cone penetration in bio-cemented sands 102

3.1 Introduction 103

3.2 Cone penetration resistance for bio-cemented sands 108

3.2.1 Large scale tests 108

3.2.2 Centrifuge model tests 109

3.3 Cone penetration numerical simulations 111

3.3.1 Axisymmetric cone penetration model 114

3.3.2 Soil model calibration 115

3.3.3 Model validation 122

3.4 Δq_c – c relationship 126

3.5 Discussion 129

3.6 Concluding remarks 132

CHAPTER 4 Extension of a sand plasticity plane-strain model for earthquake applications to bio-cemented sands 134

4.1 Introduction 135

4.2 Model reformulation 140

4.2.1 Elastic parameters 141

4.2.2 Critical state 143

4.2.3 Critical, dilatancy and bounding surfaces 144

4.2.4 Bond degradation 146

4.3 Model input parameters 149

4.3.1 Primary input parameters 149

4.3.2 Secondary input parameters 151

4.3.3 Numerical implementation 153

4.4 Model calibration 154

4.5 Model validation and performance 165

4.6 Concluding remarks 170

CHAPTER 5 One-dimensional site response analysis of bio-cemented columns: validation against centrifuge model tests 173

5.1 Introduction 174

5.2 Experimental data from centrifuge model tests 179

5.2.1 Test 1 – Darby et al. (2019) 180

5.2.2 Test 2 – San Pablo et al. (2023) 181

5.3 Nonlinear dynamic site response analyses 182

5.3.1 Numerical model setup 182

5.3.2 Input parameters and calibrations 187

5.4 Comparison of simulated and recorded dynamic responses 194

5.4.1 1D site response 194

5.4.2 Time histories (accelerations, pore pressures, and stresses) 195

5.4.3 Response spectra 201

5.5 Parametric investigation of responses to parameter uncertainties 202

5.5.1 Varying the level of cementation 203

5.5.2 Varying the degradation rate 205

5.6 Concluding remarks 208

CHAPTER 6 Conclusions and future directions 212

6.1 Summary and conclusions 213

6.1.1 Literature review (Chapter 2) 213

6.1.2 Δq_c-c relationship (Chapter 3) 214

6.1.3 PM4SandC reformulation and validation at the element level (Chapter 4) 214

6.1.4 Validation of PM4SandC at the system level (Chapter 5) 215

6.2 Future directions 216

APPENDIX A Effect of sand bio-cementation on cone tip resistance: a numerical study 220

APPENDIX B Validation of a bounding surface plasticity model against the experimental response of (bio-) cemented sands 234

BIBLIOGRAPHY 251

List of Figures

2.1. Reaction network for bio-mediated calcite precipitation using ureolysis, adapted from DeJong et al. (2010)……84

2.2. SEM images highlighting the different mineralogies of MICP bio-cementation precipitates: (a) calcite, (b) vaterite, adapted from Burdalski & Gomez (2020)…….……..……...….84

2.3. SEM images highlighting the different crystal associations and sizes of MICP bio-cementation precipitates: (a) hierarchical, (b) irregular, adapted from Nafisi et al. (2019a)……...85

2.4. SEM images highlighting the intermediate morphologies of MICP bio-cementation precipitates, adapted from Burdalski & Gomez (2020) and Burdalski (2020)……85

2.5. Schematic illustrations of (a) the potential particle-level distribution of bio-cementation precipitates, and (b) their failure mechanisms, adapted from DeJong et al. (2010)……..……...86

2.6. Modulus reduction and damping curves obtained from resonant column tests on Ottawa F-65 sand (D_R=61%) at varying levels of cementation and confining stresses of 30 and 100 kPa, adapted from Na et al. (2022)…… ……...87

2.7. Fitting of the reported small-strain shear stiffness values from experimental studies with a power equation as a function of the normalized confining stress [$G = G_o(p/p_A)^n$]…….……88

2.8. Fitting of the variation of the exponent "n" in $G = G_o(p/p_A)^n$ as a function of calcite content…….…….89

2.9. Modulus reduction and damping curves obtained from resonant column tests on Ottawa F-65 sand (D_R=61%) at increasing confining stresses (30, 100, 200 kPa), adapted from Na et al. (2022)……..89

2.10. Synthesized lab and field data correlating the change in shear wave velocity for bio-cemented sands and their and calcite content in percentage by mass……...….90

2.11. The effect of calcite content on the dry density of bio-cemented sands in terms of calcite content in percent and in grams as reported by experimental studies (top row) and the effect of calcite content on the ratio of improvement of cemented to uncemented dry densities in terms of calcite content in percent and in grams as reported by experimental studies……...……91

2.12. The effect of calcite content on the permeability of bio-cemented sands: (left column) in terms of calcite content in kg/m^3, and (right column) in terms of calcite content in %. Effect of calcite content quantified in terms of absolute permeabilities (top row) as well as in terms of ratio of permeabilities (bottom row) (grey shading indicates a change in the y-axis scale)……... ……92

2.13. The effect of bio-cementation on the cone tip resistance of sands in absolute terms (top) and in incremental terms (difference between bio-cemented and uncemented baseline tip resistances) (bottom)… ……93

2.14. Conceptual schematics of the expected monotonic response of initially loose bio-cemented sands for different levels of cementation, drained on the left and undrained on the right…….……..94

2.15. The effect of bio-cementation on the axial strain at peak stress in triaxial tests as a function of calcite content (left) and change in shear wave velocity (right)…….……..……..95

2.16. Effect of bio-cementation on strength parameters as a function of change in shear wave velocity (ΔV_s – left column) and calcite content (in % – right column): absolute cemented effective peak friction angle, ratio of final over initial (clean sand) effective friction angle, and apparent cohesion intercept (grey shading is for a change in y-axis scale)…… ……96

2.17. Cyclic response of initially loose lightly bio-cemented sands in terms of (a) stress paths, (b) stress-strain loops and (c) excess pore pressure ratio evolution. Data shown is from lab tests wherein specimens had an initial D_R of 40%, confining stress of 100 kPa and the cemented sample had a ΔV_s of 35 m/s (Lee et al. 2020, 2022)…… ……97

2.18. Effect of bio-cementation on the cyclic resistance to liquefaction with bio-cementation quantified in terms of: change in shear wave velocity (top), mass of calcite content (middle), and percent of calcite content (bottom) for a confining stress of 50 kPa. Medium dense sands correspond to relative densities around 50%. As discussed in Section 2.4.1 the authors did not attempt to reconcile the metrics for cementation and unify the data any further…….……98

2.19. The effect of bio-cementation on the cyclic resistance to liquefaction with bio-cementation quantified in terms of: change in shear wave velocity (top), mass of calcite content (middle), and percent of calcite content (bottom) for a confining stress of 100 kPa. Loose sands correspond to D_R = ~30%, medium dense sands correspond to D_R = ~50%, and dense sands correspond to D_R = ~74%. As discussed in Section 4.1 the authors did not attempt to reconcile the metrics for cementation and unify the data any further……99

2.20. The effect of bio-cementation on the cyclic resistance to liquefaction with bio-cementation quantified in terms of: mass of calcite content (top), and percent of calcite content (bottom) for a confining stress of 200 kPa. Medium dense sands correspond to D_R = ~50%.....100

2.21. Variation of parameters "a" and "b" of power law fit for the CSR versus number of cycles to liquefaction triggering [$CSR=aN^{-b}$] as a function of mass of calcite content (in grams) for seven different datasets……...……..…….101

3.1. Proposed approach for the development of a $\Delta q_c - c$ relationship for bio-cemented sands from experimental and numerically synthesized data……...…107

3.2. Cone penetration profiles from: (a) large tank experiment (Gomez et al. 2018) and (b) centrifuge model test (Darby et al. 2019) showing an increased cone tip resistance before (both a and b) and after triggering of liquefaction (only in b)……. …….110

3.3. Geometry and boundary conditions of the numerical cone penetration model in FLAC (Moug 2017)……..…..115

3.4. Relationship between apparent cohesion and change in V_s due to the cementation, large tank data from Gomez et al. (2018), triaxial data from O'Donnell et al. (2017) and Nafisi et al. (2020)…..……118

3.5. Normalization of cemented shear wave velocity V_s across the various confining stresses resulting in an apparent cohesion c and normalized shear wave velocity V_{s1} pairs similar across all simulations….120

3.6. Proposed relationship for shear modulus reduction factor as a function of the apparent cohesion c where $c = 0$ and $c > 0$ delineate uncemented and cemented sands, respectively…….....……122

3.7. Comparison between reported experimental (open symbols) and simulated (closed symbols) tip resistances in the $q_c - V_s$ space……..……125

3.8. Comparison between reported experimental (open symbols) and simulated (closed symbols) tip resistances in the K_G framework……..……..…125

3.9. Trend between cohesion and change in tip resistance from synthesized data and its dependence on confining stress……..……..…128

3.10. 3D surface of the relationship between effective vertical stress, change in cone tip resistance and cohesion……..…….129

4.1. Schematic of yield, critical, dilatancy and bounding lines in q-p space for PM4SandC……..145

4.2. Sensitivity analysis on the effect of the strain range r_s over which cementation degrades in a drained monotonic DSS test with a stress-normalized V_{s1} of 150 m/s, V_{sr} of 2, confining stress of 100 kPa: (a) effect of range r_s on the degradation factors F_s and F_{deg}, (b) effect of range r_s on the stress-strain response…….……..…150

4.3. Evolution of cementation parameters with the accumulation of damage due to shear strains for the drained monotonic DSS with r_s = 10% shown in Figure 4.2 (V_{s1} of 150 m/s, V_{sr} of 2, confining stress of 100 kPa)……...……151

4.4. Drained monotonic DSS loading responses for V_s ratio V_{sr} of 1 (uncemented), 2, and 4 and V_{s1} of 150, 300, and 600 m/s, respectively, with vertical confining stresses of 25, 100, 400, 1600, and 6400 kPa and K_o =0.5……..…157

4.5. Undrained monotonic DSS loading responses for V_s ratio V_{sr} of 1 (uncemented), 2, and 4 and V_{s1} of 150, 300, and 600 m/s, respectively, with vertical confining stresses of 25, 100, 400, 1600, and 6400 kPa and K_o=0.5……...……..…158

4.6. Undrained monotonic DSS loading responses for V_s ratio V_{sr} of 1 (uncemented), 2, and 4 and V_{s1} of 150, 300, and 600 m/s, respectively, with vertical confining stresses of 25, 100, and 400 kPa and K_o=0.5 (similar to Figure 4.5 but without high confinements)……159

4.7. Drained monotonic PSC (plane strain compression) loading responses for V_s ratio V_{sr} of 1 (uncemented), 2, and 4 and V_{s1} of 150, 300, and 600 m/s, respectively, with vertical confining stresses of 25, 100, 400, 1600, and 6400 kPa……..……...……..160

4.8. Undrained cyclic DSS loading responses for V_s ratio V_{sr} = 1 (uncemented), 2, and 4 and V_{s1} of 150, 300, and 600 m/s, respectively, with vertical confining stresses of 100 kPa and CSR of 0.09, 0.26, and 0.62, respectively……...……...…161

4.9. Cyclic stress ratios versus number of equivalent uniform loading cycles in undrained DSS loading to cause single-amplitude shear strains of 3% for V_{sr} of 1 (uncemented), 2, 4 with D_R = 30% and a vertical effective consolidation stress of 100 kPa……..……...…….162

4.10. Drained strain-controlled cyclic DSS loading responses for D_R = 30% and V_s ratio V_{sr} of 1 (uncemented), 2, and 4 and V_{s1} of 300, and 600 m/s, respectively, with vertical confining stresses of 25, 100, 400, 1600, and 6400 kPa……..……...……164

4.11. Evaluation of PM4SandC calibrations under drained plane strain compression loading against experimental data for V_{sr} of ~ 3 for confining stresses of (a,b) 10 kPa, (c,d) 100 kPa, and (e,f) 400 kPa (experimental data from Nafisi et al. 2020)……...……...166

4.12. Evaluation of PM4SandC calibrations under monotonic undrained DSS loading against experimental data for V_{sr} of 1.3 (a) to (c) and 2.5 (d) to (f) (experimental data from Lee et al. 2022)…….……167

4.13. Evaluation of PM4SandC calibrations under cyclic undrained DSS loading against experimental data for V_{sr} of 1.25, $\sigma_{vo}^{'}$ of 100 kPa, CSR of 0.2, D_R of 33%, and $V_{s,initial}$ of 146 m/s (experimental data from Lee et al. 2022)…….……...168

4.14. Evaluation of PM4SandC calibrations under cyclic undrained DSS loading against experimental data for V_{sr} of 1.7, $\sigma_{vo}^{'}$ of 100 kPa, CSR of 0.25, D_R of 33%, and $V_{s,initial}$ of 142 m/s (experimental data from Lee et al. 2022)……..……...…169

5.1. Model plan view and cross-section with sensor and cone locations (in model units) (adapted from Darby et al. 2019)……182

5.2. Model plan view and cross-section with sensor and cone locations (in model units) (adapted from San Pablo et al. 2023)……..…182

5.3. 1D site response analysis in FLAC represented by a 1D soil column with the different layering (prototype scale) for: (a) Test 1 - Darby et al. (2019) centrifuge test, and (b) Test 2 - San Pablo et al. (2023) centrifuge test ……..184

5.4. Simulated cyclic resistance ratio (*CRR*) versus number of cycles to liquefaction curves at mid-depth (i.e., mid Ottawa layer) for (a) Test 1 – Darby et al. (2019), (b) Test 2 – San Pablo et al. (2023), and (c) sensitivity of curves to calibration parameter h_{po} for both tests……....192

5.5. Comparison of dynamic time histories in uncemented and moderately cemented sands, respectively, of (a) Δu at mid-depth, (b) surface acceleration, (c) CSR at mid-depth, (d) strain at mid-depth, and (e) base

acceleration (refer to Fig. 5.3a for color coding). Experimental results adapted from Darby et al. (2019)…….197

5.6. Dynamic response comparison of uncemented (left) and moderately cemented (right) of (a) r_u at top of profile, (b) top (or surface) acceleration, (c) CSR between mid- and top-depth, (d) strain between mid- and top-depth, (e) r_u at mid of profile, (f) mid acceleration, (g) CSR between bottom- and mid-depth, (h) strain between bottom- and mid-depth, (i) r_u at bottom of profile, (j) bottom acceleration, and (k) base acceleration (refer to Fig. 5.3b for color coding). Experimental results adapted from San Pablo et al. (2023)…….....…….199

5.7. Response spectra for the uncemented case (left) and the moderately cemented case (right) across the length of the Ottawa sand in Darby et al. (2019) – Test 1 (refer to Fig. 5.3a for color coding). Experimental results adapted from Darby et al. (2019...…….……...…200

5.8. Response spectra for the uncemented case (left) and the moderately cemented case (right) across the length of the Ottawa sand in San Pablo et al. (2023) – Test 2 (refer to Fig. 5.3b for color coding). Experimental results adapted from San Pablo et al. (2023)….…….…….……...202

5.9. Results of varying the PM4SandC cementation parameters on the moderately cemented simulation validated against San Pablo et al. (2023): (a, d, g) pore pressure ratio at mid-depth, (b, e, h) stress-strain response at mid-depth, (c, f, i) response spectra at mid-depth……...……206

5.10. Results of varying the PM4SandC degradation parameters on the moderately cemented simulation validated against San Pablo et al. (2023): (a, d) pore pressure ratio at mid-depth, (b, e) stress-strain response at mid-depth, (c, f) response spectra at mid-depth…….208

List of Tables

2.1. Summary of experimental studies on cemented cohesionless soils (table sorted by cementing agent first and then alphabetically by reference)…….……55

2.2. Summary of globally observed trends in elemental monotonic behaviors of bio-cemented sands before yielding……..66

2.3. Summary of globally observed trends in elemental monotonic behaviors of bio-cemented sands after yielding…….……..……67

2.4. Summary of globally observed trends in elemental cyclic behaviors of bio-cemented sands…….....69

2.5. Summary of available constitutive models for bio-cemented sands/structured soils/weak rocks…...…70

3.1. Mohr-Coulomb input parameters for CPT simulations through cemented sands under various confining stresses…….....119

3.2. Calibration of the cone penetration model……...…123

5.1. Summary of centrifuge tests and their corresponding site response analyses……...…183

5.2. Initial soil properties selected for both models: uncemented and moderately cemented, in addition to the ones for uncemented which remain unchanged…….…….189

5.3. Soil properties selected for the constitutive model PM4SandC……..……..191

ABSTRACT

Constitutive Modeling of Bio-Cemented Sands

for Earthquake Engineering Applications

The emergence of the novel bio-cementation techniques for liquefaction mitigation application has received more attention on the experimental level than the numerical level. Few studies have aimed at modeling the behavior of bio-cemented sands under various loading conditions, but their use can be restricted by the obtainability of their input parameters and the lack of a cumulative body of data to support their validation. This Dissertation presents the extension of a plasticity model for sands to bio-cemented sands (PM4SandC Version1). The motivation for this work is twofold: (1) to have a usable constitutive model which is applicable to bio-cemented sands (and by extension naturally cemented sands) under various initial and loading conditions, and (2) to advance the deployment of bio-cementation in the field as an alternative ground improvement method for liquefaction mitigation.

The extension of the original constitutive model formulation to bio-cemented sands warrants an understanding of the main behaviors of interest. An extensive and critical review of the experimental studies on bio-cemented sands is performed first to collect the available knowledge on these geomaterials and identify the remaining gaps in this relatively new research field. This critical review of the mechanical testing is supplemented with one on the numerical studies on bio-cemented sands and other relevant cemented soils and weak rocks. The critical review provides insights into the mechanical behavior of bio-cemented sands and later informs the modifications to the original formulation of the constitutive model, and gathers the approaches used by other research to achieve this goal.

In order to address the usability for the model by means of reasonable and attainable input parameters, a relationship between a field parameter, the cone tip resistance, and a constitutive parameter, the apparent cohesion, is developed to provide an estimation of the parameter most contributing to the cementation-induced changes. Readily available cone penetration measurements in a large tank experiment and a centrifuge test on bio-cemented sands in conjunction with synthesized cone penetration data from an axisymmetric penetration model using the Mohr-Coulomb constitutive model enable the development of such a relationship as a function of confining stress. The axisymmetric cone penetration model and its input parameters are described, simulations results are validated against experimental results, and simulations are extended to higher confining stresses before fitting a simple linear relationship. This relationship is later used in the estimation of cohesion for a system-level analysis using the PM4SandC model.

Once the behaviors to be prioritized in the model extension and the input parameters to characterize cementation are known, the intended modifications are implemented in the original formulation of the sand model PM4Sand Version 3.2. Modifications in PM4SandC relative to the PM4Sand model include: (1) the introduction of input parameters quantifying the effect of cementation on the shear stiffness, the peak strength and the volumetric behavior, (2) the incorporation of an additional cementation-induced strength to the mean effective stress and hence the shift of the constitutive space to reflect the enhanced tensile strength of bio-cemented sands, (3) the adjustment of the dependence of the cemented shear modulus on confining stress, and (4) the addition of evolution laws to degrade/alter the cementation parameters as a function of damage accumulation. A generalized calibration demonstrating the performance of the model under various cementation levels, confining stresses, drainage, and loading conditions is performed in FLAC 8.1 and some guidance is provided to aid users in the calibration process. The extended

model is then validated against a body of experimental data on bio-cemented sands. Overall, the model is able to qualitatively predict the trends seen in bio-cemented sands with minimal calibration effort by means of input parameters physically meaningful and obtainable from the field.

The validation of the PM4SandC model at the element level is followed by its validation at the system level. Two one-dimensional site response analyses on bio-cemented columns are performed in FLAC 8.1 to (1) demonstrate the ability of the model to predict the free-field dynamic response of a treated site, (2) present a first-of-a-kind numerical effort to simulate site response analyses in bio-cemented sands. The PM4SandC constitutive model is assigned to the bio-cemented sand columns. The numerical analysis and its input parameters as well as the calibration process are described in detail. The dynamic response from the simulations in terms of accelerations, shear strains, cyclic demand, pore pressure generation, and response spectra is compared to the measured response in centrifuge models scaled to real site conditions. The constitutive model is found to reasonably approximate the dynamic responses from the centrifuge tests. A parametric investigation is also performed to provide insights into the effects of parameter uncertainties to PM4SandC on the overall dynamic response.

ACKNOWLEDGMENTS

Throughout my PhD, I had the opportunity to meet some incredible people whose experiences, advice, work ethic, and presence greatly improved my journey. I would like to thank each of them for their contributions over the years, whether on a professional or personal level.

First and foremost, my deepest thanks go to my PhD advisor, Prof. Katerina Ziotopoulou. Our talks have spanned from constitutive modeling to Greek islands and vacations. I am grateful for her mentorship, trust, availability, thoughtfulness, humility, sharp eye, passion and wit. She has been a true ally in this journey, and at times she believed in my capabilities more than I did. She has been a role model whose passion for her work has been contagious. To sum it up in a few words, I have been lucky to be mentored by her.

I am also deeply indebted to my Dissertation committee members, Prof. Ross Boulanger and Prof. Jason DeJong who have been co-advisors on this work. Prof. Boulanger's way of thinking, passion, humility and above all, teaching and mentoring have inspired me to broaden my perspective and sharpen my critical thinking. It has been an honor working with him on his original model.

Prof. DeJong's contributions have greatly improved the quality of this work. His practical perspective and futuristic vision gave me an escape from the world of theoretical soil mechanics when I needed it. His vision for the field of biogeotechnics inspires me to pursue my ideas and continuously push forward. His energy, kindness, work ethic, and immaculate organization have been an inspiration for my career.

The work presented here would have not been possible without collaborators. I thank Prof. Michael Gomez and Minyong Lee for the countless paper reviews and the experimental data they provided for the validation of the model. Their availability, patience, and willingness to help have

been very encouraging. I thank Prof. Diane Moug for her help in setting up the cone penetration simulations and in analyzing data. She was phenomenal in her feedback and timely replies. I want to thank Alexandra San Pablo for providing her centrifuge data within a very short time of running her tests. She has been very patient with my many requests for data and clarifications. I also want to thank Prof. Brina Montoya who I grew to know through her extraordinary work. I am happy that I finally met Prof. Montoya at a conference this year and I thank her and her students for our chats and their data on bio-cementation.

A special thank you goes to one of the smartest people I know, Dr. Sumeet Sinha. Sumeet's help in softwares, coding, and automation has made the iteration cycles for this work much easier. Thank you for continuously sharing your knowledge and encouraging me to learn new things.

The Center for Bio-mediated and Bio-inspired Geotechnics (CBBG) and the UC Davis Geotechnical Graduate Student Society (GGSS) have been a second family to me. I thank the CBBG leadership for their recognition of my contributions to the Center. It was a pleasure to serve the Center and help enhance the students' experience. I thank CBBG students for our random chats and fun meetings. GGSS made this journey much more enjoyable. "Good company in a journey makes the way seem shorter". I cannot imagine going through a PhD without the interactions I had with my fellow peers. I want to thank them one by one: Kyle O'Hara for his realism, Tyler Oathes for his sarcasm, Trevor Carey for his wisdom, Alena Raymond for her brightness, Renmin Pretell for his kindness, Francisco Humire for his Pisco, and Matthew Burrall for his thoughtfulness.

Lastly, I am deeply blessed to have the best friends and family anyone could ask for. They have surrounded me with an immense love which made leaving them to come back to California harder each time. My family, Rock, Marie, Nadine, Celine, and Elie, has been supportive in tremendous ways. I appreciate their great selflessness and boundless patience. Mirla and Zeina

have been my PhD buddies, complaining about our never-ending PhDs and ironically graduating all the same year! Tina, Mira, Rebecca, and Jennifer have made California a more welcoming and a fun second home. These are only few of the people who kept checking on me and were more excited about this PhD at times when I was not.

Even when you get to the end, always remember the beginning. I will be eternally grateful to Prof. Russell Green from Virginia Tech, my previous home. In his belief in me and my capabilities to excel in the US, not only he funded my Master's degree, but also made a dream I didn't dare to dream come true.

Finally, I would like to thank the National Science Foundation and CBBG for funding my PhD.

This journey has been challenging but rewarding. It led me out of my comfort zone and helped me grow in age, grace, and wisdom. These people have made this journey unforgettable, and this is not a "goodbye", it is a "see you again one day"!

CHAPTER 1

Introduction

1.1 Background

During recent earthquakes (e.g., the 2010 Christchurch earthquake and the 2011 Darfield earthquake in New Zealand), severe damage to sites and structures has been reported due to widespread liquefaction in saturated sandy soils at level sites. The availability of such data permitted a rigorous documentation of earthquake-induced liquefaction. The goal of such a database was (1) to understand the mechanisms underlying the phenomenon of liquefaction as well as its effects on infrastructure and (2) to develop analysis methods for assessing the susceptibility of sites to liquefaction. Together with numerous observations and recordings from other earthquakes of the past, this extensive database on liquefaction in sands has led to deep understandings of the liquefaction phenomenon in sands and its manifestations, the improvement in simplified methods (e.g., Youd and Idriss 1971; Boulanger and Idriss 2014) with descriptive indices (e.g., liquefaction potential index LPI - Iwasaki et al. 1978; ejecta potential index – Hutabarat and Bray 2021), the development of constitutive models for sands for earthquake

applications (e.g., Dafalias and Manzari 2004; Boulanger and Ziotopoulou 2017; UBCSand by Beaty and Byrne 2011), and the performance of system level analyses on liquefiable deposits (e.g., Cubrinovski et al. 2019). These advances from simplified to more complex plasticity models enabled the prediction of the stress-strain response subject to a broad range of ground conditions in the field.

Studies since the 1980s (e.g., Bachus et al. 1981; Clough et al. 1989; Sitar et al. 1980) have shown that natural cementation in sand deposits improves their stiffness and strength and hence, increases their resistance to loading. However, the sampling of naturally cemented sands posed challenges related to disturbance due to stress relaxation and breakage of weak cementation, and prohibitive cost of more sophisticated sampling methods (e.g., freezing). To overcome these challenges, researchers turned to artificial cementation as a proxy for natural cementation in order to understand the effect of cementation on the overall resistance of sands to loading, whether monotonic or cyclic. While various artificial cementing agents were considered in the lab, Portland cement was the most widely used in the lab and in the field. Eventually, cement deep soil mixing became an effective ground improvement method for liquefaction mitigation of saturated sandy soils.

More recently, bio-cementation has emerged as a sustainable, and environmentally friendly ground improvement method for liquefaction mitigation. Moreover, bio-cementation i.e., calcite precipitation has been thought as analogous to natural cementation since calcite is largely present in nature. Studies on bio-cementation have focused on demonstrating its utility in improving the resistance of sands to monotonic (e.g., Feng and Montoya 2015) and cyclic loading (e.g., Lee et al. 2022). The information available from these studies most commonly included the effect of bio-cementation on soil engineering properties (e.g., shear wave velocity, permeability, dry density),

and penetration resistances (e.g., CPT tip resistance). More elaborate studies provided results from bench-scale (e.g., triaxial and direct simple shear) and field-scale (e.g., centrifuge) tests. While the database for bio-cemented sands is limited relative to sands and is still being enriched with broader initial conditions, the readily available results provide insights into the mechanical response of bio-cemented sands subject to monotonic and cyclic loading.

Drawing a parallel to clean sands, bio-cemented sands are advancing from limited empirical relationships to more complex plasticity models, even though the body of data for bio-cemented sands is more limited compared to clean sands. A constitutive model must be able to approximate the expected response of cemented sands under diverse field and loading conditions. In fact, such a model should be usable in terms of input parameters reported from the field and be validated against single-element and system-level applications.

This Dissertation presents the development of a constitutive model for bio-cemented sands used for earthquake engineering applications. The motivation behind this work is: (1) to have a usable constitutive model which is applicable to bio-cemented sands (and by extension naturally cemented sands) under various initial conditions, and (2) to advance the deployment of bio-cementation in the field as an alternative ground improvement method for liquefaction mitigation.

The constitutive model in this Dissertation is a reformulation of an existing constitutive model for sands by Boulanger and Ziotopoulou (2017, 2022). Modifications to aspects of the model are undertaken to account for the effect of cementation and enable the model to reasonably approximate the mechanical response of bio-cemented sands with minimal calibration effort. The proposed model is PM4SandC (where "C" stands for cement) and is built on the existing PM4Sand Version 3.2 model. The extension of the model to bio-cemented sands has been guided by cycles

of reformulation, implementation, calibration, and validation against the available data on these geomaterials.

1.2 Overview of Dissertation

This Dissertation presents the reformulation of an existing constitutive model for sand in order to account for the effect of cementation. The development of the proposed PM4SandC model went through the following process: (1) a validation database was collected from an extensive literature review on bio-cemented sands which also served to understand the elemental mechanical behaviors to prioritize for the reformulation, (2) an empirical relationship was developed between a field parameter and a model input parameter to make this model usable in the field, (3) successive cycles of reformulation, implementation, and calibration were performed under monotonic and cyclic loadings at the element-scale and validated against lab test results, (4) site response analyses in bio-cemented sands were performed to validate the model at the system-level against centrifuge tests. The lab and centrifuge results used in the validation process were obtained from collaborators on the project. The goal of this work is to gather a fundamental understanding of cementation and its effects on the mechanical response of sands and enable the approximation of this mechanical response numerically using a robust plasticity model applicable to earthquake engineering applications. Preambular work was done as outlined above to achieve this goal. The current version of PM4SandC was built on prior versions where the stress-strain response was examined, and improvements were made with each evaluation cycle until the present version was achieved and compared against experimental data. The iterations were mostly guided by the literature review and the limited readily available results from experiments.

Numerical analyses were performed in the two-dimensional finite difference commercial program FLAC 8.1 (Itasca 2019) with the user-defined constitutive models PM4Sand Version 3.2

and PM4SandC loaded as dynamic link libraries (dll). The dynamic link library for PM4SandC *modelpm4sandC005_64.dll* was compiled on June 13, 2022, in Microsoft Visual Studio 2015.

1.3 Dissertation organization

Following this first Chapter, the Dissertation consists of five more chapters: as of the date of this Dissertation Chapters 2 and 3 are under review for publication as journal papers while Chapters 4 and 5 will be submitted to journals for publication. Chapter 6 summarizes the main findings of this work and provides directions to future work. The four main chapters of the Dissertation are introduced hereafter and described briefly.

Chapter 2 presents an extensive critical literature review on the mechanical response of bio-cemented sands on the experimental and numerical levels. This Chapter is divided into two subtopics. The first subtopic presents a state-of-the-art review of the experimental studies, and the second subtopic summarizes some relevant numerical models. Within the experimental part, the effect of bio-cementation on individual soil properties or parameters (e.g., permeability, shear wave velocity, dry density, tip resistance) are described first, followed by a synthesis of the behaviors in terms of monotonic and cyclic response. This Chapter constitutes the collected database for the validation of the constitutive model. It is a crucial part of the Dissertation in order to (1) understand the elemental behaviors to be prioritized in the reformulation of the constitutive model, and (2) collect the available test results as part of the validation database for the reformulated constitutive model. The paper, titled "*Mechanical behavior of bio-cemented sands: state-of-the-art review of experimental and numerical developments*", authored by Maya El Kortbawi, Katerina Ziotopoulou, Michael G. Gomez, and Minyong Lee, is anticipated to be submitted for journal publication in Geotechnical and Geological Engineering.

Chapter 3 describes the development of a relationship between a field parameter (CPT tip resistance q_c) and a constitutive parameter (cohesion c) using synthesized data from an axisymmetric cone penetration numerical model validated against centrifuge results. The Mohr-The axisymmetric cone penetration model simulates the steady state drained penetration in bio-cemented sand whereby the latter is defined using the Mohr-Coulomb constitutive model for cohesive soils. Input parameters to the model are decided based on the range of values seen in the literature review from Chapter 2. A parametric study was conducted whereby preliminary cone penetration simulations were performed to understand the sensitivity of q_c to various input parameters. This companion study is included as an appendix and is titled "*Effect of sand bio-cementation on cone tip resistance: a numerical study*". It is published in the proceedings of the 5th International Symposium on Cone Penetration Testing", Bologna in June 2022. The goal of Chapter 3 is to tie a field parameter obtained after bio-cementation treatment with one important input parameter to the proposed PM4SandC model, thereby establishing a relationship to estimate cohesion *c* from indications in the field. Chapter 3 was accepted for publication in the Journal of Geotechnical and Geoenvironmental Engineering, titled "*Axisymmetric simulations of cone penetration in bio-cemented sands*" and authored by Maya El Kortbawi, Diane M. Moug, Katerina Ziotopoulou, Jason T. DeJong, and Ross W. Boulanger.

Chapter 4 presents the modifications to PM4Sand from its original formulation leading to PM4SandC Version 1. The behaviors of interest are identified and the functional forms and equations for the contribution of the cementation and subsequently its degradation are explained. While successive cycles of implementation, calibration, and validation were performed, only the working version is described here. The additional input parameters to PM4SandC are introduced and their default values are noted where applicable. A calibration process is outlined to aid the

user in the application of PM4SandC. Generalized calibrations are performed over different confining stresses, levels of cementation, loading, and drainage conditions to assess the overall performance of the constitutive model. The latter is then validated against available lab results gathered in Chapter 1, more specifically monotonic triaxial compression tests and monotonic and cyclic Direct Simple Shear (DSS) tests on bio-cemented sands subjected to uniform loading cycles. A companion study titled "*Validation of a bounding surface plasticity model against the experimental response of (bio-) cemented sands*" is included as an appendix. This preliminary study presents an evaluation of the ability of the existing PM4Sand model to capture the response of bio-cemented sands and provides guidance for the reformulation of the existing constitutive model. This companion paper was published in the proceedings of GeoCongress 2019, Philadelphia in March 2019. Chapter 4 will be published as a journal paper titled "*Extension of a sand plasticity plane-strain model for earthquake applications to bio-cemented sands*" authored by Maya El Kortbawi, Katerina Ziotopoulou, and Ross W. Boulanger.

Chapter 5 describes the application of PM4SandC to two site response analyses for sites improved with bio-cemented sands under free-field conditions. These analyses are validated against existing results from centrifuge tests under the same conditions. The centrifuge tests are introduced first then the setup for the simulations is described in order to reproduce the conditions in the centrifuge tests. A one-dimensional soil column subjected to the achieved motion from the centrifuge is considered for each analysis. The locations of sensors are identified and the responses from the simulations are tracked at those. The input parameters to PM4SandC are summarized and variations from the centrifuge measurements are noted. Ultimately, the dynamic response from the simulations is compared to the one from the centrifuge tests in terms of accelerations, shear strains, cyclic stress ratio, and pore pressure generation. Furthermore, a parametric study is performed on

the input parameters to PM4SandC to demonstrate the sensitivity of the simulation results to uncertainties in input parameters. The goal of this Chapter is to evaluate the overall performance of the proposed PM4SandC in system level applications and identify the sensitivity of the response to uncertainties in input parameters, hence guiding the user in the selection of input. Chapter 5 will be published as a journal paper titled "*One-dimensional site response analysis of bio-cemented columns: validation against centrifuge model tests*" authored by Maya El Kortbawi, Katerina Ziotopoulou, and Jason T. DeJong.

CHAPTER 2

Mechanical behavior of bio-cemented sands: state-of-the-art review of experimental and numerical developments

Original publication:

El Kortbawi M., Ziotopoulou K., Gomez M. G., and Lee M. (2022). Mechanical behavior of bio-cemented sands: state-of-the-art review of experimental and numerical developments. Geotechnical and Geological Engineering.

Author's note: This Chapter will be submitted for publication as a review journal paper in Geotechnical and Geological Engineering. Figure and table captions and intext references were modified from the original publication to conform with the format of this Dissertation.

Abstract

Extensive research has been performed on cemented sands over the past few decades to address fundamental gaps in our understanding of the effect of cementation in natural deposits and to accelerate developments in cementitious ground improvement technologies. Significant advances in these artificial cementation processes, in particular the development of bio-mediated

precipitation technologies, have produced laboratory test results at various scales that led to new understandings of the effect of cementation on sand behavior. However, the majority of these efforts have remained largely independent of one another resulting in limited collective insights and a lack of a comprehensive knowledge base for these materials. This paper synthesizes and interprets recent research on naturally and bio-cemented sands and presents a critical review of experimental and numerical studies with the goal of identifying points of agreements and deviations. The goal of the paper is to provide new insights that aim towards establishing a comprehensive dataset that can extend research impacts beyond individual studies. Conclusions drawn from the critical review include global behavior trends and knowledge gaps that future research could address. Ultimately this synthesized knowledge base is expected to lead to the understanding and formulation of engineering property correlations and laws for constitutive models for cemented materials, in a way similar to uncemented ones.

2.1 Introduction

Whether naturally occurring or artificially created, cementation of sands has been a mechanism of ground improvement that has received a lot of attention over the last 50 years and it continues being a vibrant and independent research field. Preliminary studies focused on naturally cemented sands and their undisturbed sampling for the purpose of strength testing. In parallel, researchers sought artificial proxies to natural cementation in order to overcome the challenges in undisturbed sampling of naturally cemented sands and reproduce cementation in a more controlled lab setting. Portland cement became one of the most used cementing agents. However, and despite being widely utilized nowadays in site improvement and remediation, Portland cement and its production are exacerbating the environmental challenges facing today's world. The advances in

characterization of cemented sands over the 50 years not only led to increased interest in artificial cementation, but also paved the way for the continuous improvement in testing methods and the development of more environmentally friendly alternatives to Portland cement. This extensive research has contributed to our state of knowledge on the cementation of sands, starting from natural cementation and followed by the various methods for the artificial cementation of sands and the various agents that have been used through the years. Within the context of artificial cementation, bio-inspired cementation or bio-cementation has been relatively recently introduced as a technology that is implemented in the lab or field and aims to replicate the products of natural cementation.

This paper aims to collect, summarize, and critically synthesize the experimental and numerical efforts in the field of bio-cementation towards identifying commonalities and critical gaps and through those enabling the future of this research field. Henceforth, the term *cemented* will be used for any material that has undergone cementation regardless of its origin. Where applicable, cementation will be distinguished between *natural* and *artificial*, and the latter will in turn will be distinguished based on its artificial cementing agents and/or methods.

The presence of natural cementation in sands can result from a wide variety of time-dependent abiotic and biologically controlled mineral precipitation processes (Mitchell 2008). Abiotic cementation processes occur in the absence of biological activity and can include the deposition of a variety of minerals (e.g., carbonate, silica, sulphate, and hydroxide-based minerals) on and/or between sand particles (Baxter and Mitchell 2004). Abiotic precipitates result from reactions between aqueous chemical species including those related to groundwater mixing, atmospheric equilibration, and other chemical processes. Biologically mediated precipitation processes can form similar cementing minerals, but instead result from changes in surrounding solution

chemistry related to microbial enzymatic and metabolic activities including urea hydrolysis, and nitrate, iron, and sulphate reduction (DeJong et al. 2010). These biological processes can occur naturally, but, as will be described later, can also be anthropogenically-induced through manipulating the groundwater chemistry, enabling biological activity, super-saturating pore fluids with respect to mineral phases, and thereby initiating precipitation.

Over the time after deposition, mineral precipitation processes alter the engineering properties of clean sands. These changes typically include increases in stiffness and strength, which can alter geotechnical behaviors including, for example, in-situ penetration resistance and cyclic strength against earthquake-induced liquefaction (e.g., Bwambale and Andrus 2019). Over the past few decades, research groups (e.g., Amoly et al. 2015; Andrus et al. 2009; Arango et al. 2000; Bwambale et al. 2017; Eslaamizaad and Robertson 1996; Hayati and Andrus 2009; Kiyota et al. 2009; Kokusho et al. 2012; Maurer et al. 2014; Moss et al. 2008; Roy 2008; Troncoso et al. 1988) have proposed methods for quantifying the contributions of natural cementation to soil strength and stiffness based on observations made during laboratory and field testing as well as case history analyses. Through these studies researchers have recognized challenges related to: (1) the testing of naturally cemented sands due to sampling-associated disturbances, (2) the limited geographic examination of this phenomenon (e.g., Charleston, South Carolina, and Christchurch, New Zealand) (Bwambale and Andrus 2019), and (3) the normalization of results from reconstituted sample testing to a common reference temporal state.

Due to the challenges associated with naturally cemented sand sampling and characterization, the body of field and laboratory test data on naturally cemented sands has remained limited especially compared to existing data for clean sands. Further complexities arise from the typically non-uniform distribution of cementation in natural deposits, which hinders our ability to obtain

representative uniform samples. Even when near-homogeneous samples are encountered, the unavoidable and unquantifiable disturbances due to the sampling process can degrade or destroy any cemented bonds and the microstructure of the specimen overall. While researchers (e.g., Clough et al. 1981; Collins and Sitar 2009) have shown that low disturbance block- and frozen-sampling methods can be used, such techniques can be prohibitively expensive, time-consuming, and can still suffer from disturbances related to stress relief. Alternatively, many researchers have attempted to use in-situ testing (e.g., CPT) to characterize naturally cemented sands and avoid these sampling challenges. However, such methods are generally only capable of identifying high magnitudes of cementation (e.g., Darby et al. 2019; Gomez et al. 2018). When low magnitudes of cementation are present such as those encountered in many naturally cemented deposits, strains imposed by in-situ testing instruments can render light cementation undetectable. Conversely, when higher levels of cementation are encountered but not correctly identified, observed responses can be incorrectly attributed to differences in the sand's relative density (Puppala et al. 1995). Although some non-destructive geophysical tests can effectively detect cementation (Stokoe and Santamarina 2000), oftentimes these methods provide average small-strain properties over large soil volumes, and hence cannot resolve small differences in the mechanical properties of cemented sands in the presence of other complicating factors such as variations in density, overburden stress, and soil type. Recently proposed methods which leverage both in-situ penetration test and geophysical measurements have shown the ability to further improve cementation detection through parameters similar to rigidity indices (Gomez et al. 2018; Rix and Stokoe 1991; Schnaid et al. 2004; Schneider and Moss 2011).

Artificial cementation has developed as a field of research in response to the efforts aimed at understanding natural cementation through field measurements and sampling as well as leveraging

it towards ground improvement technologies. Researchers have attempted to recreate natural cementation in the laboratory using artificial cementing agents with the intention of: (1) improving our understanding of natural cementation, (2) characterizing the effect of cementitious ground improvement processes (e.g., Darby et al. 2019; Lee et al. 2022; Lee et al. 2020; Montoya et al. 2013; Simatupang et al. 2018; Xiao et al. 2018), and (3) developing and contributing new and environmentally conscious methods in the broader field of ground improvement. Artificial cementation processes can offer the ability to prepare lightly cemented specimens for laboratory testing while eliminating sampling-related disturbances (e.g., Rios et al. 2014), however, many of these cementation agents are unable to yield fabrics and mineralogical characteristics representative of naturally cemented materials.

More recently, bio-mediated cementation processes have been developed, which leverage biogeochemical processes to artificially cement soils and achieve improvements in soil engineering properties while requiring less energy and material usage when compared to conventional soil improvement methods (DeJong et al. 2013; Mitchell and Santamarina 2005). Many of these bio-mediated processes, such as microbially-induced calcite precipitation (MICP), enzyme-induced calcite precipitation (EICP), and microbially-induced desaturation and precipitation (MIDP) can generate calcium carbonate ($CaCO_3$) minerals thereby cementing soil particle surfaces and contacts. MICP (Fig. 1) is performed by first injecting soils with treatment solutions containing either exogenous lab-cultured ureolytic microorganisms (e.g., *Sporosarcina pasteurii*) (e.g., DeJong et al. 2006; Ferris et al. 1997; San Pablo et al. 2020; Stocks-Fischer et al. 1999) or nutrients intended to stimulate native ureolytic microorganisms (e.g., Fujita et al. 2004; Gomez et al. 2016; San Pablo et al. 2020). Once these microorganisms become capable of hydrolyzing the supplied urea, cementation solutions containing urea and calcium salts are

introduced to initiate the cementation process. EICP involves a similar reaction network, but instead uses extracted free urease enzymes supplied in treatment solutions to hydrolyze urea rather than ureolytic microbial cells (e.g., Hamdan and Kavazanjian 2016). Lastly, MIDP uses microbial dissimilatory nitrate reduction (denitrification) to generate alkalinity and carbonate species (e.g., O'Donnell et al. 2017; van Paassen et al. 2010) which can induce $CaCO_3$ precipitation when calcium is supplied. In contrast to other processes, MIDP also generates nitrogen gases which can simultaneously desaturate soils, thus altering pore fluid compressibility and hydraulic conductivity.

Advances with respect to our fundamental understanding of the microbiological and chemical process involved in the above technologies have allowed researchers to achieve a substantially improved control of cementation magnitudes and spatial uniformity (e.g., Gomez et al. 2016; Martinez et al. 2013; Montoya et al. 2021; San Pablo et al. 2020; Sharma et al. 2021; Xiao et al. 2021). In particular, advances with respect to reactive transport modelling (e.g., Fauriel 2012; Martinez et al. 2014; Minto et al. 2019; Nassar et al. 2018) have allowed for the interplay between changes in flow regimes and process reaction rates and their collective impacts on cementation distributions to be better understood. These developments have allowed researchers to produce spatially uniform cemented soil specimens at target cementation magnitudes more consistently and have facilitated the systematic investigation of the effect of cementation on soil behaviors (e.g., Gomez et al. 2018; Montoya et al. 2021).

Artificial bio-cementation methods have grown to be particularly appealing and promising in the field of liquefaction mitigation due to their effects on soil properties and their overall environmental consciousness. Furthermore, the ability of artificial bio-cementation methods to yield cemented soils with behaviors similar to naturally cemented ones has been proven key

towards using them as representative laboratory proxies (DeJong et al. 2006). While Portland cement, gypsum, and calcium carbonate-based cementing agents have all been used in attempts to recreate natural cementation in the laboratory, they have shown varying success. Several comparative studies (e.g., DeJong et al. 2006; Ismail et al. 2002; Wang et al. 2021) have examined differences between these artificial cementing agents, ranging from differences in the size, shape, and morphology of resulting cementation to differences in their macro-scale mechanical response, and even differences in associated environmental impacts. Collectively, these studies have suggested that soils treated with Portland cement and various polymers (e.g., polyacrylamide) exhibit significantly different fabrics (e.g., cementation distributions and interparticle bonding), are composed of different cementing minerals (e.g., calcium silicate hydrates), and generally exhibit more ductile responses than those expected for naturally cemented soils. In contrast, the recently developed calcium carbonate-based bio-cementation processes (e.g., MICP) offer a unique opportunity to address these limitations by producing cemented specimens that are more representative of natural deposits. In particular, bio-cementation can: (1) eliminate stress relief and sampling-induced damage by allowing soils to be cemented under representative stresses within laboratory testing devices themselves, (2) prepare spatially uniform cemented specimens at controlled levels of cementation with uniform void ratios achieved both during pluviation and after treatment by avoiding issues related to non-uniform mixing and powder segregation and non-homogenous cementation found in natural soils, (3) reproduce soil responses that are mechanically representative of naturally cemented soils including increased brittleness at lower confining stresses and large increase in soil stiffnesses with minimal increases in dry densities, and (4) generate cemented bonds, fabrics, and mineral compositions that are chemically- and physically-representative of natural deposits. The latter aspect allows for prepared specimens to exhibit more

representative stress-strain responses and higher permeabilities than those observed for soils cemented using other artificial agents (e.g., minerals are precipitated on particle surfaces and contacts rather than occurring in free pore space thereby constricting pore channels). For originally clean and later bio-cemented sands, minimal reductions in permeabilities of about one order of magnitude (e.g., Gomez and DeJong 2017; Montoya et al. 2021) have been observed after bio-cementation to moderate cementation levels (e.g., ≈5% calcite by mass). This is particularly important for obtaining more representative pore pressure generation and dissipation behavior during dynamic loading.

Significant ongoing work is pursuing both the investigation of natural cementation and the establishment and optimization of bio-cementation as a sustainable ground improvement technology. All developments with respect to bio-cementation processes have already enabled experimental research on bio-cemented geomaterials and sands in particular (e.g., Duraisamy and Airey 2012; Lee et al. 2022; Lee et al. 2020; Montoya et al. 2013; Nafisi et al. 2019a; Simatupang and Okamura 2017). To date, these existing datasets have largely remained independent, with limited synthesis of key sand behavioral insights between studies, which remain needed to support the development of theoretical frameworks at the level of rigor that currently exists for clean sands (e.g., Idriss and Boulanger 2008). Today, the number of available data is sufficient enough for a timely synthesis and a critical review such that future developments can be better contextualized, better guided, and thus faster converging.

In this paper, a comprehensive and critical review of data on bio-cemented sands is performed to synthesize individual datasets and enable a broader understanding of their behavior as well as that of naturally cemented sands which bio-cementation is found to approximate well. Although many data sets exist on various aspects of cemented sands overall, this review focuses strictly on

the physical attributes and mechanical behavior of naturally- and (artificial) bio-cemented sands. Following the synthesis, the primary goals of this critical review are to: (1) identify commonalities and discrepancies between studies to better understand geotechnical behaviors as well as identify the largest gaps in current knowledge, (2) unify data from various researchers and through those, explore and identify the parameters most influential to a bio-cemented sand's response (i.e., change in shear wave velocity, or calcite content), and (3) support the development of comprehensive continuum-based models that can capture multiple aspects of cemented sand behaviors rather than individual responses.

The paper is organized in two parts corresponding to experimental and numerical findings, respectively. First, in Sections 2.3 and 2.4 behaviors are summarized with regards to bio-cementation and natural cementation and their effects on the physical properties, monotonic (drained and undrained), and cyclic behavior of sands. Second, in Section 2.5, constitutive models for cemented sands are presented and their capabilities and limitations are discussed. Recommendations for further testing to address existing knowledge gaps are provided in each respective section.

2.2 Considered experimental studies

Experimental and numerical research included in this review followed specific selection criteria with the overarching goal of capturing, quantifying, and summarizing knowledge on the mechanical response of bio-cemented sands, with naturally cemented sands and very sparingly few other artificially cemented sands offering auxiliary insights. Seventy experimental studies were examined that involved different parent sands and cementing agents. Only studies that have presented both physical properties as well as insights regarding mechanical responses are included

in the review. This included triaxial compression/extension, direct simple shear (DSS), and tensile tests on naturally and artificially cemented sands, as well as centrifuge tests on bio-cemented sands. Although such studies oftentimes included unconfined compression tests and shear wave velocity measurements, any studies which did not provide significant mechanical data were excluded including those involving solely unconfined compression tests or field scale testing. Tests considered were on naturally cemented sands and artificially bio-cemented sands, with specific focus on calcium carbonate-based cementing agents generated using either abiotic reactions (e.g., Calcite In situ Preparation System) or urea hydrolysis (e.g., MICP or EICP). Data from other artificial methods of inducing cementation were not considered (e.g., MIDP) due to other complexities (e.g., biogas generation and de-saturation). Only for certain behaviors where data on bio-cemented and naturally cemented specimens remained limited, the review included a few select cases of sands treated with other cementing agents such as Portland cement, sodium silicate, and gypsum. These have been included as exceptions and only to elucidate expected behaviors while acknowledging important underlying differences between cementing agents (e.g., cementation fabrics, mineralogy, ductility) and motivating that these gaps should be closed with further testing on bio-cemented sands. With respect to numerical modelling efforts, 32 constitutive models are discussed and summarized in order to appreciate the multitude of ways with which researchers choose to constitutively represent the mechanical response of cemented sands. While most of these models were developed specifically for cemented sands, without of course distinguishing between the source of cementation as natural or artificial, some additional models developed for structured clays and weak rocks were also included, which were believed to feature key constitutive formulations and behaviors that would be applicable as well. Most of these models were validated against experimental data which were intentionally not included in the summary

tables (Tables 2.1 to 2.4) because of their use of cementing agents other than bio-cemented sands. Whenever constitutive models were validated against bio-cemented sands, the experimental data were included.

Table 2.1 summarizes the considered experimental studies which are separated into laboratory (bench-scale) and centrifuge (field-scale) tests. Studies 1 to 14 refer to studies performed on naturally cemented sand samples and studies 15 to 70 refer to those on artificially cemented sand samples. Out of the 56 studies on artificially cemented sands, 53 feature MICP- or EICP- based bio-cementation with calcium carbonate as the cementing agent, while the rest feature CIPS-(calcite), Portland cement-, gypsum-based cementation. Column 1 of Table 1 provides a reference number for each study while columns 2, 3, 4, and 5 provide the reference for the study, the parent sand, the cementation type (natural versus bio-cemented or otherwise), and the cementing agent, respectively. Columns 6 to 10 summarize the experimental details. Column 6 reports the tests performed and column 7 reports the parameters varied within the testing program. Columns 8 and 9 list quantification parameters for the achieved cement content as percent cement by mass and/or change in shear wave velocity (V_s), respectively. Column 10 provides the number of tests performed in each study. Variations between tests include different confining stresses, levels of cementation, and types of loading. It should be noted that the data for the plots were digitized by the authors where direct access to data was not possible. The data from Gomez et al. (2018), Lee et al. (2022), Montoya et al. (2021), Na et al. (2022) were requested and obtained from the corresponding authors.

2.3 Experimental observations from past studies on bio-cemented sands

This section summarizes observations about the individual properties of bio-cemented sands on the basis of data collected following the aforementioned criteria while the next section presents a critical synthesis of element behaviors in terms of effects on the mechanical response. Cumulatively, Sections 2.3 and 2.4 present element behaviors in terms of changes in soil properties and effects on the mechanical response, and conclude with a discussion on commonalities, differences, and gaps. Out of the four total cases of artificial treatments, the references pertaining to Portland cement as a cementing agent are appended with an asterisk*, those pertaining to sodium silicates with double asterisks**, and those pertaining to natural cementation with triple asterisks***.

2.3.1 Microstructure changes

One of the primary ways of studying bio-cementation has been by means of scanning electron microscopy (SEM) images which are commonly used to investigate the microstructure of bio-cemented sands (e.g., as in Burdalski and Gomez 2020 and Nafisi et al. 2019a), draw conclusions about their fabric, and eventually connect those with macroscopically observed mechanisms of behavior (Figs. 2.2, 2.3, and 2.4). Characterization of the microstructure and fabric (e.g., Cheng et al. 2013; DeJong et al. 2010; Terzis and Laloui 2019; van Paassen et al. 2010) is also necessary for understanding differences between bio-cemented sands that have the same calcite content by mass but demonstrate different macroscopic behaviors. This is frequently observed and indicates that calcite content alone is not an adequate metric for the verification of a bio-cementation treatment and the prediction of any subsequent responses.

Research in this area has studied and characterized bio-cemented precipitates including their mineralogy, crystal associations and sizes, morphology, particle-level distribution, and associated failure mechanisms. It has been found that these attributes primarily depend on particle and pore size, particle surface area, degree of saturation, type of cementing agent, and cementation process (Cheng et al. 2013; Lin et al. 2016; Nafisi et al. 2018; Simatupang et al. 2018; Terzis and Laloui 2017). However, select works have been fully dedicated to studying the microstructure aspect closely.

Burdalski and Gomez (2020), Nafisi et al. (2019a), and Burdalski (2020) studied the mineralogy of MICP-cemented sands (Fig. 2.2) and agreed that precipitates are largely calcite with other polymorphs including vaterite, aragonite, and amorphous calcium carbonate. Furthermore, these researchers described that precipitate mineralogy is controlled by a variety of factors including treatment techniques (i.e., reaction rates, chemical additives) and environmental factors (e.g., groundwater chemistry, soil mineralogy, and biological factors). Nafisi et al. (2019a) further studied crystal associations and sizes (Fig. 2.3) and described that these vary from hierarchical (layered) to irregularly scattered, and from small to large crystals, noting that this aspect also depends on precipitate mineralogy, treatment techniques (e.g., reaction rates, cell densities), and environmental factors (e.g., saturation, surrounding ions).

The morphology of bio-cementation (Fig. 2.4) was studied by Burdalski and Gomez (2020) and Burdalski (2020) who outlined four major descriptive categories: rhombohedral (calcite), spherical (vaterite), needle-like (aragonite), and poorly-structured (amorphous calcium carbonate), and mentioned the potential of intermediate morphologies due to crystal ripening and other possible but less frequently found structure variations. The morphology was found to depend

primarily on biogeochemical conditions during mineral formation, including the presence of various treatment reactants and trace ions.

Cuccovillo and Coop (1999) were the first ones to describe and connect micro- to macro-behaviors of naturally cemented sands and the increase in peak strengths specifically. The distribution of bio-cementation on particle surfaces and contacts (Fig. 2.5) was later studied by DeJong et al. (2010) who recognized that it can control the improvements in global engineering properties for the same cementation content. Three major possible distributions were outlined regarding this aspect recognizing that actual distributions include combinations of all three: *bridging* of particle contacts, *coating* of particle surfaces, and *infilling* of voids between particles with little particle associations (e.g., Fig. 2.5a). DeJong et al. (2010) found these distributions to depend on precipitate mineralogy, treatment techniques (e.g., reaction rates, cell densities), and environmental factors (e.g., saturation and surrounding ions). Understanding and naming these types of distributions later became key in connecting micro- to macro-behaviors: for example, bridging at sand particle contacts can increase peak strength more than simply coating sand particles, as also later supported by Cheng et al. (2013), Simatupang and Okamura (2017), and Riveros and Sadrekarimi (2020b) who all also worked on bio-cementation. DeJong et al. (2010), as well as Cui et al. (2017), Lin et al. (2016) and Montoya et al. (2021) further recognized and agreed that, regardless of the cementation distribution, the dry density of specimens increases as soil voids are filled with cementing agents.

Failure mechanisms at the microstructure level were also included in the study by DeJong et al. (2010) who delineated between two major types of failures while recognizing that actual failures consist of combinations of both mechanisms (Fig. 2.5b): failure of $CaCO_3$ bonds internally ($CaCO_3$ – $CaCO_3$) or failure of soil particle to $CaCO_3$ bonds ($CaCO_3$ – silica). This aspect was

found to depend on the soil mineral – to $CaCO_3$ bond strength, the $CaCO_3$ bond geometry, as well as the internal $CaCO_3$ shear strength.

As will later be seen in the Section 2.5, the characterization, and ideally the quantification, of some or all microstructural aspects of bio-cementation is key in our ability to choose the proper modeling vehicles for the ensuing behaviors.

2.3.2 Stiffness-related engineering properties

Bender element measurements from bench-scale and resonant column tests provide insights regarding the small-strain shear stiffness, modulus reduction, and energy dissipation or damping behavior of bio-cemented sands during shearing. Shear wave velocity (V_s) measurements on bio-cemented sands show that bio-cementation increases the initial shear stiffness of the soil matrix (Figs. 2.6a and d) (e.g., Darby et al. 2019; Gomez et al. 2016; Lin et al. 2016; Montoya et al. 2013; Na et al. 2022; Riveros and Sadrekarimi 2020b; Terzis and Laloui 2019). Resonant column tests on Portland cement-treated sands and sodium silicate-cemented sands (e.g., Acar and El-Tahir 1986*; Camacho-Padron 2006**, respectively) and more recently on MICP-cemented sands (Na et al. 2022) also support this conclusion. Indicative results from Na et al. (2022) are reproduced in Fig. 2.6. Shear stiffness is conceptually a function of the number of interparticle bonds such that, upon shearing, a rapid decay is expected for high levels of cementation and high densities (Cuccovillo and Coop 1999***). In terms of modulus reduction curves (Figs. 2.6b and e), G/G_{max} values at low strains define a plateau followed by a yield point at a certain threshold strain γ_t (the strain at which secant shear modulus G_{sec} is about 0.99 of G_{max}) and a rapid decrease at higher strains (Camacho-Padron 2006**). The sharpness/smoothness and clear/unclear distinction of yield are a function of low and high confining stresses, respectively. The threshold strain γ_t for cemented sands is initially lower than that for clean sands with increasing cementation up until a

certain cementation level, after which it becomes larger than clean sands (Camacho-Padron 2006**; Saxena et al. 1988b*; Van Hoff 1994*). Na et al. (2022) reported a decrease in γ_t from 0.002% to 0.0002% for an uncemented and a moderately MICP-cemented sand (ΔV_s = 350 m/s), respectively. The subsequent increase in γ_t at higher levels of cementation was not seen in Na et al. (2022) which may be due to the tested levels of cementation. Therefore, the corroboration of this nuance for bio-cemented sands remains unexplored. Due to the variability of yield stress with the number of loading cycles and the stress level, there is no unique threshold strain corresponding to the onset of yielding for cemented sands (Cuccovillo and Coop 1997***; Sharma and Fahey 2003b). In addition, the influence of confining stresses on V_s decreases for increasing levels of cementation (Fig. 2.7). However, the shear stiffness becomes independent of confining stress at high levels of cementation (i.e., 7% calcite content or ΔV_s = 650 m/s) (DeJong et al. 2022). Figure 2.7 synthesizes studies with G_{max} measurements at increasing confining stresses. Ideally, these stiffnesses can be fitted using a power law [$G = G_o(p/p_A)^n$] where G_o is a constant, p is the mean effective stress and is normalized by the atmospheric pressure p_A, and n is an exponent controlling the dependency of stiffness on effective stress (and through that depth). Three studies, Montoya et al. (2013), Nafisi et al. (2018), and Simatupang et al. (2018) have conducted tests at different confining stresses while measuring G_{max}. Zamani et al. (2021) also reported values of G_{max} at different confining stresses which are included in Fig. 2.7, however the effects of cementation could be influenced by the complexities of the test (bio-cementation blocks underlain by clean sands in a centrifuge container). Three major observations can be drawn from Fig. 2.7: (1) as the level of cementation increases, G_{max} increases as already mentioned, (2) for all levels of cementation, the fitted curve flattens towards high confining stresses indicating that at the influence of bio-cementation is overshadowed by the high confining stresses, and (3) at higher

levels of cementation (i.e., > 4% calcite content), the fitted curve becomes almost flat (the exponent n goes to 0). The exponent n can also be plotted against the respective calcite content and a relationship can be deduced as shown in Fig. 2.8. The exponent n, which represents the slope of the G versus p/p_A curve, decreases as the cementation becomes heavier. These values of n fall within the typical range of 0.5 for clean uncemented sands and 0 for rocks (e.g., Nafisi et al. 2018). This relationship can be further used in the normalization of the cemented shear wave velocity according to $V_{s1} = V_s\,(p/\sigma'_v)^{n/2}$ by Andrus and Stokoe (2000) where n/2 for clean sands is 0.25. Nafisi and Montoya (2018) developed a framework to estimate the level of cementation from the exponent n and applied it in Nafisi et al. (2020). Furthermore, confining stress leads to a shift in the modulus reduction to higher strain levels (Fig. 2.9b) and extends the elastic range of G_{max} thereby increasing γ_t from 0.0002% for a confinement of 30 kPa to 0.0008% for a confinement of 200 kPa, as reported by Na et al. (2022).

The effect of cementation on the damping ratio has not been extensively investigated for bio-cemented sands with the exception of one study. Thus, the following observations are drawn from the resonant column tests from Na et al. (2022) and experiments on other cementing agents. Damping ratio may depend on the distribution of cementation on particles surfaces and contacts. For example, the damping ratio increases with cementation when the dominant cementation mechanism is coating sand particles (Camacho-Padron 2006**; Fernandez and Santamarina 2001*; Saxena et al. 1988b*; Saxena et al. 1988c*; Valle et al. 2003**) and decreases at higher levels of cementation due to the formation of strong binding between sand particles (Acar and El-Tahir 1986*; Rad and Clough 1982*). Although a stiffer soil would be expected to have a lower damping ratio, Saxena et al. (1988c*) suggested that more energy is dissipated when propagating a wave (i.e., increased damping) through lightly cemented sands compared to clean uncemented

sands. The damping ratio decreases when the sand becomes heavily cemented, however, because less energy is needed for a wave to propagate through a uniformly cemented matrix than through the contacts of a clean sand. The increase in damping ratio is evident in the results by Na et al. (2022) for bio-cemented sands as well (Figs. 2.6c and f). However, the decrease in damping ratio at high levels of cementation was not seen in this set of tests, potentially due the tested levels of cementation. Similar to the modulus reduction curves, more testing is needed to corroborate or refute this nuance for bio-cemented sands. Figs. 2.6c and 2.6f show also that the damping increases at small strains compared to uncemented sands and then the curve picks up faster after the threshold strain is attained. It is expected that damping will decrease as confining stress increases due to increased interparticle forces (Camacho-Padron 2006**; Fernandez and Santamarina 2001*; Saxena et al. 1988c*) and is less sensitive to confining stress at higher levels of cementation (Camacho-Padron 2006**). This is corroborated by the Na et al. (2022) results on MICP-cemented Ottawa sand (Fig. 2.9c) where damping is higher for sands with a comparable cementation level tested at 30 kPa (damping ~7%) and 200 kPa (damping ~5%).

2.3.3 Strength-related engineering properties

Extensive experimental research that has investigated the effect of cementation on the strength of sands generally agrees on its qualitative mechanistic effects. The strength increase of (initially) loose cemented sands is the result of two phenomena: densification and cementation. Furthermore, the effect of cementation on strength parameters decreases as confinement increases (Feng and Montoya 2015). Findings are synthesized herein for both monotonic and cyclic loading conditions.

Monotonic loading experiments on cemented sands show an increase in the yield stress (stress at which cohesive bonds break and the de-structured matrix of broken cement and sand particles cumulatively carry stresses), the peak and residual strengths, dilative tendencies, as well as a shift

in the critical state line depending on the level of cementation and confining stress (e.g., Lin et al. 2016; Montoya and DeJong 2015; Riveros and Sadrekarimi 2020a; Terzis and Laloui 2017).

The increase in peak strength can be characterized by an apparent cohesive intercept, resulting in a tensile capacity (Nafisi et al. 2019b; van Paassen 2009) and a higher friction angle (Cui et al. 2017; Feng and Montoya 2015; Nafisi et al. 2020). As the cementation level increases, the increase in peak strength coincides with a decrease in the strain at which the peak occurs (Montoya and DeJong 2015). This cohesion increase is the primary contributing factor to the improvement in bio-cemented sand behavior and is significant for higher cementation levels (Feng and Montoya 2015; Nafisi et al. 2020). The residual strength increase is due to the remaining intact cohesive bonds in the soil matrix and the slight increase in residual friction angle resulting from changes in roughness and angularity of particles (DeJong et al. 2010). The increase in residual strength is more important for higher cementation levels where degraded cement produces fines in the final soil matrix (Feng and Montoya 2015; Montoya and DeJong 2015; Riveros and Sadrekarimi 2020a).

Bio-cementation increases the dilative tendencies of initially loose cemented sands compared to loose clean sands, but to a lesser extent relative to dense clean sands (Feng and Montoya 2015; Montoya and DeJong 2015; Porcino and Marciano 2017**). For clean sands, the maximum rate of dilation corresponds to the peak stress (dilation due to dense packing), whereas for cemented sands, the maximum rate of dilation occurs after the peak stress (dilation due to cementation) (Asghari et al. 2003 (hydrated lime); Leroueil and Vaughan 1990***). At the early stages of shearing, dilatancy is suppressed by the intact cohesive bonds between sand particles leading to an initial volumetric compression followed by a volumetric expansion at the onset of bonds

degradation. Faster and stronger dilative behavior has been observed for higher levels of cementation (Feng and Montoya 2015; Lo et al. 2003*; Rios et al. 2014*).

Lastly, monotonic tests on bio-cemented sands have suggested that the critical state line (CSL) can also be altered following MICP-treatment with lower critical state void ratios (i.e., denser) and steeper slopes (i.e., more compressible) relative to uncemented sands. This difference in the CSL has been attributed to the densification of the sand matrix from the presence of the calcite and its increased compressibility after the degradation of the cementation bonds (Riveros and Sadrekarimi 2020a).

Similarly, bio-cemented sands exhibit an increase in cyclic resistance relative to uncemented loose sands when subjected to cyclic / seismic loading, and thus the potential of bio-cementation to mitigate soil liquefaction has been one of the leading motivations for investigating this soil improvement method (e.g., (Burbank et al. 2013; Darby et al. 2019; Lee et al. 2022; Lee et al. 2020; Montoya et al. 2012; Riveros and Sadrekarimi 2020b; Simatupang et al. 2018; Xiao et al. 2018; Zamani and Montoya 2019). The reduced liquefaction potential may be attributed to: (1) cementation increases dilative tendencies, thus reducing the potential for contraction and excess pore pressure generation, (2) cementation increases strength at low confining stresses where liquefaction is more likely to occur, and (3) cementation fills the interparticle void space, densifies the soil, and thereby renders it stiffer and less prone to liquefaction (Darby et al. 2019; Lee et al. 2022; Riveros and Sadrekarimi 2020b; Simatupang et al. 2018). For the same cyclic loading, less pore pressure is generated and over more loading cycles compared to uncemented sands, however, the time needed for the dissipation of these excess pore pressures can be increased even due to the minimal precipitation-induced hydraulic conductivity reductions (Montoya et al. 2012; Xiao et al. 2019a). Sasaki and Kuwano (2016) further indicate that, based on cyclic triaxial compression tests

on MICP-treated Toyoura and Urayasu sand, there is a bias in the asymmetric strain accumulation towards extension (Saxena et al. 1988b*). This observation has not been investigated further in the literature.

The effects of cyclic loading duration have also been studied but observations have mostly remained inconclusive (see Section 2.4.3.1. and 2.4.3.4.), numerous researchers (Hernandez 2018; Lee et al. 2022; Riveros and Sadrekarimi 2020b; Simatupang et al. 2018; Xiao et al. 2018; Xiao et al. 2019a) have studied liquefaction resistance curves (CSR versus Number of Cycles to liquefaction N_L) for both untreated (baseline) and treated sands. CSR-N_L curves are commonly described by fitting a power law ($CSR = a \cdot N_L^b$) wherein the a-value controls the vertical position of the curve and the b-value controls the slope. These research groups have indicated that the shape of the CSR-N_L curves for MICP-treated sands is similar to that of untreated sands. However, the relative position and slope are controlled by the initial relative density D_R and the cementation level. As D_R and cementation level increase, the curves shift upward indicating that a larger demand is needed to trigger liquefaction and thus a higher cyclic strength.

2.4 Synthesis and discussion of behaviors of bio-cemented sands

This section builds on synthesized experimental observations, the various metrics of cementation adopted, and discusses them in terms of effects observed on the mechanical response of the soil, agreements and disagreements between the data, and gaps.

2.4.1 Metrics of cementation

One of the immediate observations that follows from the study of research work on the bio-cementation of sands is the breadth of metrics used to describe the product. This breadth poses challenges to unifying the findings even for similar treatment methods and parent materials. MICP-

treated sands are typically ranked as light, medium, and heavily cemented with metrics of cementation being calcite content by mass (typically in grams) and calcite in percentage by mass (%). A pragmatic approach followed by numerous researchers has been to characterize cementation through its effects on soil properties. The most commonly measured soil property has been stiffness by measuring the increase in shear wave velocity (ΔV_s) so as to essentially quantify the small-strain stiffness gain due to cementation. Figure 2.10 synthesizes and illustrates the relationship between ΔV_s and calcite content (%) from tests that have reported both (e.g., Gomez et al. 2018; Lee et al. 2022; Montoya and DeJong 2015; Nafisi et al. 2020; and others). Although the data points are seemingly scattered, a linear relationship can be fitted to relate the two metrics. The scatter in the data can be attributed to the differences in initial conditions such as treatment, parent soil, levels of cementation, spatial variability of cementation and in testing procedures such as treating under confinement, confining stresses, and instrument calibration. There is agreement between researchers on the linear fit in Fig. 2.10 (e.g., Darby et al. 2019; Gomez et al. 2018). In fact, this relationship has been used in numerical simulations of axisymmetric cone penetration to inform the properties of bio-cemented sands and has yielded results that were validated against centrifuge model tests (Chapter 3). Relating calcite content to ΔV_s can be very important for upscaling applications and connecting laboratory findings to the field implementation of this treatment method.

While most researchers only report the level of cementation as a percent cement by mass (cement content, %), some also report shear wave velocities (V_s) as being representative of a certain cementation level. Other studies only describe the cementation level qualitatively (e.g., lightly cemented, moderately cemented). It should be noted that relative density (D_R) may not be an appropriate metric for describing the post-treatment state of bio-cemented sands due to the

precipitation process increasing the solid phase. In the present paper, all reported metrics in the studies have been included in all summary plots. While these metrics could have been reconciled (e.g., calcite content by mass in % and in grams) if other properties and measurements were reported for the conversions, the authors did not wish to make this reconciliation to honor the work of the researchers.

Calcite content (in % or absolute mass) has also been correlated to its effects on dry density by Cui et al. (2017), Xiao et al. (2018), Xiao et al. (2019a), and Wu et al. (2021) as shown in Fig. 2.11. The effects on dry density show a clearer trend and this is quite promising given the impact that dry density has on several of the strength-related responses of these materials. As illustrated in Fig. 2.11, another approach has also been used to correlate the ratio of final over initial dry density to calcite content. A cleaner trend is seen in terms of dry density ratios than in terms of absolute values. There is an agreement between the studies that the dry density is expected to increase with the level of cementation. Although not quantified at the time, the impact of increasing calcite content to decreasing void ratio, increasing relative density and through those, increasing dry density had also been described by O'Rourke and Crespo (1988)*, DeJong et al. (2006), DeJong et al. (2010), Montoya et al. (2013).

Another approach has been to quantify the effects of calcite content based on its effects on permeability. Here, the synthesis of available data (Fig. 2.12), either in terms of absolute permeability or ratio of final over initial, demonstrates that these effects are neither predominant nor conclusive. Any reductions observed in permeability are of one order of magnitude at most (e.g., Gomez and DeJong 2017). Researchers agree that the permeability slightly decreases, and the trend looks clearer in terms of the ratio of treated or final to the untreated or initial permeability.

To advance the MICP implementation in various geotechnical applications, attention has been drawn to the spatial distribution of the cementation and its uniformity/nonuniformity across improved sites. Such conditions are quantified by cone tip resistance measurements q_c. Some upscaled studies on bio-cemented sands (Burbank et al. 2013; Darby et al. 2019; Gomez et al. 2018; Montoya et al. 2021) evaluated the uniformity and distribution of bio-cementation with respect to reaction and transport rates. Also, miniature CPTs were used to quantify the level of cementation at various locations. Figure 2.13 establishes a linear relationship between the difference in measured q_c and two other cementation metrics which may serve as a proxy for the estimation of the level of cementation. On the basis of upscaled experiments and numerically generated and synthesized data, Chapter 3 also developed a relationship between q_c and cohesion c for the approximation of the cemented cohesion. The upscaled experiments so far agree that q_c linearly increases as the cementation becomes heavier.

2.4.2 Monotonic behavior: Pre- and post-yielding

The following synthesis on monotonic behavior is summarized in Tables 2.2 and 2.3 and Fig. 2.14, where Tables 2.2 and 2.3 outline the elemental behaviors collected from experimental observations from monotonic laboratory tests before and after yielding, respectively, along with their respective referenced studies and Fig. 2.14 presents a conceptual schematic of the monotonic response of bio-cemented sands in the triaxial q-p' space due to the lack of availability of such a dataset. Mechanistically, the pre-yield behavior is controlled by the cohesive component of the strength (i.e., dependence on the level of the cementation) whereas the post-yield behavior is controlled by its frictional component (i.e., dependence on confinement) (Feng and Montoya 2015; Rad and Clough 1982***; Riveros and Sadrekarimi 2020a; Yun and Santamarina 2005*).

Generally, literature on the monotonic drained shearing response of bio-cemented sands before yielding agrees that increasing cementation: (i) increases the tensile strength of the material or alternatively contributes an apparent initial cohesion (Fig. 2.16), (ii) contributes to an initially stiffer response compared to clean sands corroborated by the increase of shear wave velocity and/or small-strain shear modulus (Figs. 2.7 and 2.10), (iii) increases the overall peak strength (Fig. 2.14), and (iv) leads to a decrease of the strain at which failure is observed (Fig. 2.15). The latter has been however found to increase with increasing confinement.

As a bio-cemented sand specimen is progressively loaded, it approaches a yield stress higher than clean sands and yielding occurs (Riveros and Sadrekarimi 2020a; Saxena et al. 1988a*). At first, the bond breakage occurs randomly such that the damage is accommodated by the redistribution of the load and the elastic response is preserved. During this initial stage, interparticle cohesive bonds hinder the plastic response and associated dilatancy (Terzis and Laloui 2019). As the sample is further sheared, the response transitions from stiff to less stiff and the bio-cemented sand reaches a peak strength higher than clean sand but at a smaller strain (Montoya and DeJong 2015; Terzis and Laloui 2019). Three competing mechanisms are present at the peak state: breakage of bonds, volumetric dilation, and interparticle friction. Peak strength is fully mobilized at this point and bond breakage accelerates. Various researchers have also studied the peak strength in terms of the peak friction angle, which for clean sands is state-dependent. For the peak friction angle, some disagreements can be identified in the literature with one group of researchers (Wissa and Ladd 1964*; Saxena and Lastrico 1978*; Saxena et al. 1988a*; Wang and Leung 2008*; Chou et al. 2011; Cheng et al. 2013; Feng and Montoya 2015; Montoya and DeJong 2015; Cui et al. 2017; Nafisi et al. 2020) supporting the increase of peak friction angle with cementation as well as its state dependency (decreases with increases in σ', increases with increases in D_R) and another

group (Dupas and Pecker 1979; Clough et al. 1981; Rad and Clough 1982; Abdulla and Kiousis 1997; Yu 1998; Duraisamy and Airey 2012; Lin et al. 2016; Liu et al. 2018; Riveros and Sadrekarimi 2020a) supporting that the peak friction angle is unaffected by cementation per se and that any perceived increase in it is attributed mostly to other effects such as the increase in cohesion.

Out of the research works who have produced data on the monotonic response of bio-cemented sands, only the ones that provided quantifiable effects as a function of some metric of cementation have been synthesized and plotted. Figure 2.15 shows the axial strain at peak stress measured for triaxial tests plotted against calcite content (in %) and ΔV_s (in m/s). No clear trend can be fitted but the combined data do show that the axial strain decreases with increasing cementation, regardless of how the latter is quantified. Figure 2.16 shows the relationships between a range of strength metrics (cemented friction angle, ratio of final over initial friction angle, and apparent cohesion intercept) and cementation metrics. As can be seen, the trends of Fig. 2.16 are clearer and can be fit with linear laws indicating stronger and more reliable correlations. Still, some datasets (e.g., Cui et al. 2021b) exhibit some outlying behaviors but at the same time, the continuous enrichment of these synthetic plots can further elucidate and benchmark such mechanical behaviors. These trends can be improved or the functional forms may change once more the dataset is more populated. However, there is an agreement across all studies mentioned in this paper that the cohesion increases with the level of cementation and greatly affects the behavior of initially loose treated sands. The friction angle increases to a lesser extent.

Reaching the peak typically signifies the onset of permanent deformation or plastic response. The literature is also here in agreement with regards to the effects of cementation on various aspects of this part of the response, listed in Column 1 of Table 2.3. Mechanistically, the reduction

in strength due to de-structuration exceeds the strength increases resulting from the mobilization of dilatancy and strength starts decreasing. After peak, the bond breakage is significant, the rate of dilation reaches a maximum and then gradually decreases towards zero, and the strength decreases until it reaches a residual strength (Terzis and Laloui 2019). Strain localization occurs along shear bands (DeJong et al. 2006; Waller et al. 2011). A transition from strain hardening to strain softening occurs at high cementation levels and is attributed to the transition from global to localized failure. This transition is due to the brittleness of the cementation bonds, which is a function of the cementation level and the confining stress (Lin et al. 2016; Montoya and DeJong 2015; Waller 2011). Unlike clean sands (Bolton 1986), one gap here is that no constitutive relationships have been developed for the relationship between peak and residual friction angle, although relationships between peak and residual friction angles and shear wave velocities are currently being explored (e.g., Riveros and Sadrekarimi 2020a).

The undrained behavior of bio-cemented sands is similar to the drained behavior, with the volumetric behavior under drained conditions reflected by pore pressure changes under undrained conditions. Initially, positive pore pressure is developed until yielding after which negative pore pressure builds up, suggesting initially contractive and then dilative volumetric tendencies (Montoya and DeJong 2015; Porcino and Marciano 2017**; Riveros and Sadrekarimi 2020a). The dilative behavior is hindered by the presence of the cohesive bonds at first, hence the contraction of the soil but is inevitable after yielding when these bonds are broken.

2.4.2.1 Discussion and recommendations

Following the description of observations from the populated experimental database on the mechanical response of bio-cemented sands (Table 2.1), the following list presents discussion points and recommendations that stem from the gaps identified:

- One noticeable limitation across the literature is the lack of a single, broadly accepted, metric for the quantification of the magnitude of cementation (similarly Rios et al. 2014*). It is recommended that cementation level be quantified in terms of cement content (% cement) and shear wave velocity (V_s). Similar to clean sands, the initial relative density prior to cementation should also be reported.
- Several studies (e.g., Wang et al. 2021; Wu et al. 2021) suggest that the strength behavior of bio-cemented soil is stress- and strain-dependent. Cementation dominates the behavior of bio-cemented sands at low strains and confining stresses, whereas the particle friction controls the behavior at high strains and confining stresses. This observation is important for understanding the effect of confinement on both naturally and bio-cemented sands which may be initially treated under low confining stresses but later loaded to higher stress levels due to new construction. Few experiments are available to confirm any hypothesized mechanisms, and additional lab tests on bio-cemented specimens at high confining stresses will clarify the role of confinement.
- Literature studies about friction angle are divided between concluding that the friction angle is negligibly affected by cementation (e.g., Clough et al. 1981***; Lin et al. 2016) and that it increases with cementation level (e.g., Feng and Montoya 2015; Saxena et al. 1988a*). Both conclusions agree that the angularity/roughness of the particles affect the friction angle of bio-cemented sands. The first line of thought, however, considers that the increase in friction angle is negligible relative to the gain in apparent cohesion and is thus unimportant (Rad and Clough 1982***) whereas the second considers the friction angle as a secondary contributor to the mechanical response but still important (Feng and Montoya 2015). These different interpretations may be explained in part by the range of stresses in the experiments since the

influence of cementation on the cohesion and friction angle depends on the effective stress (Lo et al. 2003). Consequently, trends in friction angle should be investigated to resolve the above inconsistency.

- Literature suggests that bio-cemented sands initially exhibit a delayed dilative behavior due to the apparent cohesion between the particles and then transition to a more dilative behavior upon bond degradation. The dilative behavior is less explored relative to other behaviors, such as stiffness or peak strength. The effect of particle shape, roughness, and arrangement (i.e., fabric) remains poorly understood and microscale studies (e.g., discrete element modelling: Dong and Fatahi 2020; Feng et al. 2017; Khoubani et al. 2016; Yang et al. 2017) have the potential to inform understanding of the macroscopic response. Experimentally, providing SEM images of bio-cemented specimens may lead to better understanding of the effect of cementation microstructure on macroscale mechanical behavior.
- Monotonic tests on lightly cemented sands imply that bio-cementation improves the mechanical response at low stresses and strains, even though for these low cementation levels shearing at high stresses and strains will produce behaviors similar to untreated sands. This is due to minimal changes in dry densities and particle surface roughnesses. Other researchers state that the residual strength of bio-cemented sands is larger than that of uncemented sands. Although this may be true for high cementation levels, it is unclear if all cohesive bonds are completely degraded at strain levels typically used to measure the residual strength of clean sands or if higher ranges of shear strains may be required to fully degraded these bonds and reach critical state. Additional monotonic tests reaching strains larger than those typical for uncemented sands are needed in order to examine the residual strength of bio-cemented sands relative to that of uncemented sands at different levels of cementation.

- Although some studies provide insights on the position of the critical state line of bio-cemented sands relative to that for clean sands, the behavior of bio-cemented sands at critical state remains largely unknown. A parametric study of monotonic tests performed at various initial void ratios and under various confining stresses will inform the shape and position of the critical state line and thus clarify the behavior of the soil when it reaches critical state.
- Knowledge gaps also exist regarding the failure modes that occur in bio-cemented sand specimens. Although it is presumed that bio-cemented sands become more brittle with increasing cementation level, there is little experimental data on the strain localization along shear bands. The size and inclination of these shear bands as well as the accompanying transition to a strain softening material have remained relatively unexplored with a few exceptions (e.g., Tagliaferri et al. 2011; Waller 2011). Additional monotonic tests are needed, focusing on the shear failure and its characteristics as a function of the particle-level spatial distribution and degree of cementation.
- In addition to addressing the above gaps in the experimental database for bio-cemented sands, effort should be put towards expanding the parametric space of initial conditions affecting the mechanical response of bio-cemented sands. Initial conditions to explore include the degree of saturation during cementation (e.g., Simatupang and Okamura 2017), the mineralogy of the parent soil (relative cement-sand particle size, particle shape, angularity and roughness) (e.g., Nafisi et al. 2018; Simatupang et al. 2018; Terzis and Laloui 2017), the mineralogy of the cementing agent (e.g., DeJong et al. 2006; Ismail et al. 2002; Nafisi et al. 2019a), the loading type (compression versus extension) (Montoya and DeJong 2015; Nafisi et al. 2019b; Nafisi et al. 2021) and the experiment scale (bench-scale versus large-scale, Gomez et al. 2016;

Montoya et al. 2021; van Paassen 2009), versus field-scale (Darby et al. 2019; Zamani et al. 2021).

- A database filled out over a broader parametric space would enable the development of bio-cemented sand behavior relationships at a rigor level similar to those for clean sands. These relationships include correlations between field measurements (CPT tip resistance) and strength parameters, and liquefaction triggering curves (e.g., q_c, V_s). Such correlations would be valuable in the formulation of a constitutive model for bio-cemented soils and thus the design of field applications for bio-cemented soils.

2.4.3 Cyclic behavior

The body of data produced on the cyclic response of bio-cemented sands is significantly smaller than that on the monotonic response of bio-cemented sands (14 datasets compared to 47) and it started increasing after realizing the potential of this technology for liquefaction mitigation. Herein, the discussion of cyclic behavior is guided by the information presented in Table 2.4 and Fig. 2.17, where Table 2.4 summarizes the elemental behaviors collected from experimental observations from cyclic laboratory tests along with their respective referenced studies and Fig. 2.17 presents plots of the cyclic response of bio-cemented sand from actual lab data by Lee et al. (2022).

2.4.3.1 Pre-triggering and triggering

In cyclic loading bio-cemented sands undergo consecutive instances of contraction and dilation where stiffness loss due to the breakage of cementation bonds is partly recovered by the generation of negative pore pressure due to densification (Fig. 2.17c). The presence of cementation specifically at the particle contacts inhibits the generation and accumulation of positive pore pressure thus the soil requires more cycles and/or a higher demand (CSR) to move the stress path

to the origin and trigger liquefaction (Fig. 2.17a). The response is stiff during these cycles and little shear strain deformations (<0.5%) are accumulated from cycle to cycle (Fig. 2.17b) (Lee et al. 2022; Riveros and Sadrekarimi 2020b; Xiao et al. 2019a). All studies performed agree on the increase of the number of cycles it takes to trigger liquefaction with increases in cementation, as well as on the decrease in the number of cycles to trigger liquefaction with increases in overburden (as is also the case with clean sands due to suppressed dilatancy that the increased overburden causes). For example, Lee et al. (2022) analyzed the pre-triggering results in terms of number of cycles to trigger liquefaction according to two different criteria: cycles to pore pressure ratio (r_u) = 0.95 and cycles to single amplitude shear strains (SASS) = 3% and corroborated the above conclusions. Both criteria yielded similar results. Even light levels of cementation reflect remarkable changes in the number of cycles for triggering according to both criteria (from 0.5 cycles for an uncemented specimen to ~650 cycles to a cemented specimen with ΔV_s of 95 m/s) and in the volumetric behavior upon initiation of shearing. One observation from these tests is that the pore pressures generated per cycle for uncemented sands were relatively similar for cycles prior to triggering whereas the pore pressures generated per cycles for bio-cemented sands were smaller upon initiation of shearing and became progressively larger as r_u progressed after 0.5. This may be attributed to the integrity of intact cementation bonds at the onset of shearing and its progressive loss of effectiveness due to fatigue with the continuous application of the loading. Results from Lee et al. (2022) further suggest that bio-cemented sands can withstand higher maximum excess pore pressure ratios before significant shear strains develop and these threshold r_u values depend on the level of cementation. For instance, for a value of $r_u = 0.6$, an uncemented sand developed nearly 1.5% shear strains compared to 0.25 % for the bio-cemented sand under similar conditions. The added tensile strength to the treated sand through the presence of the

cementation at particle contacts allowed for a higher shear stiffness which in turn prevented the rapid accumulation of shear strains. However, as the bio-cemented sand attains a certain threshold r_u, the cementation bonds are damaged and broken, their residual strength is overcome by the excess pore pressure generation, abrupt increases in shear deformations take place, and the volumetric behavior becomes more contractive fueling further increases in r_u. It was also shown that the demand (CSR) affected the failure mechanisms of the cementation bonds which in turn influenced the number of cycles for triggering. A lower CSR resulted in more gradual fatigue-like deterioration of cementation whereas a higher CSR resulted in an abrupt dissociation of cementation bonds. The former yielded longer resistance to liquefaction than the latter.

Enough data have been generated by researchers that CSR versus N_L curves can be synthesized and quantified although more work needs to be done to reach the level of understanding that we currently have on clean sands (e.g., effects of loading duration, effects of overburden stress through the K_σ factor (Montgomery et al. 2014), effects of sloping ground conditions through the K_α factor). Figures 2.18, 2.19, and 2.20 illustrate CSR versus N_L curves for overburdens of 50 kPa, 100 kPa, and 200 kPa, respectively. CSR-N_L curves are commonly described by fitting a power law ($CSR = a \cdot N_L^b$) wherein the a-value controls the vertical position of the curve and the b-value controls the decreasing slope. In Figs. 2.18 to 2.20 one can see that the power law could be fitted indicating that the shape of the CSR-N_L curves for MICP-treated sands is similar to that of untreated sands. However, this functional form was shown to not accurately depict the trends in bio-cemented sands especially at low CSRs when the number of cycles to liquefaction is very high (Lee et al. 2022). For earthquake engineering applications, a maximum of 100 cycles would be considered at most. Here, Figures 2.18, 2.19, and 2.20 extend the curves to 10^5 cycles only for complete reporting of experimental results and the datapoints are fitted for illustrative purposes.

These figures show that cementation does shift cyclic strengths to higher values, and that the fitted curves become less steep as the level of cementation increases. These aspects are further explored in terms of the parameters “a” and “b” in the above functional form. Figure 2.20 reports the values of the fitting parameters “a” and “b” as a function of the level of cementation. Parameter “a” has an increasing trend as cementation becomes heavier which reflects a higher cyclic resistance as discussed before. This aspect of the cyclic response is agreed upon by all reported studies. However, observations regarding b-value changes have remained inconclusive with Hernandez 2018, Xiao et al. 2018, and Xiao et al. 2019a indicating that b-value will decrease (i.e., flatter curve and reduced dependency on number of cycles), Okamura (2018 – pers. communication) indicating that it will more or less stay constant, and Riveros and Sadrekarimi (2020b) supporting that it will increase with cementation. Specifically, Fig. 2.21 shows that parameter “b” may decrease with the level of cementation with the exception of the values reported by Riveros and Sadrekarimi (2020b) where the “b” value is shown to increase (right plots in Fig. 2.21). Riveros and Sadrekarimi (2020b) suggested that this increase in parameter “b” (i.e., steeper slope of CSR versus N_L curves with cementation) may indicate the sensitivity of the cyclic resistance of bio-cemented sands to the number of cycles. Therefore, the trends for parameters “a” and “b” are not fitted until more data become available. Furthermore, comparison between Figs. 2.18, 2.19, and 2.20 confirms that decreases in the number of cycles to trigger liquefaction are expected with increases in overburden stresses. This observation is evident in the aforementioned figures when focusing on datasets from the same authors but at different overburden stresses i.e., green squares in Fig. 2.18 versus yellow triangles in Fig. 2.20 for cement content of 0.8% in Simatupang and Okamura (2017) and orange circles in Fig. 2.18 versus fuchsia triangles in Fig. 2.19 versus yellow cross marks in Fig. 2.20 for cement content of 12 grams in Xiao et al. (2018).

At this point, it is deduced that bio-cementation can serve as a liquefaction mitigation method because it delays the generation of excess pore pressure and shear strain accumulation depending on the duration and magnitude of shaking. While this conclusion seems evident, the lack of a consistent metric for quantifying and characterizing cementation is challenging the efficient summary of such data. For example, some researchers report cementation in terms of ΔV_s, others in absolute mass of calcite content (g) and others in percentage by mass of calcite content. Furthermore, the data reported honor different triggering criteria (some strain-based to double amplitudes of 5% and 10% and others excess pore pressure ratio-based to $r_u = 100\%$) and very few studies explore these behaviors across different overburden stresses such that extensive quantifiable conclusions can be drawn with regards to the effects of overburden on the cyclic response of bio-cemented materials.

2.4.3.2 Post-triggering

Liquefaction is triggered once cementation bonds are damaged during cyclic shearing. Excess pore pressure gradually increases, and the stress path goes to zero effective mean stress (Fig. 2.17a). Interparticle bonds no longer contribute to the cyclic resistance beyond this point and the soil sequences through cycles of contraction and dilation, leading to a significant loss in stiffness and subsequently considerable accumulation of shear strains during the post-triggering cycles (Fig. 2.17b). This is accompanied by an excess pore pressure ratio r_u close to 100% (Fig. 2.17c). Post-triggering behavior wherein this progressive controlled accumulation of shear strains takes place is typically called cyclic mobility (Castro and Poulos 1977; Seed 1979). Admittedly cyclic mobility is a behavior that has not been explicitly quantified even for clean sands with most recent efforts having made steps towards studying the mechanics of cyclic mobility under a range of conditions (Kiyota et al. 2008; Chiaro et al. 2012) and providing metrics for the rate of strain

accumulation post-triggering (Humire and Ziotopoulou 2022; Shamoto et al. 1997; Tasiopoulou et al. 2020; Wang and Wei 2016; Wei et al. 2018). As such, the quantification of post-triggering responses is also challenging in bio-cemented sands although some datasets have indicated that cementation does slow down the rate of shear strain accumulation: even though liquefaction has occurred, shear strains remain less than the corresponding strains for a clean sand subjected to the same loading. This is mainly due to the compensating effects of cementation damage and densification, which occur simultaneously (Darby et al. 2019; Riveros and Sadrekarimi 2020b; Xiao et al. 2019a). In a more recent study (Lee et al. 2022), the post-triggering behavior was explored in terms of changes in cementation magnitude and D_R for light cementation. The number of cycles to certain threshold strains (SASS of 5% and 9%, and double amplitude shear strain DASS of 24%) was considered the primary indicator of cyclic mobility in bio-cemented sands. Following liquefaction triggering in bio-cemented sands, insignificant changes in shear strain accumulation behaviors were observed compared to clean sands (e.g., 4 additional cycles for bio-cemented sands compared to clean sands for 3% SASS to 24% DASS). This may indicate that the light cementation present in the soil matrix was completely destroyed and contributed to limited densification. Cyclic tests at different D_R under similar cementation levels suggested that D_R had a bigger influence on the reduction of post-triggering shear strain accumulation than light bio-cementation. While these conclusions are in contrast with the indications by other experiments where densification might have been more evidenced, it is understood that the level of cementation plays a key role in the manifestation of post-triggering behaviors in terms of (1) number of remnant unbroken bonds, and (2) contribution of fines to the soil matrix, thus densification.

2.4.3.3 Post-liquefaction reconsolidation

Researchers (Darby et al. 2019; Riveros and Sadrekarimi 2020b; Xiao et al. 2019a) have reported that when bio-cemented sands were subjected to multiple shaking events, following their initial triggering events and post-liquefaction reconsolidation, the sands did not trigger at the level of shaking required to trigger clean sands at similar initial relative densities. This is explained by the combined effect of increased soil density, particle angularity and roughness, and some residual particle-particle bonding. This observation suggests that: (1) improvement from bio-cementation remains to a large extent even after the breakage of cementation bonds (Darby et al. 2019; Riveros and Sadrekarimi 2020b), and (2) liquefaction triggering in terms of the cone tip resistance curve (Idriss and Boulanger 2008) may be shifted upward (higher CRR) and to the left (lower q_{c1N}) for bio-cemented sands (Darby et al. 2019). Riveros and Sadrekarimi (2020b) and Simatupang et al. (2018) further explored post-liquefaction reconsolidation strains and suggested that bio-cementation has little effect on the post-liquefaction compressibility of the treated soil. This conclusion was more recently corroborated by Lee et al. (2022).

2.4.3.4 Discussion and recommendations

As seen in the preceding sections, the experimental database on the cyclic behavior of bio-cemented sands has been mainly developed and enriched over the last five years. This is most probably due to a general consensus that the understanding of the cementation effects under earthquake loading is crucial for envisioned field applications. Researchers continue to expand the database to various confining stresses, treatment procedures, shaking events and demands, and applications such as slope stability mitigation, pile capacity and foundation settlement. The synthesis of experimental findings as well as their critical review highlighted that there is a need for more laboratory tests on bio-cemented sands to: (1) expand the parametric space to higher

confining stresses, consistent failure criteria, different levels of cementation but reported with consistent metrics (e.g., ΔV_s or calcite content in % by mass), and various grain size distributions, saturation levels, and parent soils to establish a more complete database that will elucidate broader patterns in behavior and, (2) enable discrepancies in hypotheses previously developed regarding the mechanical responses of these new materials to be resolved. For these reasons, and in an attempt to inform future testing plans addressing current knowledge gaps in bio-cemented sands, areas that require more testing are:

- Cyclic lab tests on bio-cemented sands are limited but growing in number and scope. Future testing plans should therefore focus on filling the gaps in the database, which include liquefaction triggering curves and cyclic resistance versus duration curves, cyclic resistance after multiple shaking events and post-liquefaction reconsolidation cyclic resistance. Additional cyclic tests with varying levels of cementation are needed to quantify the shape of the CSR versus number of cycles to liquefaction N_L curves and the tendencies of the "a" and "b" parameters ($CSR = a \cdot N_L^b$) to, respectively, increase and decrease or increase as the level of cementation increases. Moreover, cyclic tests with varying loading patterns (i.e., high amplitude-few cycles versus low amplitude-many cycles) give insights on the degradation process and the fatigue of the cementation.
- Although the general form of the modulus reduction and damping curves for bio-cemented sands is known, the details about dynamic properties (e.g., threshold strains for G/G_{max} curves, damping ratio) and their variation with cementation level, particle-level spatial distribution, and the number of repeated cycles is lacking. Low-strain tests are needed to establish a clear relationship between dynamic properties and cementation levels.

- While most studies focus on the utility of bio-cementation in reducing liquefaction susceptibility of loose sands under level ground conditions, more attention should be drawn to sloping conditions as well especially since there is a promise in bio-cementation mitigating slope stability problems. It is reasonable that this condition is not yet evaluated due to the remaining gaps in the level ground conditions, but it is expected that such studies will enrich the database and encourage the use of bio-cementation to mitigate slope instability.
- As seen in Figs. 2.18 to 2.20, some researchers have already embarked on assessing the effect of confinement on the cyclic behavior of bio-cemented sands, but more data is needed to corroborate the present hypotheses. As more data is collected and unified, relationships relating to K_σ will be made possible. Such relationships will become valuable in the scenarios where treatment occurs for a liquefiable site followed by structural loading due to the construction of the superstructure.

2.5 Continuum models for bio-cemented sands

2.5.1 Available constitutive models and approaches

The fundamental role of a constitutive model is to relate the stress and strain increments as a material undergoes a certain loading path. The level of sophistication of any constitutive model depends on the goals under which it has been developed and the degree of understanding of the mechanical behavior of the targeted material with some materials having been more extensively sampled and tested than others. To the extent of the authors' knowledge no constitutive model in geotechnical engineering is able to capture the response of a broad range of soils (e.g., from sands to clays) to all possible loading paths (e.g., 2D and 3D, monotonic and cyclic, from low strains to crushing etc.) and for all possible applications (e.g., soil structure interaction, earthquake engineering, offshore engineering etc.). When it comes to the effects of cementation on the

constitutive behavior of sands, a few continuum constitutive models exist and are summarized herein that can incorporate the elemental mechanical behaviors observed following the cementation process and the soil's response under a variety of loading paths. Ultimately a constitutive model is the translation of physics and mechanics to a geometric space (Dafalias 2020 – personal communication), something that frequently leads to the same geometric vehicle (e.g., a surface or line) being used to capture responses that are macroscopically similar but stem from different microscopic mechanisms. As a consequence, other pertinent models have been developed for soils that macroscopically may exhibit features that resemble the response of a cemented material such as structured clays and weak rocks. These are also included in this review to (1) enrich it with a plethora of ways to incorporate cementation, and (2) assess the usability and applicability of existing models to bio-cemented sands. Table 2.5 provides a summary of available constitutive models for bio-cemented sands and other relevant soils (such as structured clays and weak rocks) used herein. All models in Table 2.5 were based on existing models for clean sands which were modified or extended to cemented sands, structured clays, or weak rocks. Columns 1 and 2 report the reference and the baseline formulation for each model, respectively. Column 3 identifies the type of soils targeted by each model. Column 4 reports any related work and publications. Columns 5 and 6 summarize the targeted behaviors from the baseline formulation and indicate whether it was a calibration (C), modification (M) or extension relative to the baseline model, respectively. A wealth of information on the incorporation of the cementation and its subsequent degradation with damage is summarized in Column 6. Columns 7 and 8 indicate whether the constitutive models were validated and if so, which validation database (i.e., laboratory tests) was used for the validation, respectively. Column 9 reports the developers' own evaluation of the model as presented in their original publications. The constitutive models are

first grouped by similar target applications and then by date of publication. Therefore, the efforts are organized into 4 major soil types: bio-cemented sands, cemented sands, structured clays, and weak rocks with other relevant materials. While a continuum model will work for light levels of cementation, it will not be appropriate for heavy cementation levels at which the materials are expected to undergo fracture and a transition from soil to rock models is warranted. Certain models attempt to account for bio-cemented sand behaviors by modifying existing models for structured clays and/or weak rocks, whereas others extend constitutive models for clean sands to include the effect of cementation. Some models have been developed that specifically target certain stress paths of bio-cemented soil behavior (e.g., Pestana and Salvati 2006).

The most common approach is for a model to macroscopically account for certain observations (e.g., increased tensile strength or apparent cohesion, increased peak strength, enhanced dilative behavior) by appropriately designating and modifying an appropriate constitutive component which of course depends on the formulation of the constitutive model and its available framework (e.g., Cam Clay-based, multiyield surface-based, bounding surface plasticity-based). For example, as seen in Section 2.3, all the experimental observations agree on the increase of peak strength with cementation. Many of the constitutive models (e.g., Fauriel 2012; Gai and Sanchez 2018; Gajo et al. 2015; Gens and Nova 1993; Lee et al. 2004; Nova et al. 2003; Rahimi et al. 2015; Rahimi et al. 2018; Yu et al. 2007) consistently account for this cementation-induced gain in peak strength by enlarging their yield surface in the positive p' direction. Similarly, the yield surface is enlarged in the negative p' direction to account for the cementation-induced tensile strength (e.g., Gai and Sanchez 2018; Yamada et al. 2022; Zhang et al. 2021). These modifications suggest that a larger yield surface is a reasonable constitutive component for adequately capturing the increase in strength due to cementation. Other models that use a multi-surface formulation (typically two

surfaces representing yield and failure) track the soil's stress history and the key characteristics of the stress path (e.g., Hirai et al. 1989; Kavvadas and Amorosi 2000; Panico and Viana da Fonseca 2018; Rahimi et al. 2018). Then, the magnitude and strength of the cementation and stress history are used to inform the size (isotropic hardening) and location (kinematic hardening) of the failure surface. These attributes are typically considered in the hardening rule of the constitutive models (e.g., Zhang et al. 2021).

Beyond the increase in the peak strength, most researchers also incorporate: (1) the small-strain response with a non-linear shear stiffness in the elastic domain (e.g., Fauriel 2012; Kavvadas and Amorosi 2000; Lee et al. 2004; Nweke and Pestana 2017; Panico and Viana da Fonseca 2018; Rahimi et al. 2015; Rahimi et al. 2018; Yu et al. 2007; Zhang et al. 2021), and (2) the shearing-induced degradation of cementation bonds by requiring damage-type relationships which reduce the yield surface size as cementation bonds break (e.g., Bruno et al. 2020; Ciantia and di Prisco 2016; Fu et al. 2022; Gai and Sanchez 2018; Gao and Zhao 2012; Gens and Nova 1993; Kavvadas and Amorosi 2000; Lee et al. 2004; Nova et al. 2003; Nweke and Pestana 2017; Panico and Viana da Fonseca 2018; Rahimi et al. 2015; Rahimi et al. 2018; Vaunat and Gens 2003; Yu et al. 2007; Zhang et al. 2021). Select models include fewer common features such as a distinction between initial yielding and major destructuration (Kavvadas and Amorosi 2000), inclusion of apparent cohesion in the stress-dilatancy relationship (Rahimi et al. 2015; Rahimi et al. 2018; Wu et al. 2021; Yu et al. 2007) or coupling between hydro-chemo-mechanical processes (Ciantia and di Prisco 2016; Fauriel 2012; Gajo et al. 2015; Gajo et al. 2019; Xiao et al. 2021).

2.5.2 Discussion and recommendations

Most of the models currently available in the literature have three main drawbacks. First, the use of Modified Cam Clay (MCC) as a baseline framework, although common, is inapplicable to soils

other than clays, because the sand behavior is fundamentally different from the clay behavior even though the cementation effects may be transferable. In addition, one underlying model assumption is that the initial void ratio for the bio-cemented soil remains at the same initial void ratio for the clean soil for which the model was initially formulated. Although this assumption may be acceptable for low levels of cementation, it may be unreasonable for higher levels of cementation where the initial void ratio decreases, and relative density increases significantly. For example, even a light level of cementation of 0.9% calcite by mass has been shown to increase the relative density by 5.8% (Lee et al. 2022) and a heavier level of cementation of 14% calcite by mass been shown to reduce the void ratio from 0.56 to 0.47 (Wu et al. 2021). Second, the apparent cohesion resulting from cementation bonds is rarely accounted for in the stress-dilatancy relationship, whereas it plays a major role in the particles' rearrangement and volumetric behavior during shearing. For example, Wu et al. (2021) report that cohesion increased from 0 to 533 kPa for a calcite content by mass of about 13% and almost doubled the dilatancy compared to uncemented sand. Third, these models are formulated and validated against monotonic lab tests on bio-cemented soils (sands or clays) and only few models can be used for cyclic loading (e.g., Xiao et al. 2021; Zhang et al. 2021). To date, only Xiao et al. (2021) have targeted the response of bio-cemented sands subjected to cyclic loading and validated the model using datasets for bio-cemented sands.

The two main challenges facing constitutive models for cemented sands are: (1) none of the above models are built considering the field application and the parameters that a model would be able to handle as inputs (e.g., calcite content versus shear wave velocity increase or q_c increase), and (2) all of these models suffer from the same limitations as the lab data used to validate them whereby no particular theoretical framework is developed but rather rational observations and

hypotheses are informed by the lab data. This lack of usable constitutive models potentially also reflects the lack of knowledge on bio-cemented sands and how they would be monitored in the field as well as the increased complexity that they carry when compared to clean sands.

2.6 Summary and concluding remarks

A critical review of experimental and numerical literature on cemented sands was performed to: (1) identify and formalize the known behaviors of cemented soil, (2) identify key unresolved mechanical behaviors and their dependence on experimental parameters, and (3) aid in the development of continuum-based models that can capture a broader range of behaviors than models based on individual case-specific responses. Based on the critical review the authors conclude that:

- Experimental data on naturally and bio-cemented sands are limited in comparison to the extensive database available for clean sands. The parametric space across which these experiments span is currently rather narrow and should be expanded to cover the range of properties of interest and typically encountered in design.
- The present synthesis of data points from the extensive literature that was collected based on the criteria set forward, should provide a database for researchers to contribute their data to. This will aid in collectively developing a comprehensive and progressively refined body of work as well as in helping researchers identify outliers in trends which can be further investigated.
- There is agreement on the general behavior of bio-cemented sands, namely the increase in stiffness, peak strength, apparent cohesion, dilatancy, and the decay of these parameters with continuous shearing. However, gaps remain with regards to the magnitudes of various effects

as well as the causal relationships between the ensuing mechanisms. Future efforts should investigate other important but less understood components such as the friction angle, residual strength, critical state line, softening and strain localization, dynamic properties, role of confinement, and impact of microstructure.

- No consensus has been reached towards establishing universal metrics to characterize bio-cementation treatment magnitudes. Similarly, there is no agreement on what range of cement contents and V_s increases are implied for a treated soil, when cementation is described qualitatively (i.e., light, medium, heavy cementation). Establishment of universal metrics to describe cementation levels would provide a common language and through that improve the understanding of the mechanical behavior of bio-cemented soils and enable discrepancies between studies to be resolved and ideally unified.
- Constitutive models developed have primarily focused on monotonic behavior, and the laws developed differ widely. There is no usable constitutive model that captures the cyclic response of bio-cemented sands.

The synthesis of data and the critical insights presented in this paper are expected to ensure that any future work on the experimental or constitutive mechanical responses of bio-cemented sands can take place within a more guided framework. This way more engineering correlations can be developed or enriched, key parameters identified, and more concrete guidance can be provided to research and industry towards the robust adoption of the environmentally conscious bio-cementation technology.

Table 2.1. Summary of experimental studies on cemented cohesionless soils (table sorted by cementing agent first and then alphabetically by reference).

Reference		Parent soil	Type of treatment*	Cementing agent	Test type**	Varied parameters (if left empty no variation studied)	Effects		Qualitative Description	Nr. of tests
							% cement	ΔV_s (m/s)		
Laboratory tests										
1	Airey (1993)	Calcarenite (Australia)	Natural		TXC (D, U)				Moderately to heavily cemented	
2	Amoly et al. (2015)	Sandy soils (Asahi and Kesen-Numa, Japan)	Natural		TXC (U)					
3	Ciantia et al. (2015)	Gravina Calcarenite (Italy)	Natural		UNC, BTT, oedometer	w_c (wet and dry), saturation fluid				
4	Clough et al. (1989)	Coastal bluffs (Pacifica, California)	Natural		TXC, cTXC (U)					20
5	Collins & Sitar (2009)	Coastal bluffs (Pacifica, California)	Natural		TXC, TX-LE, UNC (D)				Weakly cemented	
5	Collins & Sitar (2009)	Coastal bluffs (Pacifica, California)	Natural		TXC, TX-LE, UNC, BTT (D)				Moderately cemented	

Reference		Parent soil	Type of treatment*	Cementing agent	Test type**	Varied parameters (if left empty no variation studied)	Effects		Qualitative Description	Number of tests
							% cement	ΔV_s (m/s)		
6	Coop & Atkinson (1993)	Calcarenite	Natural		TXC (D)	confining stress				6
7	Cuccovillo & Coop (1997)	Calcarenite (Australia)	Natural	Calcium carbonate	TXC (D, U)	confining stress				
7	Cuccovillo & Coop (1997)	Silica sandstone (England)	Natural	Iron oxide	TXC (D, U)	confining stress				
8	Frydman et al. (1980)	Kurkar sand (Israel)	Natural	Calcite	cTXC (U)	confining stress				
9	Lagioia & Nova (1995)	Calcarenite (Bari, Italy)	Natural		TXC (D)	confining stress				
10	O'Rourke & Crespo (1988)	Volcanic Cangahua formation (Quito, Ecuador)	Natural		TXC (D), UNC, BTT	confining stress, degree of saturation			Moderately cemented	15, 15
11	Rad & Clough (1982)	Coastal bluffs (Pacifica, California)	Natural	Iron oxide, calcite	TXC (D), cTXC (D, U)	% cement, w_c			Weakly and moderately cemented	27, 6, 9
12	Salomone et al. (1978)	Vincentown formation (New Jersey, US)	Natural	Calcium carbonate	TXC (U), cTXC (U)					

Reference		Parent soil	Type of treatment*	Cementing agent	Test type**	Varied parameters (if left empty no variation studied)	Effects		Qualitative Description	Number of tests
							% cement	ΔV_s (m/s)		
13	Saxena & Lastrico (1978)	Vincetown formation (New Jersey, U.S.)	Natural	Calcite	TXC (U)	confining stress			Weakly cemented	92
14	Sitar et al. (1980), Bachus et al. (1981), Clough et al. (1981)	Coastal bluffs (Pacifica and Daly City, California), and Stanford University (excavations for Stanford Linear Accelerator)	Natural	Calcium carbonate	UNC, TXC (D)	% cement, confining stress			Weakly, heavily cemented	
15	Ismail et al. (2002)	Calcareous soil (Australia)	Artificial	Calcite (CIPS), Portland cement, gypsum	UNC, TXC (U)	type of cement, % cement, confining stress				
16	Sharma & Fahey (2003a)	Goodwyn soil (Australia)	Artificial	Calcite (CIPS)	UNC, oedometer, TXC (U), An-TXC (U), cTXC (U)	confining stress	17			
16	Sharma & Fahey (2003a)	Ledge Point Soil (Australia)	Artificial	Calcite (CIPS)	UNC, BTT, oedometer, TXC (U), cTXC (U)	% cement, confining stress	3.52-8.05			

Reference		Parent soil	Type of treatment*	Cementing agent	Test type**	Varied parameters (if left empty no variation studied)	Effects		Qualitative Description	Number of tests
							% cement	ΔV_s (m/s)		
17	Sharma & Fahey (2003b)	Goodwyn soil (Australia)	Artificial	Calcite (CIPS)	cTXC (U)					7 uncem, 17 cem
18	Almajed (2017)	Ottawa 20-30 sand (D_R=40%)	Bio-cementation	Calcium carbonate (EICP)	UNC, TXC (U)	treatment, confining stress	0.62, 0.9, 0.94, 1.305, 1.34		Weakly cemented	27, 5
19	Miftah et al. (2022)	Beach sand (Cyprus) (D_R=60%)	Bio-cementation	Calcium carbonate (EICP)	DS	% cement, confining stress	0-2.5			9
20	Simatupang & Okamura (2017), Simatupang et al. (2018)	Toyoura sand, Keisha sand (D_R=50%)	Bio-cementation	Calcium carbonate (EICP)	cTXC (U)	% cement, grain size, degree of saturation, confining stress	0, 0.4, 0.8			
21	Burbank et al. (2013)	Snake river sand (Washington, US)	Bio-cementation	Calcium carbonate (MICP)	cTXC (U)	% cement	2.4-2.6, 3.8-7.4			
22	Chou et al. (2011)	Silica sand	Bio-cementation	Calcium carbonate (MICP)	DS	confining stress, treatment			Weakly cemented	
23	Cui et al. (2017)	China iso standard sand (D_R=30%)	Bio-cementation	Calcium carbonate (MICP)	TXC (U)	% cement, confining stress	1.58-11.87			

Reference		Parent soil	Type of treatment*	Cementing agent	Test type**	Varied parameters (if left empty no variation studied)	Effects		Qualitative Description	Number of tests
							% cement	ΔV_s (m/s)		
24	Cui et al. (2021a, b)	Calcareous sand	Bio-cementation	Calcium carbonate (MICP)	TXC (D)	% cement, confining pressure	0-25			
25	DeJong et al. (2017)	Ottawa 50-70 sand (D_R=60%)	Bio-cementation	Calcium carbonate (MICP)	TXC (D)	% cement	0, 3.5, 4.8, 8.5		Weakly, moderately, heavily cemented	4
26	Feng & Montoya (2015)	Ottawa 50-70 sand (D_R=40%)	Bio-cementation	Calcium carbonate (MICP)	TXC (D)	% cement, confining stress	0, 0.9, 3, 4.3		Weakly, moderately, heavily cemented	14
27	Feng (2015)	Ottawa 50-70 sand (D_R=40%)	Bio-cementation	Calcium carbonate (MICP)	cTXC (U)	% cement	0, 0.6, 0.6, 0.84, 0.9, 1.5	0, 241, 490, 457, 331, 614	Weakly cemented	2
28	Hayashi et al. (2010)	Toyoura sand (D_R=50%)	Bio-cementation	Calcium carbonate (MICP)	cTXC (U), TXC (D)	% cement	0, 1.3, 3			
29	Lee et al. (2020, 2022)	Ottawa F-65 sand (D_R=40%)	Bio-cementation	Calcium carbonate (MICP)	DSS (D), cDSS(U)	% cement, loading	0.1-1	0-100	Weakly cemented	3, 18
30	Lin et al. (2016)	Ottawa 50-70 sand (D_R=41%), Ottawa 20-30 sand (D_R=39%)	Bio-cementation	Calcium carbonate (MICP)	TXC (D), COMP	% cement, confining stress, treatment	0-2.6		Weakly to moderately cemented	

Reference		Parent soil	Type of treatment*	Cementing agent	Test type**	Varied parameters (if left empty no variation studied)	Effects		Qualitative Description	Number of tests
							% cement	ΔV_s (m/s)		
31	Liu et al. (2018)	Calcareous sand (Xisha island, China)	Bio-cementation	Calcium carbonate (MICP)	UNC, BTT, TXC (D)	% cement, confining stress				5, 4, 9
32	Montoya & DeJong (2013)	Ottawa 50-70 sand (D_R=40%)	Bio-cementation	Calcium carbonate (MICP)	TXC (U)	treatment (healing)			Moderately cemented	
33	Montoya & DeJong (2015)	Ottawa 50-70 sand (D_R=40%)	Bio-cementation	Calcium carbonate (MICP)	TXC (D, U)	% cement, loading paths		120, 270, 470, 920, 1220	Weakly, moderately, heavily cemented	
34	Montoya et al. (2013)	Ottawa 50-70 sand (D_R=40%)	Bio-cementation	Calcium carbonate (MICP)	CENT, cDSS (U)	% cement, loading	0, 3, 2.6, 8	195, 505, 1045	Weakly, moderately, heavily cemented	
35	Mujah et al. (2021)	Natural silica sand, Australia (D_R=80-90%)	Bio-cementation	Calcium carbonate (MICP)	TXC (U)	% cement, confining stress, loading paths	0-6		Weakly, moderately, heavily cemented	
36	Na et al. (2022)	Ottawa F-65 sand (D_R=61%)	Bio-cementation	Calcium carbonate (MICP)	TRC	% cement, confining stress	0.5-3.6	100-350		

Reference		Parent soil	Type of treatment*	Cementing agent	Test type**	Varied parameters (if left empty no variation studied)	Effects		Qualitative Description	Number of tests
							% cement	ΔV_s (m/s)		
37	Nafisi et al. (2018)	Medium blasting sand and Ottawa 20-30 sand	Bio-cementation	Calcium carbonate (MICP)	TXC (D)	grain shape & size	0, 2.18, 2.28, 2.97	0, 430-510	Moderately cemented	6
38	Nafisi et al. (2019b)	Ottawa 20-30 & 50-70, Nevada sand (D_R=40%)	Bio-cementation	Calcium carbonate (MICP)	DTT, UNC	grain size		> 900	Heavily cemented	9, 3
39	Nafisi & Montoya (2018), Nafisi et al. (2020)	Ottawa 20-30 & 50-70, Nevada sand (D_R=40%)	Bio-cementation	Calcium carbonate (MICP)	TXC (D)	% cement, confining stress, grain size	variable by sand type	~150, 350, 880	Weakly, moderately, heavily cemented	38
40	Nafisi et al. (2021)	Ottawa 20-30 & 50-70 sand, Nevada sand (D_R=40%)	Bio-cementation	Calcium carbonate (MICP)	TXC (D)	% cement, grain size, loading paths	0-7.5%	0-875	Moderately, heavily cemented	32
41	Riveros & Sadrekarimi (2020a)	Fraser River sand (D_R=16-55%)	Bio-cementation	Calcium carbonate (MICP)	DSS (U)	confining stress, D_r	3-3.3	~70		16
42	Riveros & Sadrekarimi (2020b)	Fraser River sand (D_R=22, 52, 65%)	Bio-cementation	Calcium carbonate (MICP)	cDSS (U)	% cement, confining stress, treatment		~90		25
43	Sasaki & Kuwano (2016)	Toyoura sand, Urayasu sand, silt (D_R=45%)	Bio-cementation	Calcium carbonate (MICP)	cTXC (U)	% cement, % fines, loading				

Reference		Parent soil	Type of treatment*	Cementing agent	Test type**	Varied parameters (if left empty no variation studied)	Effects		Qualitative Description	Number of tests
44	Sharma et al. (2021)	Alluvial Narmada sand (India) (D_R=40%)	Bio-cementation	Calcium carbonate (MICP)	STS, UNC, TXC (U)	treatment	0-9			
45	Tagliaferri et al. (2011)	Ottawa 50-70 sand (D_R=74%)	Bio-cementation	Calcium carbonate (MICP)	TXC (D)	% cement				
46	Terzis et al. (2016)	Itterbeck sand (Netherlands)	Bio-cementation	Calcium carbonate (MICP)	TXC (U)	confining stress, treatment				5
47	Terzis & Laloui (2017)	Itterbeck sand (Netherlands), medium-grained sand (Switzerland)	Bio-cementation	Calcium carbonate (MICP)	TXC (D)	confining stress				
48	Tsukamoto et al. (2013)	Toyoura sand	Bio-cementation	Calcium carbonate (MICP)	TXC (D)	% cement, D_r				15
49	van Paassen (2009)	Itterbeck sand (Germany)	Bio-cementation	Calcium carbonate (MICP)	UNC, TXC (D, U), BTT	% cement, confining stress	27-12		Heavily cemented	45, 11, 8, 17
50	Waller (2011)	Ottawa 50-70 sand (D_R=60%)	Bio-cementation	Calcium carbonate (MICP)	TXC (D)	% cement				
51	Wu et al. (2021)	Ottawa sand	Bio-cementation	Calcium carbonate (MICP)	TXC (D)	% cement, confining stress	0, 4.48-14.25			9, 16

Reference		Parent soil	Type of treatment*	Cementing agent	Test type**	Varied parameters (if left empty no variation studied)	Effects		Qualitative Description	Number of tests
							% cement	ΔV_s (m/s)		
52	Xiao et al. (2018)	Calcareous sand (D_R=47%) (Yongxing island, China)	Bio-cementation	Calcium carbonate (MICP)	cTXC (U)	% cement, confining stress, loading	0, 0.2, 0.4, 0.6			31
53	Xiao et al. (2019a)	Calcareous sand (Yongxing island, China)	Bio-cementation	Calcium carbonate (MICP)	cTXC (U)	% cement, D_r, loading				
54	Xiao et al. (2019b)	Silica sand (D_R=72%)	Bio-cementation	Calcium carbonate (MICP)	TXC (D)	% cement, confining stress	0, 1.8, 3.5, 5.1			
55	Xiao et al. (2021)	Fujian quartz sand	Bio-cementation	Calcium carbonate (MICP)	TXC (D)	% cement, treatment	0-6			
56	Yazdani et al. (2022)	Beach sand (Newport, Oregon)	Bio-cementation	Calcium carbonate (MICP)	TXC (D)	% cement, confining stress	2.4-4.8		Weakly, heavily cemented	
57	Zamani (2017), Zamani & Montoya (2018, 2019)	Nevada sand (D_R=~50%)	Bio-cementation	Calcium carbonate (MICP)	DSS (U), cDSS (U)	% fines	1.58-3.9	~300		14, 32
58	DeJong et al. (2006)	Ottawa 50-70 sand (D_R=35%)	Bio-cementation & Artificial	Calcium carbonate (MICP), gypsum	TXC (U)	treatment, specimen size		360 (MICP), 420 (gypsum)	Moderately cemented	

Reference		Parent soil	Type of treatment*	Cementing agent	Test type**	Varied parameters (if left empty no variation studied)	Effects		Qualitative Description	Number of tests
							% cement	ΔV_s (m/s)		
59	Nafisi et al. (2019b)	Ottawa 50-70, 20-30 sand (D_R=40%)	Bio-cementation	Calcium carbonate (MICP, EICP)	TXC (D)	treatment	0-2.48	310-500	Moderately cemented	2, 3
60	Wang et al. (2021)	Ottawa sand	Bio-cementation & Artificial	Calcium carbonate (MICP), Portland cement	TXC (D)	% cement, confining pressure, treatment	0-8			15,15
Large-scale tests										
61	DeJong et al. (2014)	Ottawa 50-70 sand (D_R=84%)	Bio-cementation	Calcium carbonate (MICP)	UPSCALED			400		
62	Gomez et al. (2018)	Concrete sand (D_R=45%)	Bio-cementation	Calcium carbonate (MICP)	UPSCALED		0.5-5.3	131-967		
63	Hernandez (2018), Darby et al. (2019)	Ottawa 50-70 sand (D_R=38%)	Bio-cementation	Calcium carbonate (MICP)	CENT	% cement	0, 0.8, 1.4, 2.2	0, 80, 210, 530	Weakly, moderately, heavily cemented	4
64	Montoya et al. (2012)	Ottawa 50-70 sand (D_R=40%)	Bio-cementation	Calcium carbonate (MICP)	CENT	loading		500	Moderately cemented	
65	Montoya et al. (2021)	Poorly graded sand (D_R=30%)	Bio-cementation	Calcium carbonate (MICP)	UPSCALED	spatial variability		0-570		

Reference		Parent soil	Type of treatment*	Cementing agent	Test type**	Varied parameters (if left empty no variation studied)	Effects		Qualitative Description	Number of tests
							% cement	ΔV_s (m/s)		
66	San Pablo et al. (2020)	Concrete sand, Delta sand, Covelo River sand	Bio-cementation	Calcium carbonate (MICP)	UPSCALED	spatial variability, treatment	0.4-7.5	0-1300		
67	Sharma et al. (2022)	Alluvial Narmada sand (India) (D_R=40%)	Bio-cementation	Calcium carbonate (MICP)	UPSCALED	treatment, spatial treatment	0-10.62		Heavily cemented	
68	van Paassen et al. (2010)	Itterbeck sand (Germany)	Bio-cementation	Calcium carbonate (MICP)	UPSCALED	% cement	12.6-27.3	81-288		
69	Yazdani et al. (2022)	Beach sand (Newport, Oregon)	Bio-cementation	Calcium carbonate (MICP)	UPSCALED	wave loading, % cement	2.4-4.8		Weakly, heavily cemented	
70	Zamani et al. (2021)	Ottawa F-65 sand (D_R=40%)	Bio-cementation	Calcium carbonate (MICP)	CENT	treatment	1.2-1.5	500		

**Artificial cementation corresponds to cementing agents comparable to bio-cementation but cannot be classified as bio-cementation or natural cementation*

***Test types are: An-TXC for anisotropic triaxial compression, BTT for Brazilian tensile test, cDSS for cyclic direct simple shear, CENT for centrifuge tests, cTXC for cyclic triaxial compression, COMP for compression test, (D) for drained tests, DS for direct shear test, DSS for monotonic direct simple shear test, DTT for direct tensile test, TRC for torsional resonant column, TT for true triaxial, TXC for monotonic triaxial compression, TX-LE for monotonic triaxial lateral extension, (U) for undrained tests, UNC for unconfined compression test, and UPSCALED for large-scale tests at 1-g*

Table 2.2. Summary of globally observed trends in elemental monotonic behaviors of bio-cemented sands before yielding.

	Uncemented loose	**Cemented loose**	**Reference***
Cohesion/tensile strength	Cohesionless	Increases with increases in the magnitude of cementation	Clough et al. (1981), O'Rourke & Crespo (1988), Saxena et al. (1988a), Wang & Leung (2008), **Cheng et al. (2013), Lin et al. (2016), Cui et al. (2017), Liu et al. (2018), Nafisi et al. (2020)**
G_{max} and V_s	-	Increases with increases in the magnitude of cementation	Clough et al. (1981), Acar & El-Tahir (1986), Abdulla & Kiousis (1997), Baig et al. (1997), Cuccovillo & Coop (1997), Fernandez & Santamarina (2001), Schnaid et al. (2001), Haeri et al. (2005), Yun & Santamarina (1998), Lade & Trads (2014), **DeJong et al. (2006), DeJong et al. (2010), Duraisamy & Airey (2012), Soon et al. (2013), Feng & Montoya (2015), Montoya & DeJong (2015), Cabalar et al. (2016), Lin et al. (2016), Liu et al. (2018), Nafisi & Montoya (2018), Riveros & Sadrekarimi (2020a), Nafisi et al. (2021)**
Peak strength	-	Increases with increases in the magnitude of cementation	Clough et al. (1981), Coop & Atkinson (1993), Cuccovillo & Coop (1999), Schnaid et al. (2001), Asghari et al. (2003), Haeri et al. (2005), **DeJong et al. (2010), Chou et al. (2011), Cheng et al. (2013), Tsukamoto et al. (2013), Feng & Montoya (2015), Montoya & DeJong (2015), Lin et al. (2016), Cui et al. (2017), Terzis & Laloui (2017), Liu et al. (2018), Nafisi et al. (2020), Riveros & Sadrekarimi (2020a), Mujah et al. (2021), Nafisi et al. (2021)**
Peak friction angle	State dependent (Decreases with increases in σ', increases with increases in D_R)	Increases with increases in the magnitude of cementation, decreases with increases in σ', increases with increases in D_R	Wissa & Ladd (1964), Saxena & Lastrico (1978), Saxena et al. (1988a), Wang & Leung (2008), **Chou et al. (2011), Cheng et al. (2013), Feng & Montoya (2015), Montoya & DeJong (2015), Cui et al. (2017), Nafisi et al. (2020)**
		Unaffected (gain in strength attributed mostly to other components such as cohesion)	Dupas & Pecker (1979), Clough et al. (1981), Rad & Clough (1982), Abdulla & Kiousis (1997), Yun & Santamarina (1998), **Duraisamy & Airey (2012), Lin et al. (2016), Liu et al. (2018), Riveros & Sadrekarimi (2020a)**
Strain at failure	-	Decreases with increases in the magnitude of cementation, Increases with increases in σ'	Coop & Atkinson (1993), Schnaid et al. (2001), Asghari et al. (2003), **Montoya & DeJong (2015), Cui et al. (2017), DeJong et al. (2017), Mujah et al. (2021), Nafisi et al. (2021)**

** references in **bold** studied bio-cementation as a cementing agent while the other references studied other cementing agents and are included where information on bio-cementation was unavailable/limited.*

Table 2.3. Summary of globally observed trends in elemental monotonic behaviors of bio-cemented sands after yielding.

	Uncemented loose	**Cemented loose**	**Reference***
Post-peak stress/strain behavior (low confinement)	Strain-hardening (ductile)	Strain-softening (brittle)	Clough et al. (1981), Abdulla & Kiousis (1997), Schnaid et al. (2001), Asghari et al. (2003), **DeJong et al. (2006), Tsukamoto et al. (2013), Liu et al. (2018), Mujah et al. (2021)**
Degradation of bonds	-	Transition from global (bulging) to increasingly localized failures (shear banding more localized) with increase in the magnitude of cementation	Fernandez & Santamarina (2001), Asghari et al. (2003), Wang & Leung (2008), **DeJong et al. (2006), Waller (2011), Montoya & DeJong (2015), Lin et al. (2016), Cui et al. (2017), DeJong et al. (2017), Soriano et al. (2017), Liu et al. (2018), Nafisi et al. (2019a), Mujah et al. (2021), Yazdani et al. (2022)**
Volumetric strain/behavior (low confinement)	Contractive	Initially contractive volumetric behavior followed by dilative volumetric behavior. Increased dilatation for finer sand and rougher particle surfaces	O'Rourke & Crespo (1988), Schnaid et al. (2001), Asghari et al. (2003), Haeri et al. (2005), Wang & Leung (2008), **DeJong et al. (2010), Chou et al. (2011), Montoya & DeJong (2013), Tsukamoto et al. (2013), Feng & Montoya (2015), Montoya & DeJong (2015), Lin et al. (2016), Cui et al. (2017), Xiao et al. (2019a), Terzis & Laloui (2019), Mujah et al. (2021), Nafisi et al. (2021), Yazdani et al. (2022)**
Effect of confinement on post-peak stress/strain behavior	Strain-hardening (ductile)	Transition from strain-softening (brittle) to strain-hardening (ductile) with increases in σ', Limited influence on shear strength	Coop & Atkinson (1993), Abdulla & Kiousis (1997), Yun & Santamarina (1998), **Feng & Montoya (2015), Nafisi et al. (2020), Mujah et al. (2021)**
Effect of confinement on volumetric strain/behavior	Increasingly contractive volumetric behavior with increases in σ'	Increasingly contractive volumetric behavior with increases in σ'	Schnaid et al. (2001), Asghari et al. (2003), Yun & Santamarina (1998), **Nafisi et al. (2020), Mujah et al. (2021)**
Shear stiffness/modulus	Decreases with increasing shear strain	Decreases with increasing shear strain, Large-strain stiffness close to clean sands (with small increases from cementation related densification and remaining bonds)	Cuccovillo & Coop (1997), **Montoya et al. (2012), Montoya & DeJong (2013), Montoya et al. (2013), Lin et al. (2016), Simatupang et al. (2018), Nafisi et al. (2020)**
Rate of dilation	Maximum at yield	Fast (at low confinement, small strains), slow (at high confinement, large strains), Maximum after yield	Leroueil & Vaughan (1990), Abdulla & Kiousis (1997), Asghari et al. (2003), Lade & Trads (2014), **Feng & Montoya (2015), Lin et al. (2016), Liu et al. (2018)**

	Uncemented loose	Cemented loose	Reference*
Residual cohesion (Strains > 10%)	None – cohesionless	None to some cohesion left depending on cementation level and shearing localization (shearing reported up to 20% strain in monotonic loading)	Clough et al. (1981), **Chou et al. (2011), Lin et al. (2016), Nafisi et al. (2020)**
Residual friction angle (Strains > 10%)	-	Increases with increases in the magnitude of cementation, Decreases with increases in σ', Increases with increases in D_R	Clough et al. (1981), **Feng & Montoya (2015), Nafisi et al. (2020)**
Strain required to reach CS	Clearly goes to critical state at ~10%	Critical state not typically obtained at tested strain levels (<~20%) due to continued and incomplete bond breakage and strain localization at shear bands	Leroueil & Vaughan (1990), Lee et al. (2004), Wang & Leung (2008), Rios et al. (2012)**, Lin et al. (2016)**
Residual/ CS strength	-	Expected to increase with increases in the magnitudes of cementation	Saxena et al. (1988a), Schnaid et al. (2001), Wang & Leung (2008), Rios et al. (2012), **DeJong et al. (2006), Tsukamoto et al. (2013), Feng & Montoya (2015), Montoya & DeJong (2015), Lin et al. (2016), Hernandez (2018), Nafisi et al. (2020), Mujah et al. (2021)**
Loading paths		Failure at lower axial strain under radial extension and constant q loading compared to constant p and compression tests	**Montoya & DeJong (2015), Mujah et al. (2021), Nafisi et al. (2021)**

references in **bold studied bio-cementation as cementing agent while the other references studied other cementing agents and are included where information on bio-cementation was unavailable/limited.*

Table 2.4. Summary of globally observed trends in elemental cyclic behaviors of bio-cemented sands.

	Uncemented loose	**Cemented loose**	**Reference***
Cyclic resistance	-	Increases in the number of cycles to trigger liquefaction with increases in the magnitude of cementation; Decreases in the number of cycles to trigger liquefaction with increases in σ'; Increases in the number of cycles to trigger liquefaction for finer-grained sands	Seed (1976), Youd & Perkins (2017), Salomone et al. (1978), Dupas & Pecker (1979), Frydman et al. (1980), **Hayashi et al. (2010), Montoya et al. (2012), Burbank et al. (2013), Montoya et al. (2013), Han et al. (2016), Sasaki & Kuwano (2016), Feng & Montoya (2017), Zamani (2017), Xiao et al. (2018), Simatupang et al. (2018), Xiao et al. (2019a), Riveros & Sadrekarimi (2020b), Lee et al. (2022)**
Degradation of CRR with loading duration $CSR = aN^{-b}$	-	b value is similar to uncemented sands and/or slightly increases with cementation	**Okamura (2018, pers.com.), Riveros & Sadrekarimi (2020b)**
		b value decreases with cementation	**Hernandez (2018), Xiao et al. (2018), Xiao et al. (2019a)**
Pore pressure generation	-	Generation of excess pore pressure is suppressed with increases in the magnitude of cementation, slower pore pressure dissipation following loading due to slightly reduced hydraulic conductivity (dependent on cementation level)	**Hayashi et al. (2010), Montoya et al. (2012), Montoya & DeJong (2013), Montoya et al. (2013), Montoya & DeJong (2015), Han et al. (2016), Cui et al. (2017), Xiao et al. (2018), Xiao et al. (2019a)**
Strain accumulation	-	Larger strain increment/cycle for coarse sands and slower strain increment/cycle for fine sands	**Han et al. (2016), Sasaki & Kuwano (2016), Lee et al. (2022)**
Post-cyclic reconsolidation strains	-	Similar, no significant changes	**Simatupang et al. (2018), Riveros & Sadrekarimi (2020b), Lee et al. (2022)**

references in **bold studied bio-cementation as cementing agent while the other references studied other cementing agents and are included where information on bio-cementation was unavailable/limited.*

Table 2.5. Summary of available constitutive models for bio-cemented sands/structured soils/weak rocks.

Reference		Baseline Formulation	Target Application	Related Work	Targeted Behavior	Calibration (C) / Modification (M) / Extensions (E)	Validated	Validation Base	Developers' evaluation of model
1	Fauriel (2012) or ACMEG-B 2012	ACMEG (Laloui and François 2009)	Bio-cemented sands	none	gain in strength & stiffness	(E) introduction of scaling parameters accounting for densification and bonding+ addition of bonding hardening modulus	yes	drained triaxial compression tests on bio-cemented Itterbeck sand (van Paassen 2009) & drained triaxial compression tests on bio-cemented Ottawa 50-70 sand	reasonably reproduce all behavioral features of bio-cemented soils, dilatancy slightly underestimated by the model
					degradation of bonds	(E) degree of bonding parameter is a decreasing exponential relationship, a function of volumetric and deviatoric plastic strains			
2	Nweke and Pestana (2017)	Nor-Sand (Jefferies 1993)	Weakly bio-cemented sands	none	gain in strength	(E) failure criterion incorporating cementation	yes	drained triaxial compression tests on cemented Ottawa 50-70 sand	limited to triaxial conditions and dependent on relative density for which the measurements of maximum and minimum void ratios are not yet clear
					gain in stiffness	(E) addition of cementation to the shear modulus equation			
					degradation of bonds	(E) evolution /damage law for cementation			
3	Gai and Sanchez (2018)	MCC	Bio-cemented sands	none		(M) subloading formulation	yes	drained triaxial compression tests on Ottawa 50-70 treated with MICP	qualitatively and quantitatively captured the response of bio-cemented sands, overpredicted the dilation in the
					gain in strength	(E) enlarged yield surface to the left (tensile strength) and to the right (higher			

						strength) as a function of plastic strain increment			radial extension due to the use of a single set of input parameters for all stress paths, did not account for localization
					degradation of bonds	(E) formulation of 3 hardening parameters and their evolution/damage law			
4	Gajo et al. (2019)		Bonded or cemented soils	Gajo et al. (2015)		(M) specialized on materials with only reactive bonds such as carbonate cemented sandstone and bio-cemented sand	yes	triaxial compression tests on bio-cemented Ottawa sand, soft oedometer tests on silica sand treated with lime	overpredicted elastic volumetric strain due to simplifying assumptions such as associative flow rule, elastic isotropy, invariance of stiffness with stress level and bulk stiffness with soil densification
5	Xiao et al. (2021)		Bio-cemented (MICP) calcareous sands		gain in strength based on thermodynamics	(E) incorporation of a bonding variable (a bond structure index)	yes	undrained cyclic triaxial tests of uncemented and MICP-cemented sands (Xiao et al. 2019a)	model sufficiently captures cyclic stress-strain hysteresis & excess pore pressure generation in MICP-treated sand
					energy dissipation and plastic deformation during cyclic loading	(E) degradation law in terms of plastic strain rate			

6	Ahmed et al. (2022)	Hypoplastic material model (Fuentes 2018)- in ABAQUS	Bio-cemented sands		monotonic response	(C) calibration process of initialization and model parameters	yes	drained monotonic triaxial tests on MICP-cemented sands (Nafisi et al. 2020)	calibration process reasonably predicts initial stiffness for uncemented and lightly cemented but overestimates residual strength for moderately and heavily cemented sands
7	Lu et al. (2022)	Multisurface	Bio-cemented sands, cemented clays	Zhang et al. (2007)	tensile strength	(E) addition of cementation state parameter to represent tensile strength	yes	Isotropic, uniaxial, triaxial tests under monotonic (Horpibulsuket al. 2004; Nguyen et al. 2017) and cyclic loading (Xiao et al. 2018)	
					cementation degradation	(E) evolution law for the degradation of the cementation			
8	Pekau and Gocevski (1989)	Bounding surface plasticity	Naturally and artificially cemented sands	Pooroosh asb and Pietruszczak (1985)	tensile strength and yield	(E) addition of cementation parameter to represent tensile strength	yes	monotonic drained and undrained triaxial tests on natural weakly cemented sands and artificially cemented sands (Clough et al. 1981, Dupas and Pecker 1979), cyclic undrained tests (Ishihara et al. 1975)	
					plastic potential and yield surface forms	(M) the form of the equations for yield surface and plastic potential, and the accumulation of plastic shear strain,			

9	Reddy and Saxena (1992)	Lade's Model Kim and Lade (1988)	Portland-cemented sands	none	full response of cemented sands	(C) selection of 13 input parameters	yes	tensile tests on Monterey sand with 2% Portland Cement	underestimates the volumetric behavior of cemented sands due to the complexity in determining some input parameters
		Endrochronic model (Valanis and Peter 1988, Sengupta 1989)	Portland-cemented sands	none	full response of cemented sands	(C) selection of 12 input parameters	yes	tensile tests on Monterey sand with 2% Portland Cement	does not predict well volume change due to the selection of some input parameters
10	Sun and Matsuoka (1999)	Spatially Mobilized Plane (SMP) (Matsuoka and Nakai 1974) and t_{ij} sand model (Nakai 1989)	Cemented sands and unsaturated soils	none	gain in strength	(E) inclusion of a cohesion parameter	yes	Triaxial compression, extension, and true triaxial tests on Portland-cemented Toyoura sand (Hirai et al. 1989)	
11	Nova et al. (2003)		Bonded or cemented soils	none	gain in strength	enlarged yield surface to the left (tensile strength) and to the right (higher strength) as a function of damage	yes	drained isotropic triaxial compression tests on calcareous soft rocks, oedometers tests on calcareous materials (chalk) and chemically induced degradation of bonding	satisfactory for the simulation of brittle-ductile transition and the corresponding level of strain, limited scope of application due to the assumption of isotropy
					transition from brittle to ductile behavior	implementation of bond degradation due to mechanical and chemical weathering			

12	Yu et al. (2007) or CASM-n	CASM (Yu 1998)	Bonded or cemented soils	none	gain in strength	(E) enlarged yield surface to the left (tensile strength) and to the right (higher strength) as a function of damage	yes	drained triaxial compression tests on silty sand cemented with Portland cement	did not appropriately account for the axial strain at failure which is better modeled using a multi-surface framework
					gain in stiffness	(E) stiffness as a function of strength induced by bonding			
					volume change	(E) added cohesion in the stress-dilatancy relationship + non associative flow rule			
13	Gao and Zhao (2012)	Anisotropic failure criterion (Gao et al. 2010)	Cemented sands	none	gain in strength & stiffness	(E) introduction of tensile strength	yes	drained triaxial compression tests on cemented Ottawa sand without the consideration of fabric anisotropy (all relevant parameters set to zero) since these tests did not provide any information on anisotropy	limitations: postulation that the loading direction does not affect the tensile strength, the assumption that bonding degrades due to plastic deformations only, consideration of inherent anisotropy only and the invariance of fabric during

					degradation of bonds	(E) inclusion of a fabric tensor and damage/debonding law		true triaxial tests on clean Toyoura sand to evaluate the implementation of fabric	deformation, no particle crushing
					yield surface	(M) frictional component replaced with a hardening parameter			
14	Rahimi et al. (2015, 2018)	Imam et al. (2005)	Cemented sands	none	gain in stiffness	(E) addition of cementation to elastic parameters	yes	drained triaxial compression tests on sands cemented with Portland cement	satisfactorily captured stress-strain and volumetric responses of cemented sands but the softening behavior was not captured as well for high cement content
					gain in strength	(E) enlarged yield surface to the left (tensile strength) and to the right (higher strength) as a function of plastic strain increment			
					dilatancy	(E) cohesion term + evolution law in the dilatancy relationship			
					multisurface	(M) reformulation using bounding surface plasticity			only assessed for monotonic response
15	Rios et al. (2016)	CASM (Yu 1998)	Bonded or cemented soils	Arroyo et al. (2012)		(C) calibration process of initialization and model parameters	yes	drained and undrained isotropic triaxial compression tests on Portland-cemented silty sand	

16	Panico et al. (2018)	CASM (Yu 1998)	Bonded or cemented soils	Rios et al. (2016)	multisurface	(M) reformulation using bounding surface plasticity with a kinematic hardening rule	yes	drained and undrained triaxial compression tests on Portland-cemented Porto silty sand (Rios et al. 2014)	
17	Zhang et al. (2021) SANISA ND-C	Bounding surface plasticity	Cemented sands	Dafalias and Manzari (2004)	monotonic and cyclic loading of cemented sand	(E) / (M) incorporation of a bonding strength variable (E) link of critical state variables, stress ratio & void ratio of cemented sand to the initial cement content	yes	drained monotonic triaxial tests on Portland-cemented Ottawa sand (Wang and Leung 2008), drained monotonic triaxial tests and undrained cyclic simple shear tests on silica-based grouted sand (Porcino et al. 2012), drained and undrained monotonic triaxial tests on destructured and naturally cemented granitic residual soils (Rodrigues, 2003)	model can capture the main features of the mechanical behavior of cemented sand well, including cement-induced enhancements of stiffness, strength, dilatancy and liquefaction resistance

18	Fu et al. (2022)	Hypoplastic model (Gudehus 1996, Bauer 1996, Huang et al. 2008)	Cemented sand and gravel			(E) damage-dependent void ratio term added to account for geometrical constraints due to cementation (E) damage factor introduced to reflect the effect of cementation on the peak strength (M) reformulation of barotropy component of stiffness factor	yes	large-scale triaxial tests, consolidated-drained (CD) static tests and consolidated-undrained (CU) dynamic tests, on Portland-cemented gravel (Fu et al. 2020)	model capable of capturing most of the important behaviors of cemented materials (stiffness, strength, dilation, and brittleness)
19	Hirai et al. (1989)	MCC	Monotonic response of Tough-lock improved sandy soils	none	plastic potential surface	(M) non-associative flow rule	yes	one series of drained and undrained TXC & TXE on stabilized Toyoura sand samples	does not consider kinematic hardening & therefore not applicable to cyclic loading
					isotropic hardening	(M) plastic deformations related to deviatoric deformations also			
						(E) multisurface formulation (2 surfaces)			
20	Kavvadas and Amorosi (2000) or Model for Structured Soils (MSS)	MCC	Structured soils	none	gain in stiffness	(E) nonlinear small strain stiffness response in the elastic domain	yes	drained and undrained, isotropic and anisotropic triaxial compression tests on stiff overconsolidated Vallericca Clay (Italy)	satisfactory for the stress levels they were calibrated for but not as much for higher pressures
						(E) multisurface formulation			
					degradation of bonds	(E) inclusion of damage-type mechanism to shrink			

						yield surface upon degradation of bonds			
						(M) kinematic hardening rule for structure and anisotropy			
21	Vatsala et al. (2001)	MCC	Bonded or cemented clays	none	gain in strength and bond degradation	(E) additive elastoplastic model for the cementation bond component	yes	undrained triaxial compression test results on Osaka Clay, Calcarenite, Marl Clay and Gloucester Clay	some assumptions such as constant bond strength across all confining stresses can be improved, anisotropy not included
22	Lee et al. (2004)	MCC	Cement-treated clays	none	elastoplastic deformation at beginning of shearing	(M) parameter λ' instead of κ (slope of unload-reload portion of e-ln p' curve)	yes	drained triaxial tests on Portland cement-treated clay (illite)	quantitative agreement at low confining stresses and qualitative agreement at high confining stresses which is justified by the use of a single set of parameters in the calibrations
					gain and degradation of strength and stiffness	(E) introduction of bonding stress ratio m which is the sum of the CS stress ratio & additional strength from cementation			
23	Arroyo et al. (2012)	CASM (Yu 1998)	Cement-treated clays	none	tensile strength and yield	(M) plastic potential function	yes	undrained triaxial compression tests and oedometer tests on Bangkok clay and cement mixtures	did not quantitatively capture the experimental results, only qualitatively
					elastic parameters affected by bonding	(M) slope of unload-reload line			
					degradation of bonds	(E) evolution law for bonding			

24	Nguyen et al. (2014, 2017)	MCC	Cement-treated clays/structured clays		gain in stiffness & strength	(E) addition of mean effective stress due to cementation	yes	undrained triaxial compression tests on cement-treated Aberdeen soil, Singapore marine clay, Ariake clay, Ballina Clay and Kaolin Clay	cementation effectively captured, limitations: kinematic hardening based only on volumetric strain increment, cyclic loading cannot be accommodated
					degradation of bonds	(E) curved failure envelope (low stresses) which merges back to the envelope for uncemented (high stresses)			
					yield surface	(M) non-associative flow rule, plastic potential function based on the energy dissipation equation			
25	Gajo et al. (2015)	MCC	Bonded or cemented soils	none	gain in stiffness & bond degradation	(E) introduction of cross-scale functions for coupling chemical and mechanical processes responsible for the macrostructure behavior i.e., precipitation and the degradation of cementation	yes	uniaxial compression tests, Brazilian tensile tests and soft oedometer tests on Gravina calcarenite samples (Italy)	model initially applied for cemented clays but correctly reproduces the mechanical response of compacted silty sands
					gain in strength	(E) enlarged yield surface to the left (tensile strength) and to the right (higher strength) as a function of plastic strain increment			
26	Chong (2019)	MCC	Cement-treated clays	none	gain in strength	(E) enlarged and shifted yield surface to the left	no		

					degradation of bonds	(E) evolution/damage law for the cementation as a function of plastic shear strains (degradation rate parameter)			
27	Yamada et al. (2022)	The super-subloading Cam-Clay model (Asaoka et al. 2002)	Cement-treated soils		gain in strength	(E) translation of loading surface into the negative mean effective stress	yes	Oedometer tests and undrained triaxial compression tests on undisturbed and remolded cement-treated clayey soil	
					degradation of bonds	(E) degradation of the cementation-related translation with damage accumulation			
					gain in stiffness	(E) addition of cementation-related variable to effective mean stress to avoid negative stresses			
28	Vaunat and Gens (2003)		Soft rocks and hard soils	none	gain in strength and bond degradation	additive damage law for the brittle cementation to the clay-like ductile component	no	no	capable of capturing transition between soft rock and a hard soil and the degradation of strength and stiffness
29	Yang et al. (2011, 2008)	Bounding surface plasticity	Unsaturated structured loess	Vaunat and Gens (2003)	gain in strength	(E) incorporation of the effect of suction due to desaturation for enlarging the yield surface	yes	simple shear (Alonso et al. 1990) and cyclic triaxial tests on	The 2008 model was able to reproduce the volumetric strain accumulation with

					structure damage	(E) structure damage law		natural loess from France	the load cycles but it was complicated and described structure damage on the microscopic scale, required many input parameters and did not reflect well the hysteretic behavior under cyclic loading, the 2011 model improved structure damage on a macroscopic scale but some parameters remain difficult to be measured
30	Ciantia and di Prisco (2016)	Gens and Nova (1993), Nova et al. (2003)	Soft rocks	none	hydro-chemical weathering/ degradation of bonds	(E) weathering functions and chemical damage using a multiscale (micro to macro) simplified upscaling procedure (M) hardening rule to capture consequences of short-term and long-term debonding	yes	uniaxial compression tests, Brazilian tensile tests and soft oedometer tests on Gravina calcarenite samples (Italy)	localization not considered

31	Bruno et al. (2020)	Bounding surface plasticity	Unsaturated cemented soils	Gallipoli and Bruno (2017)	isotropic loading and the associated progressive breakage of intergranular cementation	(E) normal compression line describing the virgin behavior of cemented and uncemented soils under unsaturated and saturated conditions	yes	isotropic loading-unloading tests on Portland-cemented and uncemented silty sand (weathered Porto granite) under saturated and unsaturated conditions (Arroyo et al. 2013)	
32	Rumpelt (1990)	MCC-extended	Calcarenite (soft rocks)	none		(C) selection of input parameters	yes	uniaxial consolidation tests and simple shear tests for calcarenite and the Cap model was also validation against simple shear tests for cemented sands (Monterey sand and Portland cement)	able to handle overconsolidated materials and that the K_o prediction is not accurate
		Cap model				(C) selection of 14 model parameters			
33	Gens and Nova (1993)	Nova (1988)	Bonded soils and weak rocks	none	gain in strength	(E) enlarged yield surface to the left (tensile strength) and to the right (higher strength) as a function of damage		qualitatively compared to isotropic compression, triaxial compression and	limited scope of application due to the simplicity of the model

					degradation of bonds	(E) hardening modulus dependent on conventional plastic hardening (increase or decrease in size of yield surface) and degradation of bonds (shrinking of yield surface)		K_0-consolidated responses but not explicitly validated against experimental data	

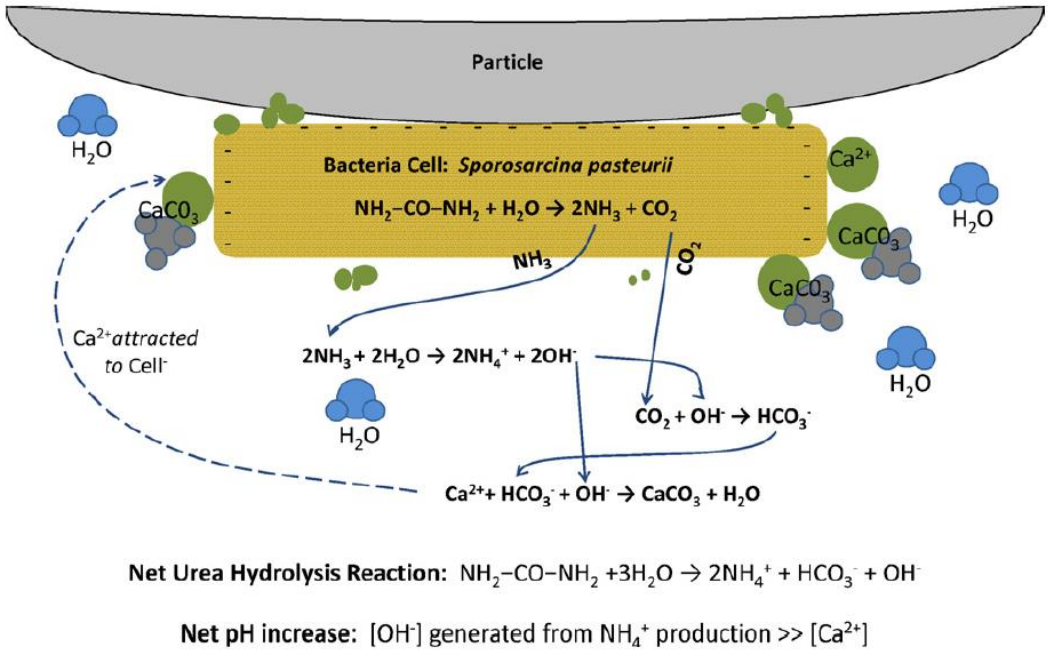

Figure 2.1. Reaction network for bio-mediated calcite precipitation using ureolysis, adapted from DeJong et al. (2010).

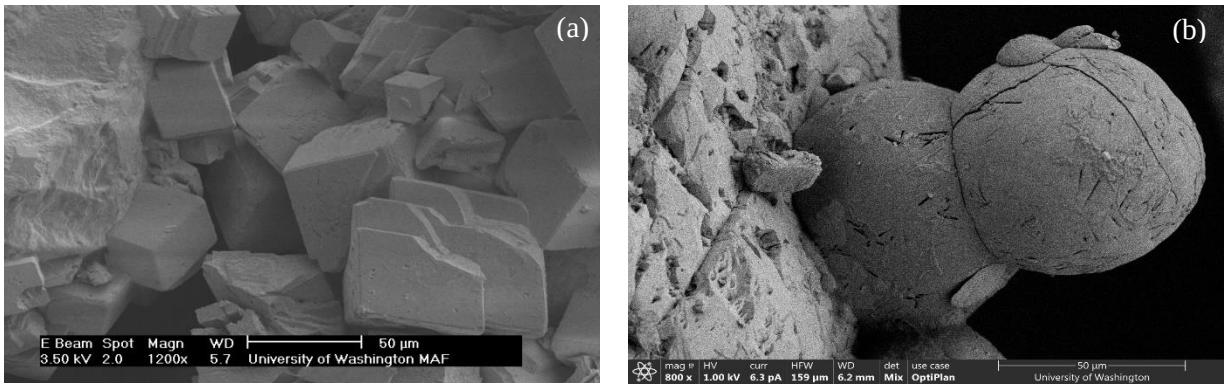

Figure 2.2. SEM images highlighting the different mineralogies of MICP bio-cementation precipitates: (a) calcite, (b) vaterite, adapted from Burdalski & Gomez (2020).

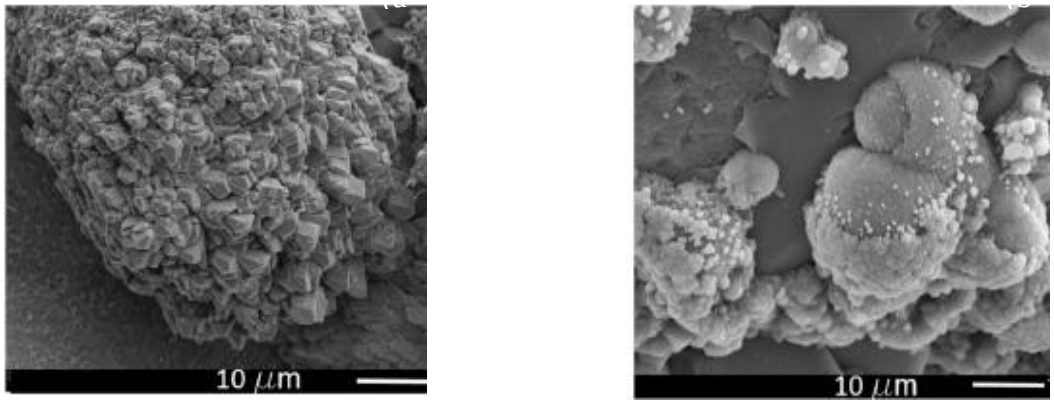

Figure 2.3. SEM images highlighting the different crystal associations and sizes of MICP bio-cementation precipitates: (a) hierarchical, (b) irregular, adapted from Nafisi et al. (2019a).

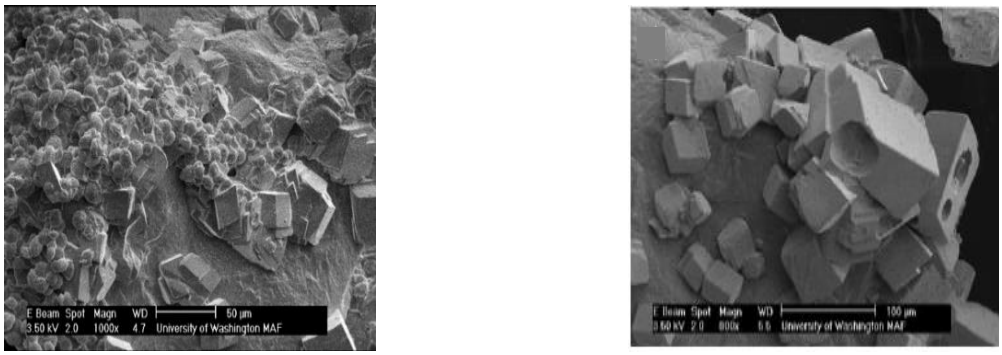

Figure 2.4. SEM images highlighting the intermediate morphologies of MICP bio-cementation precipitates, adapted from Burdalski & Gomez (2020) and Burdalski (2020).

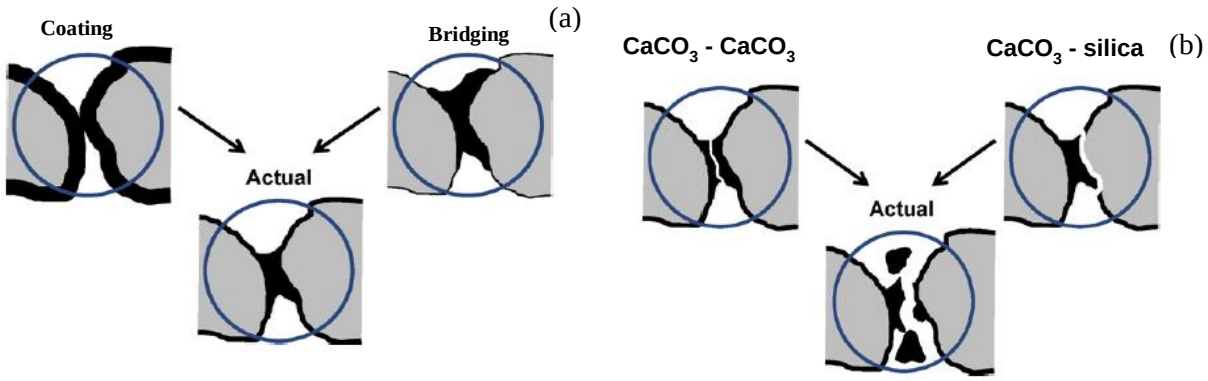

Figure 2.5. Schematic illustrations of (a) the potential particle-level distribution of bio-cementation precipitates, and (b) their failure mechanisms, adapted from DeJong et al. (2010).

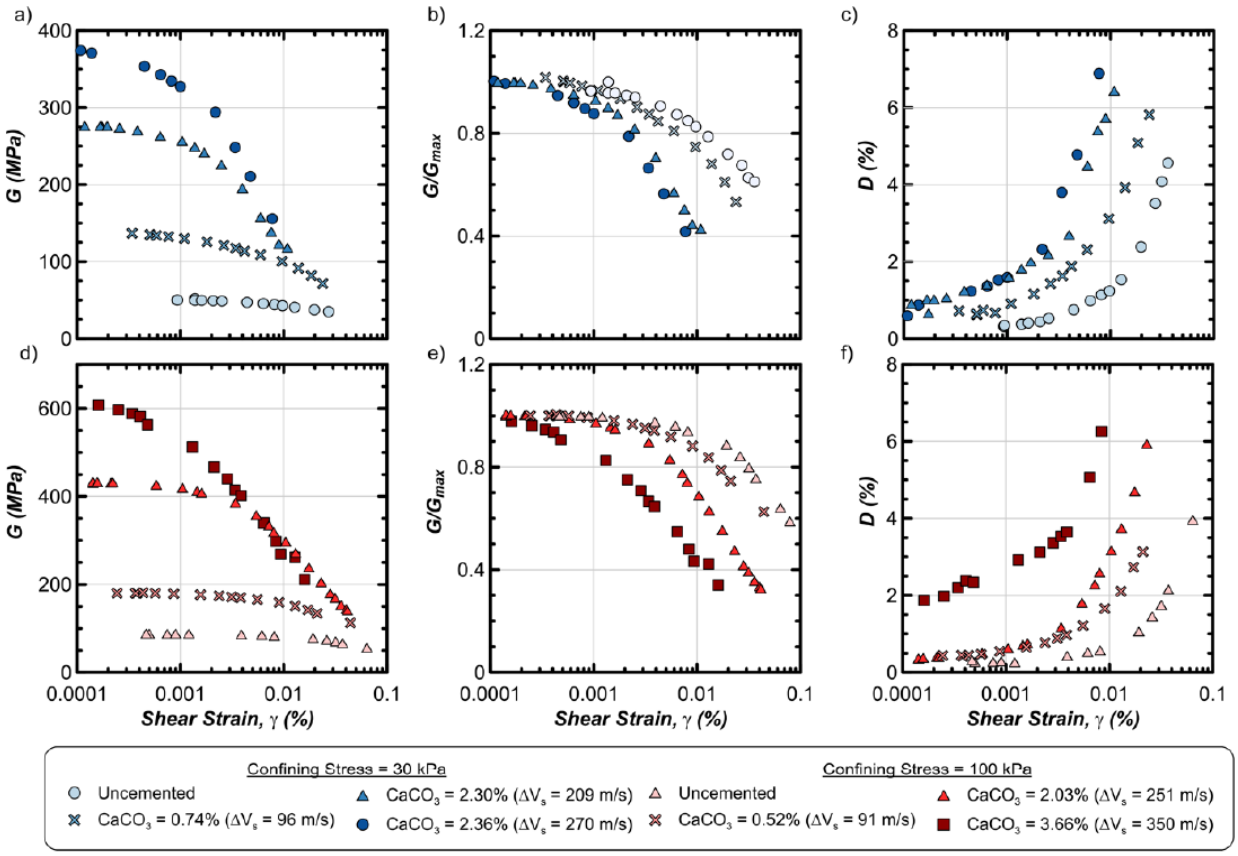

Figure 2.6. Modulus reduction and damping curves obtained from resonant column tests on Ottawa F-65 sand (D_R=61%) at varying levels of cementation and confining stresses of 30 and 100 kPa, adapted from Na et al. (2022).

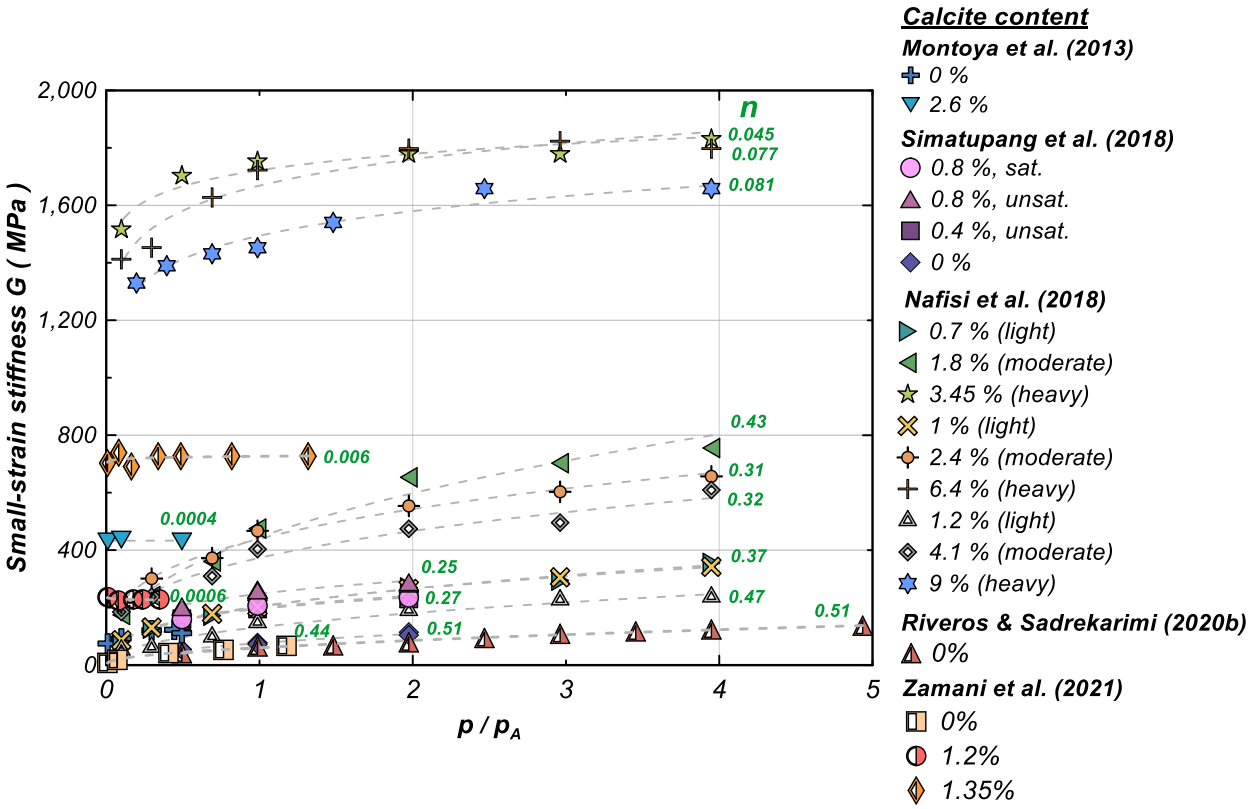

Figure 2.7. Fitting of the reported small-strain shear stiffness values from experimental studies with a power equation as a function of the normalized confining stress [$G = G_o(p/p_A)^n$].

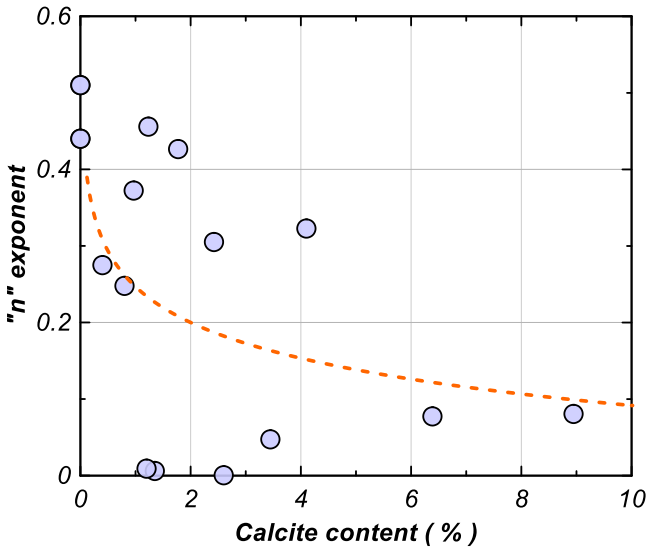

Figure 2.8. Fitting of the variation of the exponent "n" in $G = G_o(p/p_A)^n$ as a function of calcite content.

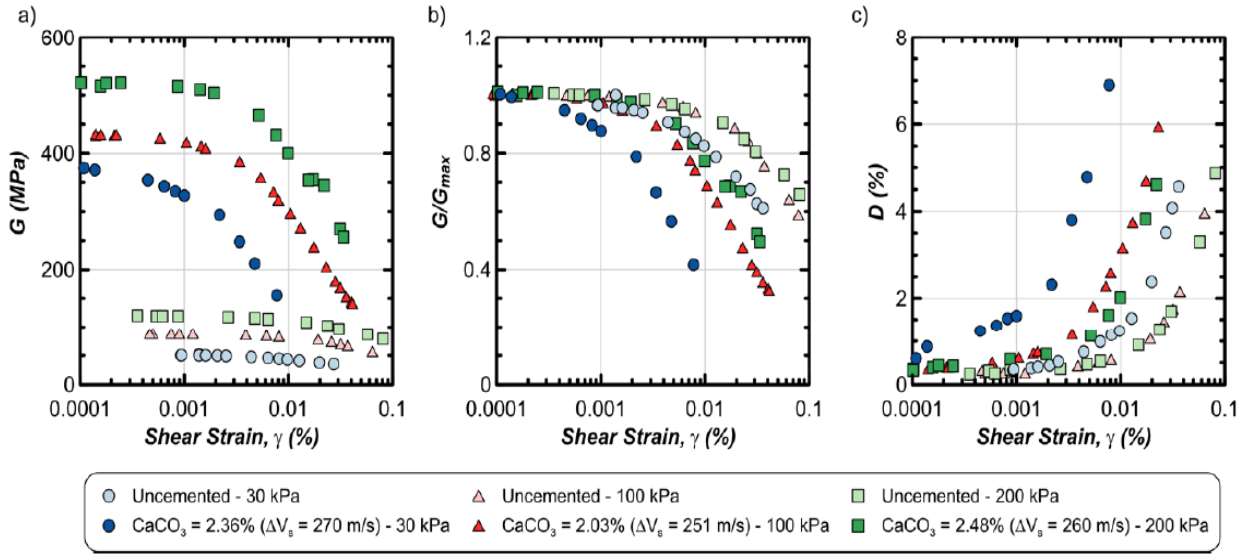

Figure 2.9. Modulus reduction and damping curves obtained from resonant column tests on Ottawa F-65 sand (D_R=61%) at increasing confining stresses (30, 100, 200 kPa), adapted from Na et al. (2022).

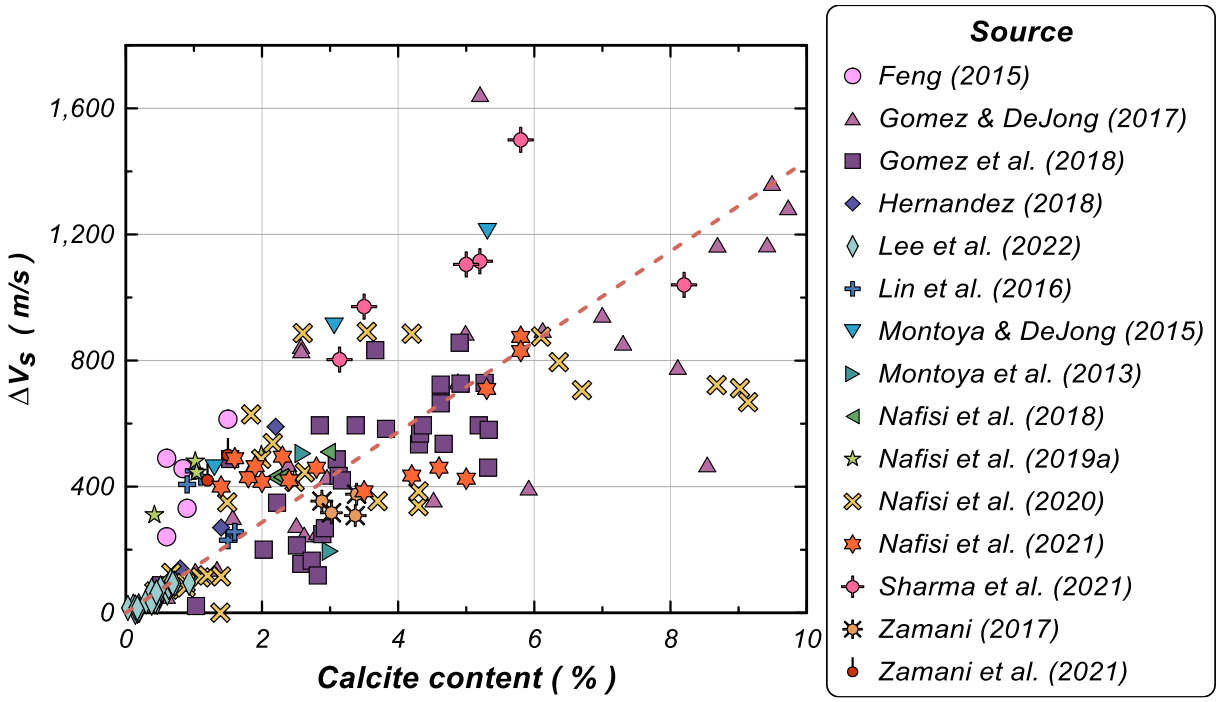

Figure 2.10. Synthesized lab and field data correlating the change in shear wave velocity for bio-cemented sands and their and calcite content in percentage by mass.

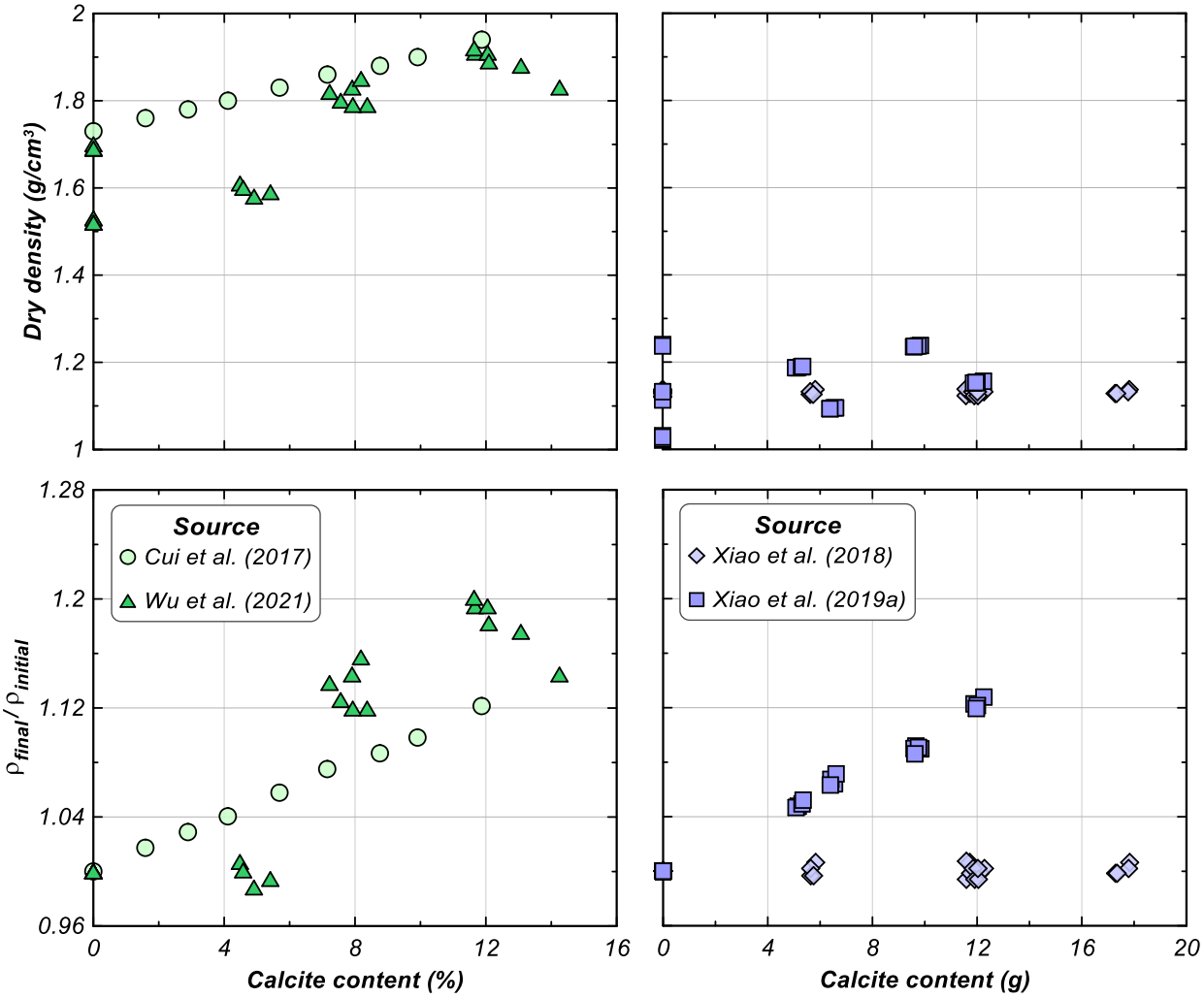

Figure 2.11. The effect of calcite content on the dry density of bio-cemented sands in terms of calcite content in percent and in grams as reported by experimental studies (top row) and the effect of calcite content on the ratio of improvement of cemented to uncemented dry densities in terms of calcite content in percent and in grams as reported by experimental studies.

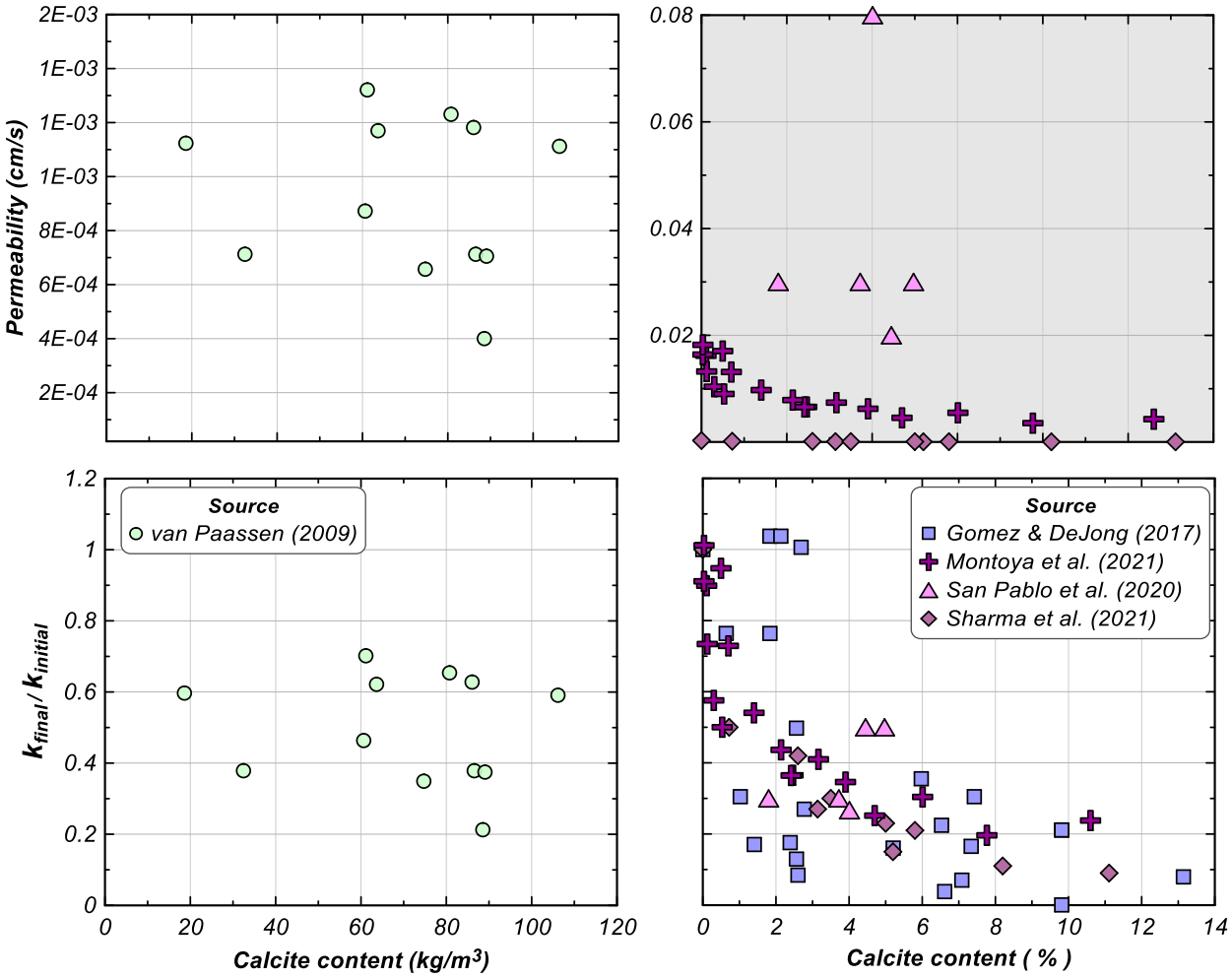

Figure 2.12. The effect of calcite content on the permeability of bio-cemented sands: (left column) in terms of calcite content in kg/m^3, and (right column) in terms of calcite content in %. Effect of calcite content quantified in terms of absolute permeabilities (top row) as well as in terms of ratio of permeabilities (bottom row) (grey shading indicates a change in the y-axis scale).

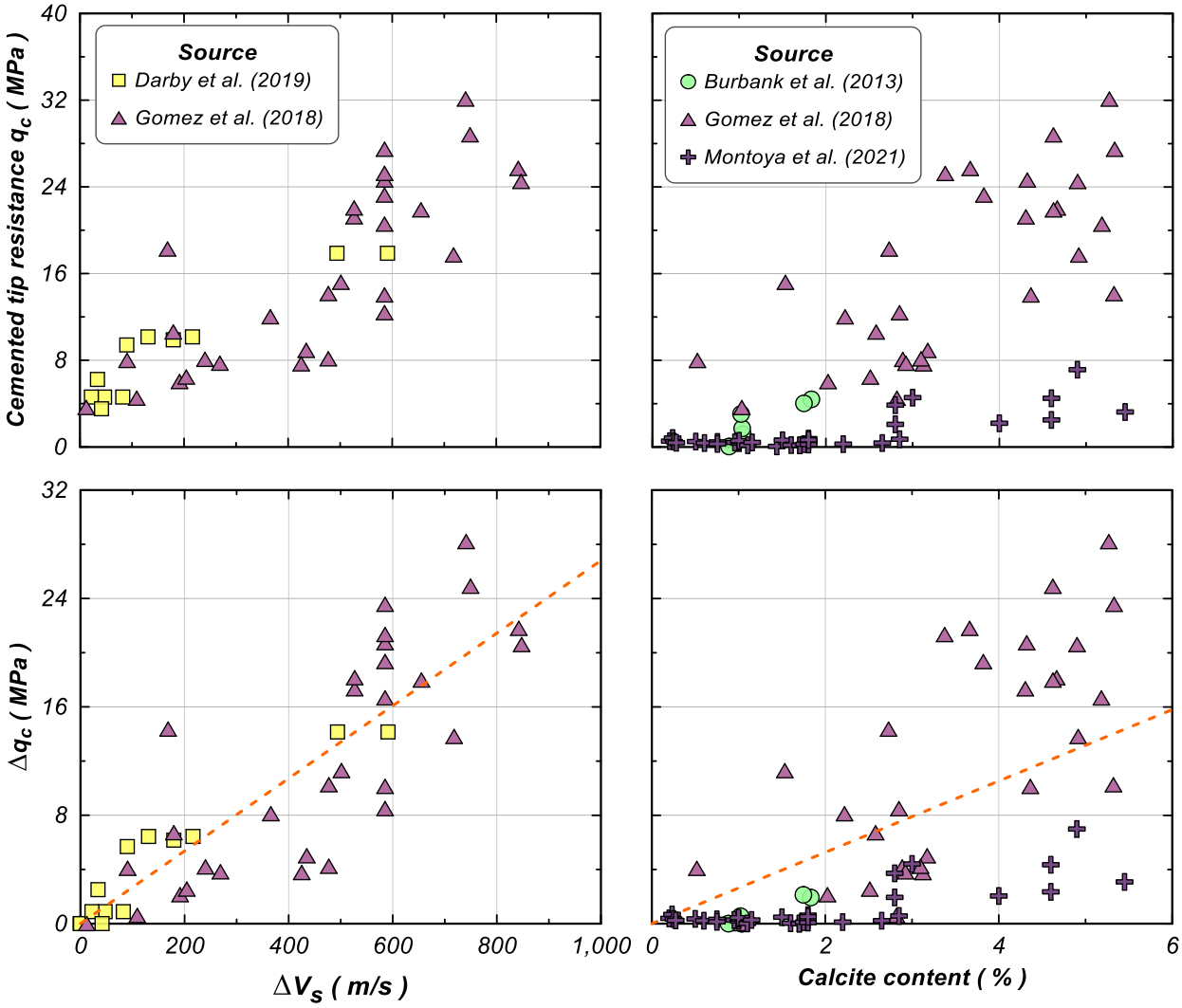

Figure 2.13. The effect of bio-cementation on the cone tip resistance of sands in absolute terms (top) and in incremental terms (difference between bio-cemented and uncemented baseline tip resistances) (bottom).

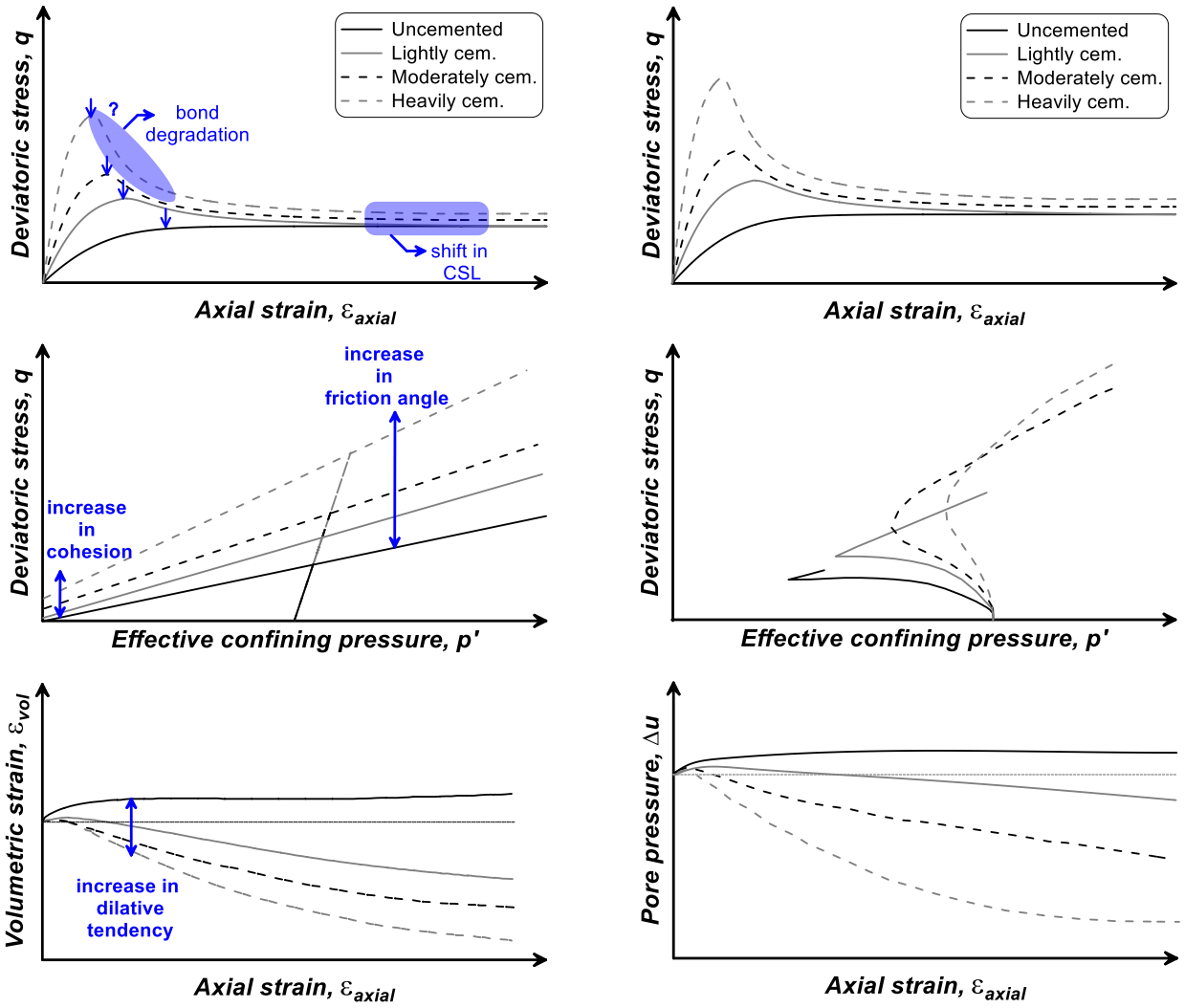

Figure 2.14. Conceptual schematics of the expected monotonic response of initially loose bio-cemented sands for different levels of cementation, drained on the left and undrained on the right.

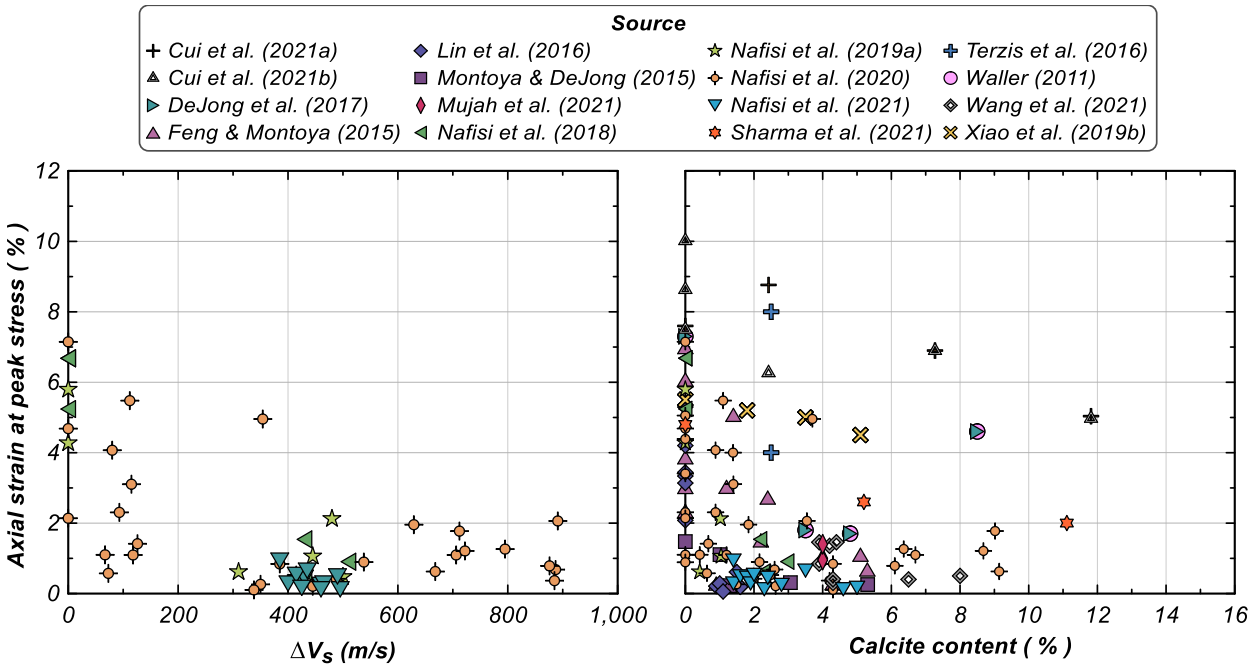

Figure 2.15. The effect of bio-cementation on the axial strain at peak stress in triaxial tests as a function of calcite content (left) and change in shear wave velocity (right).

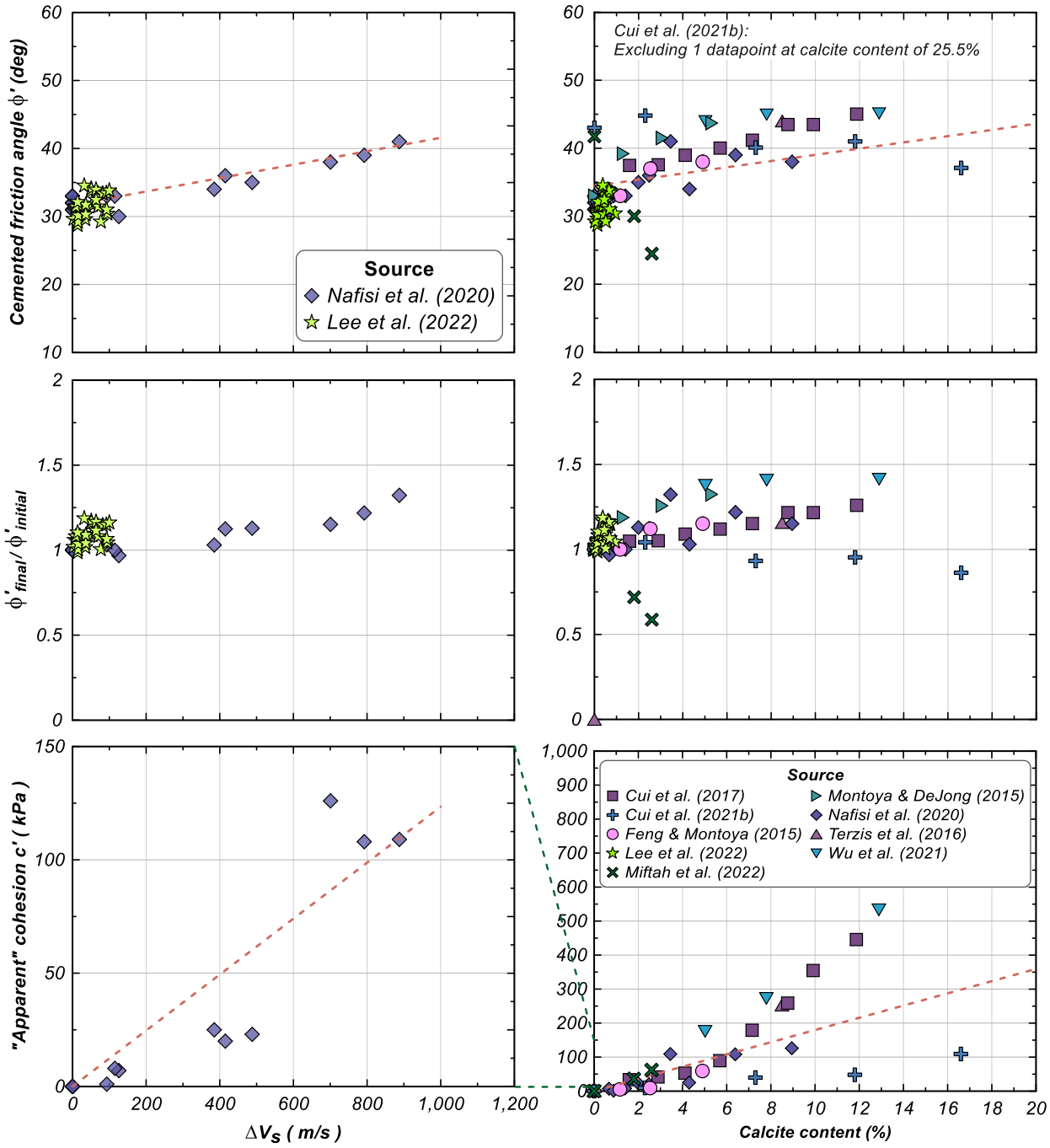

Figure 2.16. Effect of bio-cementation on strength parameters as a function of change in shear wave velocity (ΔV_s – left column) and calcite content (in % – right column): absolute cemented effective peak friction angle, ratio of final over initial (clean sand) effective friction angle, and apparent cohesion intercept (grey shading is for a change in y-axis scale).

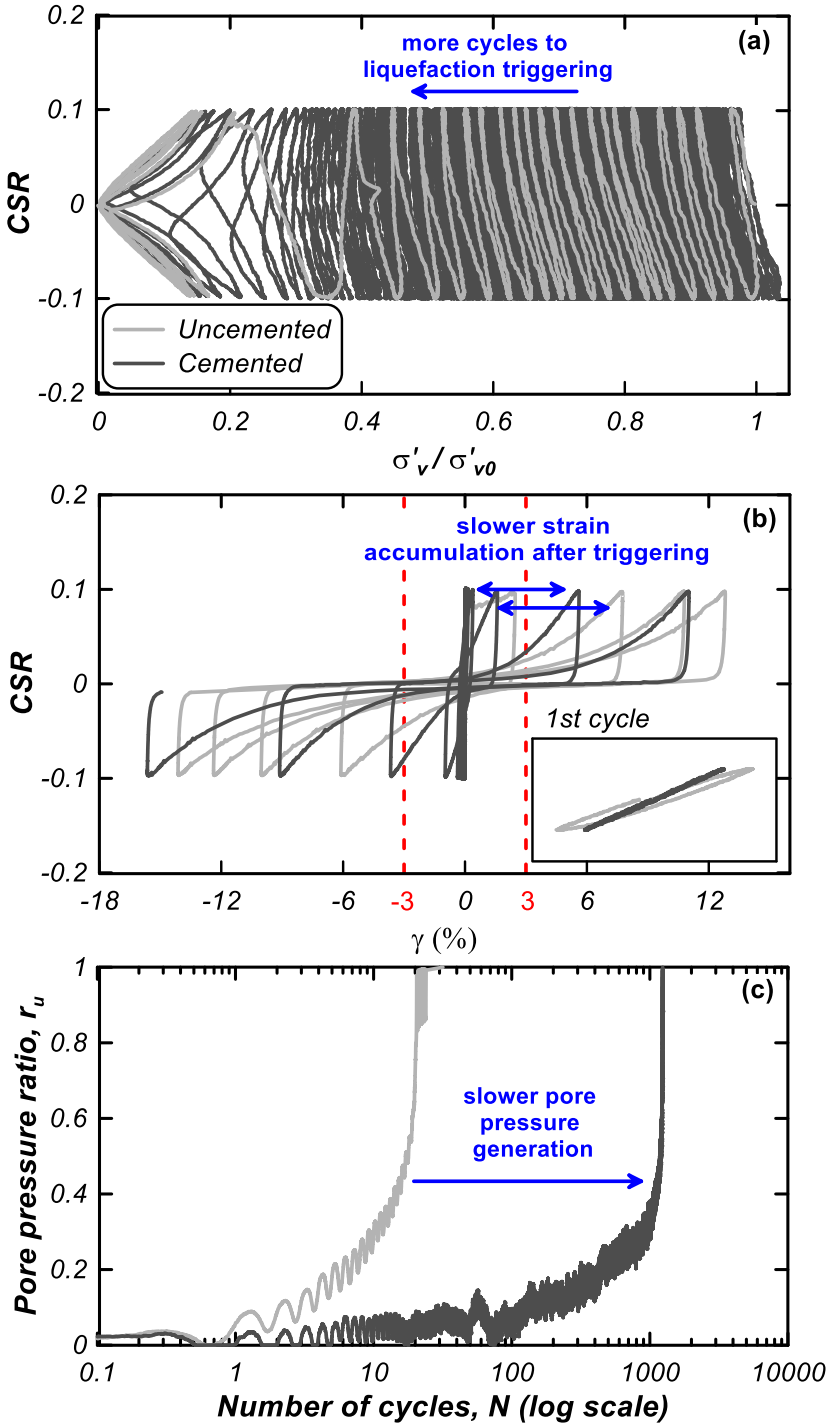

Figure 2.17. Cyclic response of initially loose lightly bio-cemented sands in terms of (a) stress paths, (b) stress-strain loops and (c) excess pore pressure ratio evolution. Data shown is from lab tests wherein specimens had an initial D_R of 40%, confining stress of 100 kPa and the cemented sample had a ΔV_s of 35 m/s (Lee et al. 2020, 2022).

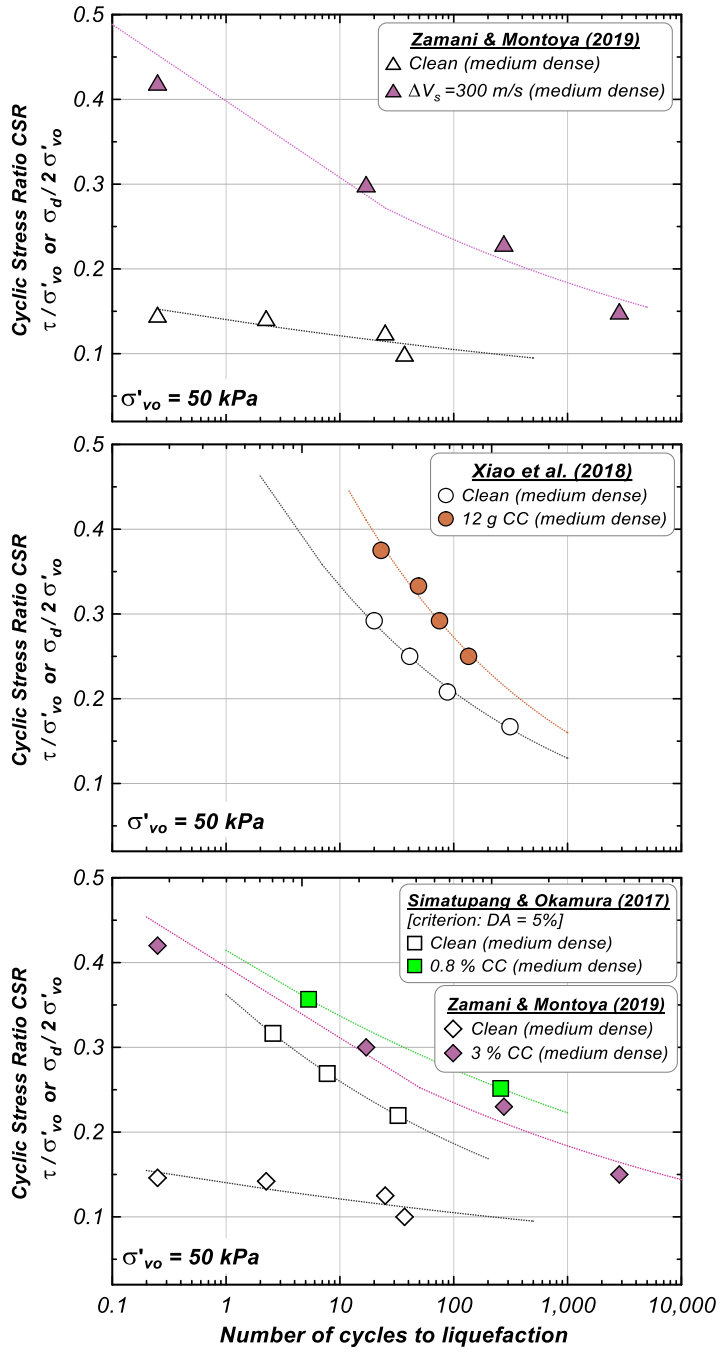

Figure 2.18. Effect of bio-cementation on the cyclic resistance to liquefaction with bio-cementation quantified in terms of: change in shear wave velocity (top), mass of calcite content (middle), and percent of calcite content (bottom) for a confining stress of 50 kPa. Medium dense sands correspond to relative densities around 50%. As discussed in Section 2.4.1 the authors did not attempt to reconcile the metrics for cementation and unify the data any further.

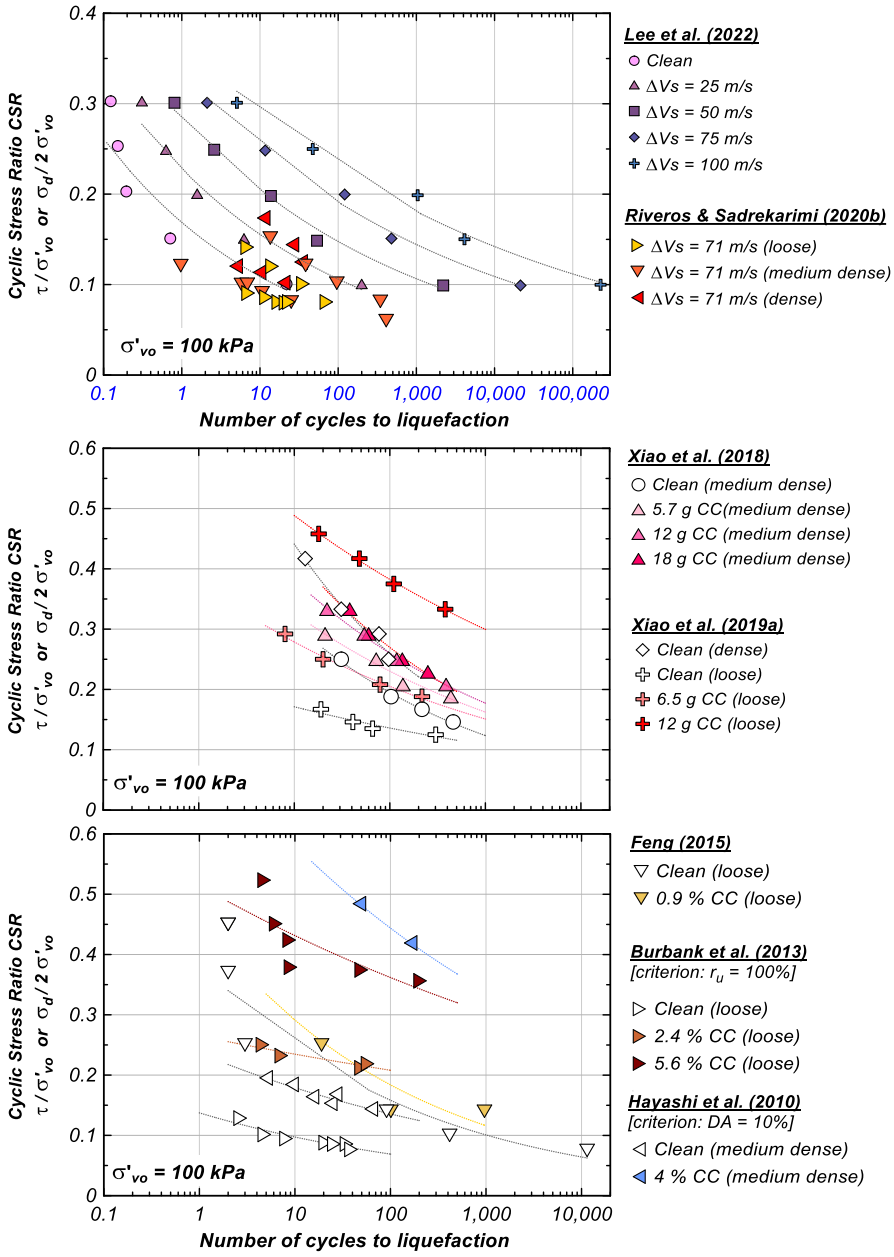

Figure 2.19. The effect of bio-cementation on the cyclic resistance to liquefaction with bio-cementation quantified in terms of: change in shear wave velocity (top), mass of calcite content (middle), and percent of calcite content (bottom) for a confining stress of 100 kPa. Loose sands correspond to D_R = ~30%, medium dense sands correspond to D_R = ~50%, and dense sands correspond to D_R = ~74%. As discussed in Section 4.1 the authors did not attempt to reconcile the metrics for cementation and unify the data any further.

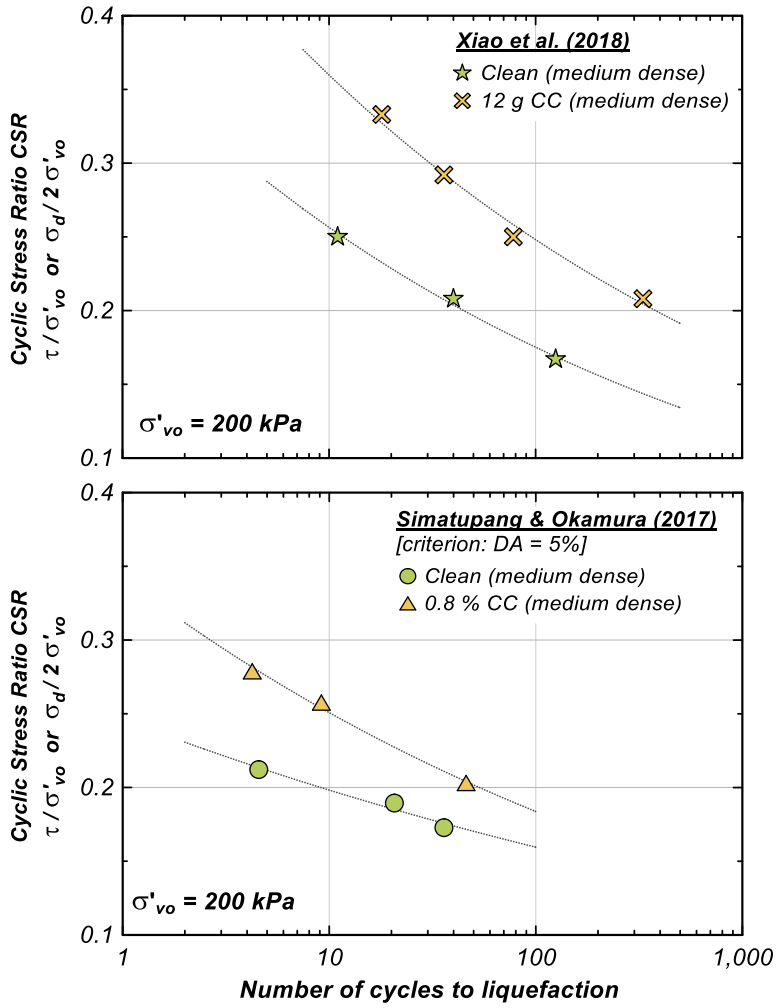

Figure 2.20. The effect of bio-cementation on the cyclic resistance to liquefaction with bio-cementation quantified in terms of: mass of calcite content (top), and percent of calcite content (bottom) for a confining stress of 200 kPa. Medium dense sands correspond to D_R = ~50%.

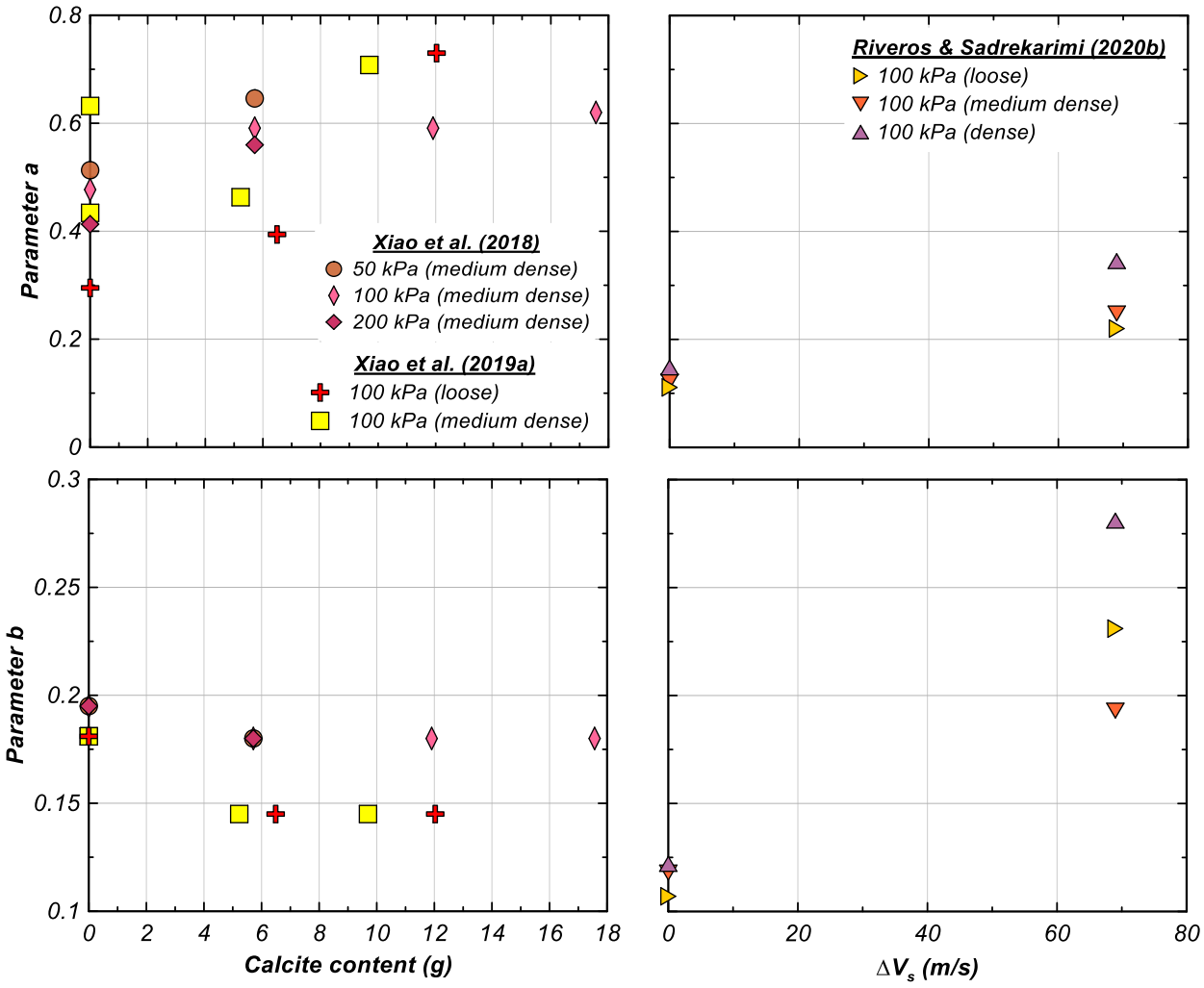

Figure 2.21. Variation of parameters "a" and "b" of power law fit for the CSR versus number of cycles to liquefaction triggering [$CSR=aN^{-b}$] as a function of mass of calcite content (in grams) for seven different datasets.

CHAPTER 3

Axisymmetric simulations of cone penetration in bio-cemented sands

Original publication:

El Kortbawi M., Moug D. M., Ziotopoulou K., DeJong J. T., and Boulanger R. W. (2022). Axisymmetric simulations of cone penetration in bio-cemented sands. Journal of Geotechnical and Geoenvironmental Engineering. https://doi.org/ 10.1061/(ASCE)GT.1943-5606.0002914.

Author's note: This paper was accepted for publication in the Journal of Geotechnical and Geoenvironmental Engineering. Figure and table captions and intext references were modified from the original publication to conform with the format of this Dissertation.

Abstract

With the recent advances in the biogeotechnics field and specifically Microbially Induced Calcite Precipitation (MICP), cone penetration testing (CPT) has become a valuable tool to overcome the challenges associated with intact sampling of improved soils, evaluate the spatial extent and magnitude of the applied MICP treatment, and assess the consequential improvement of engineering properties. While the CPT cone tip resistance (q_c) can effectively monitor the

improvement of densified clean sands, no relationship exists to estimate cementation and strength parameters in MICP-treated sands. This paper proposes a relationship between the "apparent" cohesion (c) stemming from the MICP-induced cementation bonds at particle contacts and the change in tip resistance Δq_c in initially loose sands. To develop a broadly useful correlation, available experimental CPT data in bio-cemented soils were used to guide computation simulations using a direct axisymmetric model of cone penetration in bio-cemented sands. The CPT numerical model uses the finite difference method with a rezoning algorithm for large deformation problems along with the Mohr-Coulomb constitutive model. The bio-cemented sand is characterized by Mohr-Coulomb strength parameters and an elastic shear modulus informed by shear wave velocity measurements (V_s). The correlation parameters of interest are identified (c, q_c, V_s), and results of the numerical simulations are validated against available experimental data. Once validated, the numerical simulations are extended to different initial conditions and the trends between parameters of interest are analyzed and interpreted. Results from the simulations are consistent with experimental data and show an increase in the cone tip resistance as the cementation level increases. The cementation level is modeled through "apparent" cohesion and the shear stiffness model parameters, which both increase as the cementation level increases. A linear relationship is proposed between the "apparent" cohesion and the change in cone tip resistance as a function of the confining stress.

3.1 Introduction

The cone penetration test (CPT) has been increasingly used as a tool for evaluating whether ground improvement is needed and for quantifying whether realized ground improvement methods are

effective. Current ground improvement methods include, among others, dynamic compaction, vibrocompaction, chemical grouting, and deep soil mixing, all of which are generally energy- and resource-intensive and can have significant impacts on the environment (e.g., Pinske 2011; Raymond et al. 2020). Over the past decade, alternative bio-mediated ground improvement methods that use soil microorganisms to induce calcite precipitation or desaturation have emerged. These bio-mediated ground improvement methods have received increased interest due to their potential economic advantages (e.g., cost effectiveness) and lower environmental impact (e.g., less invasive and disruptive than traditional methods) (Hall et al. 2022). Microbially-induced calcite precipitation (MICP) is a bio-mediated ground improvement method in which active urease enzymes hydrolyze supplied urea and in the presence of sufficient calcium, induces the precipitation of calcite at particle surfaces and contacts (DeJong et al. 2010). These bio-cementation bonds improve the engineering properties of the treated soil and its mechanical response (e.g., DeJong et al. 2006; Montoya and DeJong 2015; Gomez and DeJong 2017). As a result, bio-cementation has become an important alternative for mitigation of erosion, slope stability, and earthquake-induced liquefaction hazards.

Previous researchers (Bachus et al. 1981; Frydman et al. 1980; Molenaar and Venmans 1993) highlighted challenges in physical sampling naturally cemented sands due to the destruction of bonds in compression and shear during conventional sampling, and in tension when extracted from the ground. These cementation bonds are important to preserve because they alter the mechanical response of the soil by contributing to an "apparent" cohesion between soil particles, thereby increasing the strength and stiffness of the soil. Similar to naturally cemented sands, the in-situ characterization and post-treatment verification of bio-cemented sands is challenging due to the disturbance associated with the sampling process. As a result of sampling challenges and design

conservatism, the improved strength-deformation behavior of cemented sands is rarely considered in design. Furthermore, sampling may not be representative given the variable conditions (e.g., changes in density, confining stress, and microstructure with depth) present in field applications. To overcome these challenges, geophysical and CPT tests provide near-continuous in-situ measurements with depth that allow for a more direct characterization of post-treatment bio-cementation.

Despite sand bio-cementation becoming an increasingly viable ground improvement approach (e.g., Esnault Filet et al. 2016) and overcoming the challenges of sampling cemented sands for testing, relationships between their strength properties and in-situ test data remain largely uncharacterized. This is largely due to the limited availability of in-situ characterization data and complementary strength data. A comprehensive database for bio-cemented soils is still under development, but when sufficiently populated it will benefit researchers in biogeotechnics and the geotechnical community by (1) extending the knowledge from artificial bio-cementation processes to similar natural cementation processes where soil characterization may be improved despite high costs and limited available methods for soil sampling, (2) developing tools to characterize soils which may have greater resistance to certain natural hazards (e.g., erosion, liquefaction) than current practice can assess, and (3) transitioning construction to more sustainable ground improvement practices without loss of functionality or reliability. While some relationships with shear wave velocity (V_s), strength parameters (e.g., cohesion, friction angle), and cement content have been recently published (e.g., Cui et al. 2017; Hoang et al. 2020), a relationship between q_c and apparent cohesion has not been developed at this time.

The goal of this study is to enable the verification of field bio-cementation treatment through CPT testing and relate CPT-measured q_c to strength properties of initially loose MICP-treated

sands. The connection between the field measured CPT q_c as the end-of-construction quality assurance and control (QA/QC) and a strength parameter like cohesion will provide a project-specific basis for either simplified strength-based analyses or for constitutive model parameters used in more advanced numerical analyses. These numerical analyses may include the design of ground improvement techniques, the evaluation of present site conditions, and/or the post-disaster remediation of sites following a hazardous event. To this end, this paper investigates the relationship between the change in cone tip resistance (Δq_c) due to cementation and the apparent cohesion (c) for initially loose bio-cemented sands. It also proposes a mechanistic approach for synthesizing data from numerical cone penetration simulations validated against large-scale and field-scale experiments, and additional parametric simulations with varying cementation levels and confining stresses. Figure 3.1 conceptually illustrates the approach followed while the following sections describe the various data sources and analysis components. First, the published data from two experiments (a large tank experiment and a centrifuge test) with CPT q_c and V_s measurements were collected (Section 3.2). Second, numerical simulations under similar conditions were performed to reproduce the experimental results by varying the input parameters to the model. The simulation results were then validated against the experimental data. Once validated for the confining pressures from the experiments, the simulations were extended to higher confining stresses and the trends were analyzed and interpreted in order to fit a relationship between the input parameter to the Mohr-Coulomb constitutive model c and the output from the cone penetration model q_c. The following sections describe this approach in greater detail.

While other approaches have been followed for the simulation of cone penetration in cemented sands (Section 3.3), the present approach provides a valuable tool in synthesizing data which are validated against the experiments. Without disregarding the complexity of the actual mechanisms

during cone penetration, the simplicity of the Mohr-Coulomb model is still preferred at this time. Results from laboratory tests on bio-cemented sands have been used to directly map to how bio-cementation changes Mohr-Coulomb model parameters. This process provides a strong experimental basis and guidance for parametric studies for this modeling work. The Mohr-Coulomb constitutive model used here with a modified secant shear modulus and a non-degrading cohesion for the cemented sands still allows for a reasonable approximation of the constitutive behaviors due to two competing mechanisms: (1) the non-degrading cohesion inhibiting dilation, offset by (2) the enhanced dilation of cemented sands. However, the authors understand that the actual mechanisms during cone penetration are more complex due to the degradation of the bio-cementation and its effects.

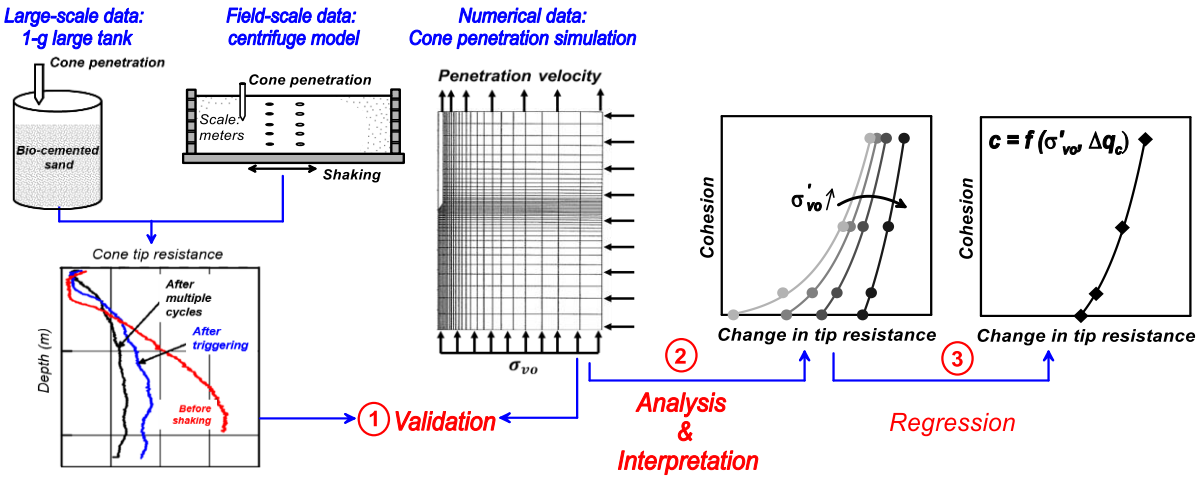

Figure 3.1. Proposed approach for the development of a $\Delta q_c - c$ relationship for bio-cemented sands from experimental and numerically synthesized data.

3.2 Cone penetration resistance for bio-cemented sands

Two published experiments evaluated the use of CPT as a site characterization tool for bio-cemented sands. These experiments are briefly summarized here since their datasets will be used in subsequent sections to validate the simulated q_c under similar conditions.

3.2.1 Large scale tests

Gomez et al. (2018) treated two 1.7 m diameter tank specimens at a relative density D_R of 45% with MICP to assess the effect of bio-cementation on CPT and shear wave velocity (V_s) measurements. Two biological treatment approaches were used (stimulation and augmentation – one in each tank) to investigate the influence of differences in the biological treatment on the spatial distribution of the cementation. They found that this variation did not significantly affect the magnitude and spatial distribution of bio-cementation, thus, for our purposes, datasets from both tanks will be used. Pre- and post-treatment CPT soundings were performed using a 1.6 cm diameter cone penetrometer at several locations where the level of cementation varied from light to heavy (Fig. 3.2a). Light cementation is defined as a soil with V_s ~ 300 m/s and heavy cementation is defined as a soil with V_s ~ 1200 m/s (after Montoya et al. 2013). V_s and calcite content by mass, measured at the same locations, were used to characterize the cementation level and they were found to have a positive linear relationship. The average confining stress at the sample locations was approximated as 13 kPa. CPT soundings reported tip resistance q_c. The q_c values were not corrected for excess porewater pressures since drained conditions were expected to prevail due to the low cone penetration velocity and the high permeability of bio-cemented sands. The reader is referred to Gomez et al. (2018) for more details on the biological treatments and the experimental setup.

Comparing pre-treatment and post-treatment CPT data showed that q_c increased with the increase of soil calcite content and V_s (i.e., the level of cementation), with more significant increases in q_c occurring at higher calcite contents. It is noted that a strong correlation between soil calcite content and V_s has been previously established (e.g., Gomez and DeJong 2017; Gomez et al. 2018; Darby et al. 2019). At lower calcite contents (i.e., less than 3%), increases in q_c were less significant probably due to the insensitivity of the cone to low levels of cementation. This limitation of the CPT was overcome by V_s measurements, which, due to their nondestructive nature, are sensitive to even the smallest changes in particle bonding. Datasets from this study were also analyzed within the K_G framework (see Section 3.3.3) which is proposed by Schneider and Moss (2011) for cemented and aged soils and is based on the small-strain (Rix and Stokoe 1991) and large-strain characteristics (Eslaamizaad and Robertson 1997) using parameters from field testing. This analysis is done to evaluate the relationship between V_s and normalized cone tip resistance (q_{c1N}) of bio-cemented sands relative to naturally cemented soils (see Section 3.3.2). The K_G boundary values were found to reasonably capture the distinction between uncemented and cemented sands.

3.2.2 Centrifuge model tests

Darby et al. (2019) performed a set of centrifuge model tests on MICP-treated Ottawa sand at a relative density D_R of 38% and different levels of cementation (i.e., light, medium and heavy cementation defined based on V_s measurements). Control tests on clean sands at loose and dense states were first performed and then the bio-cementation process was induced in loose centrifuge models. All models were spun to a centrifugal acceleration of 80g (mid-depth confining stress was approximated at 35 kPa) and subjected to 9 to 16 shaking events with acceleration amplitudes ranging from 0.02g to 0.55g. Similar to the large-tank experiment, calcite content measurements,

pre- and post-treatment CPT soundings, and bender element V_s measurements were combined to assess the effect of bio-cementation on the cone penetration resistance and the stiffness of the treated specimens. This study also investigated the effect of bio-cementation on the liquefaction resistance and the post-shaking cementation degradation (Fig. 3.2b) which are outside the scope of the present work but shown here for completeness.

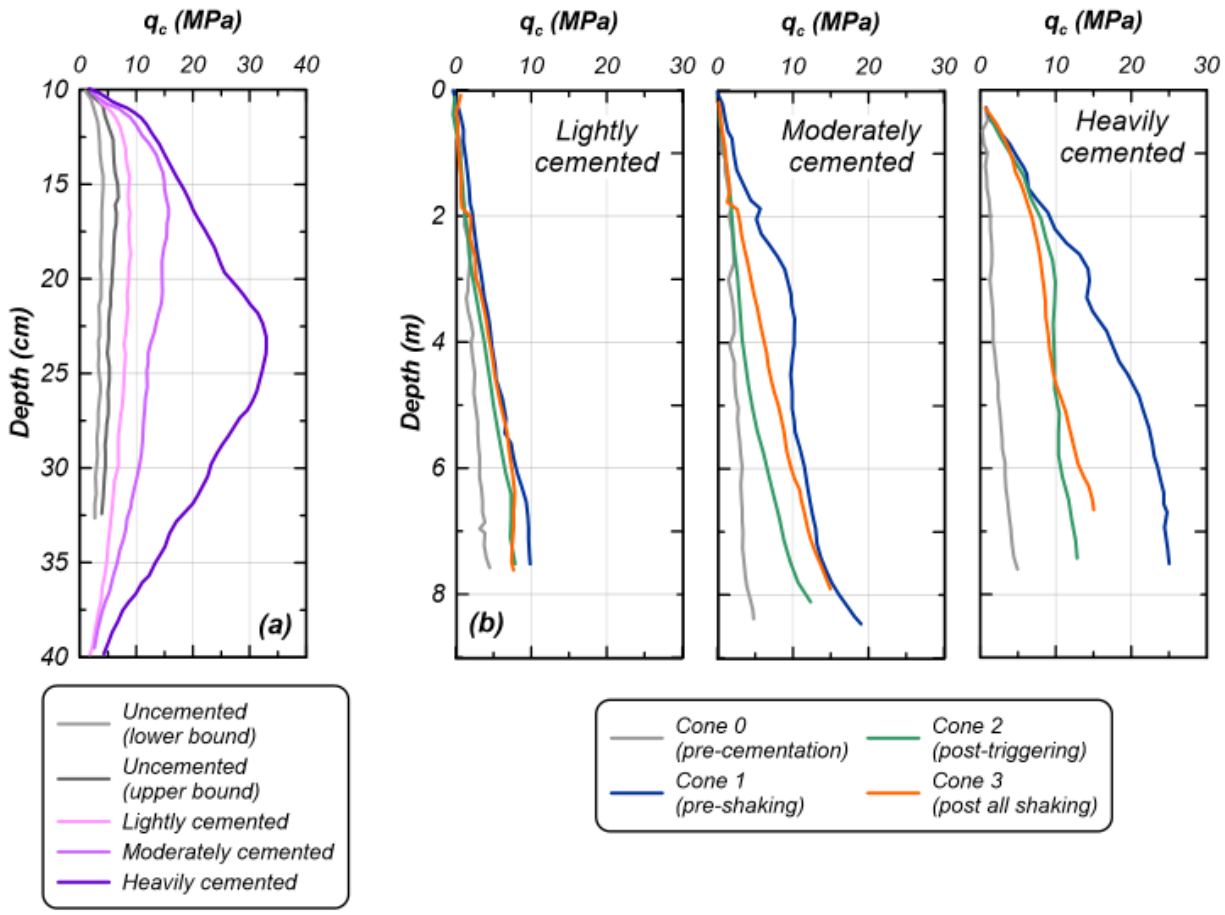

Figure 3.2. Cone penetration profiles from: (a) large tank experiment (Gomez et al. 2018) and (b) centrifuge model test (Darby et al. 2019) showing an increased cone tip resistance before (both a and b) and after triggering of liquefaction (only in b).

The present work focuses on the measured q_c prior to shaking, while the Darby et al. (2019) centrifuge study focused specifically on dynamic responses. More details on the experimental setup and post-shaking behaviors can be found in Darby et al. (2019). Compared to the pre-treatment CPT profiles, post-treatment CPT profiles showed an increase in q_c, as the level of cementation increased, due to the filling of void space with the cementation and thus the presence of the bonding between the particles. Measured q_c increased from a mid-depth value of 2.3 MPa for the uncemented loose model to 4.6, 9.9 and 17.8 MPa for the lightly, moderately and heavily cemented models, respectively with an effective vertical stress at mid-depth ranging from 32 to 36 kPa. These increases in q_c corresponded to increases in V_s and calcite contents in all models, and appeared to be linearly correlated to the increase in calcite content as reported in Gomez et al. (2018) at 1g and 13 kPa confinement.

3.3 Cone penetration numerical simulations

The availability of CPT data pre- and post-treatment is crucial for verifying that ground improvement was achieved. However, there are currently no available methods to relate changes in CPT measurements to mechanical properties of the improved soil, which limits the utility of such data. The mechanical properties of initially loose MICP-treated sands have been increasingly investigated. Research on lightly cemented sands (Puppala et al. 1995; Lee et al. 2011) and on bio-cemented sands (Burbank et al. 2013; Gomez et al. 2018; Darby et al. 2019) has reported that cementation results in an increase in the cone tip resistance and sleeve friction and a decrease in the friction ratio due the pronounced increase in tip resistance compared to the sleeve friction. This increase in q_c is a direct representation of the increase in strength of the cemented sand, which is

mostly attributed to the cohesive bonds. These studies indicate that changes in CPT data can be related to changes in soil mechanical properties due to bio-cementation.

Researchers (DeJong et al. 2010; Feng and Montoya 2015; Nafisi et al. 2020) have shown that bio-cementation increases the initial shear stiffness (G_{max}), the peak strength (τ_{pk}), and the dilative tendencies of treated sands while suppressing the initial contractive behavior due to the presence of the cementation bonds. This results in improved strength properties such as increased cohesion and friction angle. These improvements degrade after the accumulation of plastic strains and the sheared treated sand loses the cementation bonds (Chapter 2).

CPT-based relationships are advantageous since the improved strength-deformation behavior is difficult to measure accurately in the laboratory due to sampling challenges. As a result, there is a lack of understanding of how changes in CPT data relate to changes in soil strength properties. Due to the lack of CPT data coupled with conventional laboratory testing of bio-cemented sands, there is a gap in the understanding and quantification of the strength properties of these bio-cemented sands, such as "apparent" cohesion. To address this issue, a numerical direct cone penetration model is used herein. Simulations of cone penetration in cemented sands have been recently performed by Schweiger and Hauser (2021) and Rakhimzhanova et al. (2021). Schweiger and Hauser (2021) simulated undrained cone penetration in cemented clayey silt using the Particle Finite Element Method (PFEM) and the Clay and Sand Model (CASM) for structured soil. Large deformations due to the cone penetration were handled by the PFEM whereby frequent remeshing was performed in deformed regions. The numerical model consisted of a rigid cone penetrating a saturated soil at constant velocity. At approximately 25 to 30 cone radii, stationary values of tip resistance and pore pressures were obtained. Structured soils were represented by overconsolidated soils in the CASM constitutive model due to the similarities in their behaviors. The results of the

simulations confirmed that, before the degradation of the cementation, the cone tip resistance and pore pressures increased with the level of cementation while they decreased after the degradation. The authors also analyze the trends in the results in terms of changes in pore pressure, undrained shear strength, and cone correction factors in a companion study Hauser and Schweiger (2021). Rakhimzhanova et al. (2021) utilized the Discrete Element Method (DEM) to simulate constant rate vertical cone penetration in cemented sandstone. The cemented sandstone was represented by frictional elastic spheres with different bond strength values. The results of the simulations were then compared to the published Soil Behavior Type (SBT) classification system based on CPT, demonstrating the utility of numerical cone penetration simulations for relating in-situ data to cemented sand properties.

For the present study, cone penetration numerical simulations are validated against existing data and subsequently parametrically performed to produce data for development of a relationship between Δq_c and c, accounting for its dependence on confining stress. Simulations are performed in the explicit finite difference (FD) program FLAC (Fast Lagrangian Analysis of Continua, Itasca, 2019) with the Mohr-Coulomb constitutive model. The cone penetration model has been used in previous studies (e.g., Moug 2017; Moug et al. 2019a; Moug et al. 2019b) and has been validated against laboratory tests. While the present work and Schweiger and Hauser (2021) use a similar approach in terms of remeshing regions around the cone with large deformations, the tools used (FD versus PFEM, respectively) for the simulation of the cone penetration and the characterization of the cemented soil (Mohr Coulomb versus CASM, respectively) differ. The present work and Rakhimzhanova et al. (2021) also use different tools (FD versus DEM, respectively) and approaches (mesh moving up versus penetrometer moving down, respectively). Despite these differences, the aforementioned studies have similar trends in their findings.

3.3.1 Axisymmetric cone penetration model

The direct axisymmetric cone penetration model (Fig. 3.3) simulates the steady-state penetration of a standard cone with a 3.57 cm diameter (10 cm2 cone area) into a soil column using a user-defined Arbitrary Lagrangian Eulerian (ALE) algorithm coupled with FLAC's Lagrangian formulation that allows for large deformations (Moug 2017; Moug et al. 2019a). The model is developed to simulate penetration at large depths such that the cone's self-weight and ground surface effects can be neglected. The model is initialized with stress and material properties for a "wished-in-place" cone at the depth of interest. The penetration is then simulated until a steady-state stress distribution, pore pressure, and tip resistance prevail, that is approximately 25 cone diameters of simulated penetration (Lu et al. 2004). Boundary conditions simulate soil flowing upward relative to a stationary cone (i.e., soil flows from the bottom of the model and exits at the top). The far-field total vertical stress is applied at the bottom boundary, a penetration velocity of 0.02 m/s is applied at the top boundary and an infinite elastic boundary condition is assumed for the right radial boundary which is far away from the cone to prevent boundary effects. The axisymmetric boundary to the left imposes no displacement in the x-direction for the soil node at the tip of the cone and constrained vertical movement due to the rigidity of interface elements in this direction. The other soil nodes along the cone face and the shaft can deform parallel to the boundaries of the cone. The mesh near the cone face is highly discretized and the adjacent soil zones are connected by Mohr-Coulomb interface elements obeying the Mohr-Coulomb friction criterion. The interface coefficient of friction (which is the ratio of the interface friction angle and the soil's critical state friction angle) represents the friction along the cone face and ranges from 0 to 1 for a perfectly smooth and a perfectly rough cone, respectively. An interface coefficient of friction equal to 0.60 was used for these simulations, which is consistent with the value used for

simulated cone penetration in sand in Moug et al. (2019b). The soil zone sizes increase following a power distribution away from the cone. Large deformations of the model geometry, which will concentrate near the cone tip and shoulder, can lead to numerical instability and hence, are accommodated with an ALE algorithm which performs grid rezoning and model property remapping throughout the penetration depth. Details of the ALE algorithm and the model's implementation are presented in Moug (2017) and Moug et al. (2019b). Initial stress conditions correspond to a normally consolidated Ko condition. Drained conditions are imposed by minimizing the pore water bulk modulus.

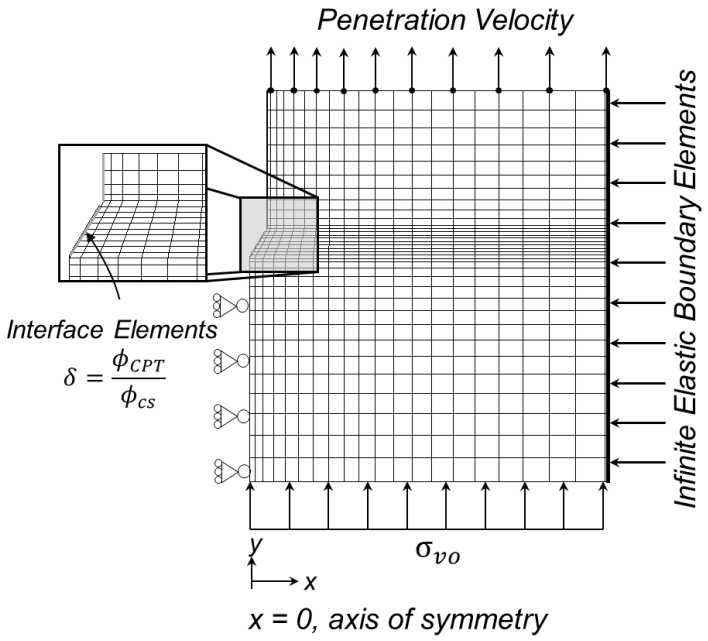

Figure 3.3. Geometry and boundary conditions of the numerical cone penetration model in FLAC (Moug 2017).

3.3.2 Soil model calibration

Mohr-Coulomb, an elastic perfectly plastic model, is used for simulating penetration in cemented sands due to its simplicity and its applicability to soils with cohesion (e.g., Cui et al. 2017; Nafisi

et al. 2020). The calibration of the Mohr-Coulomb constitutive model is guided by the aforementioned experimental data and other bench-scale tests data (e.g., triaxial and direct simple shear tests), previous research on the mechanical behavior of bio-cemented and naturally cemented sands (Chapter 2), and empirical correlations developed hereafter. Mohr-Coulomb model parameters are assigned to capture the drained penetration in uncemented and bio-cemented sands. Similar to sands, drained conditions prevail in bio-cemented sands due to their open structure reflected by the modest changes in hydraulic conductivity after cementation (Gomez and DeJong 2017). Literature on cemented sands (e.g., Dupas and Pecker 1979; Saxena et al. 1988) also suggests that while strength parameters (all in effective stress terms), cohesion c and friction angle ϕ, are both affected by cementation, changes in friction angle are of secondary importance and the main contributor to the improvement in the behavior is the apparent cohesion term c. This hypothesis is corroborated by a sensitivity analysis on the friction angle using the cone penetration model not included here for brevity (Appendix A). Furthermore, the dilation angle ψ is not activated in the simulations because preliminary calibrations suggest an overestimation in the tip resistance. This overestimation is most likely due to the double-counting of the cementation effects through a non-degrading cohesion and an enhanced dilatancy occurring simultaneously. Consequently, apparent cohesion is the primary parameter for study, while the friction angle, ϕ, and the dilation angle, ψ, are held constant at 30º (mid-range and typical value for silica sands) and 0º (restricted dilation to compensate for the non-degrading cohesion with large deformations), respectively.

Due to the interconnection between strength and stiffness for bio-cemented sands, a relationship relating a strength parameter, "apparent" cohesion, c, and a stiffness parameter, V_s, on the element level enables the estimation of the unknown "apparent" cohesion for the large-scale

experiments. Previous research on bio-cemented sands (e.g., Simatupang et al. 2018; Nafisi et al. 2020) characterizes a coupled interaction between strength and stiffness in which both entities increase post-cementation, however, initial shear stiffness increases faster and more significantly relative to strength. This mechanism is represented by a linear relationship between apparent cohesion (c) and the change in shear wave velocity (ΔV_s) due to the contribution of the cementation. Linearity is corroborated by the trends discussed above in the large-scale and centrifuge test findings. The datapoints with c and V_s measurements from triaxial test data on bio-cemented sands (O'Donnell et al. 2017; Nafisi et al. 2020) are fitted with a linear relationship. The latter is then applied to the field V_s measurements obtained during the experiments in Figs. 3.2a and 3.2b to obtain cohesion estimates. Then, the large-scale experimental data with the cohesion estimates are divided into 6 bins with cohesions from 0 to 50 kPa, in increments of 5 or 10 (0-5 kPa: 2 datapoints, 5-10 kPa: 3 datapoints, 10-20 kPa: 5 datapoints, 20-30 kPa: 7 datapoints, 30-40 kPa: 11 datapoints, 40-50 kPa: 2 datapoints). This is done to reduce the scatter obtained by fitting through all datapoints. The average of each bin is obtained and plotted in Fig. 3.4 to give a continuous relationship between cohesion and ΔV_s. Thus, the relationship between apparent cohesion and change in shear wave velocity becomes:

$$\Delta V_s = 18.9\, c \qquad (3.1)$$

where c is the apparent cohesion (kPa) and ΔV_s is the change in shear wave velocity (m/s) due to the contribution of the cementation. The cohesion term used in Eq. (3.1) and in the rest of the paper refers to the change in cohesion from an initially cohesionless sand (c = 0) due to the effects of the cementation. In the absence of bench-scale or field testing, Eq. (3.1) can be used to provide a rough estimate of the cohesion term directly from the change in shear wave velocity, however, the data

fitted by this equation is limited and hence, other means of estimation are recommended to cross check the estimated c (see Section 3.4).

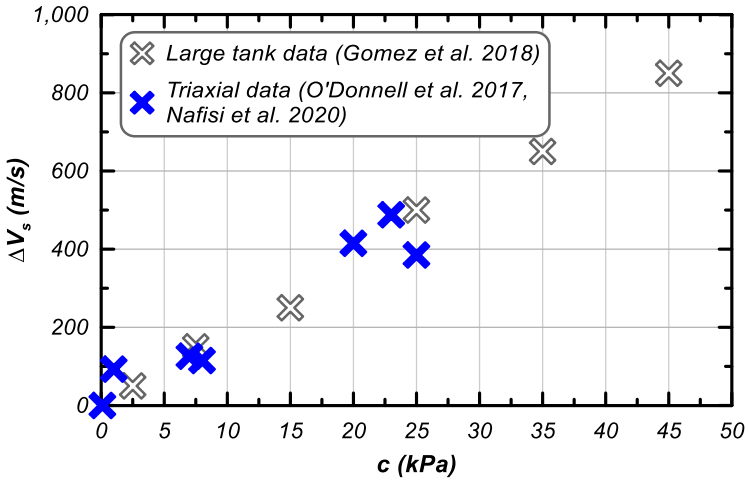

Figure 3.4. Relationship between apparent cohesion and change in V_s due to the cementation, large tank data from Gomez et al. (2018), triaxial data from O'Donnell et al. (2017) and Nafisi et al. (2020).

Based on collected experimental data (Chapter 2) and the developed correlation (Eq. 3.1), Mohr-Coulomb input parameters for the cone penetration simulations are chosen and summarized in Table 3.1. Values for apparent cohesion range from 0 (uncemented) to 40 kPa (moderately-heavily cemented). The confining stresses include 13 kPa, representing the operating confining stress for the CPTs pushed in the large tanks from Gomez et al. (2018), 35 kPa representing the operating confining stress for the CPTs pushed in the centrifuge model from Darby et al. (2019), and 100, 200, and 400 kPa in order to expand the parametric space of the simulations to operating field conditions. The values of V_s for uncemented sands (first row in Table 3.1) are either reported in the experiments (for 13 and 35 kPa) or estimated for 100 (Lee et al. 2022), 200, and 400 kPa. According to the chosen cohesion values, the change in V_s corresponding to each cohesion value is estimated from Eq. (3.1), added to the value of V_s for uncemented sand in order to obtain an

estimated V_s for cemented sands and then checked for normalization across the various confining stresses. For consistent sand properties across the different levels of stress, a stress-corrected V_{s1} (Eq. 3.2) is estimated using the correction proposed by Andrus and Stokoe (2000).

$$V_{s1} = V_s \left(\frac{P_a}{\sigma_v'}\right)^n \qquad (3.2)$$

where V_s is the shear wave velocity (m/s), P_a is the atmospheric pressure, σ_v' is the overburden stress, and n is the stress exponent. The exponent n decreases from 0.25 (for clean sands) to 0 (for rocks) depending on the level of cementation. The literature review in Chapter 2 proposes a decreasing trend for the n exponent as the level of cementation increases. In the present work, the values of the n exponent are chosen as 0.25, 0.18, 0.13 and 0.05 for c = 0, 5, 20, and 40 kPa, respectively. This choice seems reasonable for the shear wave velocity selection process. Some scatter is noticeable for the V_s at 13 kPa which is due to difficulties in the measurement of the initial V_s in the experiment. The normalization shown in Fig. 3.5 indicates that a similar V_s input is specified depending on the initial stress conditions and hence the model is initialized with an equivalent level of cementation for different initial stress conditions.

Table 3.1. Mohr-Coulomb input parameters for CPT simulations through cemented sands under various confining stresses.

c (kPa)	**ΔV_s (m/s)**	**σ'_v (kPa)**				
		13	**35**	**100**	**200**	**400**
		V_s (m/s)				
0	**0**	80	150	200	250	300
5	**95**	175	245	295	345	395
20	**378**	458	528	578	628	678
40	**756**	836	906	956	1006	1056

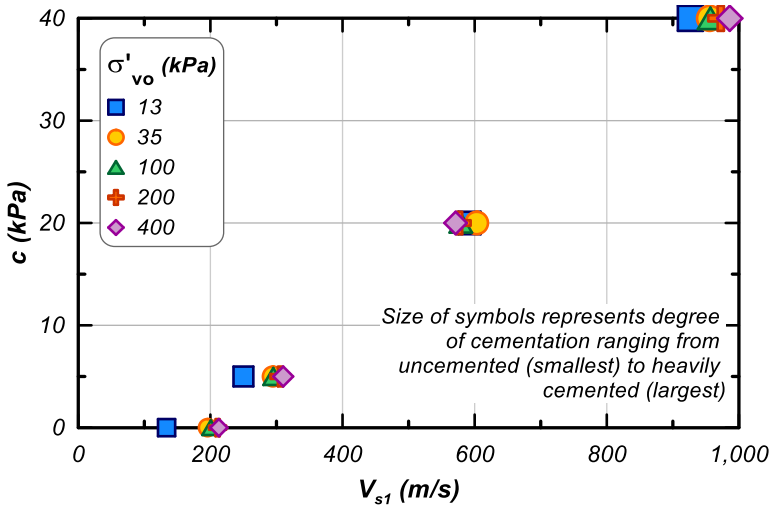

Figure 3.5. Normalization of cemented shear wave velocity V_s across the various confining stresses resulting in an apparent cohesion c and normalized shear wave velocity V_{s1} pairs similar across all simulations.

During cone penetration, a failure zone is formed around the penetrometer which generally results in a plastic region near the cone and an elastic region further away from the cone. Complex soil deformations are induced within the plastic zone which in turn affect the shear modulus (Teh and Houlsby 1991). The extent of the failure zone largely depends on the soil shear stiffness and strength, represented by its rigidity index. The current framework does not consider the effect of penetration-induced strains on the shear stiffness of deformed elements near the cone tip. At present, the model operates with a single assignment of shear modulus as opposed to accepting a strain-dependent shear modulus that would better represent the stiffness degradation in the failure zone around the cone tip as the cone penetrates (Konrad and Law 1987; Schnaid et al. 1997; Krage et al. 2014). In recognizing that the small-strain shear modulus G_{max} is overly stiff, a reduced shear modulus G_{func} is used as a reasonable approximation of the local shear stiffness for the failure zone around the cone tip (Yi et al. 2012).

To account for shear modulus softening due to large strains around the penetrating cone, a common approach is to reduce the local shear stiffness by a certain factor (Eq. 3.3) with respect to the initial small-strain shear modulus $G_{max} = \rho V_s^2$, where ρ is the soil's density and V_s is the shear wave velocity (Teh and Houlsby 1991; Lu et al. 2004). While the authors acknowledge the more common nomenclature for small-strain shear stiffness G_o in the CPT-based literature and frameworks, they choose to use the nomenclature G_{max}. The latter is more common in earthquake engineering applications which are the end-use of the proposed relationship hereafter. The two quantities denote a maximum value of shear modulus and thus, G_{max} is used in the rest of this paper. Hence, the local "functional" shear stiffness G_{func} is expressed as,

$$G_{func} = \frac{G_{max}}{F} \qquad (3.3)$$

where G_{func} is the "functional" shear modulus for large strain problems, G_{max} is the initial small-strain shear modulus, and F is the reduction factor due to penetration-induced deformations. The reduction factor is chosen for uncemented sands based on the experience of previous researchers and extrapolated to cemented sands by a calibration process as informed by the degradation of G in the response of monotonic drained triaxial tests (Feng and Montoya 2015; Montoya and DeJong 2015). The proposed relationship for the reduction factor F (Eq. 3.4) increases with the level of cementation due to the increased brittleness of the cementation at higher levels. This increase in brittleness results in a sharper decrease in stiffness with deformations for higher levels of cementation (Chapter 2). Hence, the shear stiffness is more considerably lost at higher cementation and a higher reduction factor is needed to reflect this mechanism. The reduction factor F is linearly proportional to the apparent cohesion c (kPa) and is plotted in Fig. 3.6:

$$F = 0.15\, c + 3 \qquad (3.4)$$

Additional parameters to the axisymmetric model using the Mohr-Coulomb constitutive model are summarized in Table 3.2 based on input parameters for cemented sands as summarized in Table 3.1 and on default values for clean sands wherever no information was available for cemented sands.

In what follows, results from the calibration with the "functional" shear modulus are presented and the simulated q_c values are compared to the reported ones from the experiments in the $q_c - V_s$ space (e.g., Andrus et al. 2009; Darby et al. 2019) and in the K_G framework (e.g., Rix and Stokoe 1991; Schneider and Moss 2011; Gomez et al. 2018).

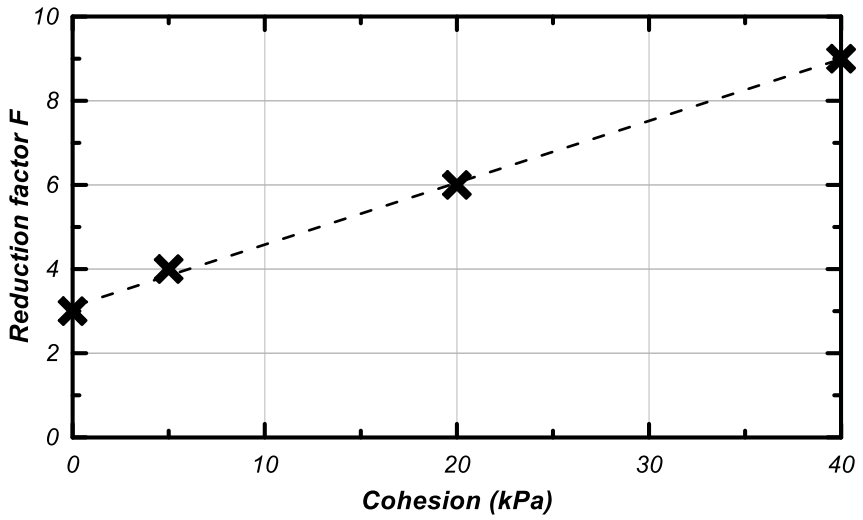

Figure 3.6. Proposed relationship for shear modulus reduction factor as a function of the apparent cohesion c where $c = 0$ and $c > 0$ delineate uncemented and cemented sands, respectively.

3.3.3 Model validation

To enable the comparison with available experimental data, the focus of the analysis is on the cone tip resistance q_c results, similar to other works (e.g., Puppala et al. 1997; Lee et al. 2010; Schneider

and Moss 2011). Simulated tip resistances for effective stresses of 13 kPa and 35 kPa are compared with the reported tip resistances from Gomez et al. (2018) and Darby et al. (2019), respectively.

Table 3.2. Calibration of the cone penetration model.

Mohr-Coulomb model parameters	**Parameter description**	**Calibration**
$\boldsymbol{c}$	Effective cohesion term (kPa)	*Refer to Table 3.1*
$\boldsymbol{\phi}$	Effective friction angle (degrees)	30
$\boldsymbol{V_s}$	Shear wave velocity (m/s)	Refer to Table 3.1
$\boldsymbol{\rho}$	Dry density (Mg/m^3)	1.7
$\boldsymbol{G}$	Functional shear modulus (kPa)	$G = \frac{G_{max}}{F}$
$\boldsymbol{K_o}$	At-rest coefficient of lateral pressure	0.5
$\boldsymbol{\psi}$	Dilation angle (degrees)	0
$\boldsymbol{\upsilon}$	Poisson's ratio	0.3

Figure 3.7 represents the simulated and experimental q_c in the $q_c - V_s$ space. The open and closed symbols refer to the experimental and simulated results at different vertical stresses, respectively. The increasing sizes of the symbols delineate the classification of the cementation as uncemented (V_s ~ 80 - 300 m/s for a stress range of 13 to 400 kPa), light (V_s ~ 170 - 400 m/s for a stress range of 13 to 400 kPa), moderate (V_s ~ 450 - 680 m/s for a stress range of 13 to 400 kPa), and heavy (V_s ~ 830 - 1100 m/s for a stress range of 13 to 400 kPa), respectively. This facilitates visualization of results not only in the global sense but also on a discretized level-by-level basis. The simulated q_c values, not only fall within the same range as the experimental ones for 13 and 35 kPa but also reasonably map the cementation level (i.e., the second smallest symbols from the simulations plot near those from the experiment, delineating a match between the light level of cementation from the simulation and the experiment). This observation follows a general trend in

which an increase in shear wave velocity results in an increase in tip resistance. The trend extends similarly to higher confining stresses.

Figure 3.8 shows the trend between simulated and experimental results in the K_G framework. The parameter K_G is defined as follows:

$$K_G = \frac{G_{max}/q_c}{{q_{c1N}}^{-0.75}} \qquad (3.5)$$

where K_G is the empirical parameter relating stiffness and strength, G_{max} is the initial small-strain shear modulus, q_c is the cone tip resistance, and q_{c1N} is the stress normalized cone tip resistance. This framework was adapted by Schneider and Moss (2011) to visualize the relationship between stiffness (originally written in terms of G_o, modified for the purpose of this work) and strength for cemented sands and by Gomez et al. (2018) and Montoya et al. (2021) for bio-cemented sands. According to the soil classification from Schneider and Moss (2011), the range for cemented sands plots above and to the right of uncemented sands with the cutoff K_G value between uncemented and cemented soils being 330. With an increase in cementation and age, the parameter K_G (Eq. 3.5) is expected to increase proportionally to the level of cementation and perpendicularly to the cutoff ranges.

The small-strain shear stiffness G_{max} is affected by the coordination number, the characteristics of particle contacts, and the effective stress. It is interpreted from V_s measurements taken during the CPT profiles or from geophysical tests. The tip resistance is a large-strain measurement controlled by a large-strain shear stiffness (or a "functional" stiffness), soil characteristics (dilation and crushability), and horizontal effective stress. While these measurements are performed at different zones of the soil, the ratio of q_c to G_{max} gives reasonable indications on the cementation and geologic age of deposits.

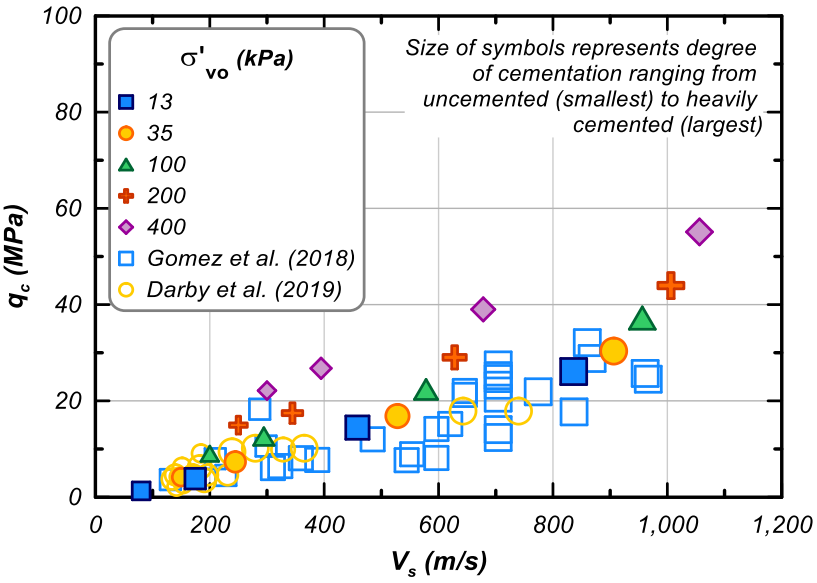

Figure 3.7. Comparison between reported experimental (open symbols) and simulated (closed symbols) tip resistances in the $q_c - V_s$ space.

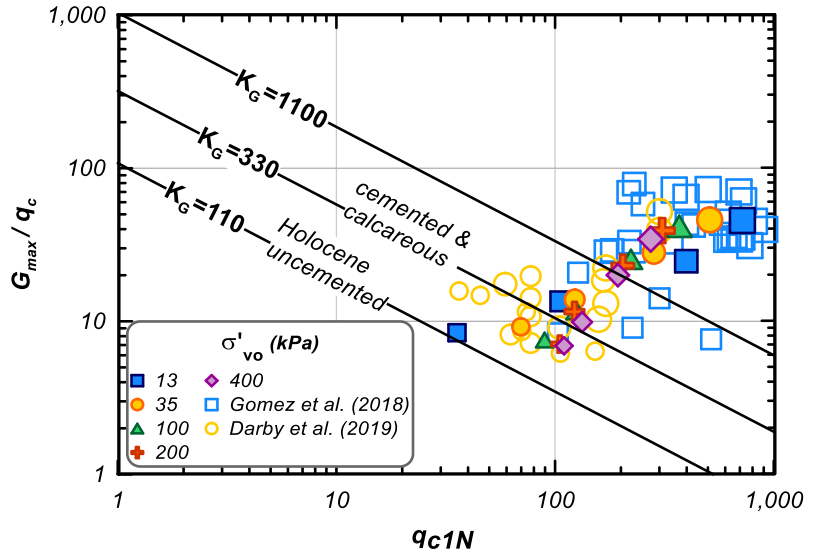

Figure 3.8. Comparison between reported experimental (open symbols) and simulated (closed symbols) tip resistances in the K_G framework.

Both the experimental and simulated results reasonably follow the aforementioned trend. Few lightly cemented experimental data plot under the cutoff K_G value of 330, while most show the cementation to generate large increases in the K_G value.

In general, the cemented simulated results plot above the K_G=330 cutoff and reasonably shift up and to the right as the apparent cohesion value (i.e., the level of cementation) increases from lightly to heavily cemented. This trend is similarly seen in the experimental work by Montoya et al. (2021) and in the numerical work on cemented sandstone by Rakhimzhanova et al. (2021). Therefore, the penetration model and soil model calibrations are resonably able to capture the effect of bio-cementation on q_c.

3.4 Δq_c – c relationship

Once the simulated tip resistances are validated against the available experimental datasets and engineering correlations, the simulations are extended to higher confining stresses (100, 200 and 400 kPa) to: (1) test the validity of the numerical model and thus the trend at relatively higher depths, and (2) extend the parametric space of the simulations and synthesize enough data to establish a relationship between the change in tip resistance due to cementation and apparent cohesion for bio-cemented sands. The tip resistance of bio-cemented sands increases with the apparent cohesion (i.e., the level of cementation) and with the confining stress and consequently, the change in the tip resistance due to cementation Δq_c follows the same trend as shown in Fig. 3.9. The performed simulations first initialize the confining stress and then apply the cementation. This approach has been chosen to be consistent with how bio-cementation has primarily been implemented in laboratory tests and how it is expected to be applied in the field. As a result, the cementation bonds are formed under the full in-situ stress conditions. Therefore, the bio-

cementation treatment is expected to increase the yield stress from the uncemented case at the given confining stress. The magnitude of this increase will depend primarily on the cementation level. Although the effect of cementation becomes less significant at higher levels of stress, it is possible that the yield stress may still affect the $\Delta q_c - c$ relationship (for example, at 500 kPa which would roughly correspond to 50 m depth in a saturated sand profile).

Eq. (3.6) presents a best-fit-line for the apparent cohesion and the change in tip resistance due to bio-cementation of loose sand. The apparent cohesion increases linearly with the change in tip resistance (Fig. 3.9), with the slope of the line being a function of the confining stress. A regression analysis using the least-squares method is performed to account for the dependence of the apparent cohesion on the confining stress. It is found that the cohesion is dependent on the square-root of the confining stress. The form of this relationship and its dependencies agree with a previously published relationship between tip resistance and cohesion (Lee et al. 2010). The latter was developed from tip resistances obtained from miniature cone penetrometers on gypsum-cemented sands in a calibration chamber, accompanied by cohesion intercept interpretations from failure envelopes obtained from triaxial tests on the same material.

$$c = a \cdot \Delta q_c \qquad (3.6)$$

where:

$$a = \frac{1}{587.3 + 12.4 \cdot \sqrt{\sigma_v'}}$$

and c is the apparent cohesion, Δq_c is the change in cone tip resistance due to cementation, and σ_v' is the initial in-situ vertical effective stress (all three parameters in units of kPa for this relationship).

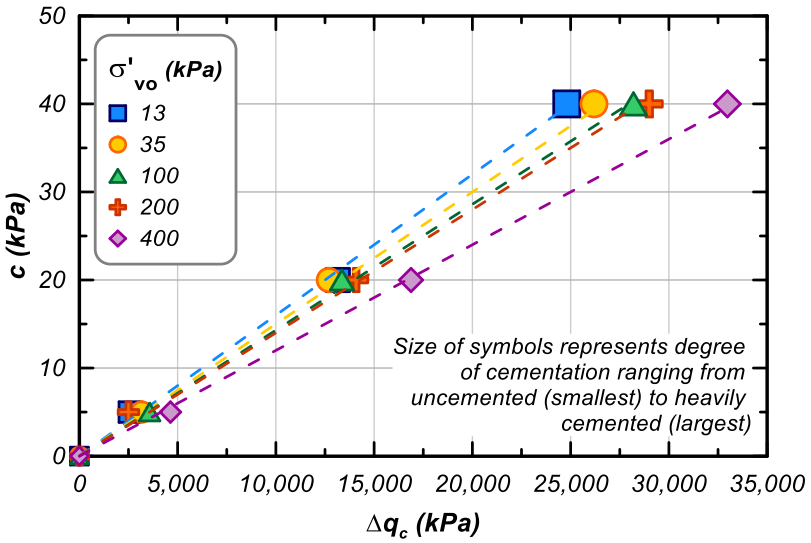

Figure 3.9. Trend between cohesion and change in tip resistance from synthesized data and its dependence on confining stress.

Plotted in a 3D space, the above relationship yields the surface shown in Fig. 3.10. Since the cone tip resistance is largely affected by the strength of the soil, a stronger or cemented soil will exert more resistance to the pushed cone and thus the tip resistance increases as the soil's strength increases. In cemented sands, the latter is mainly attributed to the increase in the apparent cohesion, hence, the upward trend for the apparent cohesion.

The confining stress also plays a major role in the soil's resistance and increase in strength. As the confining stress increases, the soil's strength increases resulting in an increased cohesion. While the ranges of tip resistances and vertical effective stresses may be comparable to "dense" clean sands, the developed relationship is only applicable to initially loose (D_R= 30-40%) MICP-treated sands contributing to a change in tip resistance due to the cementation.

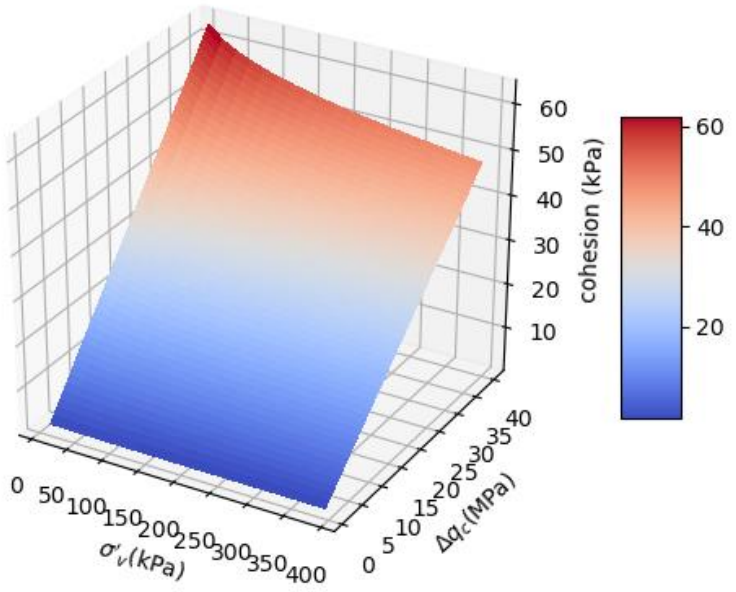

Figure 3.10. 3D surface of the relationship between effective vertical stress, change in cone tip resistance and cohesion.

3.5 Discussion

The cone penetration model using the Mohr-Coulomb constitutive model enables simulations that cover a range of soil properties and confining stresses to be performed, which is helpful in extending the analysis beyond the limited experimental data for cone penetration measurements in bio-cemented sands. The Mohr-Coulomb model can reasonably capture the elastic-plastic behavior of bio-cemented soils in the failure zone near the cone tip through defining the failure envelope with a cohesion intercept and a peak friction angle. Moreover, the Mohr-Coulomb model allows focus on two of the primary factors affecting the cone tip resistance in cemented sands: cohesion and stiffness. Cone tip resistance, and by extension strength, is largely affected by these two factors, but at different rates which is reflected by Eq. (3.1). While the application of a theoretical linear elastic-perfectly plastic continuum model with constant parameters to soil

conditions with strain-dependent parameters is fundamentally challenging, the approximation with a "functional" modulus provides useful predictions of the cone tip resistance (Schnaid et al. 1997). In the same line of thought and due to the Mohr-Coulomb formulation, the present analyses also assume a cohesion intercept which remains constant during the cone penetration. Consequently, the dilation angle is not activated to compensate for the reduction in the cohesion intercept due to bond degradation upon shearing with the simultaneous increase in dilatancy due to changes in fabric and particle shape and angularity. This approximation works for the present dataset and provides reasonable tip resistances. In addition, it is assumed that steady-state penetration is achieved and drained conditions are preserved during the cone push due to the open structure of bio-cemented sands and the slight reductions in hydraulic permeabilities from clean sands (Gomez and DeJong 2017). While the Mohr-Coulomb model provides a reasonable approximation of the mechanisms in bio-cemented sands, it is understood that the actual mechanisms around the tip are more complex due in part to the degrading effects of the bio-cementation.

The approach used to develop the $\Delta q_c - c$ relationship consists of the validation of the simulated cone tip resistances against those reported from two experimental programs on bio-cemented sands at different confining stresses. Once the tip resistances at 13 and 35 kPa gave reasonably consistent values compared to the experimental ones, the simulations are extended to higher confining stresses and shear stiffnesses, guided by laboratory data at these higher levels. As experimental results at higher confining stresses become available, the tip resistances corresponding to these stresses (100, 200, and 400 kPa) can be further validated. Thus, the $\Delta q_c - c$ relationship presented in this paper is valid for the range of parameters it was developed for. Confining stresses range from 13 to 400 kPa, cohesions range from 0 (uncemented) to 40 kPa, and shear wave velocities are proportional to the cohesion values.

It is envisioned that the proposed correlation will facilitate the evaluation of bio-mediated ground improvement at treated sites. Once the treatment process is done, it is recommended that a seismic CPT or a CPT coupled with geophysical tests is performed for the quality assurance and control of the achieved ground improvement. These in-situ tests provide a cone tip resistance profile and V_s measurements, respectively. The latter may be used for the quality control of the spatial distribution of the treatment over large areas of the site, while the former may be specified to locations of the site where structures and their foundations are expected. Therefore, the response of the foundation bearing soil is crucial for the numerical modeling and design of said foundation and structure, which leads to the importance of the estimation of strength parameters and specifically the "apparent" cohesion of the treated soil. Eqs. (3.1) and (3.6) provide two fundamentally connected variables ($\Delta V_s \; and \; \Delta q_c$) for the estimation of the "apparent" cohesion in bio-cemented sands. While the estimated values may differ due to the limited body of data used for the fitting of these relationships, the equations can be employed to cross-check their respective results and an average of the two estimates can be used to determine the "apparent" cohesion assigned to the constitutive law in the numerical model. Current practices neglect the inevitable presence of cementation in natural deposits due to the lack of understanding of the behavior of cemented sands and/or the inability to characterize them. Often this results in overly conservative designs and higher construction costs. While this work primarily applies to bio-cemented sands, an overlooked benefit is the ability to extend these findings to naturally cemented sands, since bio-cementation is thought of as a proxy to natural cementation in the lab.

3.6 Concluding remarks

This paper proposes a relationship between increase in cone tip resistance Δq_c and apparent cohesion for loose bio-cemented soils. This relationship is developed through the application of an existing axisymmetric cone penetration model using Mohr-Coulomb constitutive model calibrations. The improvement in the behavior of bio-cemented sands is attributed to the presence of cementation bonds characterized by an apparent cohesion value, hence the application of the Mohr-Coulomb constitutive model. The axisymmetric model is first calibrated and validated against control tests on clean sands, and then used to estimate cone tip resistances in bio-cemented sands for a range of cohesions and confining stresses. A simple linear relationship is found between the cohesion and the change in shear wave velocities for bio-cemented sands based on available laboratory data on MICP-treated specimens. Due to the large shear strains imposed on bio-cemented soils during cone penetration, there are likely compensating effects of reduction in cohesion and increase in dilatancy. The axisymmetric cone penetration model with the Mohr-Coulomb constitutive model using varying "functional" shear stiffness moduli yields realistic tip resistances when compared to field data at confining stresses of 13 and 35 kPa. Additional simulations across the parametric space (e.g., varying cementation level and confining stress) led to the development of a proposed relationship between cohesion and the change in cone tip resistance for bio-cemented sands. While the ranges of tip resistances and vertical effective stresses may be comparable to "dense" clean sands, the developed relationship is only applicable to initially loose (D_R=30-40%) MICP-treated sands contributing to a change in tip resistance due to the cementation. This relationship mathematically describes the causality between soil strength (in the case of bio-cemented sands, mainly attributed to cohesion) and tip resistance creating a bridge between a parameter common to modelers and one common to practitioners, respectively. It

remains that lab tests could supplement CPT soundings to fully characterize the strength parameters of bio-cemented sands for design.

CHAPTER 4

Extension of a sand plasticity plane-strain model for earthquake applications to bio-cemented sands

Anticipated publication:

El Kortbawi M., Ziotopoulou K., and Boulanger R. W. Extension of a sand plasticity plane-strain model for earthquake applications to bio-cemented sands.

Author's note: This paper will be submitted for journal publication soon. Figure and table captions and intext references were modified from the original publication to conform with the format of this Dissertation.

Abstract

Challenges in the sampling of naturally cemented sands have pushed researchers to find artificial proxies to natural cementation in the field such as bio-cementation. While most studies focused on the utility of bio-cemented sands in improving the performance of sand on the experimental level, less interest was drawn to their mechanical response on the numerical level. More specifically, a usable constitutive model which has the capability of capturing the mechanical response of bio-cemented sands, and by extension naturally cemented sands, under different loading conditions,

including cyclic, is still lacking. In this paper, the extension of a plane-strain bounding surface plasticity model for earthquake applications for sands to bio-cemented sands is proposed. The formulation of the extended model follows the baseline formulation of the plasticity model for sand PM4Sand Version 3.2 and as such it is a critical state-based, stress ratio-controlled, bounding surface plasticity model. The modifications to the original formulation include the contribution of the cementation to the shear stiffness and peak strength, and the degradation of these improvements upon accumulation of bond damage. These modifications resulted in additional input parameters to PM4Sand which carry a physical meaning related to the behavior of cemented sands. These additional input parameters and their default values are introduced herein. The extended model is implemented in FLAC 8.1 using a dynamic link library and is only applicable to lightly and moderately cemented sands where continuum models remain usable. A generalized calibration demonstrating the performance of the model under various cementation levels, confining stresses, drainage scenarios, and loading conditions is presented and guidance is provided to aid users in the calibration process. The extended model is then validated against a body of experimental data on bio-cemented sands. Overall, the extended model is able to predict the trends seen in bio-cemented sands with minimal calibration effort by means of input parameters physically meaningful and obtainable from the field.

4.1 Introduction

Naturally cemented sands are the product of time-dependent mineral precipitation processes. Despite their abundance in natural deposits, they have been studied less than clean/uncemented sands due to challenges in their sampling and characterization. Sampling of lightly-cemented sands can be difficult because of (1) disturbance from conventional drilling methods and (2) the increased

cost and time needed to get samples using hand-carved block sampling (Collins and Sitar 2009). Furthermore, fabric (i.e., particle orientation and packing) plays an important role in the strength and stability of cemented sands, and as a result, reconstituted samples of cemented sands do not produce results representative of insitu conditions (e.g., Clough et al. 1981; Collins and Sitar 2009).

In an effort to understand natural cementation, researchers have studied artificial cementation processes which are induced in a more controlled environment and are more representative of natural cementation in the field. Earlier studies (e.g., Clough et al. 1981; Rad and Clough 1982; Saxena and Lastrico 1978 and others) used Portland cement as the cementing agent in artificially cemented sands. These studies investigated the mechanical behavior of cemented sands, including evaluation of compression, tensile and shear stress-strain under monotonic and cyclic loading (e.g., Rad and Clough 1982; Saxena et al. 1988a, 1988b, 1988c), and also included complimentary constitutive modeling (e.g., Nova et al. 2003; Reddy and Saxena 1992; Rumpelt 1990; Vatsala et al. 2001). More recently, studies on cemented sands have considered more environmentally conscious and sustainable cementing agents that are also more representative of natural cementation such as microbially-induced calcite precipitation (MICP) (e.g., Ismail et al. 2002; Lee et al. 2022; Montoya and DeJong 2015).

Over the last decade, MICP has emerged as a biogeochemical process which can artificially cement soils by accelerating natural carbonate precipitation processes. It is considered a sustainable alternative to conventional soil improvement methods (Raymond et al. 2020) and a proxy for natural cementation processes in the field as the same processes naturally occur in the field. MICP soil treatment is induced by first introducing treatment solutions containing either lab-cultured ureolytic microorganisms (augmentation) or nutrients to stimulate existing soil ureolytic

microorganisms (stimulation). Then, a cementation solution containing urea and calcium salts is injected to initiate the cementation process (DeJong et al. 2006; DeJong et al. 2013; Gomez et al. 2017). Advances in the understanding of biological and chemical processes as summarized by DeJong et al. (2022) have permitted researchers to better control cementation magnitudes as well as its overall spatial uniformity (Montoya et al. 2021; San Pablo et al. 2020).

Numerous experiments have been performed on bio-cemented sands to investigate their mechanical behavior. Chapter 2 reports the state-of-the-art in the mechanical response of bio-cemented sands and conclude that the behavior of initially loose cemented sands is attributed to two concurrent mechanisms: densification and cementation. Densification is the soil skeleton's void ratio reduction due to the addition of cementation, which is distributed spatially between the formation of bridges at the particles' contacts, creating cementitious binding between particles ("apparent" cohesion), and the coating of the particles with precipitates. While the latter alters the roughness and angularity of the sand particles which in turn affect the dilatancy, strain-softening, and post-peak dilation of the soil (e.g. Montoya and DeJong 2015; Wu et al. 2021), the former is the primary contributing factor to the considerable improvement in the stiffness and strength of bio-cemented sands (e.g., Feng and Montoya 2015; Lee et al. 2022; Leroueil and Vaughan 1990; Lin et al. 2016; Montoya and DeJong 2015). This improvement is more significant for low confinements and higher levels of cementation. A full account of laboratory studies on MICP-cemented sands and their mechanical behavior, microscopically and macroscopically, is presented in Chapter 2 of this Dissertation.

The increased interest in the experimental aspects of bio-cemented sand response was closely followed by research on the ability to numerically simulate their mechanical responses, which is important in the understanding of their behavior leading to field deployment as an alternative

ground improvement method. Researchers have numerically studied the microscopic and macroscopic behavior of bio-cemented sands using discrete element modeling (DEM) (Evans et al. 2015; Feng et al. 2017; Khoubani et al. 2016; Ning et al. 2017; Yang 2018) and continuum models (Fauriel and Laloui 2012; Gai and Sanchez 2018; Mehrabi and Atefi-Monfared 2022; Nweke and Pestana 2017), respectively. The latter models incorporate the contribution of bio-cementation to existing models such as the Cam Clay model (Gai and Sanchez 2018) and the NorSand model (Nweke and Pestana 2017). While these models inherit both the capabilities and limitations of their respective baseline formulations, they also carry the limitations of the data used for validation. Such limitations may be in the form of an overall lack of data for some or more loading paths (e.g., more monotonic data available compared to cyclic) or in the form of data that are insufficient in quantity to draw robust conclusions about the mechanical response of the tested treated materials. Other limitations relate to the broad spectrum of parent materials and treatment protocols used that challenge the unification of observations. These limitations are not unreasonable given the novelty of this research field. Furthermore, the usability and practicality of constitutive models in terms of input parameters plays a major role in their potential for adoption in practice. While crucial for the forward design and mitigation of site conditions, none of the above models directly maps field measurements from the quality assurance and control process to the specification of input parameters to guide and inform ground improvement solutions.

Several constitutive models for cemented sands (regardless of their cementing agent) were extended from the original formulation of a constitutive model for sands by means of an addition of a tensile strength to indirectly produce a cohesion intercept (Gai and Sanchez 2018; Nova et al. 2003; Rahimi et al. 2018; Zhang et al. 2021). These models have also included damage mechanisms for degrading the cementation in terms of plastic strains. In the following, a bounding

surface plasticity model for sands PM4Sand Version 3.2 (Boulanger and Ziotopoulou 2022) is extended to bio-cemented sands using a similar approach to the above models but with alternative functional forms which tie better with the PM4Sand formulation. These functional forms are informed by an expanding experimental dataset reviewed in Chapter 2.

This paper presents the development and validation of a plane-strain constitutive model (PM4SandC) capable of simulating the mechanical behavior of lightly to moderately bio-cemented sands under monotonic and cyclic loading conditions. This is achieved through extension of the bounding surface plasticity plane-strain model for sands PM4Sand. The model is applicable to light and moderate cementation levels as defined by Montoya et al. (2013) to be for calcite contents up to 3% by mass and/or shear wave velocity up to 600 m/s because the failure of sands at heavier cementation levels is governed by other mechanics which cannot be accommodated in continuum models (e.g., fracture). The goal of this work is to make available a usable constitutive model for bio-cemented sands which can advance the deployment of MICP as a liquefaction mitigation technique. The modified aspects of the formulation to incorporate cementation are presented first, followed by a description of the model's input parameters and numerical implementation in FLAC 8.1 (Itasca 2019). A set of general calibrations is presented to demonstrate the capabilities of the model under various monotonic and cyclic, drained and undrained conditions, and the calibration process is described to facilitate the use of the model by others. The performance of the extended constitutive model is then evaluated via single-element simulations against readily available bench-scale tests on MICP-treated specimens, namely drained triaxial compression tests, and undrained monotonic and undrained cyclic direct simple shear (DSS) tests.

4.2 Model reformulation

The extension of a plasticity model for clean sands in earthquake engineering applications to also capturing the responses of bio-cemented sands (henceforth named PM4SandC) is presented. The extended model inherits the formulation of the baseline model PM4Sand Version 3.2 as described in Ziotopoulou and Boulanger (2016) and Boulanger and Ziotopoulou (2022). PM4Sand is a plasticity model for sand used for earthquake engineering applications. It is a critical state-based, stress ratio-controlled, bounding surface plasticity model which follows the basic framework of the Manzari and Dafalias (1997) model, later extended by Dafalias and Manzari (2004). The advantages of the PM4Sand formulation are: (1) its ability to reasonably estimate the broad range of behaviors known about sands and used as established empirical and semi-empirical relationships in practice, and (2) its ability to be calibrated with reasonable engineering effort using input parameters informed by commonly performed field investigations. The required input parameters to the model are its three primary parameters (relative density D_R, shear modulus coefficient G_o, and contraction rate parameter h_{po}). The PM4Sand model also features 21 secondary parameters which have been determined via a generalized calibration and have default values that will generally produce reasonable results compared to typical trends. Subject to the availability of data and the user's experience, secondary parameters can be assigned values other than their defaults. Readers interested in the formulation of the baseline model PM4Sand are referred to Ziotopoulou and Boulanger (2016) and Boulanger and Ziotopoulou (2017, 2022) for its full description. Only aspects of the PM4SandC model which are different from the original PM4Sand formulation are described in this paper.

Modifications in PM4SandC relative to PM4Sand model include: (1) the shear modulus constant $G_{o,cem}$ is calibrated in terms of the cemented shear wave velocity ($V_{s,cem}$) to reflect the

increase in the stiffness of bio-cemented sands, (2) the mean effective stress (p) is enhanced by the contribution of a p due to the cementation ($p_{cem,initial}$) which reflects the enhanced tensile strength of bio-cemented sands, (3) the shear modulus is proportional to p raised to a power n that is dependent on cementation level rather than a power of 0.5 for uncemented sands, and (4) evolution laws are used to degrade/alter the cementation parameters as a function of damage accumulation. The PM4Sand and PM4SandC model are constrained to plane-strain applications since the constitutive equations are cast in terms of in-plane stresses only.

4.2.1 Elastic parameters

Cementation affects the elastic part of a treated material's response in two ways: (1) an increase in stiffness, and (2) an increase in strength. The increase in stiffness is quantified by geophysical tests and more specifically the change in the shear wave velocity from the loose to the cemented state, whereas the increase in peak strength can be characterized by an "apparent" cohesive intercept ($c_{initial}$) resulting in a tensile capacity and a higher peak friction angle (ϕ_{peak}). These parameters define a Mohr-Coulomb-type failure envelope for cohesive soils which can be conveniently used as a proxy to characterize bio-cemented sands. Hence, due to the cementation bonds, the previously negligible tensile strength in soils becomes more prominent and significant to the behavior of the cemented soil at the onset of shearing. This equivalent tensile strength is estimated as a function of the level of cementation. It is mathematically described by Eq. (4.1), where $c_{initial}$ and ϕ_{peak} are the Mohr-Coulomb-type strength parameters for an intact bio-cemented sand, and is added to the mean effective stress $p_{initial}$ (Eq. 4.2) to represent a state in which there is tensile contribution to the strength. This addition eventually shifts the constitutive space and results in larger dilatancy and bounding surfaces (more details in Section 4.2.3):

$$p_{cem,initial} = \frac{c_{initial}}{\tan \phi_{peak}} \tag{4.1}$$

$$p = p_{initial} + p_{cem,initial} \tag{4.2}$$

The formulation of the model is in effective stress terms, and thus the apostrophe has been dropped for all parameters. The parameters $c_{initial}$ and ϕ_{peak} are introduced to PM4SandC as secondary input parameters and, where no tests are available to estimate their values, default values are assigned based on established relationships with available experimental results collected in Chapter 2. Due to the interconnection between strength and stiffness, the relationships for estimating the cemented strength parameters depend on some quantification of the level of cementation ($V_{sr} = V_{s,cem}/V_s$) which is the ratio of the cemented to the uncemented V_s. The addition of the tensile strength results in a shift of the original PM4Sand q-p space to the left, hence incorporating the contribution of a tensile component for an intact bio-cemented sand. As shearing occurs, bond damage accumulates, cementation bonds eventually break, and cementation-enhanced parameters revert to their original sand counterparts. The damage accumulation and bond degradation are explained in Section 4.2.4.

Beyond enhancing the peak strength, the presence of the cementation bonds at particle contacts and surfaces also increases the stiffness (G_{cem}) and dry density of the treated materials which is reflected in an increase of their shear wave velocity ($V_{s,cem}$). Accordingly, the elasticity constants in PM4SandC are enhanced to represent the stiffer bio-cemented sands. This is achieved through three parameters (Eq. 4.3): (1) the calibrated shear modulus constant $G_{o,cem}$, (2) the enhanced stress state $p = p_{initial} + p_{cem,initial}$, and (3) the stress-normalization exponent n:

$$G_{cem} = G_{o,cem}\, p_A \left(\frac{p_{initial} + p_{cem,initial}}{p_A} \right)^n \tag{4.3}$$

where $G_{o,cem}$ is a calibration parameter informed from $V_{s,cem}$ and essential to the calibration process (see Section 4.3.1) and n is the stress-normalization exponent with a default value ranging between 0 and 0.5 for bio-cemented sands. Values of n of 0 and 0.5 correspond to rock-like and soil-like material, respectively, thus the higher the level of cementation, the lower the n, which is consistent with the observations that the cementation is less affected by confinement as the latter increases (DeJong et al. 2022). Both $p_{cem,initial}$ and n degrade at the onset of bond degradation and will be further discussed later.

4.2.2 Critical state

Past research has suggested the validity of the critical state concept for cemented sands (Chong 2019). Yet, the uniqueness of the critical state line (CSL) as presented in Critical State Soil Mechanics does not apply to bio-cemented sands because the CSL may be variable depending on the level of cementation (Rahimi et al. 2015; Sharma and Fahey 2003b). Considering that the CSL will be reached at high shear strains, in order for it to be different from its clean sand counterpart, any damaged cementation needs to be significant for it to affect the location of CSL. Practically, this means that for light and moderate cementation levels, CSL will be relatively unaffected.

The PM4SandC reformulation assumes that the contribution of the broken cementation to fines in the sand matrix will be negligible for the levels of cementation where the model is applicable (light and moderate cementation), and thus, no such consideration is made in the CSL formulation. A dependency is however introduced by connecting the relative state parameter $\xi_{R,cem}$ (Boulanger 2003) and the cementation-induced $p_{cem,initial}$, such that the CSL will vary following a direct

measure of the level of cementation. Hence, the model uses $\xi_{R,cem}$ to define the state of stresses with respect to the CSL. $\xi_{R,cem}$ is the difference between the soil's relative density (D_R) at its critical and current state (Eq. 4.4) given by:

$$\xi_{R,cem} = D_{R,cs,cem} - D_R \tag{4.4}$$

The above estimate for the relative state parameter $\xi_{R,cem}$ reflects the increased density of bio-cemented sands with respect to clean sands. This increase in relative density is expected due to the cementation bridges at particle contacts, the coating of particle surfaces, and the filling of the voids between individual sand particles. The CSL may be obtained experimentally but this may be a challenging task due to the brittleness and localization mechanisms observed in bio-cemented sands. Eq. 4.5 for the critical state $D_{R,cs}$ provides enough versatility to control the position of the CSL during calibration through the constants R and Q which have default values of 1.5 and 10, respectively, as inherited from clean sands following Bolton's (1986) dilatancy relationship:

$$D_{R,cs,cem} = \frac{R}{Q - \ln\left(100\dfrac{(p_{initial} + p_{cem,initial})}{p_A}\right)} \tag{4.5}$$

4.2.3 Critical, dilatancy and bounding surfaces

The improvement in mechanical behavior due to the presence of the cementation (i.e., increase in stiffness, increase in peak strength, and increase in dilatancy due to particle angularity and roughness) is evident in monotonic tests and translates into an improved cyclic resistance to liquefaction in cyclic undrained tests. These elemental behaviors are constitutively controlled in PM4SandC by the yield, dilatancy, critical and bounding surfaces. In the constitutive q-p space for the original PM4Sand, these surfaces are represented by lines from the space origin. The inclusion of an equivalent cementation-induced tensile strength results in the shift of the PM4Sand

constitutive space leading to a cohesion intercept. Figure 4.1 presents a schematic of the yield, critical, dilatancy, and bounding surfaces in the q-p space for PM4SandC. This modification translates into larger yield, dilatancy and bounding surfaces in which a bio-cemented sand remains elastic for a longer duration of the loading until it reaches the larger yield surface or yield stress. Immediately after yielding, the cemented sand gradually mobilizes its strength but at a higher peak due to the cementation bonds initially inhibiting shear damage. However, as the strength of the cementation bonds is overcome, breakage gradually occurs, the rate of dilation reaches a maximum, friction between sand particles takes over the post-triggering behavior, and the cemented sand loses its strength and rapidly accumulates damage. The slopes of the dilatancy and bounding lines, M^d and M^b, respectively, are a function of the $\xi_{R,cem}$introduced in Section 4.2.2. These slopes increase as the level of cementation increases leading to the expansion of surfaces, and decrease as bond degradation occurs leading to the shrinking of the surfaces.

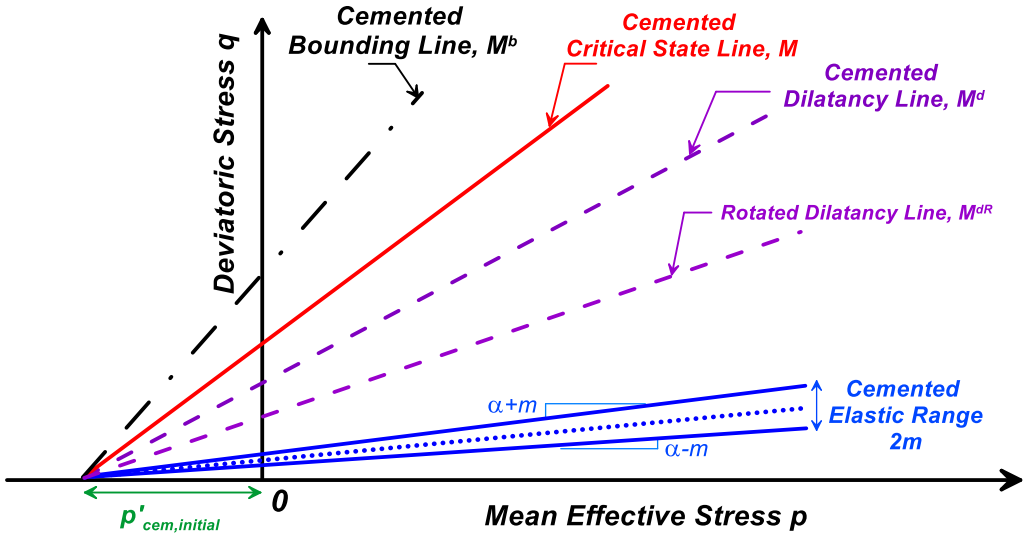

Figure 4.1. Schematic of yield, critical, dilatancy and bounding lines in q-p space for PM4SandC.

4.2.4 Bond degradation

Early stages of loading (pre-yield) are mostly controlled by the cohesion component, i.e., the resistance due to the cementation bonds. Post-yield phases of the response are dominated by the frictional interactions that take place in the soil matrix, i.e., the rearrangement of particles following the breakage of the bonds. These two components mechanistically synthesize the response of bio-cemented sands. Clearly, the cementation components presented thus far (Sections 4.2.1 to 4.2.3) correspond to an intact product of sand-cement matrix, however, realistically, they should evolve as a function of an accumulating damage index. Damage in PM4SandC is tracked through the accumulation of strains. This approach is consistent with the approaches used in other constitutive models to track cementation degradation with strain accumulation or a certain damage index (e.g., Gai and Sanchez 2018; Gao and Zhao 2012; Kavvadas and Amorosi 2000; Nova et al. 2003; Zhang et al. 2021).

The degradation of the cementation is described in terms of the accumulation of plastic shear strains over a strain space that contributes to degradation of cementation (referred to as plastic deviatoric degradation strains). The plastic component of deviatoric strain is considered here for the cementation degradation because damage is associated with irreversible plastic deformations. Moreover, plastic deviatoric strains are accumulated during shearing and cumulatively cause the degradation of the cementation. Hence, a cumulative plastic deviatoric degradation strain is introduced in the degradation law. However, the presence of the "apparent" cohesion inhibits damage accumulation initially, thus the rate of plastic deviatoric strain accumulation is controlled to reproduce a gradual cementation degradation as observed in experiments. As a result, cumulative plastic deviatoric degradation strain is activated when the total accumulated plastic deviatoric strain ($\sum d\varepsilon_{q,tot}^{p}$) reaches some elastic threshold strain (γ_{deg}) and it fully accumulates

and contributes to the damage when a "residual" strain (γ_{res}) is reached. A multiplier F_s, which increases from 0 to 1, is introduced to control the accumulation of incremental plastic deviatoric strains $d\varepsilon_q^p$ (Eq. 4.6). The sum of the product of F_s and the incremental plastic deviatoric strain $d\varepsilon_q^p$ represents the cumulative plastic deviatoric degradation strain $C_{s,cum}$. The functional form for F_s is described with a plateau at zero before γ_{deg}, it then follows a logic trend from 0 to 1 between γ_{deg} and γ_{res} where it partially accumulates strains until it reaches γ_{res}, after which it attains the value of 1, meaning that strain increments fully contribute to the damage. Mechanistically, $C_{s,cum}$ is the damage tracked by the model to initiate the degradation of $p_{cem,initial}$ to a "secant" or "degraded" p_{cem} using a similar degradation factor F_{deg}:

$$C_{s,cum} = \sum F_s . d\varepsilon_q^p \tag{4.6}$$

$$F_s = 1 - \frac{1}{1 + \left(\frac{\sum d\varepsilon_{q,tot}^p}{\gamma_{deg} + \frac{1}{8}(\gamma_{res} - \gamma_{deg})} \right)^{m_d}} \tag{4.7}$$

$$p_{cem} = F_{deg} \cdot p_{cem,initial} \tag{4.8}$$

$$F_{deg} = \frac{1}{1 + \left(\frac{C_{s,cum}}{\gamma_{deg} + \frac{1}{2}(\gamma_{res} - \gamma_{deg})} \right)^{m_d}} \tag{4.9}$$

F_{deg} follows an inverse trend relative to F_s, in that it starts at 1 and degrades to 0. At the initiation of the plastic deviatoric degradation strain accumulation ($C_{s,cum} \approx 0$), F_{deg} is at a value of 1 and remains at 1 until γ_{deg} is reached. At this elastic threshold strain, bond degradation starts and F_{deg}

decays at a degradation rate (m_d) until it reaches 0 as the "residual" strain (γ_{res}) is attained. The above equations for F_s and F_{deg} (Eqs. 4.7 and 4.9) contain three interrelated parameters γ_{deg}, γ_{res}, and m_d such that an assignment can be made for the first two parameters and the third one (m_d) can be back calculated. In the current implementation, the degradation rate m_d is given a default value which is solved for as a function of the range between the degradation and residual strains ($r_s = \gamma_{res} - \gamma_{deg}$) such that, as the range increases, the degradation rate m_d decreases, and vice versa. The default value for m_d is back calculated from Eq. 4.7 by assuming that F_s is almost zero at γ_{deg} and 0.99 at γ_{res}. Rearranging Eq. 4.7 and solving for m_d yields the following expression for its default value:

$$m_d = \frac{\ln(0.001/0.99)}{\ln(\gamma_{deg}/[\gamma_{deg} + \frac{1}{8}(\gamma_{res} - \gamma_{deg})])} \tag{4.10}$$

This flexibility in the cementation degradation functional form allows its use over a range of levels of cementation where bond breakage may start earlier or later, progress faster or slower, and end at some user-prescribed "residual" strain. Figure 4.2 presents a sensitivity exercise on the range of strains r_s and its effect on the monotonic response of a bio-cemented sand subject to shear loading in a DSS device. F_s and F_{deg} are plotted simultaneously in Fig. 4.2a to demonstrate their functionality. For the three selected ranges of strain, F_s is more than 95% accumulated by the time F_{deg} comes into play, as expected. The interplay between these functional forms is demonstrated in Fig. 4.2b where the shorter range reflects a faster degradation and softening followed by the intermediate range and then the longer range. As the range of strains r_s over which degradation occurs increases, the rate of degradation m_d decreases, and softening becomes less abrupt.

Eqs. (4.6) to (4.10) essentially slow down the accumulation of plastic deviatoric degradation strains at the onset of degradation and then speeds up this accumulation progressively. This allows for the accumulation of damage and the concurrent degradation of the cementation and is found to improve both the cyclic resistance and the slope of the relationship between the cyclic resistance ratio (CRR) and the number of cycles required to trigger liquefaction (N_{cyc}). As the degradation evolves (Fig. 4.3a), the initial intact $p_{cem,initial}$ gradually decays to p_{cem} (Fig. 4.3b) and it then follows that all other cementation components of the model degrade in the same manner (Figs. 4.3c, 4.3d). These components include: (1) the shrinking of the bounding and dilatancy surfaces toward their original PM4Sand configuration (Boulanger and Ziotopoulou 2017), and (2) the degradation of the V_{sr} from its initial value >1 toward unity (i.e., uncemented value), and (3) the degradation of the shear stiffness exponent n from its initial cemented value toward its uncemented value of 0.5.

4.3 Model input parameters

The PM4SandC constitutive model maintains the same functionality as the PM4Sand model and it handles both uncemented or clean and cemented sands, with one additional primary and 4 additional secondary parameters for the cemented mode, all of which have a physical meaning and can be estimated from and calibrated to typically available experimental results.

4.3.1 Primary input parameters

In addition to the three primary parameters of PM4Sand (D_R, G_o, and the contraction rate parameter h_{po}), a primary input parameter characterizing the level of the cementation is introduced. Quantitatively, the magnitudes of the improvement in the behavior of bio-cemented sands are more pronounced for higher levels of cementation, and vice versa, therefore, the level of cementation

should be accounted for in the model. Due to the practicality of geophysical tests for nondestructively evaluating site conditions, the ratio, V_{sr}, of the cemented ($V_{s,cem}$) to the uncemented shear wave velocity (V_s) is selected as a proxy to the level of cementation. For uncemented or clean sands, V_{sr} is equal to 1, the relationships implemented for cemented sands are inactive, and the model operates as PM4Sand.

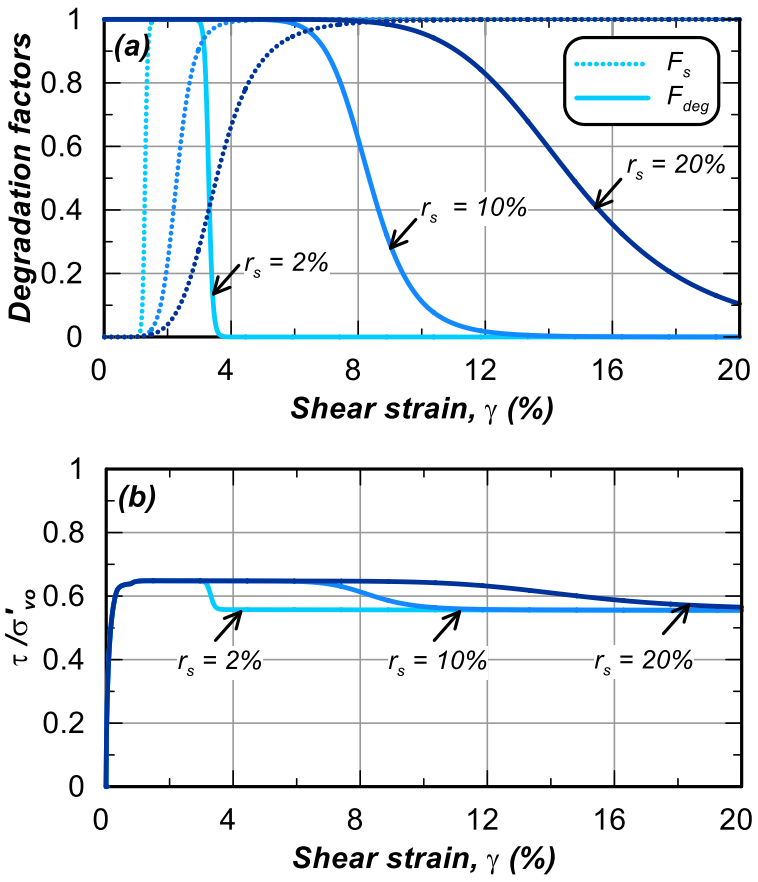

Figure 4.2. Sensitivity analysis on the effect of the strain range r_s over which cementation degrades in a drained monotonic DSS test with a stress-normalized V_{s1} of 150 m/s, V_{sr} of 2, confining stress of 100 kPa: (a) effect of range r_s on the degradation factors F_s and F_{deg}, (b) effect of range r_s on the stress-strain response.

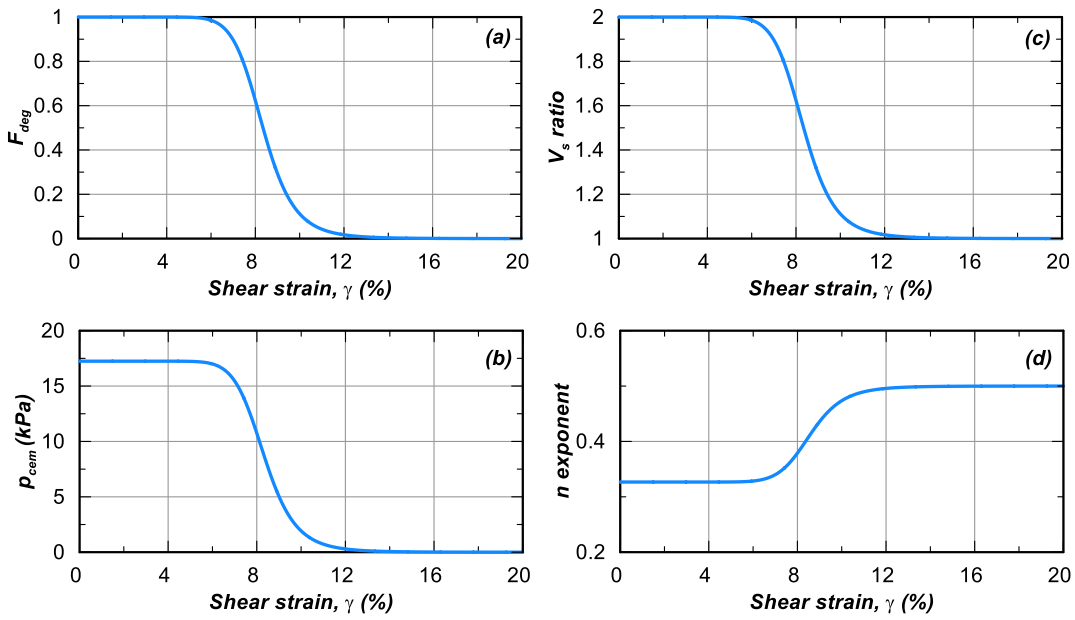

Figure 4.3. Evolution of cementation parameters with the accumulation of damage due to shear strains for the drained monotonic DSS with r_s = 10% shown in Figure 4.2 (V_{s1} of 150 m/s, V_{sr} of 2, confining stress of 100 kPa).

For cemented sands, $V_{sr} > 1$ and the cementation parameters are calculated. If sufficient shearing is applied and all cementation is destroyed, a cemented sand with an original value of $V_{sr} > 1$ converges to an uncemented sand with a $V_{sr} = 1$ (Fig. 4.3c). An upper limit of V_{sr} = 5 is assigned to the model because of the lack of experimental data at higher cementation levels for the validation of the model and the different failure mechanisms at higher cementation levels.

4.3.2 Secondary input parameters

The secondary input parameters can be grouped into 2 categories: parameters for the cementation initialization and parameters for the cementation degradation. To quantify the gained strength from the cementation, the strength parameters $c_{initial}$ and ϕ_{peak} should be initialized. These parameters can be obtained from fitting a Mohr-Coulomb type failure envelope to Mohr's circles for strength

tests run at various confining stresses on a bio-cemented sand specimen (e.g., Nafisi et al. 2020). Alternatively, $c_{initial}$ and ϕ_{peak} can be initialized by using relationships developed through the fitting of readily available experimental results as a function of V_{sr}. These relationships provide a first-estimate default value for $c_{initial}$ and ϕ_{peak} if no other values are defined by the user. These equations are empirical and thus, Eq. 4.11 and 4.12 give $c_{initial}$ in kPa and ϕ_{peak} in degrees, respectively:

$$c_{initial} = 11.5 \cdot V_{sr} - 11.5 \tag{4.11}$$

$$\phi_{peak} = \sqrt{906.04 + 331 \cdot \ln(V_{sr})} \tag{4.12}$$

An alternative relationship for the "apparent" cohesion $c_{initial}$ is developed in Chapter 3 as a function of the change in cone tip resistance (Δq_c) due to the bio-cementation. The purpose of this alternative relationship is to provide an estimate of the "apparent" cohesion value based on a measured field parameter q_c. To date, cone penetration data in bio-cemented sands are limited to two large scale tank experiments (Gomez et al. 2018; Montoya et al. 2021) and two centrifuge tests (Darby et al. 2019; San Pablo et al. 2023), therefore, cone penetration was numerically simulated using a Mohr-Coulomb constitutive model for bio-cementation, and q_c data was synthesized for the fitting of the relationship and validated against the available experimental q_c from 2 of these studies. The reader is referred to Chapter 3 for more details on the development of this relationship:

$$c_{initial} = \frac{1}{587.3 + 12.4 \cdot \sqrt{\sigma'_v}} \cdot \Delta q_c \tag{4.13}$$

where σ'_v is the effective vertical stress and $c_{initial}$, Δq_c, and σ'_v are in kPa.

The functional forms used in PM4SandC are decided based upon an extensive literature review in Chapter 2. Since the fitted experimental data on strength parameters for bio-cemented sands is limited, caution is advised when using the relationships outside of the ranges of conditions they were obtained for (e.g., calcite content up to 6%).

The parameters for the cementation degradation γ_{deg} and γ_{res} are directly provided by the user. These values can be estimated from the stress-strain response of monotonic strength tests. γ_{deg} and γ_{res} coincide with the strains at the onset of softening and critical state, respectively. The parameter m_d can also be estimated from lab results if the degradation of the V_s during the test is monitored. While this parameter may be more difficult to determine, the model is cast in a way where m_d is back calculated from γ_{deg} and γ_{res} when cementation degradation starts at γ_{deg} (refer to Section 2.4). The default value for m_d can also be overridden by the user's estimate, if available.

4.3.3 Numerical implementation

The numerical implementation of PM4SandC as a dynamic link library in the explicit finite difference program FLAC 8.1 is identical to the one for PM4Sand. In addition, the implementation of PM4SandC uses explicit integration and thus the stability of the numerical solution may be affected by the time step size. While the default time steps of FLAC in dynamic analyses of liquefaction problems in sands have ensured minimal dependence of the solution on the step size and adequate convergence of the numerical solution, the range of parameters used for cemented sands pose a numerical instability in the elemental response in monotonic loading. The numerical convergence of the current implementation is evaluated by running drained monotonic DSS tests on bio-cemented sands using the default time step computed by FLAC and smaller time steps computed internally to PM4SandC and imposed on FLAC's dynamic time step. Monotonic DSS simulation trials with PM4SandC indicate that strain increments on the order of 10^{-5} and smaller

produce consistent results and smooth responses. This is attributed to the significant increase in the shear stiffness of bio-cemented sands relative to clean sands which goes into the calculation of the default time step. The adjusted dynamic timestep for PM4SandC under monotonic conditions is given in Eq. 4.14:

$$\Delta t_{\max} = 0.01\left(\frac{mp}{G_{cem}\dot{\gamma}}\right) \tag{4.14}$$

where p is the enhanced mean effective stress equal to $p_{initial} + p_{cem,initial}$, m is the size of the elastic range, G_{cem} is the cemented shear modulus and $\dot{\gamma}$ is some constant reference strain rate. This expression can be viewed as a maximum limit on the timestep to avoid any numerical instability. For example, for m = 0.1, p =100 kPa, G_{cem}= 205 MPa (equivalent to ~ V_{sr} = 2) and $\dot{\gamma}$= 0.02 %/s, Δt_{max} will be 2.4*10^{-5}. A sensitivity of simulation results to the dynamic time step should be considered for system-level analyses.

4.4 Model calibration

The intention of the calibration approach is to approximate the main features and trends of the cemented soil behavior as indicated by the currently available body of experimental data, rather than precisely reproducing specific experimental observations. It is unlikely for one model to simultaneously fit all design correlations, however, it is desirable that it is able, after calibration to the design correlations of utmost importance to the project, to produce reasonable behaviors consistent with general trends and magnitudes.

A recommended sequence of steps for calibration is listed below to guide the calibration process, however, alternative calibration approaches may be applicable as well.

(1) Select the uncemented ($V_{s,ini}$) and cemented ($V_{s,cem}$) shear wave velocity and estimate the primary parameter V_{sr}.

(2) Select the cemented shear modulus coefficient ($G_{o,cem}$) to match the small-strain shear modulus consistent with the cemented shear wave velocity ($V_{s,cem}$).

(3) Input the relative density of the soil in its cemented condition, i.e., $D_{R,cem}$, due to the considerable densification of the soil following cementation. This will be reflected in an enhanced dilative volumetric behavior as expected for bio-cemented sands. Whenever indications of the change in relative density due to the cementation are not readily available, the uncemented relative density may be input while acknowledging that changes in the volumetric behavior may not be noticeable (see Section 4.5).

(4) Select the degradation (γ_{deg}) and residual (γ_{res}) strain values which can be informed by monotonic tests or V_s monitoring patterns.

(5) Select values for any secondary parameters which can be informed by field measurements or available correlations such as $c_{initial}$, ϕ_{peak}, and n.

(6) Perform single-element simulation of monotonic drained and undrained loading responses and use γ_{deg} and γ_{res} to adjust the degradation as necessary.

(7) Perform single-element simulation of cyclic undrained loading with uniform cyclic stress ratios and use h_{po} to adjust the slope of the simulated CRR versus number of uniform cycles to trigger liquefaction.

(8) Examine the stress-strain and stress-path responses of the cyclic loading simulations and fine-tune secondary parameters as needed.

The generalized calibration is presented herein with various loading conditions of interest to demonstrate (1) the ability of the model to predict the trends indicated by available data, as well

as (2) the effect of various input parameters on the obtained responses. It should be noted that the D_R used across this generalized calibration (bullet point # 3 above) is unified regardless of level of cementation and thus, does not represent the densification due to the increased cementation because (1) this increase in D_R cannot be estimated unless actual tests are run and measurements are taken (see Section 4.5), and (2) the effect of the modifications done to the model is better highlighted when behaviors due to stiffness and strength increase and densification increase are uncoupled and parameters related to densification are kept constant. Therefore, minimal changes in the volumetric behavior of the following simulations occurs which may be unnoticeable considering the scales of the plots. In reality, these mechanisms are concurrent and should be calibrated for as such. The effect of increase in D_R due to the cementation-induced densification is explored in Section 4.5.

Figure 4.4 illustrates the effect of confinement and the level of cementation on the drained monotonic DSS response of bio-cemented sands. The top row of plots shows the stress-strain response with Figs. 4.4a and 4.4b for uncemented sands with V_{sr} of 1, Figs. 4.4c and 4.4d for a cemented sand with a V_{sr} of 2, and Figs. 4.4e and 4.4f for a cemented sand with a V_{sr} of 4. The responses for the uncemented sands using PM4SandC with a V_{sr} of 1 are confirmed to be identical to the responses from PM4sand. To better illustrate the effects of bio-cementation on the response, the shear stress is normalized with respect to the initial confining pressure, therefore, the top-most curve corresponds to the lowest confining stress 25 kPa and vice versa. It can be observed from Figs. 4.4a, 4.4c, and 4.4e that the peak strength increases, and the strain-softening is progressively more pronounced with the increasing level of cementation, which conforms with the expected trends. As for the effect of confinement on cemented sands, the contribution of the cementation is more evident at low confinements compared to high confinements. This observation agrees well

with the expected behavior that, at high confinements, the frictional component of the strength dominates the response and cementation is not as effective. Figs. 4.4b, 4.4d, and 4.4f plot the volumetric response corresponding to the above stress-strain curves. Minimal changes can be seen across the levels of cementation because cementation-induced densification is not considered in this set of simulations as mentioned above. Also, the residual strengths for the three levels of cementation remain unchanged due to the lack of consensus on the effect of cementation on residual strength, whether it increases or this trend is associated with a cemented specimen not fully sheared to their residual state. While this deliberate omission from this model may not affect soils cemented at light levels of cementation, it may be more detrimental to soils cemented at moderate levels of cementation.

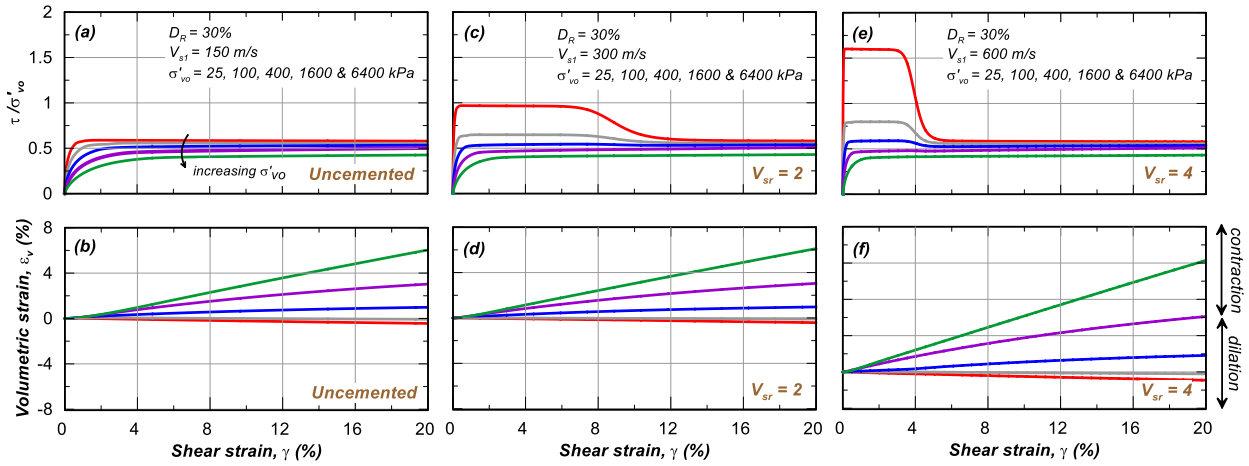

Figure 4.4. Drained monotonic DSS loading responses for V_s ratio V_{sr} of 1 (uncemented), 2, and 4 and V_{s1} of 150, 300, and 600 m/s, respectively, with vertical confining stresses of 25, 100, 400, 1600, and 6400 kPa and K_o =0.5.

Figure 4.5 presents the undrained monotonic DSS response of bio-cemented sands. The top and bottom row of plots shows the stress-strain and stress-path response, respectively, with Figs.

4.5a and 4.5b for uncemented sands with V_{sr} of 1, Figs. 4.5c and 4.5d for a cemented sand with a V_{sr} of 2, and Figs. 4.5e and 4.5f for a cemented sand with a V_{sr} of 4. In Fig. 4.5, the top-most curve corresponds to the 6400 kPa confinement since the stresses are not normalized here to view the actual respective magnitudes. As the level of cementation is increased, similar behaviors to the drained response are seen in the undrained response with a stiffer curve, a higher peak strength, and a more pronounced softening after the degradation of the cementation.

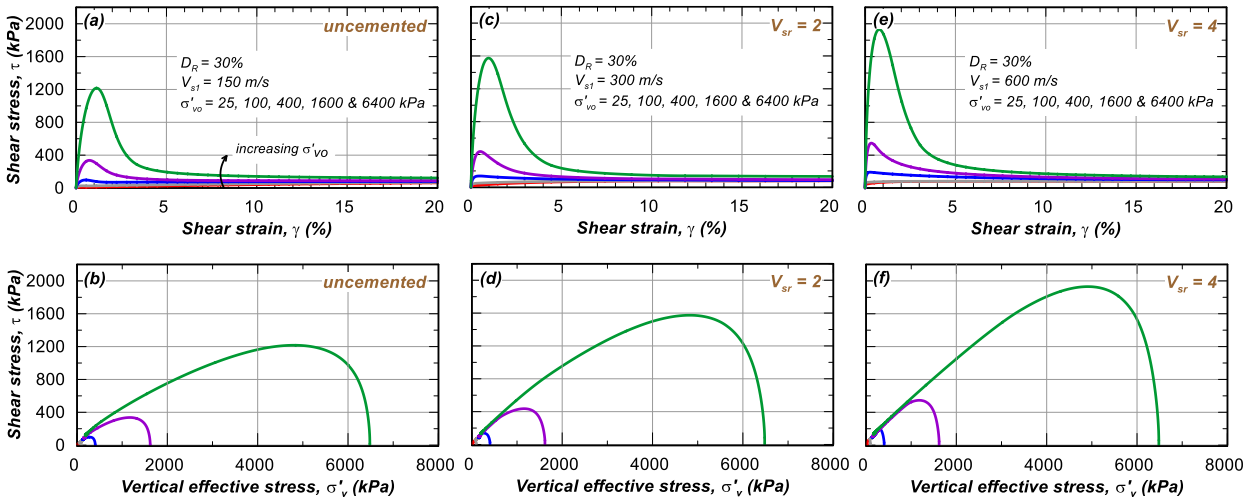

Figure 4.5. Undrained monotonic DSS loading responses for V_s ratio V_{sr} of 1 (uncemented), 2, and 4 and V_{s1} of 150, 300, and 600 m/s, respectively, with vertical confining stresses of 25, 100, 400, 1600, and 6400 kPa and K_o=0.5.

Figure 4.6 is identical to Fig. 4.5 except that the responses for the high confining stresses (1600 and 6400 kPa) are removed to better visualize the effect of the cementation at low confinements. Figures 4.6b, 4.6d, and 4.6f show that the stress paths under the lower confinement stresses show less contraction and more dilation as the level of cementation increases which, due to the simultaneous mechanisms of densification and cementation, is desired and expected. While no

changes are made for the relative density here, this behavior is inherent to the addition of the cementation to other aspects of the model.

Figure 4.7 shows the drained monotonic responses under plane strain compression loading. The general trends as seen in Figs. 4.4 and 4.5 are honored. The peaks in the principal stress ratio plots for V_{sr} of 2 and 4 are also seen in the stress paths for low confinements (25 and 100 kPa) where the stress path reaches a peak above the critical state line in brown and returns back to this line.

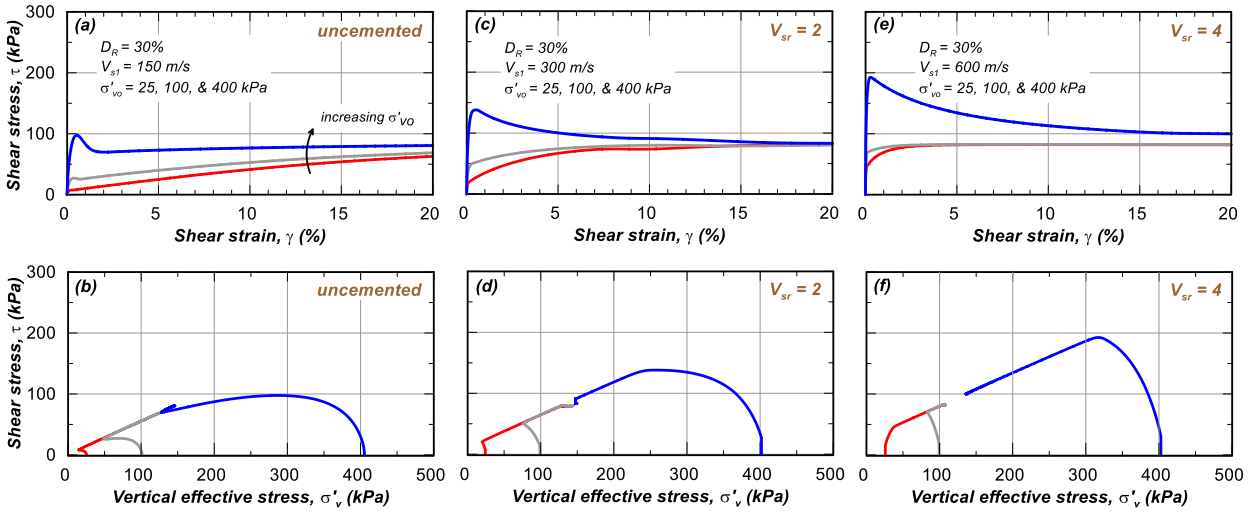

Figure 4.6. Undrained monotonic DSS loading responses for V_s ratio V_{sr} of 1 (uncemented), 2, and 4 and V_{s1} of 150, 300, and 600 m/s, respectively, with vertical confining stresses of 25, 100, and 400 kPa and K_o=0.5 (similar to Figure 4.5 but without high confinements).

In terms of cyclic response, Figs. 4.8 and 4.9 collectively show the effect of cementation on the cyclic behavior of bio-cemented sands. These simulations are performed at a confining pressure of 100 kPa and V_{sr} of 1, 2, and 4 with default secondary parameters. As expected, increasing the level of cementation leads to stiffer first few cycles and slower generation of pore pressure which

in turn results in a larger CSR and more cycles to accumulate 3% shear strain (i.e., the liquefaction triggering criterion selected here). Studying the stress paths for V_{sr} of 2 and 4 (Figs. 4.8e and 4.8h), the model initially develops a reduction in p, after which it settles into a repeating stress path while strains slowly accumulate/increase to about 1%, after which cementation begins to strongly breakdown and p can further decrease and eventually reach transient minimums of zero.

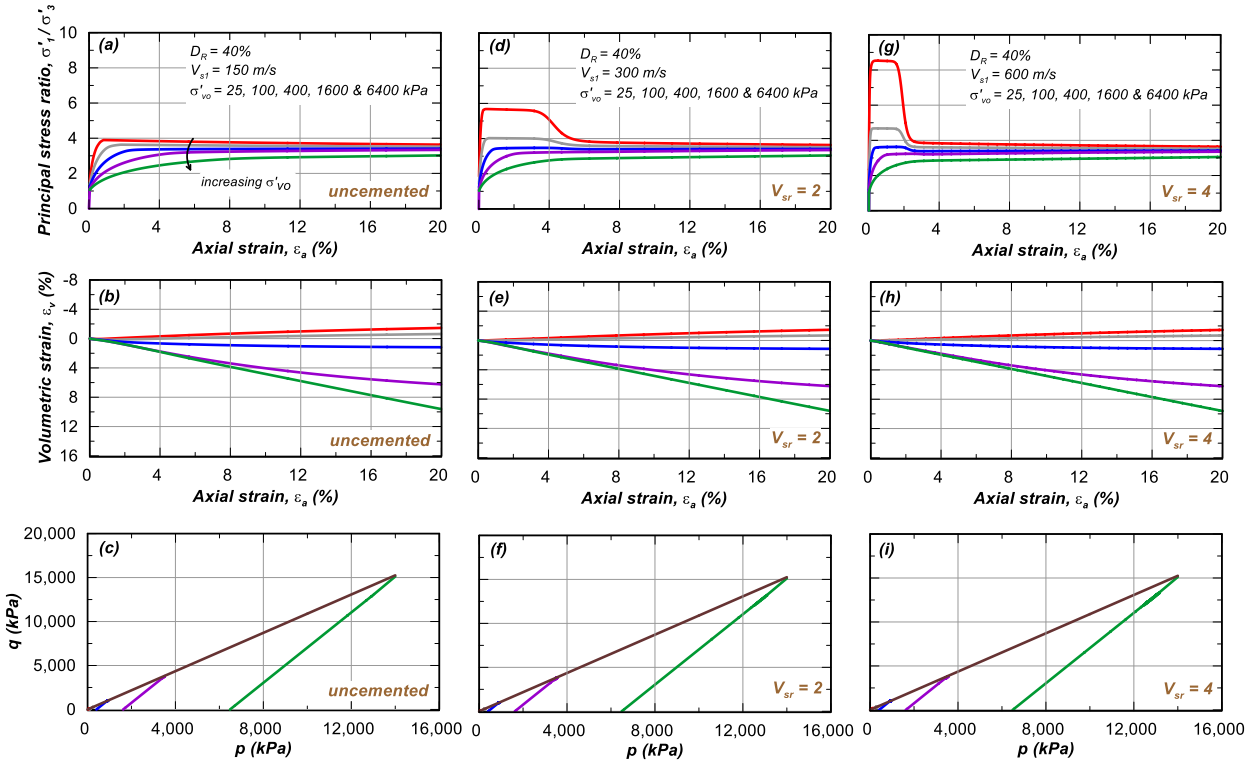

Figure 4.7. Drained monotonic PSC (plane strain compression) loading responses for V_s ratio V_{sr} of 1 (uncemented), 2, and 4 and V_{s1} of 150, 300, and 600 m/s, respectively, with vertical confining stresses of 25, 100, 400, 1600, and 6400 kPa.

These paths illustrate how, after a certain number of cycles, the improvements due to the cementation are lost and the soil behavior resolve into the typical behavior of sands until liquefaction. This relatively constant p can be attributed to the cancelling effects of the contraction

and dilation peaks evident in the r_u plots (Figs. 4.8f and 4.8i). Extending these simulations to different CSRs yields the cyclic resistance ratio (CRR) versus number of uniform cycles to trigger liquefaction. For these simulations, the choice of liquefaction criterion has little effect on the number of cycles needed for triggering, thus, the liquefaction triggering criterion considered here is the 3% single amplitude shear strain (Fig. 4.9).

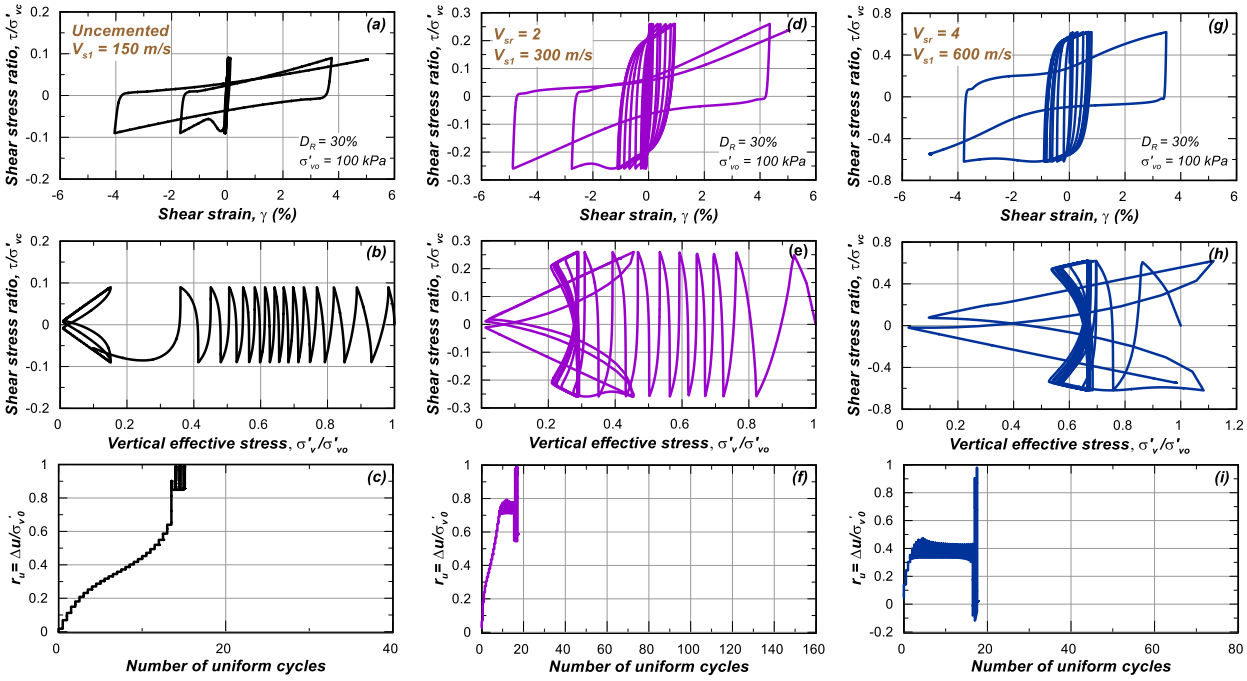

Figure 4.8. Undrained cyclic DSS loading responses for V_s ratio V_{sr} = 1 (uncemented), 2, and 4 and V_{s1} of 150, 300, and 600 m/s, respectively, with vertical confining stresses of 100 kPa and CSR of 0.09, 0.26, and 0.62, respectively.

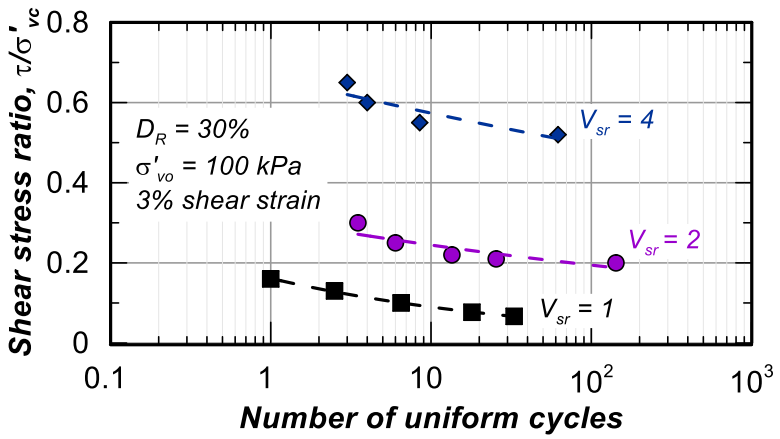

Figure 4.9. Cyclic stress ratios versus number of equivalent uniform loading cycles in undrained DSS loading to cause single-amplitude shear strains of 3% for V_{sr} of 1 (uncemented), 2, 4 with D_R = 30% and a vertical effective consolidation stress of 100 kPa.

For earthquake engineering design, the CRR versus number of cycles correlation is typically fitted with a power law:

$$CSR = a \cdot N_{cyc}^{-b} \tag{4.15}$$

where a and b are fitting coefficients representing the CSR at N_{cyc} of 1 and the slope of the curve, respectively. As evident from the literature, an increase in the level of cementation leads to an increase in the CSR at N_{cyc} of 1 (parameter a) and a decrease in the slope of the curve which becomes flatter (parameter b) (Fig.2.21). While a power law remains usable in earthquake engineering applications where the first 100 cycles may be representative of an earthquake, the authors suggest the cautious use of a power law to fit experimental or simulation data on bio-cemented sands with more than 1000 cycles. The reason behind this recommendation is the irrelevance of such as number of cycles to earthquake engineering design and the inappropriateness of the power function to fit such an extreme range of data points.

Last, the effect of the cementation and confinement on the dynamic properties of bio-cemented sands is investigated. While the available data on dynamic properties is scarce, it provides some indications on the directions of the systematic trends which can be later corroborated by additional data as they become available. Changes to the modulus reduction and damping curves depend on the confinement and the level of cementation. To assess the model's ability to capture these changes, drained strain-controlled cyclic DSS responses at confining stresses from 25 to 6400 kPa with V_{sr} of 1 (uncemented), 2, and 4 are shown in Fig. 4.10.

For the cementation levels applicable to this model, PM4SandC agrees with the trends suggested by the resonant column tests done on MICP-cemented Ottawa F65 sand at 30 and 100 kPa (Na et al. 2022) whereby the elastic threshold strain (i.e., the strain at which G_{sec} is 99% of G_{max}) decreases, the slope of the modulus reduction curves increases, and damping at a given strain amplitude increases with the level of cementation. These behaviors are clearly seen in the second and third row of Fig. 4.10 for V_{sr} of 2 and 4, respectively. As for the effect of confinement, the modulus reductions curves become flatter, and the damping curves become steeper with increasing confinement. The aforementioned trends may not translate to higher levels of cementation as indicated by tests on Portland-cemented sands (Acar and El-Tahir 1986; Camacho-Padrón 2006) but this remains unknown for bio-cemented sands and out of the scope and application of PM4SandC.

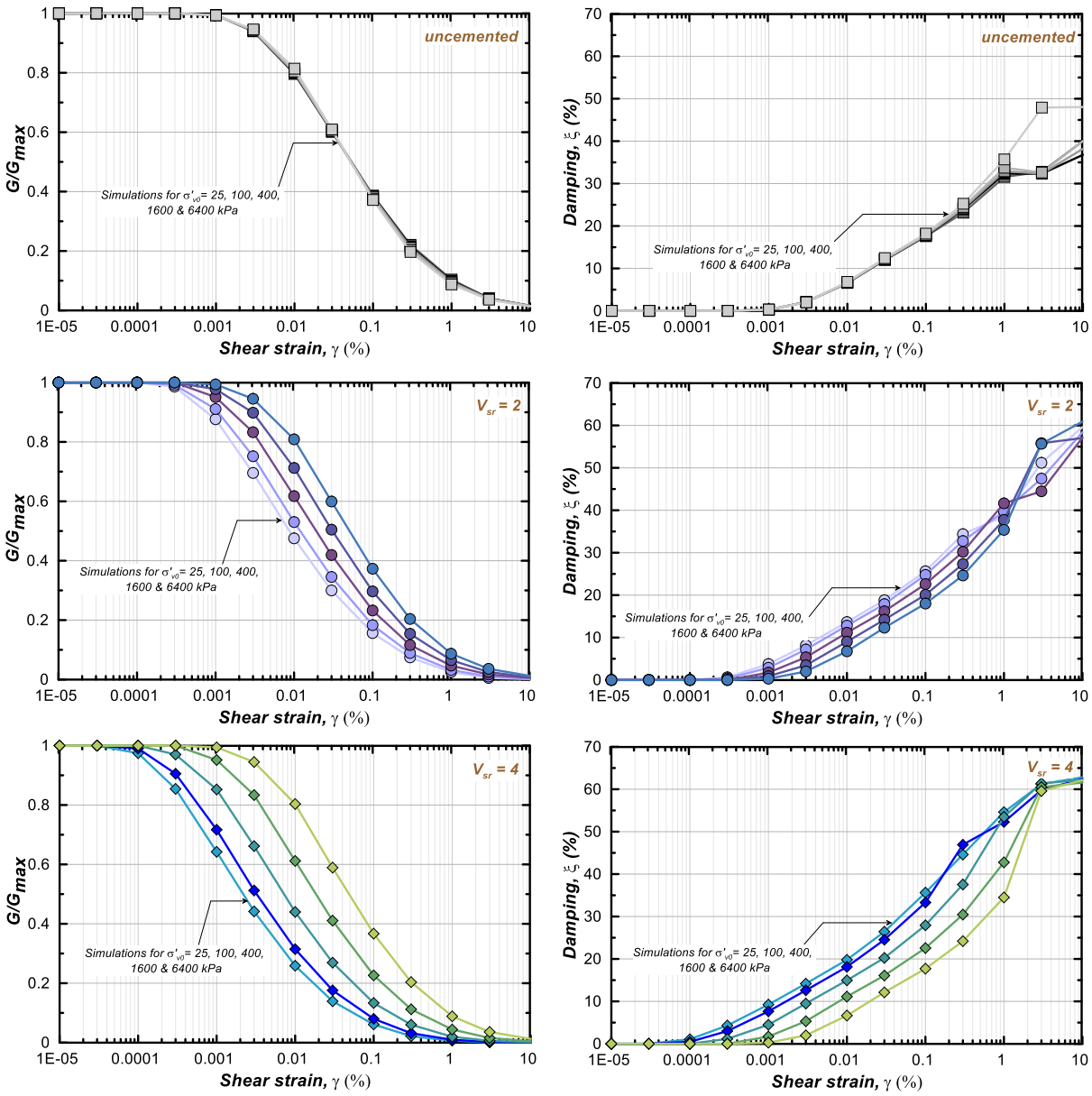

Figure 4.10. Drained strain-controlled cyclic DSS loading responses for D_R = 30% and V_s ratio V_{sr} of 1 (uncemented), 2, and 4 and V_{s1} of 300, and 600 m/s, respectively, with vertical confining stresses of 25, 100, 400, 1600, and 6400 kPa.

4.5 Model validation and performance

Sands cemented artificially in a laboratory setting can be used for the validation of the constitutive model due to their uniformity, homogeneity, and repeatability in a controlled environment. Herein, the performance of PM4SandC is evaluated against drained triaxial tests on MICP-cemented Ottawa 20-30 sand digitized from Nafisi et al. (2020) and monotonic and cyclic DSS tests on MICP-cemented Ottawa F-65 sand from Lee et al. (2022). In Nafisi et al. (2020), Ottawa sand was cemented to varying levels of cementation and confining stresses. In Lee et al. (2022), Ottawa F-65 sand was cemented to varying levels of cementation under a confining pressure of 100 kPa. The cementation process was monitored through V_s measurements taken pre- and post-cementation. The reader is referred to the original papers by Nafisi et al. (2020) and Lee et al. (2022) for more details on sample preparation and the testing procedure. The results from these tests constitute a part of the database for the validation of PM4SandC.

Plane strain compression, monotonic and cyclic DSS simulations are performed in FLAC 8.1 (Itasca 2019) in order to (1) investigate the effect of the bio-cementation on the responses of a lightly and moderately cemented sand, and (2) validate the constitutive model. These simulations are plotted against the aforementioned experimental data in Figs. 4.11 to 4.14 for different loading conditions. It should be noted that minimal calibration effort is intended for the calibration process to demonstrate the capability of the model to reproduce reasonable responses without extensive calibration.

Figures 4.11a and 4.11b present a comparison between the experimental (dotted line) and simulation (solid line) results for a drained plane strain compression or triaxial test at D_R of about 40%, an overburden stress σ'_{vc} of 10 kPa, an uncemented V_s of 114 m/s and cemented $V_{s,cem}$ of 220 m/s. This sample is qualitatively classified as “lightly” cemented according to the ranges

suggested by Montoya et al. (2013). Two simulations are performed for this set of tests to highlight the effect of densification, i.e., ΔD_R due to cementation, on the volumetric behavior (see Section 4.4). The solid line represents the simulation results without changes in D_R (i.e., $D_{R,ini}$), and the dashed line represents those with changes in D_R as informed by the experiment (i.e., $D_{R,cem}$). The black curves correspond to the results on uncemented tests shown for reference while the purple lines correspond to the cemented sand with V_{sr} of ~ 2. Figures 4.11c to 4.11f extend the comparison to higher confining stress to demonstrate the reduced effect of cementation at higher confinements. These tests are run at similar normalized conditions but under higher confinements. The shear stiffnesses for the model were reduced from the reported ones by Nafisi et al. (2020) due to their overestimation relative to the stress-strain response. The input shear wave velocities matched the slope of the stress-strain curves.

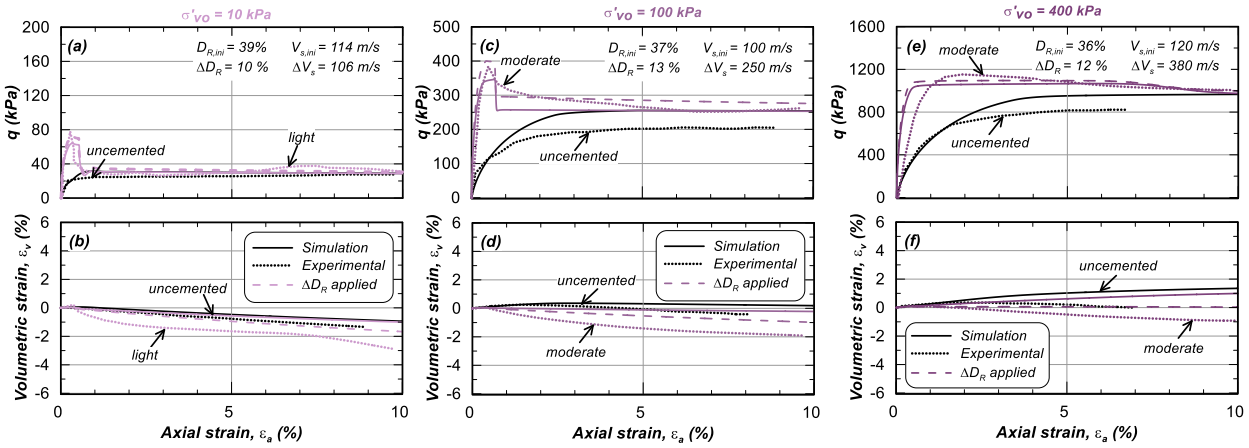

Figure 4.11. Evaluation of PM4SandC calibrations under drained plane strain compression loading against experimental data for V_{sr} of ~ 3 for confining stresses of (a,b) 10 kPa, (c,d) 100 kPa, and (e,f) 400 kPa (experimental data from Nafisi et al. 2020).

Figure 4.11 shows that the constitutive model captures the general trends seen for bio-cemented sands such as the increase in stiffness and peak strength, the pronounced softening and loss of strength upon degradation, and the effectiveness of the cementation at lower confining stresses. As confining stresses increase, the frictional mechanisms in sand dominate the behavior and the additional strength from the cementation becomes less important relative to the frictional strength. When the cementation-induced change in D_R is considered (i.e., $D_{R,cem}$), the model clearly yields more dilative volumetric responses as expected from the experimental results.

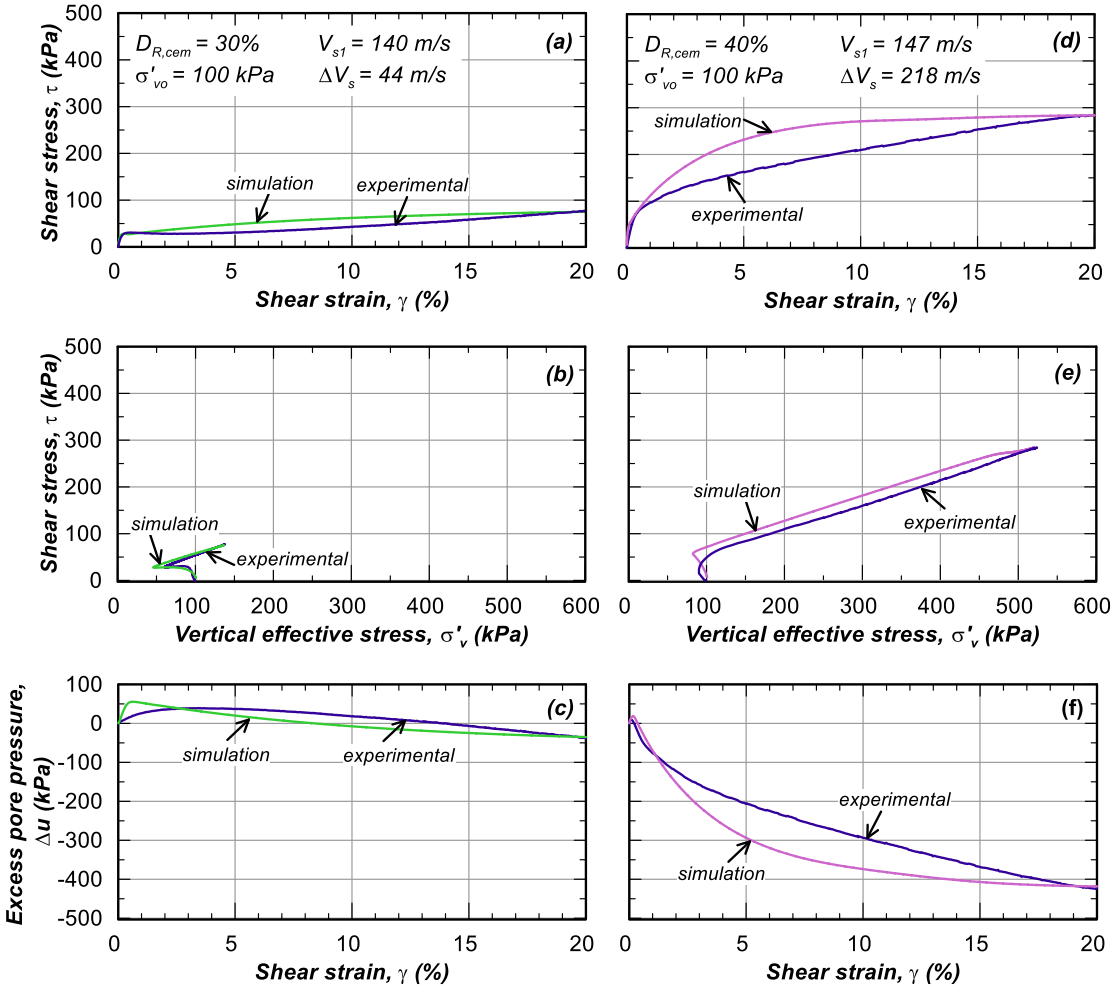

Figure 4.12. Evaluation of PM4SandC calibrations under monotonic undrained DSS loading against experimental data for V_{sr} of 1.3 (a) to (c) and 2.5 (d) to (f) (experimental data from Lee et al. 2022).

Figure 4.12 presents a comparison between the experimental and simulation results for an undrained monotonic DSS test on "lightly" cemented sand (as classified using Montoya et al. 2013) at D_R of about 30%, an overburden stress $\sigma_{vc}^{'}$ of 100 kPa, an uncemented V_s of 140 m/s and cemented $V_{s,cem}$ of 184 m/s and "moderately" cemented sand at D_R of about 40%, an overburden stress σ'_{vc} of 100 kPa, an uncemented V_s of 147 m/s and a cemented $V_{s,cem}$ of 365 m/s.

Figure 4.13 presents a comparison between the experimental and simulation results for an undrained cyclic DSS test on "lightly" cemented sand at D_R of about 33%, an overburden stress $\sigma_{vc}^{'}$ of 100 kPa, a CSR of 0.2, an uncemented V_s of 146 m/s, and cemented $V_{s,cem}$ of 182 m/s, whereas Fig. 4.14 presents the same comparison for "moderately" cemented sand at D_R of about 33%, an overburden stress σ'_{vc} of 100 kPa, a CSR of 0.25, an uncemented V_s of 142 m/s, and a cemented $V_{s,cem}$ of 242 m/s.

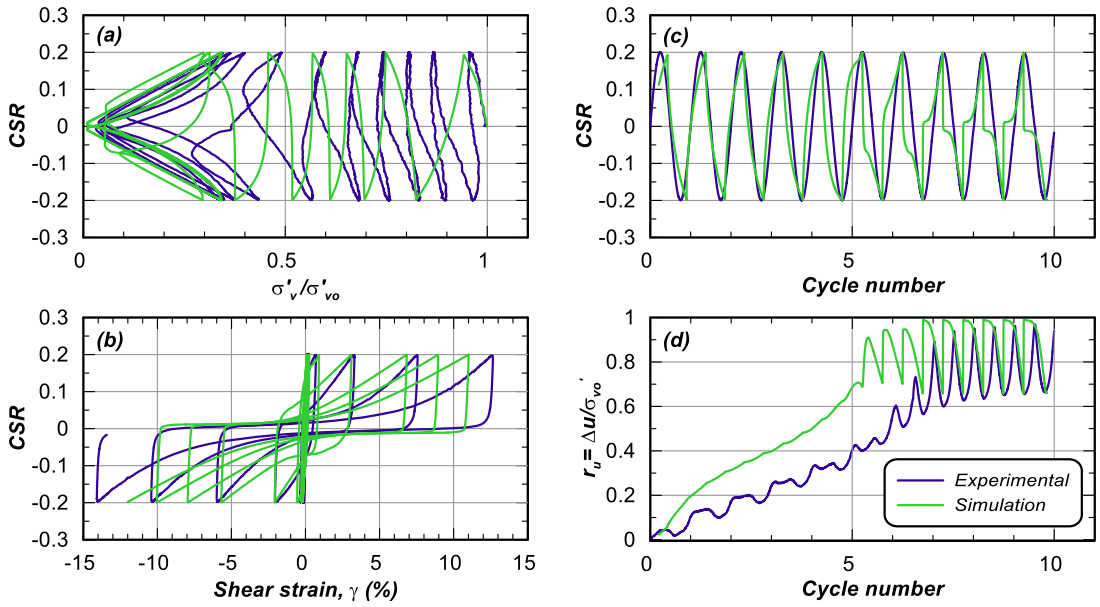

Figure 4.13. Evaluation of PM4SandC calibrations under cyclic undrained DSS loading against experimental data for V_{sr} of 1.25, $\sigma_{vo}^{'}$ of 100 kPa, CSR of 0.2, D_R of 33%, and $V_{s,initial}$ of 146 m/s (experimental data from Lee et al. 2022).

Collectively, the responses in Figs. 4.11 to 4.14 demonstrate the ability of the model to qualitatively predict the trends seen in bio-cemented sands with minimal calibration effort. The calibration can be more involved depending on the response of interest targeted by the user. The model is built such that the functional forms have enough versatility to accommodate a range of conditions (e.g., the bond degradation law in Section 4.2.4) all while remaining usable by practitioners within a minimal calibration effort. While more experimental studies may clarify certain aspects of the behavior of bio-cemented sands (e.g., post-triggering reconsolidation, damping), the validity of the current implementation remains intact.

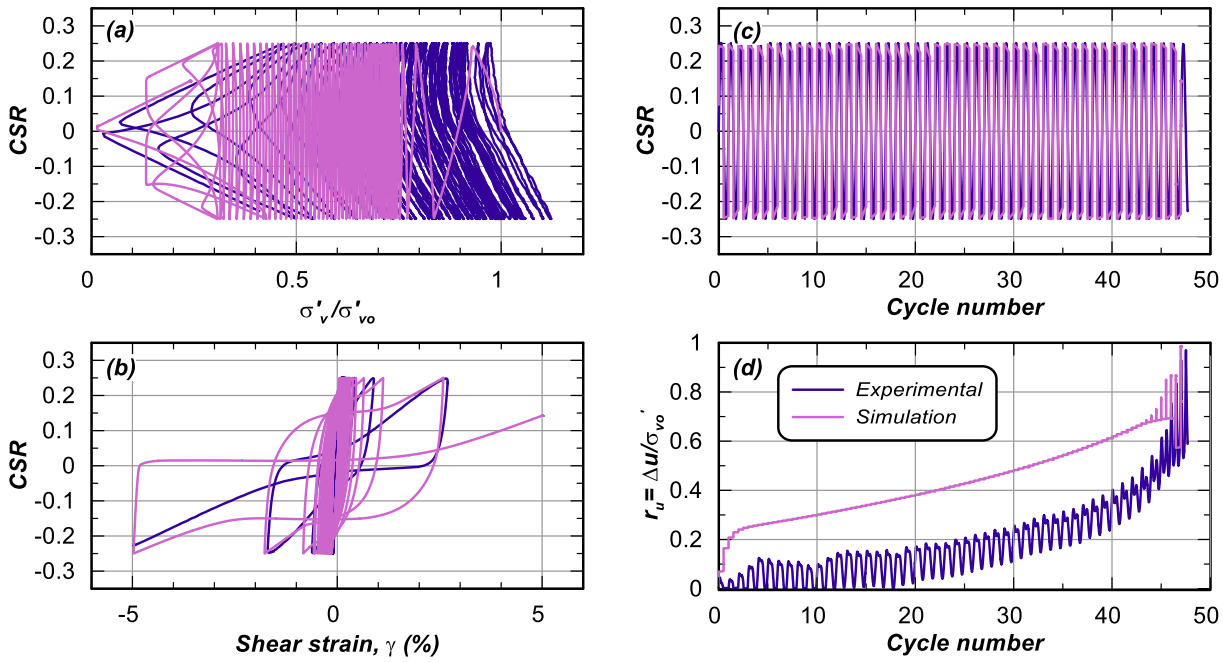

Figure 4.14. Evaluation of PM4SandC calibrations under cyclic undrained DSS loading against experimental data for V_{sr} of 1.7, $\sigma_{vo}^{'}$ of 100 kPa, CSR of 0.25, D_R of 33%, and $V_{s,initial}$ of 142 m/s (experimental data from Lee et al. 2022).

4.6 Concluding remarks

The plasticity model for cemented sands PM4SandC presented herein was built upon the framework of the plasticity model for sands PM4Sand. It is a critical state-based, stress ratio-controlled, bounding surface plasticity model applicable to the design of bio-cementation-based ground improvement towards the mitigation of earthquake-related hazards like liquefaction. It can also be used in the modeling of naturally cemented sands. The model inherits the baseline formulation and input parameters from PM4Sand and extends it to include the contributions of cementation.

A series of modifications and additions to the model were incorporated to enable the prediction of the stress-strain response of bio-cemented sands. Experimental data on bio-cemented sands guided the development of functional equations and the calibration of the model in order to provide a better approximation of the observed trends for these sands. The modifications to the model included:

- The addition of an equivalent tensile strength due to the cementation bonds;
- The enhancement of the elastic shear stiffness contributed by the presence of the cementation;
- The incorporation of the effect of cementation on the normalization of the elastic shear stiffness;
- The accumulation of damage resulting from the continuous shearing;
- The evolution of the initial cementation and its degradation as a function of accumulated damage.

The current formulation is limited to plane-strain applications. It is implemented as a user defined constitutive model with a dynamic link library (DLL) for use in the commercial software FLAC 8.1 (Itasca 2019).

Five input parameters, one primary (V_{sr}) and 4 secondary parameters ($c_{initial}$, ϕ_{peak}, γ_{deg}, γ_{res}), were added to the model to characterize the initial cementation and define the range of damage over which cementation degradation occurs. These parameters have physical meaning and can be obtained from conventional lab testing or field measurements. The shear wave velocity ratio V_{sr} can be estimated from shear wave velocity measurements pre- and post-improvement using conventional geophysical testing. The strength parameters $c_{initial}$ and ϕ_{peak} can be obtained from peak envelopes fitted to conventional strength tests at different confining stresses. $c_{initial}$ can also be estimated from in-situ CPT tip resistance measurements. The degradation and residual strain parameters γ_{deg} and γ_{res} defining the range of strains can be inferred from the interpretation of the stress-strain response of drained monotonic tests on cemented sands. While the above constitutes the parameters that were added to the model, primary input parameters from PM4Sand remain to be calibrated such as the relative density D_R, the shear modulus coefficient G_o, and the contraction rate parameter h_{po}.

Model responses to various levels of cementation and loading conditions, including drained and undrained monotonic and cyclic loading, were presented to demonstrate the changes to the responses due to the aforementioned modifications. In addition, the calibration of selected monotonic and cyclic DSS tests on MICP-cemented sands was performed to validate the performance of the model against single element tests and to evaluate its ability to capture the observed trends in behaviors. Overall, PM4SandC agrees with the expected trends from the

experimental data with minimal calibration effort. In the design process, more attention can be put on the aspects of the response of interest to the project and the model can be calibrated accordingly.

CHAPTER 5

One-dimensional site response analysis of bio-cemented columns: validation against centrifuge model tests

Anticipated publication:

El Kortbawi M., Ziotopoulou K., and DeJong J. T. One-dimensional site response analysis of bio-cemented columns: validation against centrifuge model tests.

Author's note: This paper will be submitted for journal publication soon. Figure and table captions and intext references were modified from the original publication to conform with the format of this Dissertation.

Abstract

In the past decade, Microbially-Induced Calcite Precipitation (MICP) has gained increased interest as an alternative artificial cementation technique analogous to natural cementation in the field. This increased interest led to a plethora of experimental studies on the element scale, few experiments at the large (1-g tanks) and field scale (centrifuge tests), and few numerical models. A recent bounding surface plasticity constitutive model for bio-cemented sands PM4SandC was developed to predict the stress-strain response of bio-cemented sands subject to earthquake loads

and has been shown to perform reasonably well across the broad range of element-level loading paths available from bench-scale tests. This paper aims at (1) validating PM4SandC at a system level application, and (2) presenting a first-of-a-kind numerical effort to simulate site response analyses in bio-cemented sands. The PM4SandC constitutive model is used to simulate two one-dimensional nonlinear site response analyses on bio-cemented sand columns. The numerical analysis, its input parameters, and the calibration process are described in detail. The dynamic response from the simulations in terms of accelerations, shear strains, cyclic demand, pore pressure generation, and response spectra is compared to the measured response in centrifuge models scaled to real site conditions. The constitutive model is found to reasonably approximate the dynamic responses from the centrifuge tests. A parametric investigation is also performed to provide insights into the effects of PM4SandC's parameter uncertainties on the overall dynamic response. Recommendations for the calibration process are provided and conclusions are drawn on the overall performance of the model.

5.1 Introduction

Natural cementation is abundant in sand deposits and can range from lightly cemented sands to weak rocks such as sandstones, which, in fact, are primarily formed by calcite precipitation. Cementation from calcite or calcium carbonate ($CaCO_3$) is controlled by various factors: groundwater chemistry, permeability, sand composition and texture, and presence of pre-existing carbonate substrate (DeJong et al. 2006; Molenaar and Venmans 1993). As a result of these factors, naturally cemented sands can be highly variable over small distances within a stratigraphic unit. To understand their formation process and their mechanical response, naturally cemented sands have been the focus of many studies. However, difficulties in their characterization such as

sampling-related disturbances, stress relaxation leading to bond breakage, and the cost of unconventional sampling to overcome these challenges, have hindered the collection of a rigorous testing database which may have led to their lack of consideration in engineering analyses.

In the past decade, a novel artificial cementation technique has emerged as an alternative to natural cementation whereby calcite can be artificially precipitated by a chain of chemical reactions under favorable conditions (e.g., Burbank et al. 2013; DeJong et al. 2010; DeJong et al. 2013; Mitchell and Santamarina 2005). This technique is microbially-induced calcite precipitation (MICP) in which microorganisms, whether native or added to the soil, hydrolyze urea to precipitate calcite. Calcite precipitation or bio-cementation can occur at particle surfaces and/or contacts depending on preferential conditions. MICP has rapidly gained interest amongst researchers because it has shown promise in its pilot applications as a sustainable and environmentally friendly ground improvement method compared to deep mixing and grouting. As a result, numerous studies have been conducted on MICP-cemented specimens to demonstrate its utility as an improvement method. Over the years, these studies evolved from proof-of-concept (e.g., DeJong et al. 2006) to large scale (e.g., Gomez et al. 2018; San Pablo et al. 2020) to field scale applications (e.g., Darby et al. 2019; Zamani et al. 2021). The behavior of bio-cemented sands has been studied experimentally using bench scale (e.g., Feng and Montoya 2015; Lee et al. 2022; Montoya and DeJong 2015; Nafisi et al. 2019), large 1-g scale (e.g., Gomez et al. 2018), and field scale testing (e.g., Darby et al. 2019; Montoya et al. 2013; San Pablo et al. 2023). Experimental studies on the mechanical response of bio-cemented sands at the element scale have allowed for understanding the contribution of cementation to stiffness, strength, volumetric behavior, and pre- and post-triggering behaviors under monotonic and cyclic loading. Collectively, these experimental results have established the validation database for numerical modeling efforts (Chapter 2). However,

understanding the system scale performance, which is crucial in the implementation of MICP in the field as a liquefaction hazard mitigation method, requires further development.

At the element level, researchers have shown that bio-cementation increases the stiffness as well as the monotonic and cyclic resistance of sands. These improvements are more evident in the pre-triggering portion of the response and are less visible post triggering following the degradation of the cementation. As the yield stress is reached, bio-cemented sand fully mobilizes its shear strength and eventually softens as the cementation degrades. It follows that friction between sand particles takes over the response, thereby inducing a maximum rate of dilation post-peak (Section 2.4.2). The calcite coating the sand particles and the broken calcite densifying the soil matrix collectively result in a more dilative volumetric behavior for bio-cemented sands compared to clean sands. Once their strength is overcome by the shearing, they progressively break and result in a degraded matrix of sand and calcite. It has been reasonably hypothesized that the residual strength of bio-cemented sands is higher than that of clean sands (e.g., Montoya and DeJong 2015). The observed increase in residual strength may be the result of remnant intact calcite bonds and/or the increased particle roughness due to the broken calcite. Further studies on the post-triggering behavior of bio-cemented sands are needed to accept or refute this hypothesis.

The attention drawn by MICP on the experimental front was shortly followed by an increased interest on the numerical front. The population of an experimental database on the element scale accelerated the need for numerical models able to reproduce the behaviors seen in the experiments. Numerical efforts focused on reactive transport models (e.g., Fauriel and Laloui 2012), discrete element modeling (e.g., Feng et al. 2017), and continuum modeling (e.g. Gai and Sanchez 2018). On the continuum level, which is the main interest of this paper, one of the recently developed constitutive models includes a plasticity model for bio-cemented sands for earthquake engineering

applications PM4SandC (Chapter 4). PM4SandC is a descendant and extension of an existing constitutive model for sands PM4Sand Version 3.2 (Boulanger and Ziotopoulou 2017, 2022) which was modified to incorporate the effects of cementation in its original formulation. As such, PM4SandC is a critical state-based, stress ratio-controlled, bounding surface plasticity model for bio-cemented sands. It inherits the input parameters from PM4Sand and supplements them with one primary input parameter, the shear wave velocity ratio (V_{sr}), and 4 secondary input parameters which control the initial contribution of the cementation to the stiffness and strength and its degradation with continued shearing. The PM4SandC constitutive model is described in greater detail in Chapter 4. Chapter 4 also presents a validation of PM4SandC at the element level (i.e., triaxial compression and monotonic and cyclic Direct Simple Shear tests on MICP-treated specimens).

To systematically evaluate their performance, constitutive models like PM4SandC need to be validated against available body of data at multiple scales (i.e., element scale such as lab results and system scale such as centrifuge tests). Considering the readily available system-level data on bio-cemented sands, one-dimensional site response analyses (SRA) coupled with centrifuge test results provide the potential to validate and evaluate the constitutive model at the system scale. SRAs are widely used to assess the effect of a soil deposit on the propagation of ground motions due to a shaking event. In a controlled setting, SRA is analogous to the recorded responses in a centrifuge container with layered sand subjected to a shaking event from a shake table at a given centrifugal acceleration. Centrifuge tests have been used in the validation of 1D SRA due to (1) the availability of instrumentation and recordings along the depth of the container, (2) their ability to represent field scale conditions using scaling laws, and (3) the complexity in simulating these tests and obtaining comparable results. Compared to the simpler equivalent linear method,

nonlinear site response analyses (NL-SRA) can better approximate the nonlinearity in soil behavior using appropriate constitutive models calibrated to available data. Concurrently with computational advances, NL-SRAs have been increasingly used in practice to evaluate the response of soils at sites prone to liquefaction (e.g., Hashash et al. 2010).

This paper presents two NL-SRAs of MICP-improved soil columns, under free-field conditions using the PM4SandC constitutive model, validated against two published centrifuge tests under similar conditions, and evaluates the sensitivity of the free-field response facing uncertainties in input parameters to PM4SandC. The SRA setup and results are shown in the first part of this study. The recorded free-field responses from two published centrifuge tests on bio-cemented sands (Darby et al. 2019; San Pablo et al. 2023) are presented first. Then, the dynamic analysis setup in the explicit finite difference program FLAC 8.1 (Itasca 2019) is described and the selection of the input parameters to the PM4SandC constitutive model is explained. Simulation results are presented and compared to centrifuge results and conclusions are drawn regarding the effect of bio-cementation on the free-field dynamic response of sands and the performance of the constitutive model. In the second part of this study, a parametric study on select input parameters to the PM4SandC model is performed based on which recommendations for the calibration of the constitutive model are provided.

The validation exercise of the two SRAs in this paper is important for two reasons: (1) it serves as a validation of the recent PM4SandC constitutive model for bio-cemented sands on the system level which is needed for complete evaluation of such models (e.g., Hashash et al. 2015; Ramirez et al. 2018), and (2) it constitutes the first-ever-system-level numerical simulation of a bio-cemented deposit. As a result, this first validation study paves the way for future analyses capable of capturing field responses (e.g., for the design of MICP field trials). Moreover, the parametric

study on PM4SandC's input parameters provides insights into the effects of variability on the dynamic response in the field such that our understanding of the range of possible responses is extended to more treatment conditions which would eventually render the treatment design process more affordable and efficient.

5.2 Experimental data from centrifuge model tests

Two published centrifuge tests (Darby et al. 2019; San Pablo et al. 2023) are used to validate the free-field dynamic responses of an MICP improved soil column at comparable levels of cementation. The series of centrifuge model tests were performed at a range of cementation levels from light to moderate to heavy cementation. However only the tests at about V_s of 300 m/s are used for the simulations instead of the lightly cemented ones (V_s < 300 m/s, based on the classification of Montoya et al. 2013). This selection was made to focus on the effects of the bio-cementation which are more evident at a higher cementation level than the light cementation. All centrifuge tests considered were performed at the UC Davis Center for Geotechnical Modeling on the Schaevitz 1-m-radius centrifuge. The two centrifuge model tests are similar in their construction with some improvements in the most recent one (San Pablo et al. 2023). The improvements focused on (1) increasing the number of sensors, and (2) applying a ramping motion instead of a sine wave to minimize resonance. The model preparation and testing sequence are briefly summarized in the following subsections. More details on these tests and results are available in their respective publications (Darby et al. 2019; San Pablo et al. 2023). All dimensions and units presented herein are in the prototype scale unless noted otherwise.

5.2.1 Test 1 – Darby et al. (2019)

A series of centrifuge model tests were performed on uniform MICP-cemented sands treated at varying levels of cementation representing level ground free-field conditions. The imposed demands were repeated shaking events with increasing magnitudes. A flexible shear beam container was used for all tests and the centrifugal acceleration was set to 80g, yielding a scaling factor of 80. Control tests to establish baseline reference conditions were performed on uncemented uniform Ottawa F-65 sand, air-pluviated at loose and dense relative densities (D_R). Cemented models consisted of the same sand layer underlain by a mix of Monterey sand and pea gravel that facilitated drainage and the bottom-up cementation of the sand layer. Once placed, the soil was saturated with a solution of methylcellulose and deionized water with a viscosity of about $5x10^{-5}$ m^2/s (nearly 50 times the viscosity of water) to assist with the scaling of the dynamic pore pressure generation and dissipation after shaking. Following saturation, the models were spun up to the centrifugal acceleration of 80 g (mid-depth effective stress of 35 kPa) and each was subjected to 15 uniform cycles of a 1.25 Hz frequency sine wave with magnitudes varying from 0.02 g to 0.55 g for each loading event, as deemed necessary to trigger liquefaction. The shaking events increased in magnitude until the initial triggering of liquefaction at mid-depth. Shaking events were followed by sufficient time for generated pore pressures to dissipate. Accelerations, pore pressures, settlements, and V_s were monitored using accelerometers, pore pressure transducers, linear potentiometers, and bender elements, respectively (Fig. 5.1). In addition, miniature cone penetrometers were pushed pre-cementation, pre-shaking, post-triggering liquefaction, and post all shaking events to track the changes in cone tip resistance during the testing sequence. The focus of this paper is on the dynamic response of the control test on uncemented sand at an achieved D_R of 41% and on the MICP-cemented sand at V_s of about 300 m/s.

5.2.2 Test 2 – San Pablo et al. (2023)

A series of four centrifuge model tests were performed on MICP-cemented sands and used the flexible shear beam container, spun to a centrifugal acceleration of 80 g. The San Pablo et al. (2023) tests were all treated to a moderate cementation level (ΔV_s of 300 m/s at 1g level) but with varying depths of treatment to investigate the effect of finite cemented zones on liquefaction-induced settlements at improved sites. Control tests on uncemented sands were performed at an achieved D_R of 52% to establish baseline reference conditions. The cemented models comprised a profile identical to that of Darby et al. (2019). Model saturation also followed the same procedure by Darby et al. (2019). The cementation finite zones extended to 100% (8 m, entire model), 75% (6 m), and 50% (4 m) below the ground surface. All models were subjected to four shaking events at 1 Hz frequency at varying magnitudes from 0.05 g to 0.35 g. The ground motion of 1 Hz frequency consisted of three consecutive phases: (1) linearly increasing amplitude, (2) constant amplitude at a target peak acceleration, and (3) an exponential decay of amplitude. More details on the design of the applied waveform are presented by Carey et al. (2022). The target peak acceleration for the shaking events increased in magnitude until the initial triggering of liquefaction at mid-depth. The models were instrumented with two arrays: a center array and an edge array. For the purposes of the present study and to isolate any potential boundary effects, only the results from the instruments in the center array are considered henceforth. The instrumentation protocol for this set of tests followed the aformentioned Darby et al. (2019) protocol. However, miniature cone penetrometers were only pushed post cementation, pre-shaking and post all shaking (Fig. 5.2). The focus of this paper is on the fully cemented model (100% depth) in order to (1) evaluate the repeatability of results from different researchers, and (2) decouple the effect of the cementation from other mechanisms such as uneven treatment at the

bottom of the block and reflected waves in the container. The reader is referred to the original publication by San Pablo et al. (2023) for a full account on the testing procedure for the four models and their results.

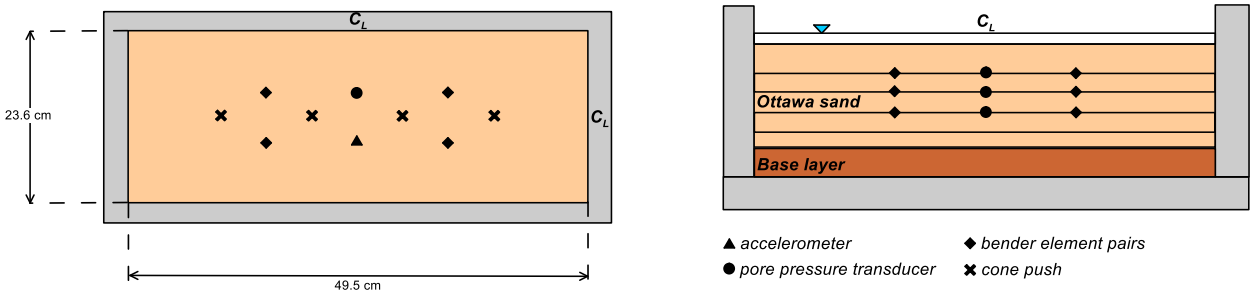

Figure 5.1. Model plan view and cross-section with sensor and cone locations (at 1g in model units) (adapted from Darby et al. 2019).

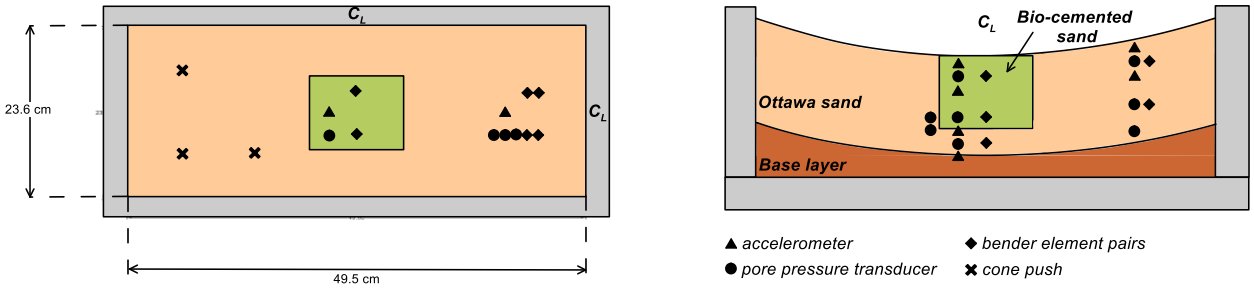

Figure 5.2. Model plan view and cross-section with sensor and cone locations (at 1 g in model units) (adapted from San Pablo et al. 2023).

5.3 Nonlinear dynamic site response analyses

5.3.1 Numerical model setup

The centrifuge tests introduced in the previous section are simulated using SRA as shown in Table 5.1. Relative densities used in the SRAs and reported in this paper correspond to the achieved (or corrected) values which differ from the ones reported in the experiments due to corrections

between the target and the achieved D_R, as explained later in this section. These initial conditions are chosen to honor the centrifuge conditions as reported by the experimentalists. The simulated analyses represent the free-field level-ground dynamic responses of uncemented and MICP-cemented soil columns.

Table 5.1. Summary of centrifuge tests and their corresponding site response analyses.

Centrifuge test	**Corresponding SRA**
Test 1 - Darby et al. (2019)	Case A: uncemented Ottawa F-65 sand (achieved D_R = 41%)
	Case B: moderately MICP-cemented Ottawa F-65 sand (achieved D_R = 53%)
Test 2 - San Pablo et al. (2023)	Case C: uncemented Ottawa F-65 sand (achieved D_R = 52%)
	Case D: moderately MICP-cemented Ottawa F-65 sand (achieved D_R = 60%)

The 1D SRA is performed in the explicit finite difference program FLAC 8.1 (Itasca 2019). It has been shown that 1D NL-SRAs along with well-understood site conditions and well-calibrated constitutive models can provide reasonable responses of a soil column subject to dynamic loading (e.g., Hashash et al. 2010). The user-defined plasticity model for bio-cemented sands PM4SandC (Chapter 4) is assigned to both uncemented and cemented Ottawa sand with different input parameters. The constitutive model handles both loose and dense, uncemented (V_{sr} = 1) and cemented (V_{sr} > 1) conditions. The numerical analyses presented here represent a 1D soil column in FLAC with boundary conditions, constraints, and soil properties which best approximate the conditions of the reference centrifuge tests (Fig. 5.3). The two centrifuge tests (Figs. 5.1 and 5.2) have slightly different dimensions and are thus reflected by the simulations. The effect of the curved surfaces in the models at the target g level are disregarded in the 1D simulations. The soil

profile of Test 1 is 11.4 m deep including a 2.4 m base layer while the profile of Test 2 is 10.8 m deep including a 1.6 m base layer.

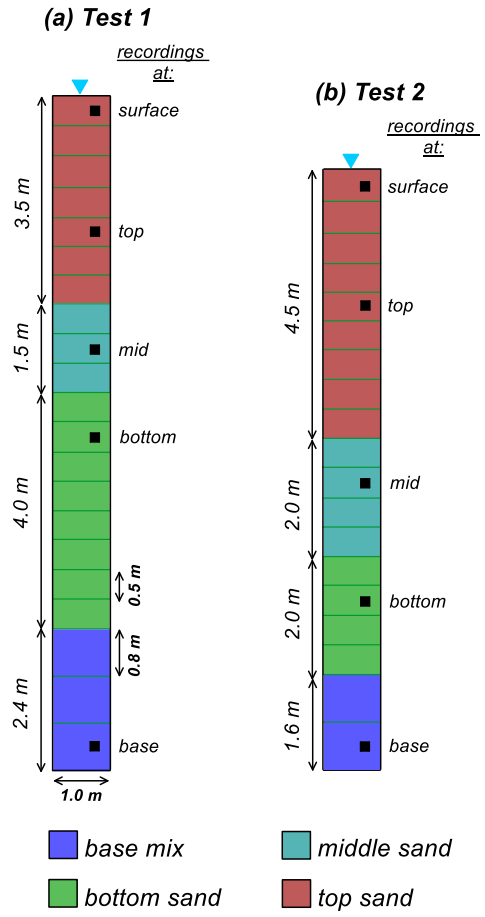

Figure 5.3. 1D site response analysis in FLAC represented by a 1D soil column with the different layering (prototype scale) for: (a) Test 1 - Darby et al. (2019) centrifuge test, and (b) Test 2 - San Pablo et al. (2023) centrifuge test.

The design of the centrifuge tests consists of two discretized layers: the liquefiable Ottawa sand underlain by a base layer for drainage (mix of Monterey sand and pea gravel). Initially, a grid with two soil layers was defined to reflect the design of the centrifuge tests. However, preliminary calibrations, not included here for brevity, supplemented by bender element measurements showed

that the bio-cementation may not be uniform along the full layer depth and hence, the liquefiable sand layer is further divided to account for the nonuniformity in the MICP treatment within the centrifuge model as indicated by the V_s measurements. The liquefiable layer is divided into three sublayers (bottom, middle, and top) based on the location of the instrumentation and more specifically the bender elements reporting V_s measurements (refer to Fig. 5.3). The sub layering of the Ottawa sand layer allows the input of three different sets of parameters to best approximate the conditions present in the centrifuge. For each of the three layers, a discretization is determined based on (1) the minimum wavelength of propagation of a motion through the model, and (2) the depth of the instrumentation in the centrifuge tests. Based on the range of V_s in Test 1 between 150 and 230 m/s (reported at 80 g), and for an input motion of 1.25 Hz frequency, the maximum wavelength (λ) of propagation ranges from 120 to 184 m. The maximum zone size is limited to λ/10 and therefore the grid size ranges from 12 to 18.4 m. To account for liquefaction-induced softening, V_s is reduced by a factor of 10 and thus the maximum zone discretization becomes approximately 1.2 to 1.84 m. The same process is repeated for Test 2 with V_s ranging from 151 to 270 m/s and an input motion frequency of 1 Hz. The maximum zone discretization for Test 2 is estimated to be 1.51 to 2.7 m. In both tests, the smallest of the maximum zones controls the discretization. Next, the placement of the instrumentation is evaluated, and according to both the maximum zone estimate and the instrumentation, a vertical discretization of 0.5 m is chosen for the liquefiable sand layer in both models. As for the base layer, it is discretized into 0.6 m elements in Test 1 and 0.8 m in Test 2 based on the thickness of this layer. The horizontal dimension for all zones is 1 m. The colors of the sublayers in Fig. 5.3 will be used henceforth to delineate the responses corresponding to each sublayer (Section 5.4).

The soil column is fixed at the base in both the x and y directions prior to initializing stresses. First, a static analysis is run. Initial stresses due to gravity are initialized using the elastic model and K_o conditions are imposed by setting horizontal stresses. Horizontal stresses increase from zero to about 50 kPa at the bottom of each profile. The model is run for static equilibrium in its dry condition (pre-saturation). After static equilibrium is confirmed, pore pressures are initialized by fully saturating the model and the coupled analysis is now solved for equilibrium. Pore pressures hydrostatically increase from zero at the surface of the model to about 100 kPa at the bottom of each profile. All values of stresses and pore pressures in FLAC are checked using hand calculations.

The PM4SandC model is assigned to the liquefiable Ottawa sand while the elastic model is assigned to the base layer. Six input parameters should be assigned at a minimum: (1) the relative density D_R, (2) the coefficient of stiffness G_o, (3) the contraction rate parameter h_{po}, (4) the shear wave velocity ratio V_{sr}, (5) the degradation strain γ_{deg}, and (6) the residual strain γ_{res}. More details on the input parameters and the calibration of the analysis are discussed in the following section. Next the dynamic analysis is performed.

The motion applied at the bottom of the centrifuge container as recorded by the base accelerometers is prescribed at the bottom of the soil column in the x- and y-component (i.e., horizontal and vertical acceleration, respectively), knowing that the x-component is the detrimental one for the soil and is larger than the y-component. While each of the centrifuge model tests was subjected to a series of successive shaking events, only the shaking event at which liquefaction was triggered in the middle layer is used in the simulations. The shaking events preceding liquefaction triggering only had a negligible densification effect on the model in the centrifuge container since liquefaction was not triggered and reconsolidation did not take place, as confirmed

by both pore pressure transducer and linear potentiometer measurements. The triggering criterion used in this paper and in the experiments is an excess pore pressure ratio r_u of 0.95. In Test 1, liquefaction was initially triggered in Shake 2 with a peak base acceleration (PBA) of 0.06 g for the uncemented case, and in Shake 5 with a PBA of 0.17 g for the bio-cemented case. In Test 2, liquefaction was initially triggered in Shake 3 with a PBA of 0.19 g for the uncemented case, and in Shake 6 with PBA of 0.29 g for the bio-cemented case. The different demand required to liquefy the uncemented sand of Tests 1 and 2 is attributed to the denser placement of the Ottawa sand in Test 2. In order to simulate shearing due to earthquake loading, the lateral nodes of the column at each elevation are connected to each other and, as such, forced to move together as would be the 1D case in the free field. The input parameters to the analyses and the calibration of the PM4SandC constitutive model are detailed in the following.

5.3.2 Input parameters and calibrations

5.3.2.1 Static model parameters

Soil properties input for the simulations (Table 5.2) are determined based on the reported values from the centrifuge tests. Whenever the latter is not available, typical values from published empirical relationships in the literature are used. The values for the minimum and maximum void ratio and specific gravity are obtained from previous available testing on Ottawa F-65 sand (Carey et al. 2020a) within the Liquefaction Experiments and Analyses Projects (LEAP-UCD-2017 in Kutter et al. 2020). The target initial relative density D_R is reported on the basis of mass-based measurements performed during the construction of the model centrifuge test. Corrections are subsequently made using the measured cone tip penetration resistance q_c and the linear trend method at 2 m penetration depth (Carey et al. 2020b). Following these corrections, the D_R is assigned in the simulations. For Test 1, the D_R of the Ottawa sand layer is adjusted from the

reported 38% to the corrected 41%. Similarly for Test 2, the D_R of the sand layer is adjusted from the reported 40% to the corrected 52%. The base layer was not instrumented in the centrifuge tests, therefore a D_R measurement was not available. In this study, the base layer only acts as a stiff drainage layer and does not affect the response of the liquefiable Ottawa sand layer, hence its D_R is estimated to be 70%. The permeability of the base layer (Monterey sand and pea gravel mix) is set to $2x10^{-3}$ m/s for both tests. Yet, the permeability of the Ottawa sand layer differs between the tests due to differences in the D_R and the viscosity of the saturation fluid. The permeability of Ottawa F-65 sand typically ranges between 1 and $2x10^{-4}$ m/s based on constant head tests performed on Ottawa F-65 specimens at different densities (Kutter et al. 2017, Chapter 3). In this study, the permeability of the Ottawa sand layer is set to $1.3x10^{-5}$ m/s and $1.3x10^{-4}$ m/s, respectively, for Test 1 and Test 2 to better approximate the pore pressure generation. Table 5.2 summarizes the soil properties for both the uncemented and cemented models.

5.3.2.2 Selection of V_s

The assignment of V_s honors the reported V_s measurements from the bender elements. No bender elements were placed in the base layer, thus the V_s for this layer is estimated to be 300 m/s. This estimate is obtained from available relationships between V_s, D_R, and vertical effective stress and the knowledge that the base layer is stiffer than the liquefiable layer (e.g., Andrus and Stokoe 2000; Biryaltseva et al. 2016). The sand layer was instrumented along its depth in both tests, and measurements were taken towards the bottom, the middle, and the top of the layer. The placement of the bender elements and the V_s distribution from these measurements warranted the sub layering of the cemented Ottawa sand. Preliminary calibrations showed an overestimation of the V_s measurements compared to the dynamic responses, thus the V_s from the experiments were slightly reduced for the cemented cases to better represent the dynamic responses. While the uncemented

Ottawa sand is more uniform, it is also subdivided into three layers for consistency between the analyses. Table 5.2 summarizes the V_s for both the uncemented and cemented models.

Table 5.2. Initial soil properties selected for both models: uncemented and moderately cemented, in addition to the ones for uncemented which remain unchanged.

Soil	**Base layer**	**Bottom Ottawa sand layer**	**Mid Ottawa sand layer**	**Top Ottawa sand layer**	**Bottom Ottawa sand layer**	**Mid Ottawa sand layer**	**Top Ottawa sand layer**
UNCEMENTED MODEL							
		Darby et al. (2019)			**San Pablo et al. (2023)**		
e_{min}	0.536	0.51	0.51	0.51	0.51	0.51	0.51
e_{max}	0.843	0.78	0.78	0.78	0.78	0.78	0.78
G_s	2.64	2.67	2.67	2.67	2.67	2.67	2.67
D_R (%)	70	41	41	41	52	52	52
V_s (m/s)	300	155	150	150	183	172	151
MODERATELY CEMENTED MODEL							
		Darby et al. (2019)			**San Pablo et al. (2023)**		
V_s (m/s)	300	155	150	150	183	172	151
$V_{s\ cem}$ (m/s)	300	217	230	200	200	270	229
$D_{R,cem}$ (%)	70	53	53	53	60	60	60

5.3.2.3 Dynamic properties of liquefiable layer: PM4SandC calibration

Input parameters to the PM4SandC model differ between the uncemented and cemented cases. For the uncemented sand, it suffices to give values to three primary parameters: the D_R, the coefficient of stiffness G_o, and the contraction rate parameter h_{po}. When the V_{sr} is not provided by the user, it defaults to 1 and the PM4SandC model runs in uncemented mode (identical to PM4Sand). In addition to the three mentioned parameters, a fourth primary parameter V_{sr} and two secondary

parameters (the degradation, γ_{deg}, and the residual, γ_{res}, strains) are required for the cemented sand. The calibrated parameters for the four analyses (cases A, B, C, and D) are provided in Table 5.3.

V_{sr} is the ratio of the cemented to the uncemented V_s, thus V_{sr} equals 1 for uncemented sands and V_{sr} > 1 for cemented sands. The higher the level of cementation, the stiffer the sand, the higher the V_{sr}. The V_{sr} parameter and the strength parameters "apparent" cohesion c and the peak friction angle ϕ (discussed hereafter) represent the contribution of the initial cementation to stiffness and strength. When PM4SandC is run in cemented mode (V_{sr} > 1), the $D_{R,cem}$ (Section 4.4) and the cemented $G_{o,cem}$ estimated from the cemented shear wave velocity $V_{s,cem}$ should be assigned and h_{po} should be calibrated for. It should be noted here that the shear stiffness initialization in PM4SandC considers its stress dependency which allows the model to internally handle the change of shear stiffness with depth. Hence, the proposed sub layering of the Ottawa sand layer is not intended for the stress dependency but instead for the cementation nonuniformity. When data from strength tests (e.g., triaxial tests) on bio-cemented sands are available, the default values of the "apparent" cohesion c and the peak friction angle ϕ should be overridden by estimates from these tests. The default values within PM4SandC are estimates based on cohesion and friction angle values from Nafisi et al. (2020). When, instead, the cone tip resistance q_c from a cone penetration test (CPT) performed pre- and post-cementation in the field is available, the "apparent" cohesion c can be estimated from the relationship in Chapter 3. For Tests 1 and 2 in this paper, pre-cemented and post-cemented q_c were indeed reported and as result, the "apparent" cohesion values c for both tests are the average of the estimate from the relationship in Chapter 3 and the default value in PM4SandC from the V_{sr} (Table 5.3). Two additional parameters are calibrated for the degradation of the cementation with damage accumulation: the degradation strain γ_{deg} which is

the shear strain at the onset of degradation, and the residual strain γ_{res} which is the shear strain at which the cementation is presumably fully broken. The range between γ_{deg} and γ_{res} implicitly represents the rate of degradation. As the range of accumulated strains is increased, the rate of degradation over this range decreases, and vice versa. These strains are input by the user based on indications from monotonic strength tests (such as triaxial or direct simple shear tests).

Table 5.3. Soil properties selected for the constitutive model PM4SandC.

Soil	**Base layer**	**Bottom Ottawa sand layer**	**Mid Ottawa sand layer**	**Top Ottawa sand layer**	**Bottom Ottawa sand layer**	**Mid Ottawa sand layer**	**Top Ottawa sand layer**
UNCEMENTED MODEL							
		Darby et al. (2019)			**San Pablo et al. (2023)**		
dynamic model	hysteretic	PM4SandC	PM4SandC	PM4SandC	PM4SandC	PM4SandC	PM4SandC
hp_o	-	0.2	0.44	0.44	0.06	0.4	0.1
G_o	-	547.8	513	513	770.5	680.6	524.6
V_{sr}	-	1.0	1.0	1.0	1.0	1.0	1.0
c (kPa)	-	0	0	0	0	0	0
MODERATELY CEMENTED MODEL							
		Darby et al. (2019)			**San Pablo et al. (2023)**		
dynamic model	hysteretic	PM4SandC	PM4SandC	PM4SandC	PM4SandC	PM4SandC	PM4SandC
hp_o	-	0.05	0.3	0.02	1.5	0.01	0.02
$G_{o,cem}$	-	1084	1218	921	926.5	1689	1215
V_{sr}	-	1.4	1.5	1.3	1.09	1.57	1.52
γ_{deg}	-	0.002	0.002	0.002	0.001	0.001	0.001
γ_{res}	-	0.01	0.01	0.01	0.025	0.025	0.025
c (kPa)	-	9.4	8.8	4.7	5.4	6.5	4.6

One calibration approach for the PM4Sand and PM4SandC models is to calibrate h_{po} using single element simulations in order to capture the corresponding cyclic resistance ratio (CRR). Although advisable, this is not done here due to the lack of lab tests and empirical correlations corresponding to the present conditions. The availability of these tests helps guide the range of reasonable values for the calibrated parameters. The approach followed here consists of calibrating h_{po} to the dynamic responses directly through a trial-and-error process.

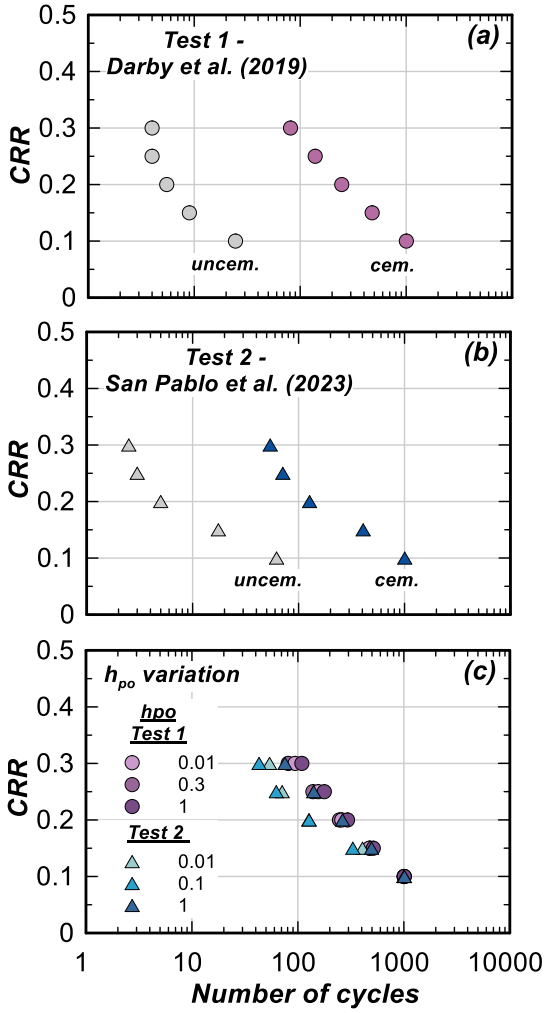

Figure 5.4. Simulated cyclic resistance ratio (*CRR*) versus number of cycles to liquefaction curves at mid-depth (i.e., mid Ottawa layer) for (a) Test 1 – Darby et al. (2019), (b) Test 2 – San Pablo et al. (2023), and (c) sensitivity of curves to calibration parameter h_{po} for both tests.

The calibration of h_{po} to the dynamic response prioritizes the pore pressure generation response since an r_u of 0.95 is considered as the liquefaction triggering criterion. Consequently, the combination of h_{po} values chosen for the 3 sublayers gives the closest match to the shape and magnitude of the pore pressure generation at each recoding point. Figure 5.4 presents the simulated CRR versus the number of cycles to liquefaction curves as obtained from single element cyclic undrained DSS simulations performed on an element at mid-depth in the Ottawa sand and under the same initial conditions (i.e., $D_{R,cem}$, $G_{o,cem}$, V_{sr}, γ_{deg}, and γ_{res}). Figure 5.4a presents a comparison of the CRR for the uncemented case (case A) and the cemented case (case B) for Test 1 – Darby et al. (2019). The cemented input parameters along with the calibrated h_{po} from the middle layer element result in a shifted CRR curve to the right indicating a stronger cyclic resistance and a longer duration (i.e., number of cycles) needed for liquefaction triggering. Figure 5.4b shows a similar behavior for the CRR curves for Test 2 – San Pablo et al. (2023). A variation of h_{po} for the middle layer element is performed in Fig. 5.4c to demonstrate the effect of h_{po} on the CRR versus number of cycles curves. As the contraction rate parameter h_{po} increases, contraction increases resulting in an increased number of cycles to trigger liquefaction and thus a less steep CRR versus number of cycles curves. Physically, it means that an earthquake with a certain demand needs to span over a longer duration in a cemented site to trigger liquefaction due to the increased cyclic resistance of the cemented site. In retrospect, a stronger earthquake with a certain duration is required to trigger liquefaction at a cemented site compared to an uncemented sand. These conclusions conform with the expected behaviors from Chapter 2 and the model performance in Chapter 4.

The uncertainties accompanying the additional parameters to PM4SandC are evaluated parametrically later in this paper. The reader is referred to Chapter 4 for a full description of the PM4SandC model, its formulation, and its calibration process.

5.3.2.4 Dynamic properties of base layer

For the base layer, the dynamic behavior is represented by the hysteretic model (sig3 model) with selected parameters of a = 1.014, b = -0.4792 and x_o= -1.249 fitted to the curves recommended by Seed and Idriss (1970).

5.4 Comparison of simulated and recorded dynamic responses

5.4.1 1D site response

The dynamic response of 1D soil columns can be understood numerically and physically by considering the profile's equivalent fundamental frequency relative to the input motion's frequency. The site's fundamental frequency can be estimated using $T = \frac{4H}{V_s}$ or $f = \frac{V_s}{4H}$ where T is the site's fundamental period, f is the site's fundamental frequency, H is the site's height, and V_s is the site's average shear wave velocity. At small strains, the average secant V_s ranges between 150 and 200 m/s for an uncemented sand. Therefore, for an 11 m deep site, the natural frequency of the site is estimated between 3.4 and 4.5 Hz. For Tests 1 and 2 described in Section 5.2, the frequency of the input motions ranges from 1 to 1.25 Hz indicating that the system will largely respond as a rigid block. As the system is shaken with stronger or longer motions such that cementation breaks or liquefaction is triggered, the system softens, and its natural frequency reduces. In the event the site's natural frequency becomes close to the input motion's frequency, resonance occurs resulting in large amplifications of the motion. If the site gets even softer,

deamplification of the motion takes place. This behavior is evident in the response spectra; however, it should be noted that response spectra represent the peak response of a single degree of freedom (SDOF) system which engineers often use to simplify structures. Thus, the spectral accelerations of a ground motion with a significant drop in intensity at some time in the record reflect only the response of the SDOF prior to the strong drop in motion intensity. As a result, response spectra may not show any difference from changes in site response later in the shaking. In Tests 1 and 2, the surface acceleration in the simulations is expected to be the richest around the same frequency as the input motion (i.e., at 1 Hz for Test 1 and 1.25 Hz for Test 2). Similarly, the response spectra for the surface motion are expected to peak at a period of 1 sec (or frequency of 1 Hz) due to the input motion's frequency. These aspects of the site response will be examined in more detail hereafter.

5.4.2 Time histories (accelerations, pore pressures, and stresses)

The validation of numerical results against recorded centrifuge data requires the selection of recording points along the soil column at locations close to the actual instrumentation in the centrifuge test. Numerical time histories are obtained at three locations representing each of the sublayers for the Ottawa sand. In Test 1, time histories are extracted at about 2 m (i.e., top), 4 m (i.e., mid), and 5.5 m (i.e., bottom) from the ground surface (Fig. 5.1). For brevity, only the results at mid-depth are presented here. In Test 2, time histories are extracted at about 2 m (i.e., top), 5 m (i.e., mid), and 7 m (i.e., bottom) from the ground surface (Fig. 5.2). Results from Test 2 are discussed below in more detail.

Figure 5.5 shows time histories of excess pore pressure generation (Δu), surface acceleration (at 2 m below ground level), cyclic stress ratio (CSR), shear strain (γ), and peak base acceleration (PBA) at mid-depth for the baseline uncemented model (left) and for the moderately cemented

model (right) in Test 1 (Darby et al. 2019). The responses in Fig. 5.5 correspond to shaking events 2 (PBA = 0.06g) and 5 (PBA = 0.17g) which triggered initial liquefaction in the uncemented and moderately cemented models, respectively. As expected, the imposed demand in terms of PBA required for liquefaction was more than two times higher for the cemented sand. The reader is referred to Darby et al. (2019) for further interpretation of these results in terms of liquefaction triggering curves which are outside the scope of the present study. For both the uncemented and the moderately cemented sand, the numerically simulated dynamic responses agree well with the experimentally recorded ones in terms of pore pressure generation (Fig. 5.5a), surface acceleration (Fig. 5.5b), CSR (Fig. 5.5c), and shear strains (Fig. 5.5d). For the uncemented sand, the simulated shear strains and CSR are 0.07% and 0.22, respectively, which are different from the measured ones (0.2% shear strain and 0.15 CSR). This is due to prioritizing liquefaction triggering due to excess pore pressure generation over other behaviors during calibration and the lack of single element test results to calibrate for the CSR. For the moderately cemented sand, the maximum shear strain from the simulation is 0.28% which is an increase from the uncemented one. Both the centrifuge and the simulation (0.59% and 0.28%, respectively) show a higher maximum shear strain which may be attributed to the different demands (i.e., loading) applied to the system for the uncemented and cemented cases. The maximum achieved CSR in the simulation is 0.92 which is slightly higher than the experimental one (CSR of 0.79). Comparing the surface acceleration (Fig. 5.5b) to the base acceleration (Fig. 5.5e), both experimental and simulated results show that the accelerations are de-amplified in uncemented sands (peak PBA of about 0.06 g to peak surface acceleration of about 0.03 g) and amplified in cemented sands (peak PBA of about 0.17 g to peak surface acceleration of about 0.4 g) from the bottom to the top of the profile.

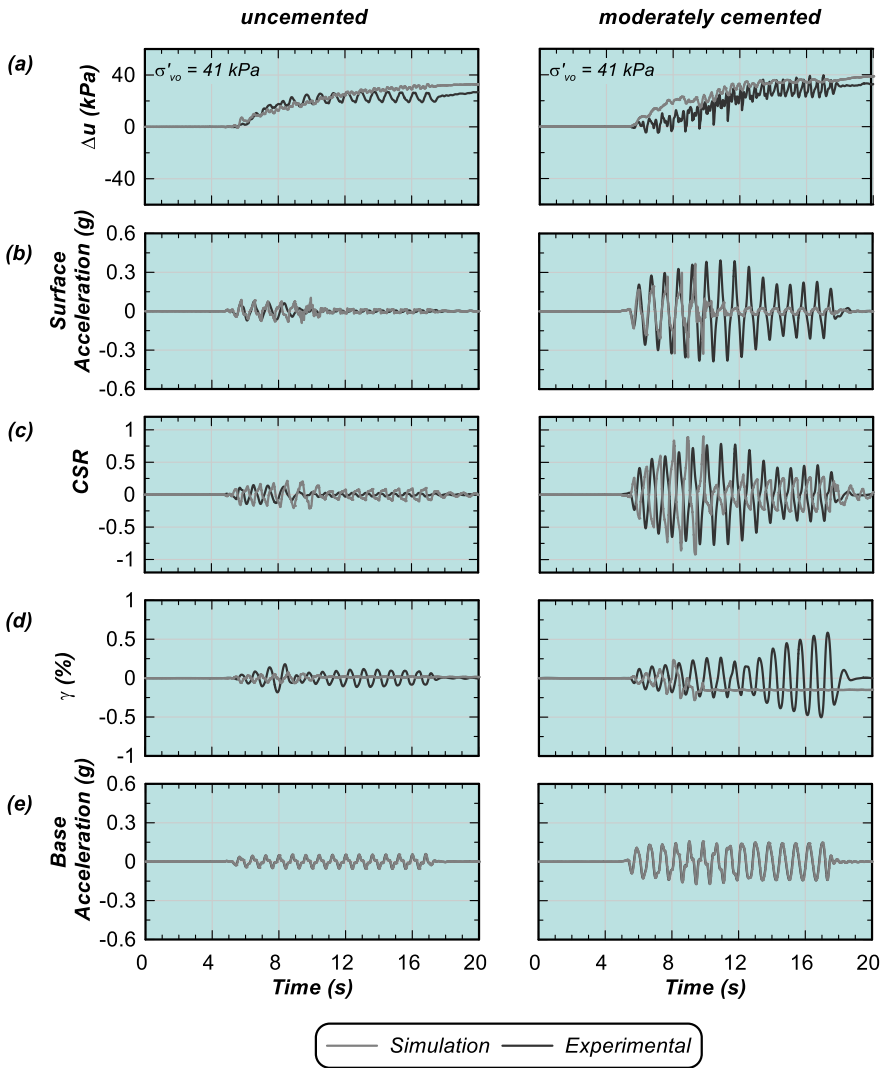

Figure 5.5. Comparison of dynamic time histories in uncemented and moderately cemented sands, respectively, of (a) Δu at mid-depth, (b) surface acceleration, (c) CSR at mid-depth, (d) strain at mid-depth, and (e) base acceleration (refer to Fig. 5.3a for color coding). Experimental results adapted from Darby et al. (2019).

Figure 5.6 summarizes the time histories of excess pore pressure generation (r_u), accelerations, cyclic stress ratio (CSR), shear strain (γ), and peak base accelerations (PBA) across the profile depth for the baseline uncemented model (left) and for the moderately cemented model (right) for the tests by San Pablo et al. (2023). The responses in Fig. 5.6 correspond to shaking events 3 (PBA

= 0.19g) and 6 (PBA = 0.29g) which triggered initial liquefaction in the uncemented and moderately cemented models, respectively. The PBAs are higher than the ones for the Darby et al. (2019) tests because of the higher D_R for the San Pablo et al. (2023) tests. The increase in PBA between the uncemented and the cemented sand is similarly credited to the stronger and stiffer sand resulting from the cementation process and requiring stronger shaking to liquefy. For both the uncemented and the moderately cemented sand, the dynamic response from the simulation generally agrees well with the one recorded in the centrifuge test in terms of pore pressure generation (Fig. 5.6a, e, i), accelerations (Fig. 5.6b, f, j), CSR (Fig. 5.6c, g), and shear strains (Fig. 5.6d, h) along the depth of the sand layer (delineated by the color coding in Fig. 5.3) apart from some discrepancies near the ground surface. These discrepancies may pertain to the dynamic response from the centrifuge and are an artifact of the small centrifuge container size and its boundary effects. As evident, these differences (i.e., amplifications) are more visible towards the ground surface (the shallower sensors) and are more pronounced in Test 2 (stiffer) than Test 1. They may be due to the accumulation of high frequency noise and reflected waves present in the centrifuge container due to boundary effects. As a result of these amplifications, sensors reached their maximum values and clipped the histories at about 6.5 sec as indicated on Figs. 5.6b and c. While these erratic measurements are not considered in the comparison, they are shown here for completeness.

The measurements from the center array of sensors are least affected by the boundary effects and thus, are more suited for numerical simulation validation. For the uncemented sand, the simulated shear strains and CSR at mid-depth are 0.54% and 0.67, respectively, compared to 0.92% and 0.56 as averaged from the centrifuge results over a certain depth.

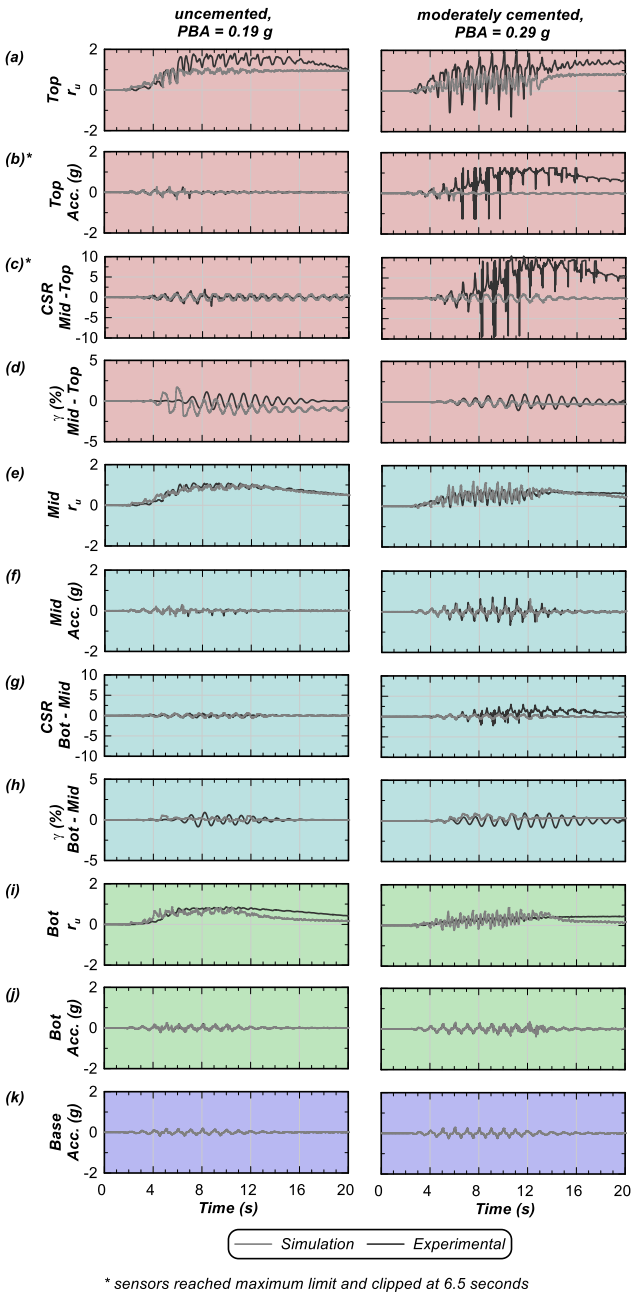

Figure 5.6. Dynamic response comparison of uncemented (left) and moderately cemented (right) of (a) r_u at top of profile, (b) top (or surface) acceleration, (c) CSR between mid- and top-depth, (d) strain between mid- and top-depth, (e) r_u at mid of profile, (f) mid acceleration, (g) CSR between bottom- and mid-depth, (h) strain between bottom- and mid-depth, (i) r_u at bottom of profile, (j) bottom acceleration, and (k) base acceleration (refer to Fig. 5.3b for color coding). Experimental results adapted from San Pablo et al. (2023).

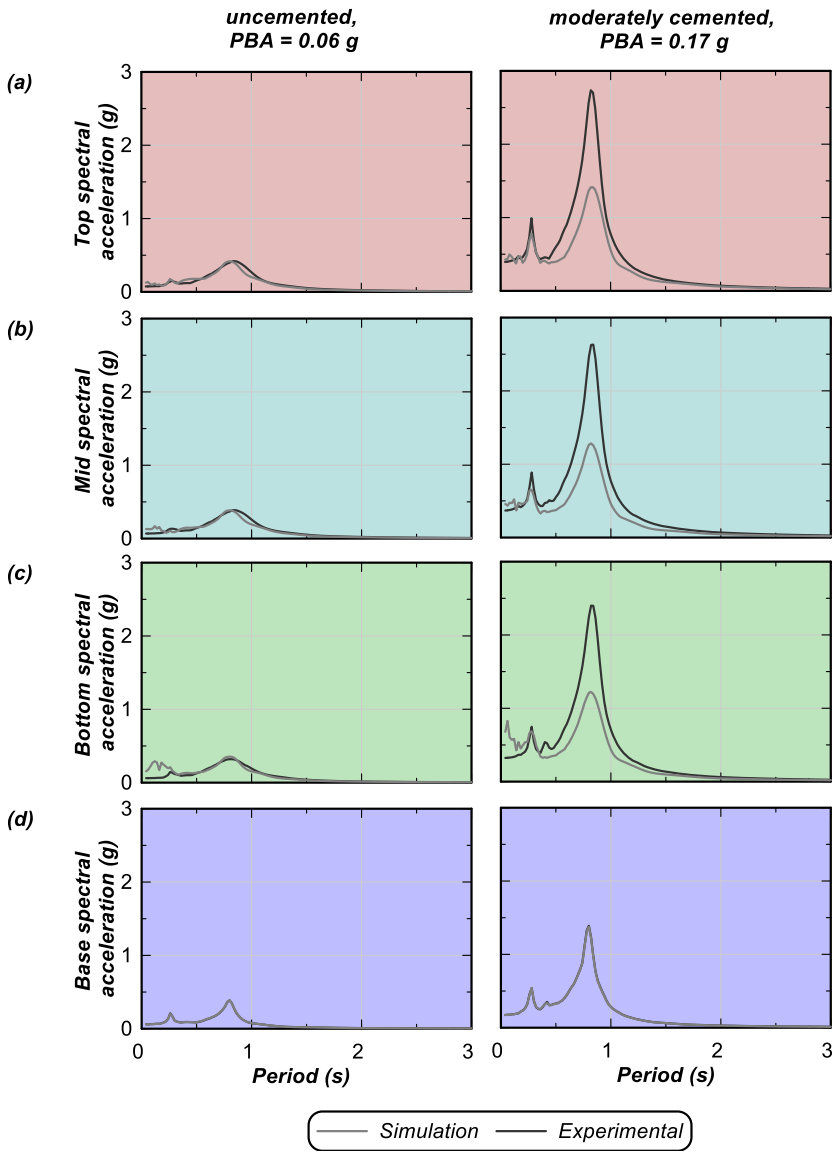

Figure 5.7. Response spectra for the uncemented case (left) and the moderately cemented case (right) across the length of the Ottawa sand in Darby et al. (2019) – Test 1 (refer to Fig. 5.3a for color coding). Experimental results adapted from Darby et al. (2019).

For the moderately cemented sand, the simulated shear strains and CSR at mid-depth are 0.76% and 1.10, respectively, which differ by 0.18% and 1.91 respectively, as averaged from the centrifuge results over the depth.

These discrepancies may be attributed to the depth averaging done for the centrifuge results and possibly the exaggerated amplifications in the stiffer cemented case due to the reflected waves as discussed before. In light of the above, the comparison between the shear strains and CSR in this case may be considered reasonable.

5.4.3 Response spectra

To highlight the effect of the bio-cementation on the dynamic response of a liquefiable site, acceleration response spectra are also compared along the depth of the soil column. Figures 5.7 and 5.8 illustrate the response spectra for the uncemented and moderately cemented sand for Test 1 and Test 2, respectively. These spectra are computed at various locations within the liquefiable Ottawa sand as reported by the placement of the accelerometers in the centrifuge (discussed in Section 5.3.1). Due to the clipping of the sensors, the response spectra for the top sand are omitted from the comparison (Fig. 5.8a). Along the full depth of the soil profile, the response spectra show a peak at a period of 1 sec (or frequency of 1 or 1.25 Hz) due to the input's motion frequency. Comparing the uncemented to the moderately cemented sand in Figs. 5.7 and 5.8, it is noticeable that the response spectra get amplified in the cemented sand as the waves travel through the soil column. These amplifications are attributed to the cemented site's higher initial stiffness compared to the uncemented site and the subsequent softening of the natural frequency to one closer to the input motion's frequency (refer to Section 5.4.1). Regardless of the relative magnitude of this amplification, the observation is consistent for both the experimental and simulated results. It can also be observed that the response spectra from the simulations reasonably match the ones from the centrifuge tests for both Tests 1 and 2 with little calibration effort of the PM4SandC model.

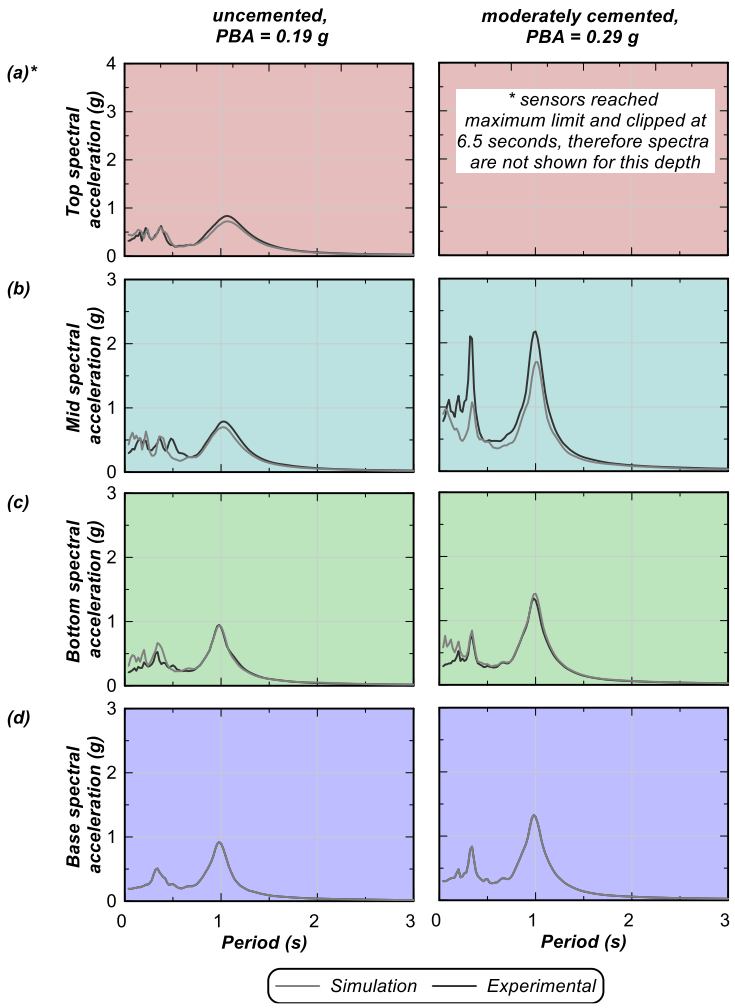

Figure 5.8. Response spectra for the uncemented case (left) and the moderately cemented case (right) across the length of the Ottawa sand in San Pablo et al. (2023) – Test 2 (refer to Fig. 5.3b for color coding). Experimental results adapted from San Pablo et al. (2023).

5.5 Parametric investigation of responses to parameter uncertainties

Input parameter uncertainties may be unavoidable for any site-specific analysis, and they may be even more challenging to quantify at an improved site where additional complexities come into play such as the spatial nonuniformity of treatment. While field trials will further explore these uncertainties experimentally, a parametric analysis is performed to numerically investigate the

effect of PM4SandC user input parameter uncertainties on the dynamic response of a 1D soil column subject to earthquake loading. The goal of this exercise is (1) to highlight the effects of each cementation-related input parameter and its inherent uncertainty, and (2) to guide the analyst in navigating the calibration process such that the behaviors of importance to each site are prioritized in the calibration. The moderately cemented sand simulation from San Pablo et al. (2023) (Test 2) serves as a reference case for the parametric study. The variation of input parameters focuses on three PM4SandC parameters: the level of cementation informed by the shear wave velocity V_s, the degradation strain γ_{deg}, and the residual strain γ_{res}.

5.5.1 Varying the level of cementation

The reference case results correspond to the simulation shown in Fig. 5.6 (right column) and Fig. 5.8 (right column). The input parameters to this simulation are reported in Tables 5.1 and 5.2. The uncertainty for the level of cementation is assessed as a potential measurement error of V_s. This measurement error is quantified to be 15% in lab and field V_s measurements. Consequently, the $V_{s,cem}$ in each of the three sublayers is varied ± 15% of the original sublayer's V_s. The lower bound for $V_{s,cem}$ is set to the uncemented V_s such that the V_{sr} does not go below 1. Therefore, the V_s for the bottom, mid, and top sand becomes 183, 230, and 195 m/s, respectively, for a lower bound for $V_{s,cem}$. The V_s for the bottom, mid, and top sand becomes 230, 311, and 263 m/s, respectively, for an upper bound for $V_{s,cem}$. These soils are considered lightly and moderately cemented, respectively, based on the classification by Montoya et al. (2013). The contraction rate parameter h_{po} is also varied to highlight its effect on the liquefaction triggering at the given conditions. h_{po} controls the contraction rate of the soil and thus affects its liquefaction resistance and the number of cycles to trigger liquefaction (refer to Section 5.3.2.3). It is a calibration parameter, and it is calibrated for the reference simulation (validated against the centrifuge test).

In this parametric study, h_{po} is taken from the reference simulation and simulations are run with half the value of h_{po} and twice its value. This is done to bracket the responses and obtain a representative set of results. Thus, $0.5h_{po}$ for the bottom, mid, and top sand corresponds to 0.75, 0.005, and 0.01, respectively. Similarly, h_{po} corresponds to 1.5, 0.01, and 0.02, and $2h_{po}$ corresponds to 3, 0.02, and 0.04. The columns in Fig. 5.9 represent a different set of h_{po} values and the rows in Fig. 5.9 represent the different responses of interest at mid-depth of the Ottawa sand layer (prototype scale). The top row shows the excess pore pressure generation r_u as a function of the duration of loading, the middle row shows the cyclic shear stress CSR versus the shear strain γ, and the bottom row shows the acceleration response spectra S_a versus period. The colors for the curves darken as V_s increases and the soil becomes more cemented.

Figure 5.9 indicates that, in terms of liquefaction triggering, the case with the lower V_s bound (i.e., -15% uncertainty) is the one where liquefaction is most likely triggered based on the r_u criterion (r_u > 0.95). In addition to the r_u triggering criterion, the stress-strain responses in Figs. 5.9b, 5.9e, and 5.9h show that shear strain accumulates to about 1%, further indicating liquefaction triggering. The reference case triggers at the validated h_{po} as seen in Section 5.4. The upper V_s bound (i.e., +15% uncertainty) does not trigger with increasing h_{po}, as expected for a higher level of cementation needing more cycles to liquefy. Thus, r_u for the simulations with higher V_s (Figs. 5.9a, 5.9d, 5.9g) dissipate faster and the volumetric behavior tends towards more dilation reflected by the dilation peaks and the slightly negative r_u. The stress-strain loops for the lower V_s bound simulations accumulate more shear strains while the ones for the upper V_s bound remain relatively elastic and do not accumulate enough shear strains to liquefy (Figs. 5.9b, 5.9e, 5.9h). It is also noticeable that the stress-strain loops are stiffer for the simulation with higher V_s (i.e., higher level of cementation) due to the relationship between V_s and the coefficient of stiffness G_o.

The response spectra for the lower V_s bound and the reference simulations (Figs. 5.9c, 5.9f, 5.9i) show a slight shift in the predominant period which can be attributed to liquefaction triggering and significant strain accumulation in these cases. It remains at 1 sec for the upper V_s bound. The peaks of the response spectra are comparable for all these cases with spectral accelerations around 1.5 g. Overall, the spectral shape is preserved. As for h_{po}, it directly affects the pore pressure generation, the shear strain accumulation, and to a lesser extent the amplification of the response spectra. As h_{po} increases, pore pressure dissipation happens faster and the shear strain accumulation happens slower due to an increase in the cyclic resistance as can be seen for the upper V_s bound simulation in Fig. 5.9a compared to Fig. 5.9g, and Fig. 5.9b compared to Fig. 5.9h, respectively.

5.5.2 Varying the degradation rate

The results presented in Section 5.5.1 above correspond to one set of degradation parameters: degradation strain γ_{deg} of 0.1% and residual strain γ_{res} of 2.5%. These values are chosen based on the generalized calibration of PM4SandC against element test data from the literature. In the absence of any lab strength tests and given that the mechanical response of bio-cemented soils is still being formalized (e.g., Chapter 2), these parameters may introduce some uncertainty in the simulated response. In what follows, the reference V_s and a set of h_{po} values equal to the reference (validated) h_{po} are preserved. The values of γ_{deg} and γ_{res} are varied to understand their effect on the overall dynamic response. γ_{deg} is increased from 0.1% to 1% shear strain with a fixed γ_{res} of 5%, whereas γ_{res} is increased from 2.5% to 5% (strain of interest for liquefaction problems) with a fixed γ_{deg} of 0.1%.

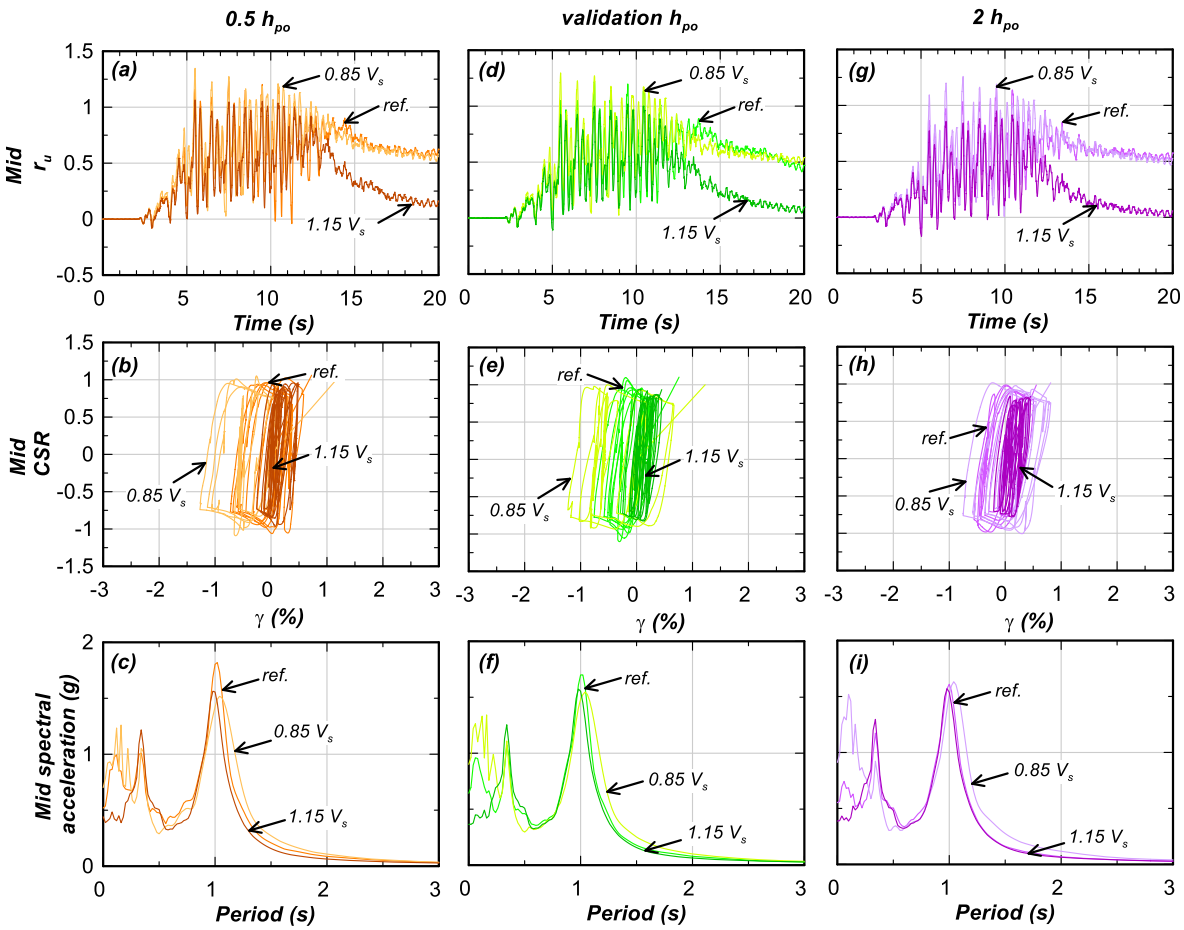

Figure 5.9. Results of varying the PM4SandC cementation parameters on the moderately cemented simulation validated against San Pablo et al. (2023): (a, d, g) pore pressure ratio at mid-depth, (b, e, h) stress-strain response at mid-depth, (c, f, i) response spectra at mid-depth.

In this manner, the range between γ_{res} and γ_{deg} varies from 2.4% to 4.9% which directly affects the rate of cementation degradation. A smaller range yields a faster degradation and vice versa. Figure 5.10 shows the results from a set of simulations performed on the reference case from the moderately cemented sand in San Pablo et al. (2023). The organization of Fig. 5.10 is comparable to that of Fig. 5.9 in that the columns are for different PM4SandC parameters, the rows are for the responses of interest, and the colors from light to dark denote an increase in the investigated parameter. The column to the left shows the results for a fixed γ_{deg} of 0.1% and varying γ_{res}.

While little effect is seen in the response spectra (Fig. 5.10c) due to their ability in only capturing peak responses, a more considerable effect is observed in the pore pressure generation (Fig. 5.10a) and the stress-strain response (Fig. 5.10b). As γ_{res} increases, the range of degradation becomes larger, and hence, the degradation of the cementation becomes slower. This is reflected on the dynamic response by a slower pore pressure generation after 10 seconds which may still be inhibited by the presence of the cementation at the sand contacts (γ_{res}=5% in Fig. 5.10a), and a slower accumulation of shear strains (or damage) (γ_{res}=5% in Fig. 5.10b). These differences may not be significant in this set of calibrated simulations, however the mentioned trends provide insights for other site response analyses where the cementation is heavier and the degradation is more important.

The column to the right shows the results for a fixed γ_{res} of 5% and varying γ_{deg}. As such, the range between these strains decreases from 4.9% to 4%. Although degrading at different rates, the results of γ_{deg} of 0.1% and 1% coincide because the degradation with γ_{deg} of 0.1% starts earlier and over a 4.9% range and the degradation with γ_{deg} of 1% starts later and over a 4% range. This choice of γ_{deg} and range eventually yields a similar degradation curve for these 2 cases leading to similar results. The response spectra (Fig. 5.10f) remain insignificantly affected by the 2 parameters γ_{deg} and γ_{res}, however differences in responses are slightly more obvious for the shear strain accumulation (Fig. 5.10e). When the onset of the degradation is delayed to 1%, the rate of pore pressure generation remains the same as γ_{deg} = 0.1% and the soil liquefies but the pore pressure ratio dissipates slightly faster. This is more intuitive in the stress-strain response whereby increasing γ_{deg} results in delayed degradation and less shear strain accumulation.

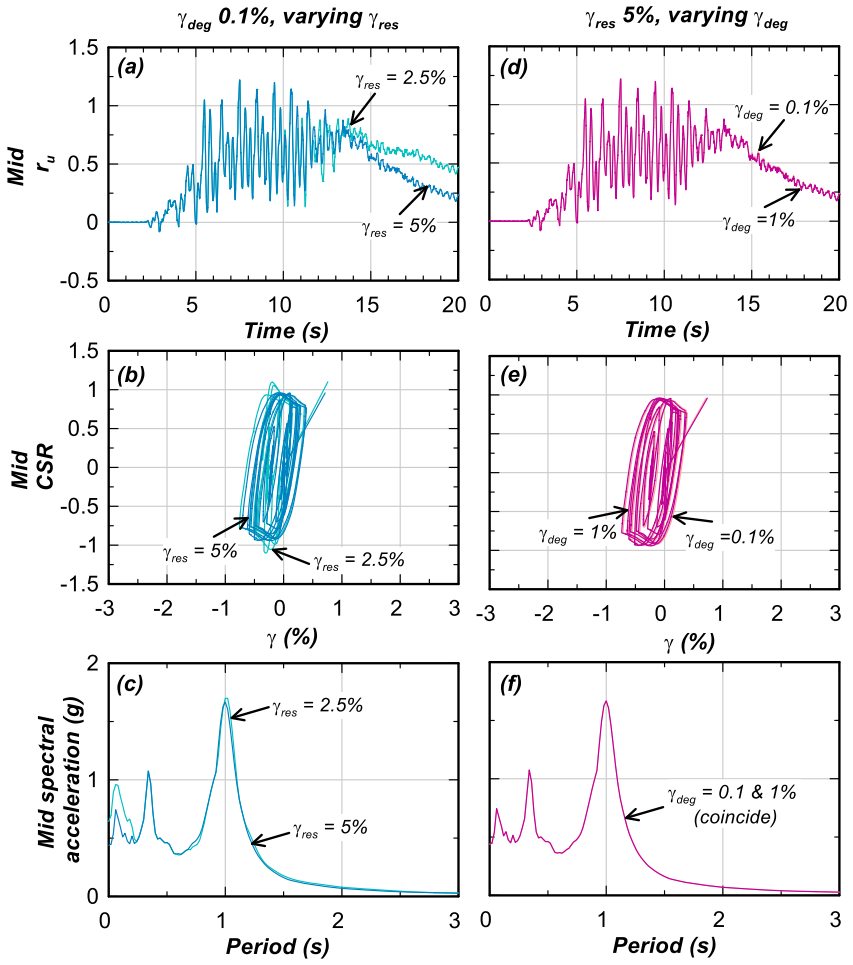

Figure 5.10. Results of varying the PM4SandC degradation parameters on the moderately cemented simulation validated against San Pablo et al. (2023): (a, d) pore pressure ratio at mid-depth, (b, e) stress-strain response at mid-depth, (c, f) response spectra at mid-depth.

5.6 Concluding remarks

A series of nonlinear dynamic 1D site response analyses were performed to validate the recently developed PM4SandC constitutive model in a system-level analysis and subsequently investigate the effect of bio-cementation on the free-field dynamic response of an improved site. The results from the simulations were validated against two centrifuge tests. Therefore, two soil column models were described in this paper along with their boundary conditions and soil profiles.

Due to the nonuniformity and the spatial variability of the cementation, the cemented sand layer was divided into three sublayers as guided by the location of the instrumentation. For each layer was assigned a set of input parameters to the PM4SandC model.

The comparison of the simulated and the recorded dynamic responses showed that the PM4SandC constitutive model is able to capture the changes in behaviors due to the cementation. These changes were reflected in the dynamic response tracked from the base to the surface of the profile. According to this validation, the effect of bio-cementation on the free-field dynamic response of an MICP-improved site included:

- A larger peak base acceleration was required to trigger liquefaction in bio-cemented sands (an increase of ~ 0.1 g for both tested models).
- The accumulated shear strain was larger for a bio-cemented sand than an uncemented sand because they were tested under larger peak accelerations. The post-triggering behavior of bio-cemented sands is not well experimented or understood yet, and more considerations could be given to this aspect in future studies.
- The cyclic stress ratio was higher for bio-cemented sands than an uncemented sand which corroborates the conclusion that larger shaking is needed to trigger liquefaction. The cyclic stress ratio resulting from the simulation was comparable to the one seen in the centrifuge.
- Pore pressure generation was slower for the bio-cemented sand than the uncemented sands and the dilation peaks were more pronounced due to the enhanced dilative behavior coming from the cementation.
- The base accelerations were de-amplified at the surface for an uncemented sand and were amplified at the surface for a bio-cemented sand. This was seen in both the centrifuge tests and the simulations.

- Similarly, the amplification of the accelerations was seen in the response spectra and the predominant period of the motion was seen shift to the right as liquefaction occurs in bio-cemented sands. The simulations and the centrifuge tests corroborate this finding.

A parametric study was performed to clarify how the PM4SandC constitutive model works. This study aimed at emphasizing the effect of each input parameter on the dynamic response and providing insights into a more targeted calibration process. It is recommended that the user starts the calibration process by (1) inputting an estimate of the level of cementation, correlated here with the cemented shear wave velocity, (2) adjusting the relative density to the measure after cementation, (3) assigning estimates for the degradation and residual strains, and (4) inputting a value for the contraction rate parameter h_{po}. What follows is an iterative process to calibrate h_{po}. It can be done in two ways: (1) if centrifuge data or field data are available, h_{po} can be calibrated to best approximate the measured response, as was done in this paper, and (2) if lab strength data is available, h_{po} can be calibrated using single-element simulations to approximate a cyclic resistance ratio (CRR) and the h_{po} corresponding to the CRR is input in the site response analysis. In the absence of both, the constitutive model generally yields a reasonable prediction of the overall dynamic response, and the analysis can be further tweaked once more data becomes available. It is also recommended in this case to bracket the dynamic response by performing simulations with the lowest level of cementation estimates (conservative) and the highest level of cementation estimates (optimistic). The decision for a given project can then be made based on the user's confidence in the measured level of cementation. The degradation and the residual strains can be further fine-tuned if a monotonic strength test is available where the degradation of the cementation is more visible.

The work presented in this paper is unique for the novel bio-cemented sands. It has been made recently possible by the development of a constitutive model for bio-cemented sands following the elemental behaviors suggested by bench scale (lab) and large scale (1-g tanks) tests. The constitutive model has been validated against single-element tests (Chapter 4) and this work constitutes its first validation study on a system level. The aim of this study was to evaluate the general response of the model and provide some insights into its usability. The aspects of the response shown here are considered based on the available data to validate against.

CHAPTER 6

Conclusions and future directions

This Dissertation describes the extension of the sand plasticity model PM4Sand (Version 3.2) for geotechnical earthquake engineering applications to bio-cemented sands. The extended model PM4SandC ("C" for cement) is built upon the same framework as PM4Sand and inherits its original formulation and input parameters. A series of modifications and additions to the model were done to the original formulation of PM4Sand (Version 3.2) to enable the model to predict the stress-strain responses of bio-cemented sands, and by extension, naturally cemented sands. The reformulation was performed at the equation level of some aspects of the model where the effect of the cementation was the greatest. The goal of this Dissertation was to present an implemented plasticity model for bio-cemented sands promoted as a potential mitigation to liquefiable sands that is built on a robust original formulation, usable in practice, and is relatively easy to calibrate.

The work presented in this Dissertation included the following steps: (1) comprehensive literature review of the elemental behaviors of bio-cemented sands, (2) an empirical relationship between a field parameter and a constitutive input parameter, (3) implementation, calibration, and

validation of the extended PM4SandC model on the element level, (4) implementation, calibration, and validation of the model on the system level.

This Chapter presents the main conclusions from the aforementioned components of this work and provides suggestions for future research.

6.1 Summary and conclusions

6.1.1 Literature review (Chapter 2)

An extensive literature review on bio-cemented sands was performed to (1) synthesize, critically review, and understand the elemental behaviors of these geomaterials, (2) inform constitutive modifications to the PM4Sand model, and (3) highlight knowledge gaps and provide recommendations for further research and testing. The literature review consisted of a critical review of available experimental studies on MICP-cemented sands on the bench, large, and field scale as well as available constitutive models for bio-cemented sands and other relevant geomaterials such as Portland-cemented soils, structured clays, and weak rocks. The effect of bio-cementation on engineering properties of sands was first presented followed by a synthesis of the affected elemental responses with emphasis on the stress-strain and volumetric behaviors under monotonic and cyclic loading, drained and undrained conditions. Available constitutive models for cemented sands and other relevant geomaterials along with their modifications and validation programs were then summarized. Points of agreements and deviations on both the experimental and the numerical levels were identified to provide insights into establishing a comprehensive dataset useful for the formulation of engineering property correlations and laws for constitutive models for cemented sands. This Chapter was essential to inform the work in the subsequent Chapters of this Dissertation.

6.1.2 Δq_c-c relationship (Chapter 3)

Axisymmetric cone penetration simulations were performed in FLAC 8.1 to simulate cone penetration in bio-cemented sands, aiming to synthesize numerical data to complement the readily available experimental data for the development of a relationship between a field parameter (Δq_c) and a constitutive parameter (c). The axisymmetric cone penetration model (Moug 2017) was used in conjunction with the Mohr-Coulomb constitutive model for cohesive soils to represent bio-cemented sands. A preliminary sensitivity analysis presented in Appendix A was done to distinguish the input parameters most important to the simulation of cone penetration in bio-cemented sands. Findings from this sensitivity analysis informed the prioritization of the cohesion and shear stiffness in the calibration of the numerical model. Cone penetration simulations were initially performed at two confining stresses similar to the ones from available experimental data on a large tank experiment and a centrifuge test. Results from the simulations were compared to the ones from the experiments and were found to be satisfactory. Once validated, the simulations were extended to higher confining stresses to expand the dataset needed for the development of a relationship between tip resistance and cohesion. The results were analyzed in the K_G (analogous to rigidity index) space against previously published ranges for cemented sands and were found to fall within the expected ranges. An empirical relationship between the cementation-induced cone tip resistance and the cohesion of cemented sands is presented as a function of confining stress. This relationship may be used in the estimation of the cohesion term for constitutive models such as the proposed PM4SandC from field measurements.

6.1.3 PM4SandC reformulation and validation at the element level (Chapter 4)

An extension of the PM4Sand constitutive model to bio-cemented sands was described on the equation level and was implemented as a dynamic link library in the explicit scheme program

FLAC 8.1 (Itasca 2019). Only modifications from the original PM4Sand Version 3.2 formulation were presented here. These modifications included:

- the shear modulus constant $G_{o,cem}$ is calibrated in terms of the cemented shear wave velocity to reflect the increase in the stiffness of bio-cemented sands;
- the mean effective stress (p) is enhanced by the contribution of a p due to the cementation which reflects the enhanced tensile strength of bio-cemented sands;
- the shear modulus is proportional to p raised to a power n rather than a power of 0.5 whereby n depends on the level of cementation;
- evolution laws are used to degrade/alter the cementation parameters as a function of damage accumulation.

The PM4SandC model is applicable to lightly and moderately cemented sands as classified by Montoya et al. (2013) and is constrained to plane-strain applications in the FLAC program.

Input parameters to the model were introduced and the calibration process was outlined to guide the user in the calibration process. The numerical implementation in FLAC was described and a set of general calibrations was presented to demonstrate the capabilities of the model under various monotonic and cyclic, drained, and undrained conditions. The performance of the extended constitutive model was also evaluated against readily available element tests on MICP-treated specimens for drained triaxial compression tests and undrained monotonic and undrained cyclic Direct Simple Shear (DSS) tests. The PM4SandC constitutive model reasonably predicts the mechanical behavior of bio-cemented sands under the tested initial conditions.

6.1.4 Validation of PM4SandC at the system level (Chapter 5)

Chapters 4 and 5 constitute the validation of the PM4SandC constitutive model at the element and system level, respectively. Two one-dimensional site response analyses on bio-cemented columns

were performed in FLAC 8.1 (Itasca 2019) using the PM4SandC to model the bio-cemented columns. Two centrifuge tests on uncemented and bio-cemented sands were simulated as 1D columns and simulation results were compared against the measurements from the instrumented experiments. The bio-cemented columns were divided into sublayers to account for the spatial variability and heterogeneity of the treatment along the depth of the centrifuge container. Motions which corresponded to the first triggering of the cemented Ottawa sand using the pore pressure ratio > 95% liquefaction criterion were prescribed at the bottom of the 1D columns. The input parameters to each of the four simulations (Test 1-uncemented, Test 1-cemented and Test 2-uncemented, Test 2-cemented) were summarized and the selected properties were justified. Results from the dynamic analyses for the four simulations reasonably agreed with the experimental results from their respective centrifuge tests. Acceleration, pore pressures, cyclic stress ratio, and shear strain time histories as well as response spectra were presented and discussed. The spatial variability of the cementation led to a parametric investigation of responses to input parameter uncertainties. For this parametric study, parameters related to the level of cementation (i.e., V_{sr}) and the bond degradation (i.e., γ_{deg} and γ_{res}) were varied for the "Test 2-cemented" simulation and observations were made regarding the changes in behavior of the 1D columns.

6.2 Future directions

The extensive literature review on bio-cemented sands was initiated in the early stages of this research to synthesize the knowledge and gaps on the mechanical response of these geomaterials, and it kept being extended until July, 4th 2022. In recent years, the number of experimental studies on bio-cemented sands increased exponentially which improved our understanding of their mechanisms and behaviors. However, some areas remain unexplored in which case insights were

taken from studies on other cemented sands. While the summary plots and tables include all studies up to the publication of this Dissertation, publications on bio-cemented sands continue to increase, and thus a continuous effort should be made to maintain the database up to date with the recent publications, findings, and refinements to prior knowledge, and improve the fits of the proposed relationships. One of the major contributions of this Dissertation is that through this review it paves the way for further extensions and valuable findings.

During the reformulation of the PM4SandC constitutive model, the model has been calibrated and validated against readily available element lab tests. While the available lab data was enough to demonstrate the performance of the model, the model should be continuously and systematically validated under broader ranges of initial conditions as the experimental database becomes more enriched. The continuous validation of the model will expand its use to broader geotechnical engineering applications and create a database of analyzed cases that are systematically validated.

The validation of the model at the system level covered the 1D site response analysis of the bio-cemented centrifuge models. These system-level analyses can be extended to 2D simulations of these tests using the PM4SandC model, and to well-instrumented field trials currently being planned. The current collaborative effort between the Center of Bio-mediated and Bio-inspired Geotechnics (CBBG) institutions provides the opportunity to disseminate the model to users other than the developers and promote its use as a predictive tool in the area of liquefaction mitigation.

The PM4SandC constitutive model has enough robustness to accommodate a broad range of input parameters, e.g., V_{sr} from 1 to 5. It is acknowledged that the MICP treatment, although becoming more controlled, may yield different end-products, morphologies, and cement contents. The spatial variability of the cementation and its uniformity versus nonuniformity become important at the system scale such as large tanks, centrifuge tests, and field trials. In the present

implementation, spatial variability of the cementation is acknowledged by prescribing different input parameters to sublayers. As spatial variability in the field becomes more quantifiable, the functional forms related to the initial cementation contribution in the model may be refined to reflect this variability within a sand matrix. The aforementioned field trial is an excellent starting point to collaborate on this notion.

In addition to liquefaction analyses, the model can be tested under sloping ground conditions to lead the effort in understanding the dependence of the response of cemented sands on static shear stresses and developing empirical relationships similar to sands (i.e., K_α relationships) that are reasonably consistent with the expected behaviors and their magnitudes. In the same line of thought, the dependence of the response on the confining stress, which was considered in this work, can be further explored to develop an empirical relationship similar to sands and advance one of the goals of this work which is to mitigate shallow liquefiable sands.

Post-liquefaction reconsolidation of bio-cemented sands is largely unexplored by experimentalists and modelers alike. With very little indications on the behavior of bio-cemented sands following multiple triggering events and pore pressure dissipation, this aspect of the model remained unchanged relative to the original sand formulation. There may be room for refinement on this aspect.

A 3D implementation of PM4Sand is underway. Similarly, a 3D implementation of PM4SandC is needed to enable its application to 3D problems.

Although validated constitutive models should be able to reproduce the stress-strain behavior of soils, the mechanisms leading to the response are often more detailed and complex. As a result, constitutive models, including PM4SandC, have limitations which may be important in bigger scale analyses. As the model is continuously tested, it is expected that users should be able to

recognize these limitations in light of their projects and exercise their engineering judgement on what seems like an erroneous result. It is hoped that this Dissertation, along with the single-element drivers and manual by El Kortbawi et al. (2022) available to the public, constitute a complete documentation of the PM4SandC extension model and that other researchers contribute to its general validation and identification of limitations through their work.

APPENDIX A

Effect of sand bio-cementation on cone tip resistance: a numerical study

Original publication:

El Kortbawi M., Ziotopoulou K., DeJong J.T., and Moug D. M. (2022). Effect of sand bio-cementation on cone tip resistance: a numerical study. Proceedings of the 5th International Symposium on Cone Penetration Testing, Bologna, Italy, 8-10 June 2022.

Author's note: This companion paper serves as a parametric study on the input parameters to the cone penetration model using the Mohr-Coulomb constitutive model. This preliminary work preceded the final work presented in Chapter 3 of this Dissertation and is included in the appendix for completeness.

Abstract

Understanding the effect of soil cementation on cone measurements is important for the identification of naturally cemented soil deposits and for the verification of soil improvement achieved by various forms of artificial cementation, including bio-cementation. This paper presents the results of an effort to connect cone tip resistances with fundamental, constitutive level,

bio-cementation-induced changes in soil behavior. To this end, a direct axisymmetric cone penetration model using the Mohr-Coulomb constitutive model and grid rezoning and remapping algorithms is used to model cone penetration in bio-cemented sands. By connecting the results of cone penetration simulations in a Mohr-Coulomb material to real data and established relationships, this work will guide selection of equivalent strength properties of these challenging materials. More specifically, the apparent cohesion, peak friction angle, dilation angle, and small-strain shear modulus within the Mohr-Coulomb constitutive model are varied parametrically across a reasonable range of parameter values informed by past laboratory, bench-scale, and centrifuge tests. Results show that cone penetration resistance in bio-cemented sands is mostly influenced by the interconnected apparent cohesion and the small-strain shear modulus, while other parameters play a secondary role.

A.1 Introduction

The cone penetration test (CPT) is a widely used field test for soils in subsurface explorations due to its ability to provide continuous information on the stratigraphy, and to be correlated to physical and engineering properties of the subsurface strata (e.g., Robertson & Campanella 1983, Lunne et al. 1997, Robertson 2016). While the CPT has been mostly used for the characterization of sands and clays, it may also be used for the identification of naturally cemented soils deposits (e.g., Puppala et al. 1995, Roy 2008) and artificially cemented and improved soils, including bio-cemented ones (e.g. Gomez et al. 2018, Darby et al. 2019).

Bio-cementation is a relatively new ground improvement technique in which microorganisms present in the soil are stimulated under specific conditions to precipitate calcite which coats and bridges soil particle contacts. The artificially precipitated calcite is analogous to natural

cementation and can be considered as a proxy for naturally cemented sands (e.g., DeJong et al. 2006, DeJong et al. 2010). To date, the characterization of bio-cemented sands and, similarly, naturally cemented sands in the field remains a challenging task due to difficulties in sampling and its high cost.

Classification and characterization approaches for bio-cemented sands developed to date have been primarily derived through empirical analyses of field data obtained in cemented soils, although some full scale 1-g and reduced scale centrifuge modeling data are also available. Therefore, the CPT has been proposed as a field test able to overcome the limitations of sampling and to provide direct indications of the presence of the cementation in the field. In general, the cone tip resistance and the shear wave velocity both increase with cementation, which suggests the development of a framework relating these two parameters as an indicator of possible cementation. Currently, such a framework is not available for the interpretation of the CPT data and their correlation to soil strength parameters for bio-cemented sands.

This paper presents the results of an effort to connect cone tip resistances with fundamental, constitutive level, bio-cementation-induced changes in soil behavior. To this end, a direct axisymmetric cone penetration model using the Mohr-Coulomb constitutive model and grid rezoning and remapping algorithms (Moug 2017) is used to model cone penetration in bio-cemented sands. By connecting the results of cone penetration simulations in a Mohr-Coulomb material to real data and established relationships, this work will guide selection of equivalent strength properties of these challenging materials. More specifically, the apparent cohesion, peak friction angle, dilation angle, and small-strain shear modulus within the Mohr-Coulomb constitutive model are varied parametrically across a reasonable range of parameter values informed by past laboratory, bench-scale, and centrifuge tests.

The axisymmetric penetration model is briefly introduced, followed by a summary of the equivalent Mohr Coulomb input parameters. Simulation results are presented, interpreted, and compared against a published soil behavior type chart as well as experimental data from a reduced scale centrifuge model test. Conclusions pertaining to the validity of the proposed framework and the results are drawn.

A.2 Numerical Investigation

A.2.1 Axisymmetric penetration model

The axisymmetric model presented in Fig. A.1 simulates the steady-state penetration of a standard 10 cm^2 (3.57 cm-diameter) cone into the soil column. Boundary conditions are imposed for a soil flowing into the bottom of the model upwards relative to a fixed cone. Mohr-Coulomb interface elements are applied at the interfaces between the cone and soil to represent an interface roughness factor of 0.60, which is the ratio of the interface friction angle to the soil friction angle. Stresses and Mohr-Coulomb material properties are initialized for a "wished-in-place" condition at the depth of interest. Initial stress conditions correspond to an at-rest K_o condition and a fully drained penetration is simulated. The cone penetration is velocity-controlled at the gridpoints across the top boundary. The right radial boundary is far enough from the cone to avoid any boundary effects and is thus defined as an infinite elastic boundary. The bottom boundary is sufficiently far from the cone's zone of influence to maintain the prescribed in-situ stress conditions. Large deformations are handled with a user-implemented Arbitrary Lagrangian-Eulerian (ALE) algorithm which performs grid rezoning and remapping during the cone penetration. Penetration is simulated until a steady state penetration resistance is achieved (Moug et al. 2019), which is approximately 25 cone diameters of penetration.

A.2.2 Input parameters and calibration

The application of bio-cementation treatment to sands, as well as the geologic-time scale process where sand is gradually cemented, induce changes in the stiffness and strength. While difficult to characterize in the field, coupling the simulated cone tip resistance in a Mohr-Coulomb type of material and established relationships can guide the selection of equivalent strength parameters for these challenging geomaterials. The Mohr-Coulomb constitutive model was selected because it defines a failure envelope with a cohesion intercept and a peak friction angle which can be representative of bio-cemented sands. More broadly, it is a simple model with few parameters and nicely describes a broad range of responses without unnecessary complexities. Based on numerous bench-scale and large-scale experiments on bio-cemented sands, a linear relationship between the "apparent" cohesion (c) and the change in shear wave velocity (ΔV_s) was developed to estimate the value of cohesion from the measured post-cementation in-situ V_s (Chapter 3).

$$\Delta V_s = 18.9\ c \tag{A.1}$$

where ΔV_s = the change in shear wave velocity in m/s and c = the "apparent" cohesion in kPa. Following an extensive literature review on bio-cemented sands (e.g., Nafisi et al. 2019, Nafisi et al. 2020, Wu et al. 2020) and using the above empirical relationship, the values for the input parameters in Table A.1 was defined.

Due to the large strains around the penetrating cone, the small-strain shear modulus (G_{max}) as an input model parameter does not reflect the complex deformations and strain softening in the plastic region near the cone tip which would result in an overestimation of the cone tip resistance (Teh and Houlsby 1991, Lu et al. 2004).

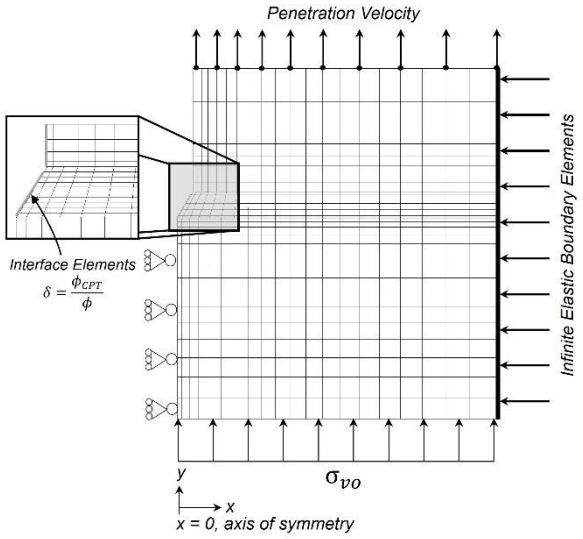

Figure A.1. Geometry and boundary conditions of the numerical cone penetration model (Moug 2017).

Table A.1. Variables for parametric study.

Variable	**Tested values**
Cohesion, c (kPa)	0, 10, 20
Friction angle, ϕ (degrees)	30, 35
Dilation angle, ψ (degrees)	0, 10
"Functional" shear modulus, G_{sec} (kPa)	Based on the relationship between ΔV_s and cohesion
Confining stress, $\sigma_{vo}^{'}$ (kPa)	35, 100

Therefore, a reduction factor is applied to G_{max} (where $G_{max} = \rho V_s^2$ and ρ is the density) to account for the shear modulus softening and a secant shear modulus (G_{sec}) is used, where $G_{sec} = G_{max}/F$ and $F = 0.15\,c + 3$ based on a calibration process and comparison of simulated cone penetration with experimental results (Chapter 3). The chosen initial V_s ($V_{s,ini}$) values normalize with respect to the varying confining stresses of 35 and 100 kPa, hence the results of these simulations are examined in absolute terms such as q_c instead of incremental terms (Δq_c).

The input to each set of simulations is summarized in Tables 2 and 3 for the confining stresses of 35 and 100 kPa, respectively.

Table A.2. Simulation input parameters for σ'_v = 35 kPa.

	Cohesion (kPa)		
	0	**10**	**20**
$V_{s,ini}$ (m/s)	150	150	150
ΔV_s (m/s)	0	189	378
Reduction factor *F*	3	4.5	6
G_{sec} (kPa)	12,750	43,149	78,262

Table A.3. Simulation input parameters for σ'_v = 100 kPa.

	Cohesion (kPa)		
	0	**10**	**20**
$V_{s,ini}$ (m/s)	200	200	200
ΔV_s (m/s)	0	189	378
Reduction factor *F*	3	4.5	6
G_{sec} (kPa)	22,667	56,814	93,783

A.3 Results

The focus of the subsequent analyses and illustrations is the cone tip resistance q_c. Open and closed symbols correspond to confining stresses of 35 and 100 kPa, respectively. Circle and square symbols correspond to friction angle of 30 and 35 degrees, respectively. Figure A.2a presents the variation of the absolute q_c with an increasing shear stiffness (proportional to V_s according to $G_{max} = \rho V_s^2$), friction angle, and confining stress at a dilation angle of 0º. Figure A.2b illustrates the change in q_c with the change in V_s due to the presence of a cohesion (Eq. A.1) for the given combinations of stress states and friction angles. Figure A.2c illustrates the effect of the confining

stress on q_c by normalizing it according to $Q_t = (q_t - \sigma_{vo})/\sigma'_{vo}$. Collectively, these figures confirm that: (1) the cone tip resistance increases considerably with the increase in the cementation level, (2) the change in q_c is due to the changes in cementation only, and (3) the "cemented" friction angle may have an effect on the increase in q_c but to a lesser extent than the shear stiffness.

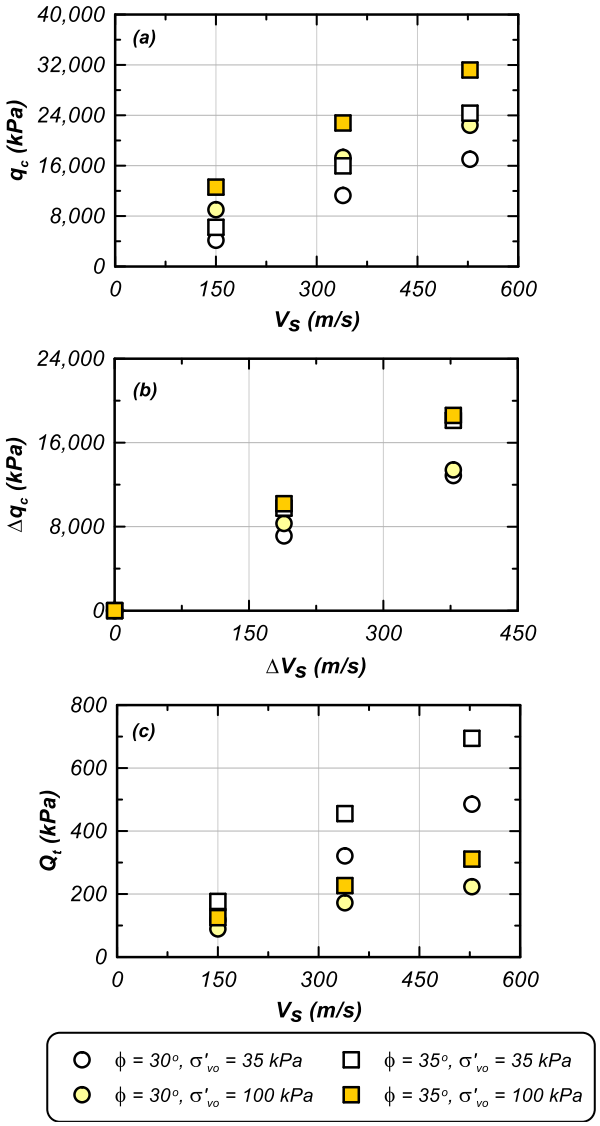

Figure A.2. (a) Variation of q_c as a function of V_s, (b) variation of Δq_c with varying ΔV_s, and (c) variation of normalized Q_t as a function of V_s, for varying ϕ of 30º and 35º and different confining stresses at ψ of 0º.

Figure A.3 presents the variation of the tip resistance as a function of the confining stress with varying strength parameters, cohesion from 0 to 20 kPa, and friction angle from 30 to 35 degrees. Circle and square symbols correspond to friction angles of 30 and 35 degrees, respectively, whereas the shading corresponds to increasing the cohesion from 0 to 20 kPa.

Similar to Fig. A.2, a positive trend exists between q_c and $\sigma_{vo}^{'}$ where the following observations are made: (1) for σ'_{vo} =35 kPa, q_c for c = 20 kPa is around 4 times the q_c for c = 0 kPa, whereas for a higher $\sigma_{vo}^{'}$= 100 kPa, this ratio decreases to 2.5 times regardless of the friction angle, (2) for c = 0 kPa, q_c for σ'_{vo}= 100 kPa is around twice the q_c for σ'_{vo}= 35 kPa, whereas for c = 20 kPa, this ratio decreases to 1.3 times regardless of the friction angle, and (3) for $\sigma_{vo}^{'}$= 35 kPa, q_c for ϕ = 35º is around 1.5 times q_c for ϕ = 30º whereas for σ'_{vo} =100 kPa this ratio slightly decreases to 1.4 times, regardless of the cohesion. These observations suggest that: (1) cohesion is the major contributor to the enhanced tip resistance, followed by the confining stress, and then followed by the friction angle, and (2) the effect of the cementation is more significant at low confining stress.

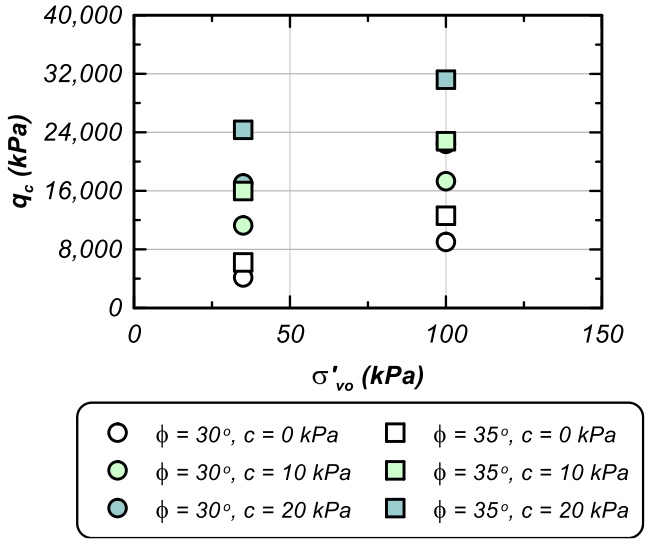

Figure A.3. Variation of q_c as a function of $\sigma_{vo}^{'}$ for varying ϕ and c at ψ of 0º.

Figure A.4 incorporates, in addition to the cohesion, friction angle and confining stress, the effect of the dilation angle ψ. Figs. A.4a and A.4b correspond to ϕ = 30º and 35º, respectively, and the diamond and triangle symbols correspond to a ψ of 0º and 10º, respectively. The results show that the increase in the dilation angle leads to a larger cone tip resistance, due to stronger dilation of the soil which in turn results in a higher resistance of the soil to shearing. The q_c with a ψ = 10º (a limit for bio-cemented sands suggested by the literature e.g., Wu et al. 2020) is 3 to 4 times higher relative to q_c with a ψ = 0º, depending on the strength parameters with this ratio increasing for a higher confining stress ($\sigma_{vo}^{'}$ of 100 kPa).

The current state of practice uses previously established charts for the interpretation of CPT data and classification of soils which include cemented sands. As the change in shear stiffness plays a major role in the behavior of bio-cemented sands and cemented sands in general, the small-strain shear modulus G_{max} and the stress-normalized cone tip resistance Q_t can be correlated to guide the soil behavior type and extend it to these cemented soils. Figure A.5a presents the simulation results for the different scenarios. In addition to the simulation results from this work, experimental data obtained from cones pushed in a bio-cemented specimen in a centrifuge model (Darby et al. 2019) are plotted. Several levels of cementation were established by the experimentalists targeting light, moderate, and heavy cementation levels. The datapoints from the cones pushed in treated sands plot reasonably within the region corresponding to soils with "ageing cementation", with few datapoints plotting close to the "uncemented" region due to their light level of cementation (Darby et al. 2019). Specimens with higher levels of cementation follow the trend discussed earlier. Moreover, Fig. A.5a shows that the simulation results for σ'_{vo}= 35 kPa fall within the range of the experimental data from Darby et al. (2019) with a similar confining stress of 35 kPa, hence validating the proposed approach.

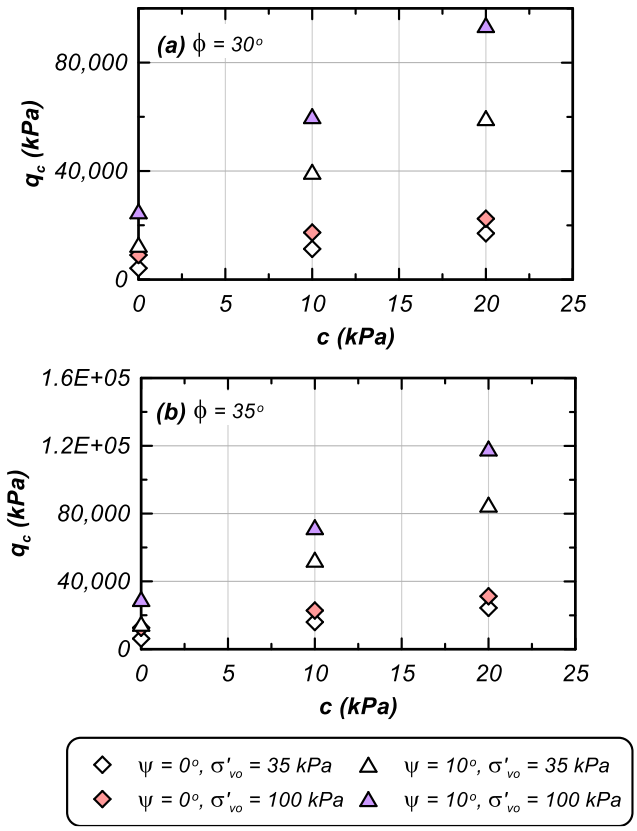

Figure A.4. Variation of q_c as a function of c for varying ψ and σ'_{vo} at, (a) ϕ of 30º, and (b) ϕ of 35º.

The CPT-based classification chart according to Q_t and G_o/q_t is reproduced in Fig. A.5b and the simulation and experimental results are overlaid. Figure A.5b shows a reasonable agreement between the expected soil behavior from the input parameters (i.e., uncemented sands with zero cohesion versus cemented sands with nonzero cohesion) and the suggested soil behavior from the chart. For example, the simulations with c = 0 kPa plot in the "sand" behavior type on the chart as expected for a cohesionless uncemented sand. Similarly, the simulations with c > 0 kPa plot in the region corresponding to soils with "ageing cementation" on the chart. Moreover, the aforementioned relative magnitude of Q_t and G_o/q_t between the cemented sands and the uncemented sand is also evident on the soil classification chart.

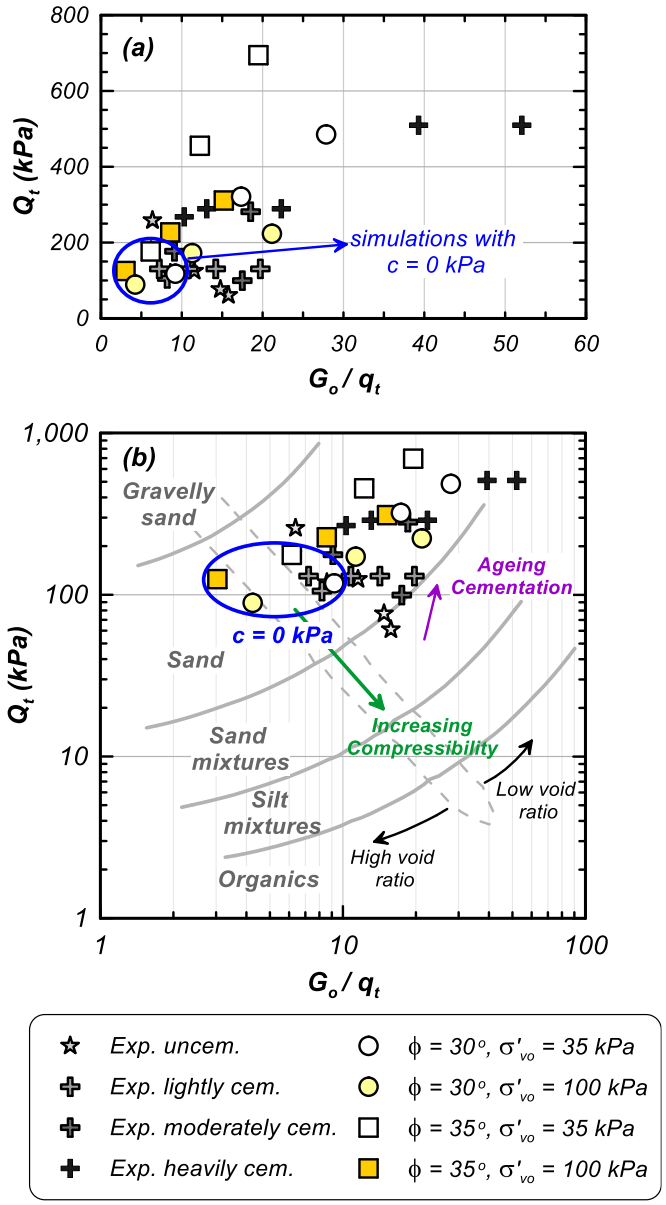

Figure A.5. Soil classification chart based on normalized cone resistance and small-strain shear modulus, reproduced from Lunne et al. (1997), and overlaid with simulation results from this work and experimental data from the centrifuge test from Darby et al. (2019).

A.4 Concluding remarks

The cone penetration test has been commonly used in soils to indicate the soil behavior type and to assess the soil's resistance in bearing capacity and liquefaction mitigation applications. Its use can be extended to bio-cemented or cemented sands. Some limitations are associated with pushing cones in cemented sands, such as the inability of the cone to detect light cementation (equivalent to calcite content less than 3%) and the destructive nature of the test to any pre-existing cementation in the soil. However, it is still a common and valuable test able to provide proxies of the expected soil behavior and its degree of cementation in the absence of more viable exploration methods.

In this paper, a parametric study on the input parameters to an axisymmetric cone penetration model for sands was presented in the context of its application to bio-cemented sands. The numerical model implemented the Mohr-Coulomb constitutive model which was used to estimate equivalent "cemented" strength parameters. Although the Mohr-Coulomb constitutive model prescribed constant strength parameters to strain-dependent soil conditions, the approximation with a "functional" shear modulus allows the model to reasonably predict the elastic-plastic behavior of bio-cemented soils in the failure zone near the cone tip. The input parameters varied in this paper are the cohesion, friction angle, dilation angle, and confining stress. The results were analyzed in terms of cone tip resistance, and the study confirmed that it increased with increasing the level of cementation, and suggested that the cohesion value is the main contributor to this improvement in the soil resistance. The dilation and friction angles also affect the soil's resistance but to a lesser extent. Simulation results were also compared to experimental data from CPTs pushed in bio-cemented sands and to previously established soil behavior type charts for "unusual" soils. The simulation results fell within the range of the experimental data and they both plotted in

the “ageing cementation” region of the chart. Hence the proposed framework appears reasonable to estimate the soil’s strength and overcome the challenges in sampling cemented sands.

Oftentimes, considerable effort is put into the selection of input parameters for numerical models. The above observations related to the effect of input parameters on the cone tip resistance are insightful for prioritizing the choice of input parameters and can be potentially used to guide parameter selection for numerical models, based on CPT data, to represent cemented materials in numerical simulations.

The ranges of input parameter values used in this study reflect the typical ranges found in the literature for lightly and moderately bio-cemented sands. The trends presented here may be cautiously extrapolated to reasonably higher strength parameters and confining stresses; however, the relative magnitudes may warrant further exploration.

In the developing field of bio-cemented sands, numerical models that are validated and calibrated against existing data can be leveraged to populate and synthesize data that are not yet available. While some approximations such as the estimation of the cohesion value and the reduced secant shear modulus are made herein, the numerical model is still a valuable tool to, in the first stage, study the sensitivity of the results to input parameters and, in the second stage, synthesize data needed to develop correlations between these various parameters. Chapter 3 extends this work to develop a correlation between the cone tip resistance and the cohesion in order to implement it in a plasticity constitutive model for bio-cemented sands.

Adding to the importance of the CPT in indicating the behavior of the present soil, it can and should be a preferred method for post-cementation verification in the field. The CPT can thus serve as a tool in the design of ground improvement methods and in the QA/QC of the final improvement, especially in the field of bio-cementation ground improvement techniques.

APPENDIX B

Validation of a bounding surface plasticity model against the experimental response of (bio-) cemented sands

Original publication:

El Kortbawi M., Ziotopoulou K., Gomez G.M., and Lee M. (2019). Validation of a bounding surface plasticity model against the experimental response of (bio-) cemented sands. Proceedings of ASCE GeoCongress 2019, Philadelphia, Pennsylvania, 24-27 March 2019.

Author's note: This companion paper serves as a preamble to the extension of the PM4Sand Version 3.2 model to inform the modifications needed for the model based on its current performance compared to experimental data on bio-cemented sands. This preliminary work preceded the final work presented in Chapter 4 of this Dissertation and is included in the appendix for completeness.

Abstract

Microbially-Induced Calcite Precipitation (MICP) has been increasingly investigated as a novel ground improvement technique for the mitigation of earthquake-induced soil liquefaction.

Experimental results including those from triaxial, direct simple shear, and small centrifuge tests have demonstrated the ability of MICP to increase the resistance of loose sands to liquefaction triggering and improve the post-triggering response of these materials when compared to similar untreated soils. Despite significant advances in the development of this technology for field-scale applications, currently no quantitative frameworks exist, which can accurately predict the behavior of cemented sands in the field. In this paper, we present an evaluation of the ability of an existing stress-ratio controlled, critical state compatible, bounding surface plasticity model (PM4Sand) to capture the response of (bio-) cemented sands. The results of this study will guide the reformulation of the existing constitutive model to capture experimentally observed soil behaviors.

B.1 Introduction

Geotechnical ground improvement methods can be used to improve the mechanical properties of soils for engineering applications including slope stability, seepage reduction, and mitigation of earthquake-induced liquefaction. Although effective, conventional techniques oftentimes result in significant environmental consequences resulting from the use of high mechanical energy and/or energy-intensive cementing agents. Recently, biologically-based alternative technologies have emerged (Mitchell and Santamarina 2005) as means to obtain similar improvements in soil engineering properties with reductions in energy, materials usage, and environmental impacts by leveraging natural biological and chemical processes. Microbially-Induced Calcite Precipitation (MICP), or bio-cementation, is one such technology that offers the potential for mitigation of earthquake-induced liquefaction through the bio-mediated precipitation of calcium carbonate on soil particle surfaces and contacts (e.g. Montoya et al. 2013; Xiao et al. 2018).

The MICP bio-cementation process is made possible by ureolytic microorganisms, which can hydrolyze provided urea to generate carbonate. When calcium is sufficiently available, the process can super-saturate soil solutions and initiate mineral precipitation. The resulting bio-cementation can bind soil particles together, coat particle surfaces, and reduce soil void space thus altering the overall engineering behavior of the soil (e.g. DeJong et al. 2006). Despite significant recent interest in the liquefaction behavior of MICP in laboratory experiments (Duraisamy and Airey 2012; Montoya et al. 2013; Simatupang and Okamura 2017; Xiao et al. 2018), significant gaps remain with respect to understanding the behavior of bio-cemented soils at the field-scale for practical engineering purposes. An improved understanding of the mechanical response of MICP-treated soils may not only aid in the advancement of this technology towards field-scale applications, but may also improve our understanding of the behavior of naturally-cemented geo-materials commonly encountered in the geotechnical subsurface resulting from other abiotic and bio-mediated mineral formational processes. It is suspected that such deposits may have engineering behaviors and cementation mineralogy similar to that observed for MICP-treated soils.

Despite the prevalence of natural cementation in aged soil deposits, the contribution of cementation to soil strength and stiffness is generally ignored due to challenges with respect to material characterization. The use of MICP as a method for preparing cemented materials in the lab may allow representative cemented materials to be further studied experimentally as well as the development of models that can capture cemented soil behaviors.

Herein, a review of experimental observations on the behavior of bio-cemented sands under monotonic and cyclic loading is presented. An overview of currently available constitutive models for sands is provided and their applicability is briefly discussed. Results of single element simulations of untreated and MICP-treated sand responses using PM4Sand (Boulanger and

Ziotopoulou 2017) are presented and discussed. The simulated responses (monotonic and cyclic) are compared to those obtained from monotonic and cyclic direct simple shear (DSS) tests (Zamani and Montoya 2017). Differences in shearing behavior following bio-cementation are identified and future improvements to the model are proposed.

B.2 Effect of bio-cementation on behavior of loose sands

B.2.1 Effect of bio-cementation on the peak and residual strength of sands

Past experiments on MICP-treated sands show an increase in peak and residual strengths depending on the level of cementation and confining pressure (e.g. Montoya and DeJong 2015). These shear strength increases can be attributed to both soil densification through precipitation of minerals solids and the formation of cohesive bonds from cementation. Scanning electron microscopy (SEM) images suggest that bio-cementation may not only result in the formation of cemented bonds at particle-particle contacts, but that it may also coat soil particle surfaces. As a result, soil pore spaces are filled and the initial void ratio can decrease significantly after cementation. Feng and Montoya (2015) performed drained triaxial compression tests on untreated and bio-cemented Ottawa 50-70 specimens at different initial relative densities (D_R), levels of cementation, and confining pressures, and observed increases in peak strength with increasing bio-cementation. Peak friction angles φ_{pk} were also found to increase with cementation and decrease with increased confining pressure. Increases in φ_{pk} were expected and likely resulted from both inter-particle bonding and increases in particle surface roughness. While the change in cohesion appeared to be negligible for lightly-cemented materials, it was more pronounced for moderately and heavily-cemented samples resulting in an enhanced tensile strength. Similar trends were observed for residual friction angles φ_r, wherein lightly-cemented values were not significantly

different to untreated sands, however, for moderately-cemented sands φ_r was considerably larger. This suggests that at higher cementation levels, a shift in critical state may result from the presence of sheared calcite solids and their effects on particle roughness, shape, and material gradation.

B.2.2 Effect of bio-cementation on small-strain properties of sands

Bio-cementation has been shown to increase soil matrix initial shear stiffness permitting the use of shear wave velocity (V_s) as a method to non-destructively monitor changes in soil cementation (e.g. Gomez et al. 2018). Past experiments show reliable increases in V_s values during MICP treatments resulting from precipitation of calcium carbonate at particle contacts (e.g. Montoya et al. 2013). During shearing, gradual reductions in stress-normalized V_{s1} values can be monitored to track the degradation of bio-cementation independent of effective stress changes. At large strains, the shear stiffness of bio-cemented sands can reduce dramatically and approach that of clean sand resulting from the breakage of particle bonding. Despite significant geophysical characterizations, the effect of bio-cementation on other small strain dynamic properties including damping ratio remains relatively unknown. These properties may be of primary importance for constitutive modeling of this material and may therefore merit further investigation.

B.2.3 Effect of bio-cementation on soil dilatancy

Bio-cementation has been shown to influence the volumetric tendencies of sands during undrained and drained shearing. For the same initial density, more pronounced increases in soil dilation can be observed for bio-cemented loose sands when compared to initially denser materials. While a traditional strain-hardening response can be observed for untreated loose sands, undrained triaxial compression tests on bio-cemented loose sands show a clear peak strength followed by strain-softening. The transition from strain-hardening to strain-softening becomes more pronounced as the level of cementation increases (e.g. Feng and Montoya 2015). This may result from increases

in soil density and the transition from a global to a localized shearing failure (shear band) with increased cementation (e.g., DeJong et al. 2017). During undrained shearing at large-strains, bio-cemented loose sands can develop negative excess pore pressures that are comparable or less than those observed for similar uncemented dense samples depending on the level of cementation.

B.2.4 Effect of bio-cementation on cyclic resistance

When subjected to seismic loading, bio-cemented sands can exhibit increased cyclic resistance relative to untreated loose sands resulting from both soil "densification" and increases in cohesive cementation of the soil matrix. These mechanisms have been observed in element tests (Xiao et al. 2018) as well as centrifuge model experiments (Montoya et al. 2013; Darby et al. 2018). Mechanistically, cementation can act to bond particles together, thus allowing for improved load transfer between particles and minimal particle rearrangement (shearing) at similar shear stress amplitudes. For the same intensity and duration of loading, soil particles in cemented specimens may exhibit delayed generation of excess pore pressures resulting from reductions in shear strain amplitudes and therefore limited mobilization of soil volumetric tendencies. Despite this, increases in time required for pore pressure dissipation may result from precipitation related decreases in soil hydraulic conductivity and should be considered to reliably predict the consequences of soil liquefaction. Although element tests have shown large reductions in soil shear stiffness and pore pressure induced reductions in effective stresses during cyclic loading, the number of cycles required to trigger liquefaction remains generally greater for bio-cemented soils when sufficient cementation is present. Observed failure envelopes for cyclic tests also indicate increased φ_{cv} following the presence of cementation.

B.3 Constitutive models for sands

Numerous constitutive models for sands have been developed over the years which incorporate specific aspects of sand behavior. Models that follow the framework of Critical State Soil Mechanics (CSSM) and account for the combined effects of void ratio and stress on sand behavior have been widely adopted. Still, few models exist which can incorporate the evolving micro-mechanical behaviors observed following the bio-cementation of sands. This section briefly mentions some of the available constitutive models for reconstituted and cemented sands, which may be of particular relevance to the modeling of bio-cemented materials.

B.3.1 Current constitutive models for sands (uncemented)

Constitutive models for sands include the work of Elgamal et al. (2003) (PDMY02) and Khosravifar et al. (2018) (PDMY03) who followed the framework of multi-surface plasticity, Byrne et al. (2004) who developed UBCSAND following classic plasticity theory and targeting the response of liquefiable sands, and Dafalias and Manzari (2004) who combined the effect of D_R and effective confining stress in one bounding surface plasticity model using the state parameter (Been and Jefferies 1985) and included the effect of fabric. Recent work by Boulanger and Ziotopoulou (2017) led to the plane-strain PM4Sand model. This work extended the work of Dafalias and Manzari (2004) to better capture engineering design relationships used to estimate stress-strain behaviors important for the prediction of liquefaction-induced ground deformations during earthquakes. The work presented herein uses PM4Sand as a baseline model due to its ability to capture the fundamental aspects of sand behavior and its formulation around parameters that are commonly obtained in the field.

B.3.2 Current models for lightly cemented sands

The geotechnical community has been long aware of the effect of cementation on the soil response and the challenges accompanying the modeling of cemented sands. There are various constitutive models which have considered the effect of cementation on the response of sands. While some models have succeeded in some parts, they have generally not captured the full behavior (i.e, the increase in strength as well as the degradation of cementation after shearing). Recent work by Nweke and Pestana (2017) resulted in the development of a model which has successfully incorporated key aspects of the response of MICP-treated sands. This work focused on identifying changes in shear strength and stiffness following the degradation of calcite bonds leading to empirical rules that were subsequently incorporated into the Nor-Sand model (Jefferies 1993) to ultimately develop a constitutive model for lightly cemented sands. Still, there is no complete framework that considers the effect of microstructure on all the aspects of the monotonic and cyclic response of bio-cemented sands, with the changes in cementation integrity during dynamic loading being the most challenging ones to constitutively capture. The work presented herein is part of the overarching goal of developing a new constitutive model for (bio-)cemented sands. Following the framework of PM4Sand (Boulanger and Ziotopoulou 2017) the objective is to enable the prediction of the response of (bio-)cemented sands during cyclic loading. During its development phase, this model will be formulated and validated against experimental data for bio-cemented soils, but ultimately it will be generalized to capture the behavior of multiple types of cemented materials (e.g., via chemical grouts, natural cementation, etc.). This paper focuses on evaluating the ability of PM4Sand to capture the behavior of bio-cemented soils by identifying critical shortcomings via comparisons of calibrated single element numerical simulations against

experimental data from the monotonic and cyclic direct simple shear testing of bio-cemented sands.

B.4 Single element calibrations for cemented sands using PM4Sand

B.4.1 PM4Sand as a baseline for the proposed model

The behavior of cemented sands is expected to build upon baseline behaviors observed for clean sands by incorporating the effects of cementation. As such, it is rational to build upon available advanced models developed for clean sands and subsequently incorporate the effects of cementation. The proposed constitutive model used for simulating bio-cemented sands is PM4Sand V3.1 (Boulanger and Ziotopoulou 2017) (Fig. B.1), a stress-ratio controlled, critical-state compatible, bounding-surface plasticity model. As a framework it offers a high versatility to allow for extending it to other materials. The model has 22 input parameters, from which only three are considered primary and are required as model input. These are the initial relative density (D_{Ro}), the shear modulus coefficient (G_0) used to define the elastic shear modulus, and the contraction rate parameter (h_{p0}) used for calibration of the undrained cyclic shear strength. The other 19 can be either left with their preset default values, that are generally functions of an index property, if no other information is available, or calibrated to the desired response based on the available lab data. The reader is referred to Boulanger and Ziotopoulou (2017) for a detailed discussion of the formulation of the model as well as its parameters.

B.4.2 Calibration process

Single-element simulations prescribing the conditions of an undrained monotonic and cyclic DSS were run in FLAC8 (Itasca 2016). The calibration aims at: (1) evaluating PM4Sand's ability to capture the response of bio-cemented sands with rational modifications of its parameters, and (2)

obtaining insights on which constitutive features may be revised. Zamani and Montoya (2017) performed a series of DSS tests on Nevada sand mixed at different percentages with silt. Out of those, only the undrained monotonic and cyclic DSS tests on Nevada sand with 0% silt are used. Four sets of calibrations are performed for the present study (all undrained): monotonic untreated (DSSm_U) and MICP-treated (DSSm_T), and cyclic untreated (DSSc_U) and MICP-treated (DSSc_T). Details on the treatment and the experimental testing procedure are provided in Zamani and Montoya (2017). Table B.1 summarizes the calibrated model parameters. The initial relative density D_{Ro}, the shear modulus coefficient G_0, and the contraction rate parameter h_{p0} are primary input parameters. Unless noted otherwise, secondary parameters of PM4Sand have retained their default values.

The calibration approach followed was to identify the behaviors of interest and vary the model parameters accordingly. Only parameters related to the stress-strain response were varied, while the remaining parameters were set to their default values (e.g., parameters controlling post-shaking reconsolidation, which is not of interest in these calibrations). Parameters were obtained using an iterative process by comparing the response from single-element undrained direct simple shear simulations to the experimental data. D_{Ro} was calculated based on the reported initial void ratio (about 0.7) and the minimum and maximum void ratios. The shear modulus G_0 controls the elastic stiffness and was estimated based on the reported shear wave velocity measurements. It was found however that it should be reduced to a sixth and an eight of the value corresponding to shear velocity measurements (V_{s_untr} = 164m/s and V_{s_tr} = 462m/s) respectively in order to better match the small strain response of the experiments. This is reasonable given that stiffness may be overestimated in lab specimens. The contraction rate parameter h_{p0} was obtained through an iterative process to match the experimental response, particularly in terms of the number of cycles

it takes to reach a certain triggering criterion. The critical state friction angle φ_{cv} was obtained from the literature for Nevada sand for the untreated specimen while for the treated specimen it was adjusted to match the experimental data.

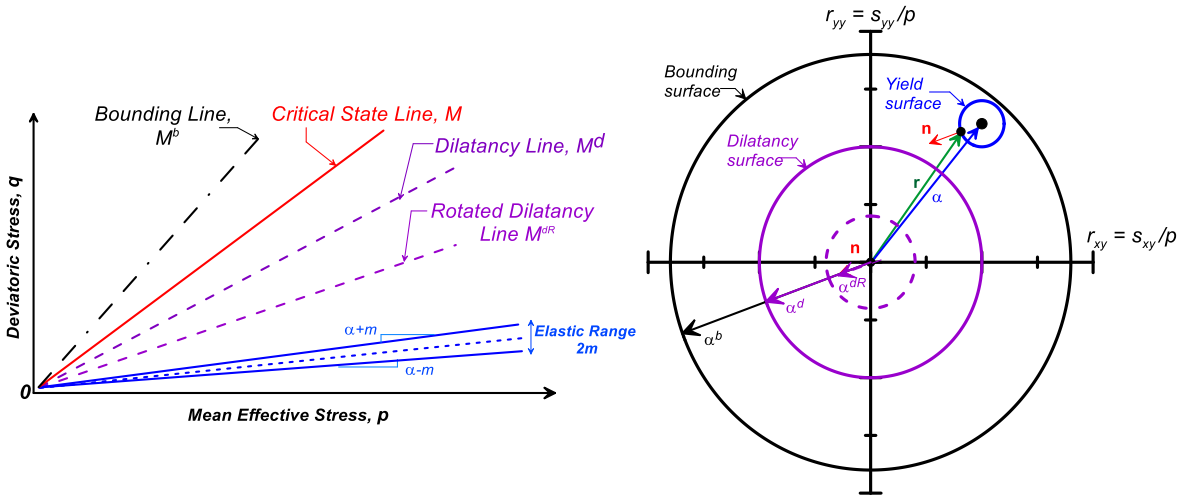

Figure B.1. Constitutive space of PM4Sand: yield, critical, dilatancy, and bounding lines in q-p space (left) and in r_{yy}-r_{xy} stress-ratio plane (right) (Boulanger and Ziotopoulou 2017).

n^b controls the slope of the bounding line and by extension the rate of strain accumulation in the post-triggering phase of loading. z_{max} controls the maximum fabric accumulated by the model and was adjusted to control the shape of the loops. G_{degr} controls the rate of the elastic modulus degradation, while p_{min} and p_{min2} control the maximum excess pore pressure ratio in cyclic loading. *R* (along with Q) defines the critical state according to Bolton's (1986) relationship and was adjusted in order to obtain the undrained shear strength under monotonic loading following the procedure described in Boulanger and Ziotopoulou (2018).

Table B.1. Primary input parameters for the four calibrations

Parameters		**DSSm_U**	**DSSm_T**	**DSSc_U**	**DSSc_T**
Primary	D_{Ro}	0.49	0.47	0.49	0.49
	G_0	144.1	855.6	216.1	1715
	h_{p0}	0.4	5.0	0.7	0.4
Secondary	e_{min}	0.511	0.511	0.511	0.511
	e_{max}	0.887	0.887	0.887	0.887
	φ_{cv}	30	40	30	40
	n^b	default	default	5.0	0.2
	z_{max}	default	default	0.5	default
	G_{degr}	default	default	4.0	default
	p_{min}, p_{min2}	default	default	2.5 kPa / 10 kPa	6 kPa / 10 kPa
	R	3.7	2.9	default	default

The results from this first set of calibration exercises are illustrated in Figs. B.2Figure B.*1* and B.3 for monotonic and cyclic loading respectively. Overall, the monotonic and cyclic responses of untreated specimens are captured reasonably. Secondary parameters were activated in order to better capture critical state, small strain response, and contraction rate, respectively. The peak strength is not captured without changing more secondary parameters but this was considered unnecessary at this stage. Figure B.2a also shows there is some reasonable agreement between the large strain range of the simulated and the experimental response for the treated samples. The discrepancy between the reported G_o and the calibrated G_o is not surprising for two reasons: (i)

elastic stiffness of treated samples is affected by cementation and the model does not incorporate a mechanism to capture that, and (ii) stress-strain response measured in DSS tests is known to underestimate small strain stiffness due to various limitations with standard testing equipment. It also seems like the critical state is not captured properly for the treated specimen (Fig. B.2b) even after changing the critical state friction angle. Last but not least, there is some discrepancy in the strain-hardening response between experiment and simulation (Fig. B.2b) and this hints at the inability of the model to properly capture the effects of cementation in that stage of loading.

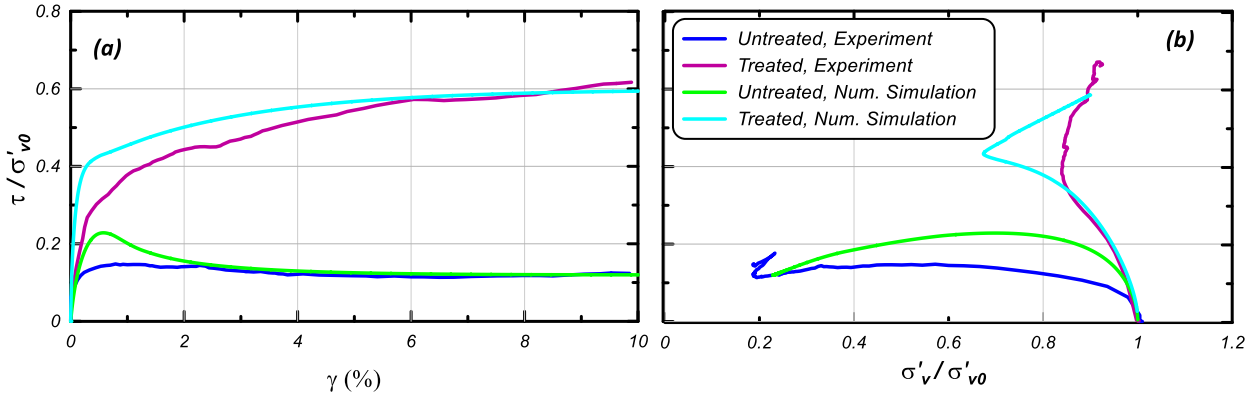

Figure B.1. Comparison of DSS monotonic response between simulations and experiments for untreated and treated samples: (a) stress-strain responses, and (b) stress paths.

Figures B.3 and B.4 illustrate comparisons of DSS cyclic responses between single element simulations and experimental data for untreated and treated samples respectively. The untreated and treated specimens were tested under cyclic stress ratios CSR=0.125 and CSR=0.3, respectively. Looking at the experimental data between the untreated and treated specimens, it can be seen that the major differences in the behavior correspond to the number of cycles to reach the 3% criterion for liquefaction and to the strain accumulation. The mentioned behaviors are controlled by h_{p0} and n^b, respectively. Thus, h_{p0} was changed to reproduce the number of cycles

seen in the experiment and n^b was increased to account for the faster rate of dilation. Extra secondary parameters were activated (p_{min}, $p_{min2,}$ G_{degr}) in order to better match the stress-strain loop and stress path experimental responses of Figs. B.3a and B.3b respectively, particularly with regards to the shape and size of the loops and the limited excess pore pressure ratio of ~85%.

For the untreated specimen (Figs. B.3a and B.3b), the simulation reasonably captures the behavior observed in the experiment with h_{po} iteratively adjusted to capture the desired cyclic resistance (criterion set at same number of cycles to 3% shear strain). For the treated specimen (Fig. B.4), the responses are –as expected– not comparable. Discrepancies are observed in the shape and size of the stress-strain loops and the implied damping ratio as well as the contractiveness in stress path terms. It can be noticed however (Fig. B.4a) that the number of cycles can however be captured. The model is challenged in capturing the change in the shear modulus upon initiation of degradation of cementation. Figure B.4b suggests that the degradation of the cementation and thus the generation of pore pressure is gradual as opposed to an immediate loss of strength shown by the model. Furthermore, it is worth noting that the steepness of the failure envelope from the experiment is different from the one from the model. This suggests that the model (formulated for clean sands) and the bio-cemented material have different critical states.

Overall, the baseline constitutive model PM4Sand has enough versatility to accommodate some of the behaviors observed in the experimental program by Zamani and Montoya (2017). Its formulation needs however to be revisited in order to better approximate the fundamental mechanisms that cementation adds to the response of clean sands to monotonic and cyclic loading. In particular, the formulation needs to be revisited in order to more globally capture the observed individual aspects of the response rather than relying on a case-by-case calibration.

Based on the observations from the calibrations illustrated in Figs. B.2, B.3, and B.4 the following major changes to the current PM4Sand are envisioned:

1) adding an apparent cohesion to account for the effects cementation during the initial stages of loading;
2) shifting the critical state line from its original position to better account for the effects of broken cementation on the final material;
3) accounting for the degradation of cementation via the shear and/or plastic modulus and potentially revisiting the hardening rule of the model.

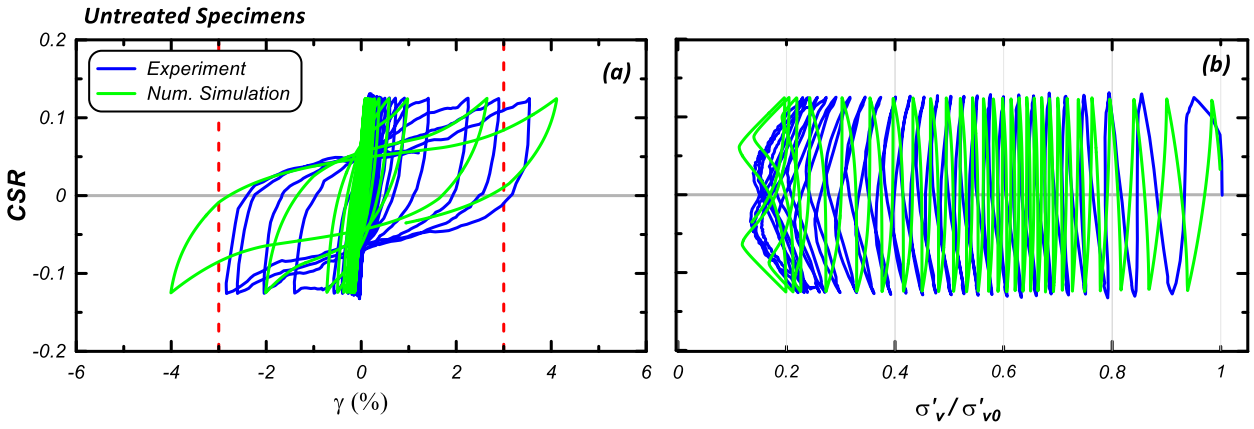

Figure B.3. Comparison of DSS cyclic response between simulations and experiments for untreated samples cyclically loaded (CSR = 0.125) under σ'_{vo}=50 kPa: (a) stress-strain responses, and (b) stress paths.

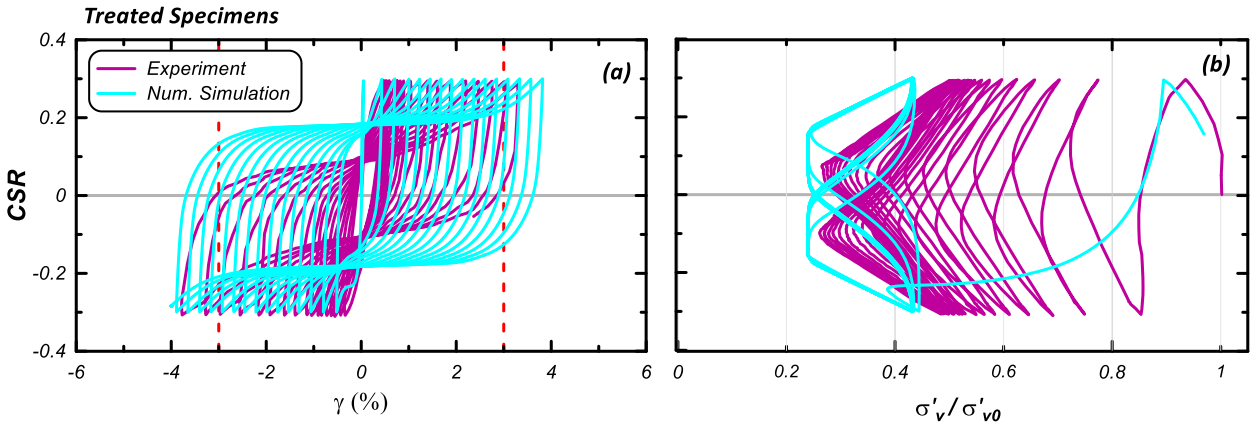

Figure B.4. Comparison of DSS cyclic response between simulations and experiments for treated samples cyclically loaded (CSR = 0.3): (a) stress-strain responses, and (b) stress paths.

B.5 Concluding remarks

A brief review of experimental results demonstrating the effect of (bio-)cementation on the engineering behavior of sand was provided. Next, an overview of constitutive models which may be of primary relevance to future modeling of bio-cemented materials was presented. Finally, a calibration study was performed to evaluate the ability of PM4Sand to capture the behavior of cemented sands during cyclic loading and identify critical shortcomings in our ability to predict the behavior of these challenging geo-materials. A new constitutive model based on the formulation of PM4Sand (Boulanger and Ziotopoulou 2017) is proposed to enable prediction of the response of cemented sands during monotonic and cyclic loading. This model may have important implications for the prediction of the shearing response of sands when natural or artificial cementation is present. Based on this study, the following conclusions are highlighted:

1) Previous laboratory experiments and physical modeling has demonstrated the ability of bio-cementation to significantly improve the monotonic and cyclic response of sands through increases in shear stiffness, shear strength, and cyclic resistance to liquefaction, while

minimizing soil deformations. While a wealth of laboratory data exists for clean sands, MICP, which is a relatively recent ground improvement technology, lacks the body of past experimentation needed to fully understand material behaviors. Multiple complex mechanisms occurring simultaneously during shearing of bio-cemented materials suggest the need for further advancement in the characterization of this material.

2) Despite significant efforts to capture the response of uncemented and cemented soils, currently there exists no constitutive models capable of predicting the cyclic response of cemented sands. In order to reliably predict the behavior of cemented sands in field-scale geotechnical systems, a constitutive model that can capture cemented sand behavior is needed. This model may improve the material efficiency and performance of both bio-cementation and other cementitious ground improvement methods and significantly advance the use of MICP for practical field-scale applications.
3) An initial calibration exercise using PM4Sand to match the response of untreated sands showed reasonable agreement between observed experimental responses and results obtained from the numerical model. When attempting to capture the behavior of bio-cemented sand specimens using the PM4Sand framework, reasonable model parameters were used which honored laboratory test data. The results of this exercise suggest that simple modifications of model parameters may not be sufficient to globally capture key features of the bio-cemented sand response. A revised constitutive framework is likely required to reasonably capture the behavior of cemented sand materials during monotonic and cyclic loading.

BIBLIOGRAPHY

Abdulla, A. A., and Kiousis, P. D. (1997). Behavior of cemented sands—I.Testing. *International Journal for Numerical and Analytical Methods in Geomechanics*, 21(8):533-547.

Acar, Y. B., and El-Tahir, E. T. A. (1986). Low strain dynamic properties of artificially cemented sand. *J. Geotechnical Engineering*, 112(11):1001-1015.

Ahmed, F., Montoya, B. M., and Gabr, M. A. (2022). Sensitivity analyses of hypoplastic model parameters to simulate the stress-strain behavior of MICP-treated sands. In *Proceedings of GeoCongress 2022*, Charlotte, North Carolina.

Airey, D. W. (1993). Triaxial testing of naturally cemented carbonate soil. *J. Geotechnical Engineering*, 119(9):1379-1398.

Almajed, A. A. (2017). Enzyme-induced carbonate precipitation (EICP) for soil improvement. *PhD dissertation*, Arizona State University, Tempe, AZ, USA.

Alonso, E. E., Gens, A., and Josa, A. (1990). A constitutive model for partially saturated soils. *Géotechnique*, 40(3):405-430.

Amoly, R. S., Ishihara, K., and Bilsel, H. (2015). Relations between liquefaction resistance and shear wave velocity as affected by aging of sand deposits. *J. Seismological Earthquake Engineering*, 17(1):19–30.

Andrus, R. D., Hayati, H., and Mohanan, N. P. (2009). Correcting liquefaction resistance for aged sands using measured to estimated velocity ratio. *J. Geotechnical and Geoenvironmental Engineering*, 135(6), 735–744.

Andrus, R. D., and Stokoe, K. H. (2000). Liquefaction resistance of soils from shear-wave velocity. *J. Geotechnical and Geoenvironmental Engineering*, *126*(11):1015–1025.

Arango, I., Lewis, M. R., and Kramer, C. (2000). Updated liquefaction potential analysis eliminates foundation retrofitting of two critical structures. *Soil Dynamics and Earthquake Engineering*, 20(1-4):17–25.

Arroyo, M., Amaral, M. F., Romero, E., and Viana da Fonseca, A. (2013). Isotropic yielding of un- saturated cemented silty sand. *Canadian Geotechnical J.*, 50 (8): 807–819.

Arroyo, M., Ciantia, M., Castellanza, R., Gens, A., and Nova, R. (2012). Simulation of cement-improved clay structures with a bonded elasto-plastic model: a practical approach. *Computers and Geotechnics*, 45:140-150.

Asaoka, A., Noda, T., Yamada, E., Kaneda, K., and Nakano, M. (2002). An elasto-plastic description of two distinct volume change mechanisms of soils. *Soils and Foundations*, 42(5):47-57.

Asghari, E., Toll, D. G., and Haeri, S. M. (2003). Triaxial behaviour of a cemented gravely sand, Tehran alluvium. *Geotechnical and Geological Engineering*, 21(1):1-28.

Bachus, R. C., Clough, G. W., Sitar, N., Shafii-Rad, N., Crosby, J., and Kaboli, P. (1981). Behavior of weakly cemented soil slopes under static and seismic loading conditions. Volume II, USGS Report No. 51.

Baig, S., Picornell, M., and Nazarian, S. (1997). Low strain shear moduli of cemented sands. *J. Geotechnical and Geoenvironmental Engineering*, 123(6):540–545.

Bauer, E. (1996). Calibration of a comprehensive hypoplastic model for granular materials. *Soils and Foundations*, 36(1):13-26.

Baxter, C. D. P., and Mitchell, J. K. (2004). Experimental study on the aging of sands. *J. Geotechnical and Geoenvironmental Engineering*, 130:1051-1062.

Beaty, M. H., and Byrne, P. M. (2011). UBCSAND constitutive model:version 904aR. Documentation report: UBCSAND constitutive model on Itasca UDM website.

Been, K., and Jefferies, M.G. (1985). A state parameter for sands. *Géotechnique*, 35(2):99-112.

Biryaltseva, T., Lunne, T., Kreiter, S., and Morz, T. (2016). Estimation of shear wave velocity based on SPT profile data. In A.-M. & K. Lehane (Ed.), Geotechnical and Geophysical Site Characterization 5 (pp. 389–394).

Bolton, M. D. (1986). The strength and dilatancy of sands. *Géotechnique*, 36(1):65-78.

Boulanger, R. W. (2003). Relating Kα to relative state parameter index. *J. Geotechnical and Geoenvironmental Engineering*, 129(8): 770–773.

Boulanger, R. W., and Idriss, I. M. (2014). CPT and SPT based liquefaction triggering procedures. Report No. UCD/CGM-14/01, University of California, Davis.

Boulanger, R. W., and Ziotopoulou, K. (2017). PM4Sand (version 3.1): A sand plasticity model for earthquake engineering applications.

Boulanger, R. W., and Ziotopoulou, K. (2018). On NDA practices for evaluating liquefaction effects. In *Proceedings of Geot Earthq Eng and Soil Dyn V (GEESDV)*, June 10 – 13, 2018, Austin, Texas.

Boulanger, R. W., and Ziotopoulou, K. (2022). PM4Sand (version 3.2): A sand plasticity model for earthquake engineering applications.

Bruno, A. W., Gallipoli, D., Rouainia, M., and Lloret-Cabot, M. (2020). A bounding surface mechanical model for unsaturated cemented soils under isotropic stresses. *Computers and Geotechnics*, 125:103673.

Burbank, M., Weaver, T., Lewis, R., Williams, T., Williams, B., and Crawford, R. (2013). Geotechnical tests of sands following bioinduced calcite precipitation catalysed by indigenous bacteria. *J. Geotechnical and Geoenvironmental Engineering*, 139(6):928-936.

Burdalski, R. J., and Gomez, M. G. (2020). Investigating the effect of microbial activity and chemical concentrations on the mineralogy and morphology of ureolytic bio-cementation. In *Proceedings of GeoCongress 2020*, Minneapolis, MN.

Burdalski, R. J. (2020). Investigating the effect of biological and chemical factors on the reaction kinetics and mineralogy of ureolytic bio-cementation. *Master's thesis*, University of Washington, Seattle, WA, USA.

Bwambale, B., Andrus, R. D., and Cubrinovski, M. (2017). Influence of age on liquefaction resistance of Holocene alluvial and marine soils in Christchurch and Kaiapoi, New Zealand. In *Proceedings of the 3rd International Conference on Performance-based Design in Earthquake Geotechnical Engineering* (PBD-III), July 16-19, Vancouver, Canada.

Bwambale, B., and Andrus, R. (2019). State of the art in the assessment of aging effects on soil liquefaction. *Soil Dynamics and Earthquake Engineering*, 125:105658.

Byrne, P. M., Park, S., Beaty, M., Sharp, M., Gonzalez, L., and Abdoun, T. (2004). Numerical modeling of liquefaction and comparison with centrifuge tests. *Canadian Geotechnical Journal*, 41:193–211.

Cabalar, A. F., Karabash, Z., and Erkmen, O. (2016). Stiffness of a biocemented sand at small strains. *European Journal of Environmental and Civil Engineering*.

Camacho-Padron, B. I. (2006). Effect of particle cementation on the stiffness of uniform sand as measured with stress wave velocities. *PhD dissertation*, University of Texas, Austin, TX, USA.

Carey, T. J., Chiaradonna, A., Love, N. C., Wilson, D. W., Ziotopoulou, K., Martinez, A., and Dejong, J. T. (2022). Effect of soil gradation on embankment response during liquefaction: a centrifuge testing program. *Soil Dynamics and Earthquake Engineering*, 157:107221.

Carey, T. J., Gavras, A., and Kutter, B. L. (2020). Comparison of LEAP-UCD-2017 CPT results. In Z. M. Kutter B., Manzari M. (Ed.), Model Tests and Numerical Simulations of Liquefaction and Lateral Spreading. Springer, Cham.

Carey, T. J., Stone, N., and Kutter, B. L. (2020). Grain size analysis and maximum and minimum dry density testing of Ottawa F-65 sand for LEAP-UCD-2017. In Z. M. Kutter B., Manzari M. (Ed.), Model Tests and Numerical Simulations of Liquefaction and Lateral Spreading. Springer, Cham.

Castro, G., and Poulous, S. J. (1977). Factors affecting liquefaction and cyclic mobility. *J. of the Geotechnical Engineering Division*, 103(6):501-516.

Cheng, L., Cord-Ruwisch, R., and Shahin, M. A. (2013). Cementation of sand soil by microbially induced calcite precipitation at various degrees of saturation. *Canadian Geotechnical J.*, 50(1):81–90.

Chong, S. H. (2019). Development of constitutive model for simulation of cemented soil. *Geotechnical and Geological Engineering.*

Chou, C., Seagren, E. A., Aydilek, A. H., and Lai, M. (2011). Biocalcification of sand through ureolysis. *J. Geotechnical and Geoenvironmental Engineering*, 137(12):1179-1189.

Chiaro, G., Koseki, J., and Sato, T. (2012). Effects of initial static shear on liquefaction and large deformation properties of loose saturated Toyoura sand in undrained cyclic torsional shear tests. *Soils and Foundations*, 52(3): 498–510.

Ciantia, M. O., Castellanza, R., and di Prisco, C. (2015). Experimental study on the water-induced weakening of calcarenites. *Rock Mechanics and Rock Engineering*, 48:441-461.

Ciantia, M. O., and di Prisco, C. (2016). Extension of plasticity theory to debonding, grain dissolution, and chemical damage of calcarenites. *International Journal for Numerical and Analytical Methods in Geomechanics*, 40:315-343.

Clough, G. W., Sitar, N., Bachus, R. C., and Rad, N. S. (1981). Cemented sands under static loading. *J. Geotechnical Engineering Division*, 107(6):799–817.

Clough, G. W., Iwabuchi, J., Shafii Rad, N., and Kuppusamy, T. (1989). Influence of cementation on liquefaction of sands. *J. Geotechnical Engineering*, 115(8):1102–1117.

Collins, B. D., and Sitar, N. (2009). Geotechnical properties of cemented sands in steep slopes. *J. Geotechnical and Geoenvironmental Engineering*, 135(10):1359-1366.

Coop, M. R., and Atkinson, J. H. (1993). The mechanics of cemented carbonate sands. *Géotechnique*, 43(1):53-67.

Cubrinovski, M., Rhodes, A., Ntritsos, N., and Van Ballegooy, S. (2019). System response of liquefiable deposits. *Soil Dynamics and Earthquake Engineering*, 124:212-229.

Cuccovillo, T., and Coop, M. R. (1997). Yielding and pre-failure behavior of structured sands. *Géotechnique*, 47(3):491-508.

Cuccovillo, T., and Coop, M. R. (1999). On the mechanics of structured sands. *Géotechnique*, 49(6):741-760.

Cui, M., Zheng, J., Zhang, R., Lai, H., and Zhang, J. (2017). Influence of cementation level on the strength behavior of bio-cemented sand. *Acta Geotechnica*, 12: 971-986.

Dafalias, Y. F., and Manzari, M. T. (2004). Simple plasticity sand model accounting for fabric change effects. *J. Engineering Mechanics*, 130(6): 622–634.

Darby, K. M., Hernandez, G. L., DeJong, J. T., Boulanger, R. W., Gomez, M. G., and Wilson, D. W. (2019). Centrifuge model testing of liquefaction mitigation via microbially induced calcite precipitation. *J. Geotechnical and Geoenvironmental Engineering*, 145(10):04019084.

Darby, K.M., Hernandez, G.L., Gomez, M.G., DeJong, J.T. (2018). Centrifuge Model Testing of Liquefaction Mitigation via Microbially Induced Calcite Precipitation. *GEESDV*, 127-137).

DeJong, J. T., Fritzges, M. B., and Nüsslein, K. (2006). Microbially induced cementation to control sand response to undrained shear. *J. Geotechnical and Geoenvironmental Engineering*, 132(11):1381-1392.

DeJong, J. T., Gomez, M. G., San Pablo, A. C. M., Graddy, C. M. R., Nelson, D. C., Lee, M., Ziotopoulou, K., El Kortbawi, M., Montoya, B., and Kwon, T. (2022). State of the art: MICP soil improvement and its application to liquefaction hazard mitigation. In *Proceedings of the 20th International Conference on Soil Mechanics and Geotechnical Engineering*, Sydney, Australia, 1-105.

DeJong, J. T., Mortensen, M. B., Martinez, B. C., and Nelson, D. C. (2010). Biomediated soil improvement. *Ecological Engineering*, 36(2):197–210.

DeJong, J. T., Soga, K., Kavazanjian, E., Burns, S., van Paassen, L. A., Al Qabany, A., Aydilek, A., Bang, S. S., Burbank, M., Caslake, L. F., Chen, C. Y., Cheng, X., Chu, J., Ciurli, S., Esnault-Filet, A., Fauriel, S., Hamdan, N., Hata, T., Inagaki, Y., Jefferis, S., Kuo, M., Laloui, L., Larrahondo, J., Manning, D. A. C., Martinez, B., Montoya, B. M., Nelson, D. C., Palomino, A., Renforth, P., Santamarina, J. C., Seagren, E. A., Tanyu, B., Tsesarsky, M., and Weaver, T. (2013). Biogeochemical processes and geotechnical applications: progress, opportunities and challenges. *Géotechnique*, 63(4):287-301.

DeJong, J. T., Martinez, B. C., Ginn, T. R., Hunt, C., Major, D., and Tanyu, B. (2014). Development of a scaled repeated five-spot treatment model for examining microbial induced calcite precipitation feasibility in field applications. *Geotechnical Testing Journal*, 37(3):1–12.

DeJong, J. T., Gomez, M. G., Waller, J. T., and Viggiani, G. (2017). Influence of bio-cementation on the shearing behavior of sand using X-Ray computed tomography. In *Proceedings of Geotech. Frontiers*, 871-880.

Dong, Y., and Fatahi, B. (2020). Discrete element simulation of cavity expansion in lightly cemented sands considering cementation degradation. *Computers and Geotechnics*, 124:103628.

Dupas, J. M., and Pecker, A. (1979). Static and dynamic properties of sand-cement. *J. Geotechnical Engineering Division*, 105(3):419–436.

Duraisamy, Y., and Airey, D. W. (2012). Strength and stiffness of bio-cemented liquefiable sand soil. In *Proceedings of International Conference on Ground Improvement and Ground Control*, University of Wollongong, Australia.

El Kortbawi, M., Ziotopoulou, K., and Boulanger, R.W. (2022). PM4SandC (version 1): A bio-cemented sand plasticity model for earthquake engineering applications. Report No. UCD/CGM-22/05, University of California, Davis.

Elgamal, A., Yang, Z., Parra, E., and Ragheb, A. (2003). Modeling of cyclic mobility in saturated cohesionless soils. *International Journal of Plasticity*, 19:883–905.

Eslaamizaad, S., and Robertson, P. K. (1996). Seismic cone penetration test to identify cemented sands. In *Proceedings of the 49th Canadian Geotechnical Conference*, 352–360.

Eslaamizaad, S., and Robertson, P. K. (1997). Evaluation of settlement of footings on sand from seismic in-situ tests. In *Proceedings of the 50th Canadian Geotechnical Conference*, Surrey, BC, Canada, 755–764.

Esnault Filet, A., Gutjahr, I., Mosser, J., Sapin, L., and Ibrahim, K. (2016). A novel grouting process for the reinforcement of low permeability soils with the use of biocementation by Biocalcis. In the *Proceedings of 19th Southeast Asian Geotechnical Conference and 2nd AGSSEA Conference.*

Evans, T. M., Khoubani, A., and Montoya, B. M. (2015). Simulating mechanical response in bio-cemented sands. *Computer Methods and Recent Advances in Geomechanics*, 1569–1574.

Fauriel, S. (2012). Multiphysical modelling of soils with a focus on microbially induced calcite precipitation. *PhD dissertation*, Ecole Polytechnique Fédérale de Lausanne, Switzerland.

Fauriel, S., and Laloui, L. (2012). A bio-chemo-hydro-mechanical model for microbially induced calcite precipitation in soils. *Computers and Geotechnics*, 46:104–120.

Feng, K. (2015). Constitutive response of microbial induced calcite precipitation cemented sands. *PhD dissertation*, North Carolina State University, USA.

Feng, K., and Montoya, B. M. (2015). Influence of confinement and cementation level on the behavior of microbial induced calcite precipitated sands under monotonic loading. *J. Geotechnical and Geoenvironmental Engineering*, 142(1):1-9.

Feng, K., and Montoya, B. M. (2017). Quantifying level of microbial-induced cementation for cyclically loaded sand. *J. Geotechnical and Geoenvironmental Engineering*, 06017005.

Feng, K., Montoya, B. M., and Evans, T. M. (2017). Discrete element method simulation of biocemented sands. *Computers and Geotechnics*, 85:139-150.

Fernandez, A. L., and Santamarina, J. C. (2001). Effect of cementation on the small-strain parameters of sands. *Canadian Geotechnical J.*, 38(1):191-199.

Ferris, F. G., Stehmeier, L. G., Kantzas, A., and Mourits, F. M. (1997). Bacteriogenic mineral plugging. *J. Canadian Petroleum Technology*, 36(9).

Frydman, S., Hendron, D., Horn, H., Steinbach, J., Baker, R., and Shaal, B. (1980). Liquefaction study of cemented sand. *J. Geotechnical Engineering Division*, 106(3):275–297.

Fu, Z., Chen, S., and Han, H. (2020). Large-scale triaxial experiments on the static and dynamic behavior of an artificially cemented gravel material. *European Journal of Environmental and Civil Engineering*.

Fu, Z., Chen, S., Zhong, Q., and Ji, E. (2022). A damage hypoplasticity constitutive model for cemented sand and gravel materials. *Acta Geotechnica*, 17:1–18.

Fuentes, W. (2018). ISA-hypoplasticity (cyclic).

Fujita, Y., Ferris, F. G., Lawson, R. D., Colwell, F. S., and Smith, R. W. (2000). Subscribed content calcium carbonate precipitation by ureolytic subsurface bacteria. *Geomicrobiology Journal*, 17(4):305-318.

Fujita, Y., Redden, G. D., Ingram, J. C., Cortez, M. M., Ferris, F. G., and Smith, R. W. (2004). Strontium incorporation into calcite generated by bacterial ureolysis. *Geochimica et Cosmochimica Acta*, 68(15):3261-3270.

Gai, X., and Sánchez, M. (2018) An elastoplastic mechanical constitutive model for microbially mediated cemented soils. *Acta Geotechnica*.

Gajo, A., Cecinato, F., and Hueckel, T. (2015). A micro-scale inspired chemo-mechanical model of bonded geomaterials. *International Journal of Rock Mechanics & Mining Sciences*, 80:425–438.

Gajo, A., Cecinato, F., and Hueckel, T. (2019). Chemo-mechanical modelling of artificially and naturally bonded soils. *Geomechanics for Energy and the Environment*, 18:13-29.

Gallipoli, D., and Bruno, A. W. (2017). A bounding surface compression model with a unified virgin line for saturated and unsaturated soils. *Géotechnique*, 67(8): 703–712.

Gao, Z. W., Zhao, J. D., and Yao, Y. P. (2010). A generalized anisotropic failure criterion for geomaterials. *International Journal of Solids and Structures*, 47:3166–3185.

Gao, Z., and Zhao, J. (2012). Constitutive modeling of artificially cemented sand by considering fabric anisotropy. *Computers and Geotechnics*, 41:57–69.

Gens, A., and Nova, R. (1993). Conceptual bases for a constitutive model for bonded soils and weak rocks. In *proceedings of Geotech. Eng. of Hard Soils-Soft Rocks*, Athens, Greece, 485-494.

Gomez, M. G., and DeJong, J. T. (2017). Engineering properties of bio-cementation improved sandy soils. In *proceedings of Grouting 2017*.

Gomez, M. G., DeJong, J. T., and Anderson, C. M. (2018). Effect of bio-cementation on geophysical and cone penetration measurements in sands. *Canadian Geotechnical J.*, 55:1632-1646.

Gomez, M. G., Anderson, C. M., Graddy, C. M. R., DeJong, J. T., Nelson, D. C., and Ginn, T. R. (2017). Large-scale comparison of bioaugmentation and biostimulation approaches for biocementation of sands. *J. Geotechnical and Geoenvironmental Engineering*, 143(5):04016124.

Gudehus, G. (1996). A comprehensive constitutive equation for granular materials. *Soils and Foundations*, 36(1):1-12.

Haeri, S. M., Hosseini, S. M., Toll, D. G., and Yasrebi, S. S. (2005). The behaviour of an artificially cemented sandy gravel. *J. Geotechnical and Geoenvironmental Engineering*, 23(5):537-560.

Hall, C., Kavazanjian, E., Van Paassen, L., Kamalzare, S., and Parmantier, D. (2022). Techno-economic assessment of liquefaction mitigation by microbially induced desaturation. In *proceedings of 2021/2022 ASCE Lifelines Conference*.

Hamdan, N., and Kavazanjian, Jr E. (2016). Enzyme-induced carbonate mineral precipitation for fugitive dust control. *Géotechnique*, 66(7):546-555.

Han, Z., Cheng, X., and Ma, Q. (2016). An experimental study on dynamic response for MICP strengthening liquefiable sands. *Earthquake Engineering and Engineering Vibration*, 15:673-679.

Hashash, Y. M. A., Dashti, S., Ines, M., Ghayoomi, M., and Musgrove, M. (2015). Evaluation of 1-D seismic site response modeling of sand using centrifuge experiments. *Soil Dynamics and Earthquake Engineering*, 78:19–31.

Hashash, Y. M. A., Phillips, C., and Groholski, D. R. (2010). Recent advances in non-linear site response analysis. In *proceedings of International Conferences on Recent Advances in Geotechnical Earthquake Engineering and Soil Dynamics*, 1–22. San Diego, California.

Hauser, L., and Schweiger, H. F. (2021). Numerical study on undrained cone penetration in structured soil using G-PFEM. *Computers and Geotechnics*, 133:104061.

Hayashi, K., Yasuhara, H., and Okamura, M. (2010). Effects of calcite precipitation on liquefaction resistance of sand. In *proceedings of 7th Int. Conf. on Urban Earth. Eng. & 5th International Conference on Earthquake Engineering*, Tokyo, Japan, 485-491.

Hayati, H., and Andrus, R. D. (2009). Updated liquefaction resistance correction factors for aged sands. *J. Geotechnical and Geoenvironmental Engineering*, 135(11):1683–92.

Hernandez, G. L. (2018). Centrifuge model testing of liquefaction mitigation via microbially induced calcite precipitation. *Master's thesis*, University of California, Davis, CA, USA.

Hirai, H., Takahashi, M., and Yamada, M. (1989). An elastic-plastic constitutive model for the behavior of improved sandy soils. *Soils and Foundations*, 29(2):69–84.

Hoang, T., Alleman, J., Cetin, B., and Choi, S. (2020). Engineering properties of biocementation coarse- and fine-grained sand catalyzed by bacterial cells and bacterial enzyme. *Journal of Materials in Civil Engineering*, 32(4), 04020030.

Horpibulsuk, S., Miura, N., and Bergado, D. T. (2004). Undrained shear behavior of cement admixed clay at high water content. *J. Geotechnical and Geoenvironmental Engineering*, 130(10):1096–1105.

Huang, W. X., Sloan, S., and Fityus, S. (2008). Incorporating a predefined limit condition in a hypo-plastic model by means of stress transformation. *Mechanics of Materials*, 40(10):796-802.

Humire, F. A., and Ziotopoulou, K. (2022). Mechanisms of shear strain accumulation in laboratory experiments on sands exhibiting cyclic mobility behavior. *Canadian Geotechnical Journal*, 00:1-13.

Hutabarat, D. and Bray, J. (2021). Effective stress analysis of liquefiable sites to estimate the severity of sediment ejecta. *J. of Geotechnical and Geoenvironmental Engineering*, 147(5):04021024.

Idriss, I. M., and Boulanger, R. W. (2008). Soil liquefaction during earthquakes. Earthquake Engineering Research Institute.

Imam, S. M. R., Morgenstern, N. R., Robertson, P. K., and Chan, D. H. (2005). A critical-state constitutive model for liquefiable sand. *Canadian Geotechnical J.*, 42:830–855.

Ishihara, K., Tatsuoka, F., and Yasuda, S. (1975). Undrained deformation and liquefaction of sand under cyclic stresses. *Soils and Foundations*, 15(1):29-44.

Ismail, M. A., Joer, H. A., Sim, W. H., and Randolph, M. F. (2002). Effect of cement type on shear behavior of cemented calcareous soil. *J. Geotechnical and Geoenvironmental Engineering*, 128(6):520-529.

ITASCA (2019). *Finite Lagrangian Analysis of Continua*.

Iwasaki, T., Tatsuoka, F., Tokida, K., and Yasuda, S. (1978). A practical method for assessing soil liquefaction potential based on case studies at various sites in Japan. In *proceedings of 2nd International Conference on Microzonation*, National Science Foundation, Washington, DC.

Jefferies, M. G. (1993). Nor-Sand: a simple critical state model for sand. *Géotechnique*, 43(1):91-103.

Kavvadas, M., and Amorosi, A. (2000). A constitutive model for structured soils. *Géotechnique*, 50(3):263-273.

Khoubani, A., Evans, T. M., and Montoya, B. M. (2016). Particulate simulations of triaxial tests on bio-cemented sand using a new cementation model. In *proceedings of Geo-Chicago 2016*, 84-93.

Khosravifar, A., Elgamal, A., Lu, J., and Li, J. (2018). A 3D model for earthquake-induced liquefaction triggering and post-liquefaction response. *Soil Dynamics and Earthquake Engineering*, 110:43-52.

Kim, M. K., and Lade, P. V. (1988). Single hardening constitutive model for frictional materials, I. Plastic potential function. *Computers and Geotechnics*, 5(4):307-324.

Kiyota, T., Koseki, J., Sato, T., and Kuwano, R. (2009). Aging effects on small strain shear moduli and liquefaction properties of in-situ frozen and reconstituted sandy soils. *Soils and Foundations*, 49(2):259–74.

Kiyota, T., Sato, T., Koseki, J., and Abadimarand, M. (2008). Behavior of liquefied sands under extremely large strain levels in cyclic torsional shear tests. *Soils and Foundations*, 48:727–739.

Kokusho, T., Nagao, Y., Ito, F., and Fukuyama, T. (2012). Aging effect on sand liquefaction observed during the 2011 earthquake and basic laboratory studies. In *proceedings of the International Symposium on Engineering Lessons Learned from the 2011 Great Japan Earthquake*, 759-770.

Konrad, J. M., and Law, K. T. (1987). Undrained shear strength from piezocone tests. *Canadian Geotechnical J.*, 24, 392–405.

Krage, C. P., Broussard, N. S., and DeJong, J. T. (2014). Estimating rigidity index (Ir) based on CPT measurements. In *proceedings of 3rd International Symposium on Cone Penetration Testing (CPT14)*, 727–735.

Kutter, B. L., Manzari, M. T., and Zeghal, M. (2017). Model tests and numerical simulations of liquefaction and lateral spreading, LEAP-UCD-2017.

Lade, P. V., and Trads, N. (2014). The role of cementation in the behaviour of cemented soils. *Geotechnical Research*, 1(4):111-132.

Lagioia, R., and Nova, R. (1995). An experimental and theoretical study of the behaviour of a calcarenite in triaxial compression. *Géotechnique*, 45(4):633–648.

Laloui, L., and François, B. (2009). SCMEG_T:soil thermoplasticity model. *J. of Engineering Mechanics*, 135(9):932-944.

Lee, K., Chan, D., and Lam, K. (2004). Constitutive model for cement treated clay in a critical state framework. *Soils and Foundations*, 44(3):69-77.

Lee, M. J., Choi, Y. M., Kim, M. T., and Lee, W. J. (2010). Evaluation of cementation effect of sand using cone resistance. In *proceedings of 2nd International Symposium on Cone Penetration Testing*.

Lee, M., Choo, H., Kim, J., and Lee, W. (2011). Effect of artificial cementation on cone tip resistance and small strain shear modulus of sand. *Bulletin of Engineering Geology and the Environment*, 70:193–201.

Lee, M., Gomez, M. G., El Kortbawi, M., and Ziotopoulou, K. (2022). Effect of light biocementation on the liquefaction triggering and post-triggering behavior of loose sands. *J. of Geotechnical and Geoenvironmental Engineering*, 148(1), 1–19.

Lee, M., Gomez, M. G., El Kortbawi, M., and Ziotopoulou, K. (2020). Examining the liquefaction resistance of lightly cemented sands using microbially induced calcite precipitation (MICP). In *proceedings of GeoCongress 2020*, Minneapolis, MN.

Leroueil, S., and Vaughan, P. R. (1990). The general and congruent effects of structure in natural soils and weak rocks. *Géotechnique*, 40(3):467-488.

Lin, H., Suleiman, M. T., Brown, D. G., and Kavazanjian, E. (2016). Mechanical behavior of sands treated by microbially induced carbonate precipitation. *J. Geotechnical and Geoenvironmental Engineering*, 142(2).

Liu, L., Liu, H., Stuedlein, A. W., Evans, M. T., and Xiao, Y. (2018). Strength, stiffness, and microstructure characteristics of biocemented calcareous sand. *Canadian Geotechnical J.*, 1-12.

Lo, S. C., Lade, P. V., and Wardani, S. P. R. (2003). An experimental study of the mechanics of two weakly cemented soils.

Lu, Q., Randolph, M. F., Hu, Y., and Bugarski, I. C. (2004). A numerical study of cone penetration in clay. *Géotechnique*, 54(4), 257–267.

Lu, Y., Zhu, W., Ye, G., and Zhang, F. (2022). A unified constitutive model for cemented/non-cemented soils under monotonic and cyclic loading. *Acta Geotechnica*, 17:2173-2191.

Lunne, T., Robertson, P. K., and Powell, J. J. M. (1997). Cone penetration testing in geotechnical practice.

Manzari, M. T., and Dafalias, Y. F. (1997). A critical state two-surface plasticity model for sands. *Géotechnique*, 47(2), 255–272.

Martinez, B. C., DeJong, J. T., Ginn, T. R., Montoya, B. M., Barkouki, T. H., Hunt, C., Tanyu, B., and Major, D. (2013). Experimental optimization of microbial-induced carbonate precipitation for soil improvement. *J. Geotechnical and Geoenvironmental Engineering*, 139(4):587-598.

Martinez, B. C., DeJong, J. T., and Ginn, T. R. (2014). Bio-geochemical reactive transport modeling of microbial induced calcite precipitation to predict the treatment of sand in one-dimensional flow. *Computers and Geotechnics*, 58:1-13.

Matsuoka, H., and Nakai, T. (1974). Stress-deformation and strength characteristic of soil under three different principal stresses. In *proceedings of the Japan Society of Civil Engineers*, 232: 59-70.

Maurer, B., Green, R., Bradley, B., and Cubrinovski, M. (2014). Assessment of aging correction factors for liquefaction resistance at sites of recurrent liquefaction. In *proceedings of the 10th U.S. National Conference on Earthquake Engineering*, July 21-25, Anchorage, AK, USA.

Mehrabi, R., and Atefi-Monfared, K. (2022). A coupled bio-chemo-hydro-mechanical model for bio-cementation in porous media. *Canadian Geotechnical J.*, 59:1266-1280.

Miftah, A., Tirkolaei, H. K., Bilsel, H., and El Naggar, H. (2022). Erodibility improvement and scour mitigation of beach sand by enzymatic induced carbonate precipitation. *Geomechanics for Energy and the Environment*.

Minto, J. M., Lunn, R. J., and El Mountassir, G. (2019). Development of a reactive transport model for field-scale simulation of microbially induced carbonate precipitation. *Water Resources Research*, 55(8):7229-7245.

Mitchell, J. K., and Santamarina, J. C. (2005). Biological considerations in geotechnical engineering. *J. of Geotechnical and Geoenvironmental Engineering*, 131(10):1222-1233.

Mitchell, J. K. (2008). Aging of sand-a continuing enigma. In *proceedings of International Conference on Case Histories in Geotechnical Engineering (6ICCHGE)*, Arlington, VA, USA.

Molenaar, N., and Venmans, A. A. M. (1993). Calcium carbonate cementation of sand: a method for producing artificially cemented samples for geotechnical testing and a comparison with natural cementation processes. *Engineering Geology*, (35), 103–122.

Montgomery, J., Boulanger, R. W., and Harder, L. F. (2014). Examination of the K_σ overburden correction factor on liquefaction resistance. *J. of Geotechnical and Geoenvironmental Engineering*, 140(12):04014066.

Montoya, B. M., DeJong, J. T., Boulanger, R. W., Wilson, D. W., Gerhard, R., Ganchenko, A., and Chou, J. (2012). Liquefaction mitigation using microbial induced calcite precipitation. In *proceedings of GeoCongress 2012*, Oakland, CA, USA.

Montoya, B. M., and DeJong, J. T. (2013). Healing of biologically induced cemented sands. *Géotechnique Letters*, 3:147-151.

Montoya, B. M., DeJong, J. T., and Boulanger, R. W. (2013). Dynamic response of liquefiable sand improved by microbial-induced calcite precipitation. *Géotechnique*, 63(4):302.

Montoya, B. M., and DeJong, J. T. (2015). Stress-strain behavior of sands cemented by microbially induced calcite precipitation. *J. of Geotechnical and Geoenvironmental Engineering*, 141(6):04015019.

Montoya, B. M., Do, J., and Gabr, M. A. (2021). Distribution and properties of microbially induced carbonate precipitation in underwater sand bed. *J. of Geotechnical and Geoenvironmental Engineering*, 147(10):04021098.

Moss, R. E. S., Thornhill, D. M., Nelson, A. I., and Levulett, D. A. (2008). Influence of aging on liquefaction potential: preliminary results. In *proceedings of Geotechnical Earthquake Engineering and Soil Dynamics Congress IV*,1–10.

Moug, D. M. (2017). Axisymmetric cone penetration model for sands and clays. *PhD dissertation*, University of California, Davis.

Moug, D. M., Boulanger, R. W., DeJong, J. T., and Jaeger, R. A. (2019a). Axisymmetric simulations of cone penetration in saturated clay. *J. of Geotechnical and Geoenvironmental Engineering*, 145(4).

Moug, D. M., Price, A. B., Parra Bastidas, A. M., Darby, K. M., Boulanger, R. W., and DeJong, J. T. (2019b). Mechanistic development of CPT-based cyclic strength correlations for clean sand. *J. of Geotechnical and Geoenvironmental Engineering*, 145(10).

Mujah, D., Shahin, M. A., Cheng, L., and Karrech, A. (2021). Experimental and analytical study on geomechanical behavior of biocemented sand. *International J. of Geomechanics*, 21(8):04021126.

Na, T. K., Cabas, A., and Montoya, B. M. (2022). Resonant column testing procedure for microbial induced carbonate precipitated sands. *Geotechnical Testing Journal*.

Nafisi, A., and Montoya, B. (2018). A new framework for identifying cementation level of MICP-treated sands. In *proceedings of International Foundations Congress & Equipment Expo (IFCEE)*, Orlando, FL, USA.

Nafisi, A., Khoubani, A., Montoya, B., and Evans, T. M. (2018). The effect of grain size and shape on mechanical behaviour of MICP sand I: experimental study.

Nafisi, A., Liu, Q., and Montoya, B. M. (2021). Effect of stress path on the shear response of bio-cemented sands. *Acta Geotechnica*.

Nafisi, A., Safavizadeh, S., and Montoya, B. (2019a) Influence of microbe and enzyme-induced treatments on cemented sand shear response. Technical note, *J. of Geotechnical and Geoenvironmental Engineering*, 145(9): 06019008.

Nafisi, A., Mocelin, D., Montoya, B., and Underwood, S. (2019b). Tensile strength of microbially induced carbonate precipitation treated sands. *Canadian Geotechnical J.*, 57:1611-1616.

Nafisi, A., Montoya, B., and Evans, T. M. (2020). Shear strength envelopes of biocemented sands with varying particle size and cementation level. *J. of Geotechnical and Geoenvironmental Engineering*, 146(3):04020002.

Nakai, T. (1989). An isotropic hardening elastoplastic model for sand considering the stress path dependency in three-dimensional stresses. *Soils and Foundations*, 1:119-137.

Nassar, M. K., Gurung, D., Bastani, M., Ginn, T. R., Shafei, B., Gomez, M. G., Graddy, C. M. R., Nelson, D. C., and DeJong, J. T. (2018). Large-scale experiments in microbially induced calcite precipitation (MICP): reactive transport model development and prediction. *Water Resources Research*, 54(1):480-500.

Nguyen, L. D., Fatahi, B., and Khabbaz, H. (2014). A constitutive model for cemented clays capturing cementation degradation. *International J. of Plasticity*, 56:1–18.

Nguyen, L. D., Fatahi, B., and Khabbaz, H. (2017). Development of a constitutive model to predict the behaviour of cement-treated clay during cementation degradation: C3 model. *International J. of Geomechanics*, 17(7):04017010.

Ning, Z., Khoubani, A., and Evans, T. M. (2017). Particulate modeling of cementation effects on small and large strain behaviors in granular material. *Granular Matter*, 19(1).

Nova, R. (1988). Sinfonietta classica: an exercise on classical soil modelling. In *proceedings of the Symposium on Constitutive Equations for Granular Non-cohesive soils*, 501-520.

Nova, R., Castellanza, R., and Tamagnini, C. (2003). A constitutive model for bonded geomaterials subject to mechanical and/or chemical degradation. *International J. for Numerical and Analytical Methods in Geomechanics*, 27(9):705-732.

Nweke, C. C., and Pestana, J. M. (2017). Modeling bio-cemented sands: shear strength and stiffness with degradation. In *proceedings of Grouting 2017*, 34–45.

O'Donnell, S. T., Rittmann, B. E., and Kavazanjian, E. (2017). MIDP: Liquefaction mitigation via microbial denitrification as a two-stage process. I: Desaturation. *J. Geotechnical and Geoenvironmental Engineering*, 143(12):04017094.

O'Rourke, T. D., and Crespo, E. (1988). Geotechnical properties of cemented volcanic soil. *J. of Geotechnical Engineering*, 114(10):1126–1147.

Panico, F., and Viana da Fonseca, A. (2018). Modelling the small strain behaviour of a cemented silty sand with bounding plasticity. In *proceedings of the 9th European Conference on Numerical Methods in Geotech. Eng. (NUMGE 2018)*, Porto.

Pekau, O. A., and Gocevski, V. (1989). Elasto-plastic model for cemented and pure sand deposits. *Computers and Geotechnics*, 7:155-187.

Pestana, J. M., and Salvati, L. A. (2006). Small-strain behaviour of granular soils. I: model for cemented and uncemented sands and gravels. *J. Geotechnical and Geoenvironmental Engineering*,132(8):1071-1081.

Pinske, M. A. (2011). Life cycle assessment of ground improvement methods.

Porcino, D., and Marcianò, V. (2017). Bonding degradation and stress-dilatancy response of weakly cemented sands. *Geomechanics and Geoengineering*, 12(4):221-233.

Porcino, D., Marciano, V., and Granata, R. (2012). Static and dynamic properties of a lightly cemented silicate-grouted sand. *Canadian Geotechnical J.*, 49(10):1117-1133.

Poorooshasb, H. B., and Pietruszczak, S. (1985). On yielding and flow of sand: a generalized two-surface model. *Computers and Geotechnics*, 1:33-58.

Puppala, A. J., Acar, Y. B., and Tumay, M. T. (1995). Cone penetration in very weakly cemented sand. *J. of Geotechnical Engineering*, 121(8):589-600.

Puppala, A. J., Acar, Y. B., and Tumay, M. T. (1997). Low strain dynamic shear modulus of cemented sand from cone penetration test results. *Transportation Research Record*, (1548), 60–66.

Rad, N. S., and Clough, G. W. (1982). The influence of cementation on the static and dynamic behaviour of sands. Final report, United States Geological Survey (USGS), Contract No. USGS 14-08-0001-19763.

Rahimi, M., Chan, D., and Nouri, A. (2015). Bounding surface constitutive model for cemented sand under monotonic loading. *International J. of Geomechanics*, 16(2):1–11.

Rahimi, M., Chan, D., and Nouri, A. (2018). Constitutive model for monotonic and cyclic responses of loosely cemented sand formations. *J. of Rock Mechanics And Geotechnical Engineering*, 10:740–752.

Rakhimzhanova, A., Thornton, C., Amanbek, Y., and Zhao, Y. (2021). Numerical simulations of cone penetration in cemented sandstone. *EPJ Web of Conferences*, 249(14010):1–4.

Ramirez, J., Barrero, A. R., Chen, L., Dashti, S., Ghofrani, A., Taiebat, M., and Arduino, P. (2018). Site response in a layered liquefiable deposit : evaluation of different site response in a layered liquefiable deposit : evaluation of different numerical tools and methodologies with centrifuge experimental results. *J. of Geotechnical and Geoenvironmental Engineering*, 144(10): 1–22.

Raymond, A. J., Kendall, A., and DeJong, J. T. (2020). Life cycle sustainability assessment (LCSA): a research evaluation tool for emerging geotechnologies. In *proceddings of GeoCongress 2020*, 330–339.

Reddy, K. R., and Saxena, S. K. (1992). Constitutive modelling of cemented sand. *Mechanics of Materials*, 14:155-178.

Rios, S., Viana da Fonseca, A., and Baudet, B. A. (2012). Effect of the porosity/cement ratio on the compression of cemented soil. *J. of Geotechnical and Geoenvironmental Engineering*, 138(11):1422-1426.

Rios, S., Viana da Fonseca, A., and Baudet, B. A. (2014). On the behaviour of an artificially cemented soil. *Acta Geotechnica*, 9:215-226.

Rios, S., Ciantia, M., Gonzalez, N., Arroyo, M., and Viana da Fonseca, A. (2016). Simplifying calibration of bonded elasto-plastic models. *Computers and Geotechnics*, 73:100-108.

Riveros, G. A., and Sadrekarimi, A. (2020a). Effect of microbially-induced cementation on the instability and critical state behaviors of Fraser River sand. *Canadian Geotechnical J.*

Riveros, G. A., and Sadrekarimi, A. (2020b). Liquefaction resistance of Fraser River sand improved by a microbially-induced cementation. *Soil Dynamics and Earthquake Engineering*, 131:106034.

Rix, G. J., and Stokoe, K. H. (1991). Correlation of initial tangent modulus and cone penetration resistance. In *proceedings of the First International Symposium on Calibration Chamber Testing*, Potsdam, NY, 351-362.

Robertson, P. K. (2016). Cone penetration test (CPT)-based soil behaviour type (SBT) classification system — an update. *Canadian Geotechnical Journal, 53*, 1910–1927.

Robertson, P. K., and Campanella, R. G. (1983). Interpretation of cone penetration tests. *Canadian Geotechnical Journal*, *20*(4):1–81.

Rodrigues, C. M. G. (2003). Geotechnical characterization and geomechanical behaviour study of saprolitic granite soils from Guarda. *PhD dissertation*, Coimbra University, Coimbra, Portugal.

Roy, D. (2008). Coupled use of cone tip resistance and small strain shear modulus to assess liquefaction potential. *J. of Geotechnical and Geoenvironmental Engineering*, 134(4):519-530.

Rumpelt, T. K. (1990). Constitutive modeling of weak porous rocks. *PhD dissertation*, University of California, Berkeley, CA, USA.

Salomone, L. A., Singh, H., and Fischer, J. A. (1978). Cyclic shear strength of variably cemented sands. In *proceedings of the ASCE Geotechnical Engineering Division Specialty Conference on Earthquake Engineering and Soil Dynamics*, Vol.II, Pasadena, CA, 819-835.

San Pablo, A. C. M., DeJong, J. T., and Carey, T. J. (2023). Centrifuge tests to investigate the effect of MICP treatment zone on foundation system performance. In *proceedings of ASCE GeoCongress 2023*, Los Angeles, California (under review).

San Pablo, A. C. M., Lee, M., Graddy, C. M. R., Kolbus, C. M., Khan, M., Zamani, A., Martin, N., Acuff, C., DeJong, J. T., Gomez, M. G., and Nelson, D. C. (2020). Meter-scale Bio-cementation experiments to advance process control and reduce impacts: examining spatial control, ammonium by-product removal, and chemical reductions. *J. of Geotechnical and Geoenvironmental Engineering*, 146(11):04020125.

Sasaki, T., and Kuwano, R. (2016). Undrained cyclic triaxial testing on sand with non-plastic fines content cemented with microbially induced $CaCO_3$. *Soils and Foundations*, 56(3):485-495.

Saxena, S. K., and Lastrico, R. M. (1978). Static properties of lightly cemented sand. *J. of Geotechnical Engineering Division*, 14(12):1449–1463.

Saxena, S. K., Reddy, K. R., and Avramidis, A. S. (1988a). Static behavior of artificially cemented sand. *Indian Geotechnical Journal*, 18(2):111-141.

Saxena, S. K., Reddy, K. R., and Avramidis, A. S. (1988b). Liquefaction resistance of artificially cemented sand. *J. of Geotechnical Engineering*, 114:1395-1413.

Saxena, S. K., Avramidis, A. S., and Reddy, K. (1988c). Dynamic moduli and damping ratios for cemented sands at low strains. *Canadian Geotechnical J.*, 25:353-368.

Seed, H. B., and Idriss, I. M. (1970). Soil moduli and damping factors for dynamic response analyses.

Schnaid, F., Prietto, P. D. M., and Consoli, N. C. (2001). Characterization of cemented sand in triaxial compression. *J. of Geotechnical and Geoenvironmental Engineering*, 127:857-868.

Schnaid, F., Sills, G. C., Soares, J. M., and Nyirenda, Z. (1997). Predictions of the coefficient of consolidation from piezocone tests. *Canadian Geotechnical J.*, 34, 315–327.

Schnaid, F., Lehane, B. M., and Fahey, M. (2004). In situ characterization of unusual geomaterials. In *proceedings of the 2nd International Conference on Geotechnical and Geophysical Site Characterization*, Porto, Portugal, 49-74.

Schneider, J. A., and Moss, R. E. S. (2011). Linking cyclic stress and cyclic strain based methods for assessment of cyclic liquefaction triggering in sands. *Géotechnique Letters*, 1:31-36.

Seed, H. B. (1976). Evaluation of soil liquefaction effects on level ground during earthquakes. In *proceedings of Liquefaction Problems in Geotechnical Engineering*, ASCE National Convention, 1-104.

Seed, H. B. (1979). Soil liquefaction and cyclic mobility evaluation for level ground during earthquakes. *J. of the Geotechnical Engineering Division*, 105(2):201-255.

Sengupta, A. (1989). Application of a thermodynamic model to soils and concrete. *PhD dissertation*, Department of Civil Engineering, Illinois Institute of Technology, Chicago, Illinois.

Shamoto, Y., Zhang, J. M., and Goto, S. (1997). Mechanism of large post-liquefaction deformation in saturated sand. *Soils and Foundations*, 37(2): 71–80.

Sharma, S. S., and Fahey, M. (2003a). Evaluation of cyclic shear strength of two cemented calcareous soils. *J. of Geotechnical and Geoenvironmental Engineering*, 129(7):608-618.

Sharma, S. S., and Fahey, M. (2003b). Degradation of stiffness of cemented calcareous soil in cyclic triaxial tests. *J. of Geotechnical and Geoenvironmental Engineering*, 129(7):619-629.

Sharma, M., Satyam, N., and Reddy, K. R. (2021). Hybrid bacteria mediated cemented sand: microcharacterization, permeability, strength, shear wave velocity, stress-strain, and durability. *International J. of Damage Mechanics*, 1-28.

Sharma, M., Satyam, N., and Reddy, K. R. (2022). Large-scale spatial characterization and liquefaction resistance of sand by hybrid bacteria induced biocementation. *Engineering Geology*, 302:106635.

Schweiger, H. F., and Hauser, L. (2021). Numerical simulation of CPT with the Clay and Sand Model (CASM) including effects of bonding. In B. M., A. Di Donna, & D. Sterpi (Eds.), In *proceedings of the 16th International Conference of IACMAG* (Vol. 1, pp. 179–188). Turin, Italy: Springer.

Sitar, N., Clough, W. G., and Bachus, R. C. (1980). Behavior of weakly cemented soil slopes under static and seismic loading conditions. The John A. Blume Earthquake Engineering Center, Stanford University, Report No. 44.

Simatupang, M., and Okamura, M. (2017). Liquefaction resistance of sand remediated with carbonate precipitation at different degrees of saturation during curing. *Soils and Foundations*, 57(4):619–631.

Simatupang, M., Okamura, M., Hayashi, K., and Yasuhara, H. (2018). Small-strain shear modulus and liquefaction resistance of sand with carbonate precipitation. *Soil Dynamics and Earthquake Engineering*, 115:710-718.

Soon, N. W., Lee, L. M., Khun, T. C., and Ling, H. S. (2013). Improvements in engineering properties of soils through microbial-induced calcite precipitation *J. of Civil Engineering*, 17(4):718-728.

Soriano, I., Charalampidou, E. M., Lewis, H., Viggiani, G., Buckman, J., and Couples, G. (2017). Localised deformation of weakly cemented sands: a case study. In *proceedings of International Workshop on Bifurcation and Degradation in Geomaterials*, 381-389.

Stocks-Fischer, S., Galinat, J. K., and Bang, S. S. (1999). Microbiological precipitation of CaCO3. *Soil Biology and Biochemistry*, 31(11):1563-1571.

Stokoe, K. H., and Santamarina, J. C. (2000). Seismic-wave-based testing in geotechnical engineering.

Sun, D., and Matsuoka, H. (1999). An elastoplastic model for frictional and cohesive materials and its application to cemented sands. *Mechanics of Cohesive-Frictional Materials*, 4:525–543.

Tagliaferri, F., Waller, J., Andò, E., Hall, S. A., Viggiani, G., Bésuelle, P., and DeJong, J. T. (2011). Observing strain localisation processes in bio-cemented sand using x-ray imaging. *Granular Matter*, 13(3):247-250.

Tasiopoulou, P., Ziotopoulou, K., Humire, F., Giannakou, A., Chacko, J., and Travasarou, T. (2020). Development and implementation of semiempirical framework for modeling postliquefaction deformation accumulation in sands. *J. of Geotechnical and Geoenvironmental Engineering*, 146(1).

Teh, C. I., and Houlsby, G. T. (1991). An analytical study of the cone penetration test in clay. *Géotechnique*, 41(1), 17–34.

Terzis, D., Bernier-Latmani, R., and Laloui, L. (2016). Fabric characteristics and mechanical response to bio-improved sand to various treatment conditions. *Géotechnique Letters*, 6(1):50–57.

Terzis, D., and Laloui, L. (2017). On the application of microbially-induced calcite precipitation for soils: a multiscale study. *Geomechanics and Geoengineering*.

Terzis, D., and Laloui, L. (2019). Cell-free soil bio-cementation with strength, dilatancy and fabric characteristics. *Acta Geotechnica*, 14:639-656.

Troncoso, J., Ishihara, K., and Verdugo, R. (1988). Aging effects on cyclic shear strength of tailings materials. In *proceedings of the 9th World Conference on Earthquake Engineering*, Vol. III. Japan: Tokyo, Kyoto, 121–126.

Tsukamoto, M., Inagaki, T., Sasaki, Y., and Oda, K. (2013). Influence of relative density on microbial carbonate precipitation and mechanical properties of sand. In *proceedings of the 18th International Conference on Soil Mechanics and Geotechnical Engineering*, 2613-2616.

Valanis, K. C., and Peters, J. F. (1988). Thermodynamics of frictional materials, Report I, A constitutive theory of soil with dilatant capability. U.S. Army Engineers Waterways, Experiment Station Report.

Valle, C., Camacho, B. I., Stokoe, K. H., and Rauch, A. F. (2003). Comparison of the dynamic properties and undrained shear strengths of offshore calcareous sand and artificially cemented sand. In *proceedings of the 22nd International Conference on Offshore Mechanics and Arctic Engineering*, Cancun, Mexico 1, 133-141.

Van Hoff, D. J. (1994). Evaluation of the dynamic properties of artificially cemented sands at low confining pressures. University of Texas, Austin, Texas, USA.

van Paassen, L. A. (2009). Biogrout, ground improvement by microbial induced carbonate precipitation. Delft University of Technology, The Netherlands.

van Paassen, L. A., Daza, C. M., Staal, M., Sorokin, D. Y., van der Zon, W., and van Loosdrecht, M. C. (2010). Potential soil reinforcement by biological denitrification. *Ecological Engineering*, 36(2):168-175.

van Paassen, L. A., Ghose, R., van der Linden, T. J. M., van der Star, W.R. L., and van Loosdrecht, M. C. M. (2010). Quantifying biomediated ground improvement by ureolysis: large-scale biogrout experiment. *J. of Geotechnical and Geoenvironmental Engineering*, 136(12):1721–1728.

Vatsala, A., Nova, R., and Murthy, B. S. (2001). Elastoplastic model for cemented soils. J *J. of Geotechnical and Geoenvironmental Engineering*, 127(8):679-687.

Vaunat, J., and Gens, A. (2003). Bond degradation and irreversible strains in soft argillaceous rock. In *proceedings of the 12h Panamerican Conference on Soil Mechanics and Geotechnical Engineering*, 1:479-484.

Waller, J. T. (2011). Influence of bio-cementation on shearing behaviour in sand using X-ray computed tomography. *Masters' thesis*, University of California, Davis, CA, USA.

Wang, L., Chu, J., Wu, S., and Wang, H. (2021). Stress-dilatancy behavior of cemented sand: comparison between bonding provided by cement and biocement. *Acta Geotechnica*, 16:1441-1456.

Wang, Y. H., and Leung, S. C. (2008). Characterization of cemented sand by experimental and numerical investigations. *J. of Geotechnical and Geoenvironmental Engineering*, 134(7):992-1004.

Wang, G., and Wei, J. (2016). Microstructure evolution of granular soils in cyclic mobility and post-liquefaction process. *Granular Matter*, 18:51.

Wei, J., Huang, D., and Wang, G. (2018). Microscale descriptors for particle-void distribution and jamming transition in pre- and post-liquefaction of granular soils. *Journal of Engineering Mechanics*, 144(8): 4018067.

Wissa, A. E. Z., and Ladd, C. C. (1964). Effective stress-strength behavior of compacted stabilized soils. Department of Civil Eng., M.I.T, MA, USA, Research report R64-32, Soils Publication No. 164.

Wu, S., Li, B., and Chu, J. (2021). Stress-dilatancy behavior of MICP-treated sand. *International J. of Geomechanics*, 21(3):04020264.

Xiao, P., Liu, H., Xiao, Y., Stuedlein, A. W., and Evans, T. M. (2018). Liquefaction resistance of bio-cemented calcareous sand. *Soil Dynamics and Earthquake Engineering*, 107:9–19.

Xiao, P., Liu, H., Stuedlein, A., Evans, T. M., and Xiao, Y. (2019a). Effect of relative density and bio-cementation on the cyclic response of calcareous sand. *Canadian Geotechnical J.*

Xiao, Y., Wang, Y., Desai, C. S., Jiang, X., and Liu, H. (2019b). Strength and deformation responses of biocemented sands using a temperature-controlled method. *International J. of Geomechanics*, 19(11):04019120.

Xiao, Y., Zhang, Z., Stuedlein, A. W., and Evans, T. M. (2021). Liquefaction modeling for biocemented calcareous sand. *J. of Geotechnical and Geoenvironmental Engineering*, 147:04021149.

Yamada, S., Sakai, T., Nakano, M., and Noda, T. (2022). Method to introduce the cementation effect into existing elastoplastic constitutive models for soils. *J. of Geotechnical and Geoenvironmental Engineering*, 148(5):0422013.

Yang, C., Cui, Y. J., Pereira, J. M., and Huang, M. S. (2008). A constitutive model for unsaturated cemented soils under cyclic loading. *Computers and Geotechnics*, 35(6):853–859.

Yang, C., Huang, M. S., and Cui, Y-J. (2011). Constitutive model of unsaturated structured soils under cyclic loading. In *proceedings of Unsaturated Soils*, London. Taylor and Francis Group.

Yang, P. (2018). Discrete element modeling of the mechanical response of cemented granular materials.

Yang, P., O'Donnell, S., Hamdan, N., Kavazanjian, E., and Neithalath, N. (2017). 3D DEM simulations of drained triaxial compression of sand strengthened using microbially induced carbonate precipitation. *International J. of Geomechanics*, 17(6):04016143.

Yazdani, E., Montoya, B. M., Wengrove, M., and Evans, T. M. (2022). Bio-cementation for protection of coastal dunes: physical models and element tests. In *proceedings of ASCE GeoCongress 2022*, Charlotte, North Carolina.

Yi, J. T., Goh, S. H., Lee, F. H., and Randolph, M. F. (2012). A numerical study of cone penetration in fine-grained soils allowing for consolidation effects. *Géotechnique*, 62(8):707–719.

Youd, T. L., and Idriss, I. M. (2001). Liquefaction resistance of soils: Summary report from the 1996 NCEER and 1998 NCEER/NSF Workshops on Evaluation of Liquefaction Resistance of Soils. *J. of Geotechnical and Geoenvironmental Engineering*, 127:4(297), 297–313.

Youd, T. L., and Perkins, D. M. (1978). Mapping liquefaction-induced ground failure potential. *J. of Geotechnical Engineering Division*, 104(GT4):433-446.

Yu, H. S., Tan, S. M., and Schnaid, F. (2007). A critical state framework for modelling bonded geomaterials. *Geomechanics and Geoengineering*, 2(1):61-74.

Yu, H. S. (1998). CASM: a unified state parameter model for clay and sand. *International J. Numerical and Analytical Methods in Geomechanics*, 22:621–653.

Yun, T. S., and Santamarina, J. C. (2005). Decementation, softening, and collapse: changes in small-strain shear stiffness in k_o loading. *J. of Geotechnical and Geoenvironmental Engineering*, 131(3):350-358.

Zamani, A. (2017). Liquefaction mitigation of silty sands with microbial induced calcite precipitation. *PhD dissertation*, North Carolina State University, Rayleigh, NC, USA.

Zamani, A., and Montoya, B. M. (2017). Shearing and hydraulic behavior of MICP treated silty sand. In *Proceedings of Geotechnical Frontiers 2017*, 290–299.

Zamani, A., and Montoya, B. (2018). Undrained monotonic shear response of MICP-treated silty sands. *J. of Geotechnical and Geoenvironmental Engineering*, 144(6):1-12.

Zamani, A., and Montoya, B. (2019). Undrained cyclic response of silty sands improved by microbial induced calcium carbonate precipitation. *Soil Dynamics and Earthquake Engineering*, 120:436-448.

Zamani, A., Xiao, P., Baumer, T., Carey, T. J., Sawyer, B., DeJong, J. T., and Boulanger, R. W. (2021). Mitigation of liquefaction triggering and foundation settlement by MICP treatment. J *J. of Geotechnical and Geoenvironmental Engineering*, 147(10):1-15.

Zhang, A., Dafalias, Y. F., and Jiang, M. (2021). A bounding surface plasticity model for cemented sand under monotonic and cyclic loading. *Géotechnique*, 1–18.

Zhang, F., Ye, B., Noda, T., Nakano, M., and Nakai, K. (2007). Explanation of cyclic mobility of soils: approach by stress-induced anisotropy. *Soils and Foundations*, 47(4):635–648.

Ziotopoulou, K., and Boulanger, R. W. (2016). Plasticity modeling of liquefaction effects under sloping ground and irregular cyclic loading conditions. *Soil Dynamics and Earthquake Engineering*, 84, 269–283.